Division of Molecular Therapeutics and Formulation

School of Pharmacy

Glycoligands for targeted liposomes: design, development and *ab-initio* understanding of cell-vesicle recognition

Rosa Catania, MSc.

Thesis submitted to the University of Nottingham

for the degree of Doctor of Philosophy

September 2017

"The more the marble wastes, the more the statue grows"

Michelangelo

Dedicated to my parents

Lucia and Michele

Abstract

In nature, several known proteins are glycosylated, and carbohydrate-cell receptor interactions mediate a plethora of key biological events, *e.g.* parasitisation and immune responses. Cell membranes display carbohydrate-binding proteins (lectins), which are able to selectively recognise specific sugar-ligands, decipher sugar-encoded instructions, and convert them into downstream biological processes. To overcome low binding affinities, which are typically observed for simple monosaccharides, protein-binding sugars are typically displayed within large multivalent ligands, where biological systems rely on multivalent interactions as a way to enhance selectivity and binding avidity. Glycoliposomes, phospholipid vesicles coated with sugars, can be designed to exploit this phenomenon through the presentation of multiple glycosylated ligands for actively targeting specific receptors, enhancing uptake of nanomedicines into target cells, or both. Among all the nanocarriers, liposomes are an advantageous strategy for drug delivery for their biocompatibility and high drug encapsulation efficiency. Functionalised liposomes have been developed over the last 30 years to optimise these nanocarriers by improving stability, circulation time and targeting.

This thesis work focussed on the use of glycosylated liposomal systems for the treatment of intracellular bacterial infection in cells presenting lectin endocytic receptors. Antimicrobial resistance is one of the current main global healthcare challenges. In particular, antimicrobial resistance in *Salmonella Enterica* serotypes is responsible for 16 million cases of typhoid fever, 94 million cases of gastroenteritis and 600.000 deaths worldwide. Salmonella is able to survive in intracellular compartments of macrophages. Mannose Receptor (MR, CD206) is a potential access gate to Salmonella infected macrophages which could be selectively targeted with

mannosylate-decorated liposomes. In this work, we present the design, the development and investigation of liposomal systems to deliver antimicrobials into Salmonella-infected macrophages.

In order to investigate and identify the key structural parameters for efficient delivery of glycotargeted liposomes to selected cell targets (MR^+ macrophages), two sets of monovalent glycoligands and two sets of multivalent polyglycosides - synthetic lipid-terminated glycopolymers - bearing a range of membrane-inserting anchors were synthesised. These synthesised membrane-inserting glycoligands have been used to formulate glycosylated liposomes with different glycosylation patterns and lipid composition through the Bangham method. Concanavalin A – a carbohydrate-binding protein – has been initially utilised as model protein target to study the surface presentation of the carbohydrate ligands. Firstly, the effect of lipid composition on the rate of liposomal clustering mediated by Concanavalin A (Con A) model lectin has been established. Our results showed that the binding properties of glycoliposomes are affected by the nature of both lipid constituents and carbohydrate ligands. Next, the uptake of glycosylated liposomes was investigated in salmonella infected macrophage-like cells. This *in vitro* infection model was used to evaluate the effect of different glycosylation patterns on the liposomal surface on mannose receptor (MR, CD206) targeting efficacy. Liposomes coated with mannose-containing glycopolymer significantly enhanced uptake compared to uncoated liposome control, and showed higher gentamicin delivery, resulting in reduction in internal infection.

Acknowledgements

Firstly, I would like to thank my supervisors from the University of Nottingham, Drs Giuseppe Mantovani, Snow S. Stolnik, Franco H. Falcone and Cynthia Bosquillon for their invaluable guidance and help throughout my PhD. Thanks to GlaxoSmithKline and Dr Rita Majithiya for supporting this project.

My sincere thanks also go to Dr Alan Huett, who provided me with access to his laboratory and research facilities together with his expertise in microbiology.

I am very grateful to Dr Francesca Mastrotto for all her help and advice not only in the academic life but also as a friend.

Thanks to Sue Wen Yong, Akmal Sabri, Thomas Smith and Laura McCoubrey (MPharm Undergraduate Project Students 2015 and 2016) for their help in the collection of data shown in Chapter 3 of this thesis.

Thanks to all the past and current members of B15 lab, D13 (cell culture) lab and B28 office. (The list of names would be far too long).
I also want to express my thanks to Christy Grainger-Boultby, Paul Cooling, Tom Boots, Tammy Lydamore, Esmé Ireson, Amy Nair, Julia Crouch, Carol Turrill and Colin Rowe. Without them Boots Science Building would not be such an amazing, efficient and safe place to work.
A massive thanks goes to the CDT, especially Dr Claudia Matz, and the "Ectodecto Team" (Georgina Marsh, Guðrún Andrea Friðgeirsdóttir, Monica Mistry, Claire Lewis, and Dolly) for all the amazing adventures during these years.

Thanks to my dear friends in Nottingham and around the world, especially in my sunny Sicily, for always supporting me.

Finally, I would like to thank my family for the immense support. My parents, Lucia and Michele, for always encouraging me to study, my aunt Matilde, my sister Chiara, my sister Itria with my brother-in-law Andrea and my sweet nephew Alessandro. Your smiles and love have been the energy that has fuelled this work over the years (and coffee of course).

Conference presentations

Catania R, Ricard F, Bosquillon C, Falcone FH, Stolnik S, Mantovani G. (2015) Targeted liposomal formulations: design, development and investigation of binding properties. Poster Presentation, UKICRS, University of Nottingham.

Catania R, Majithiya R, Bosquillon C, Falcone FH, Stolnik S, Mantovani G. (2016) Sweet liposomes: when sweetness is stuck in a 'lipid-zone'. Poster Presentation, Warwick Polymer Chemistry Conference, University of Warwick.

Catania R, Majithiya R, Bosquillon C, Falcone FH, Stolnik S, Mantovani G. (2017) Towards targeting of Salmonella-infected Macrophage using bespoke glycoliposomes. Oral Presentation, MacroGroup YRM, University of Edinburgh.

Catania R, Majithiya R, Bosquillon C, Falcone FH, Stolnik S, Mantovani G. (2017) Towards targeting of Salmonella-infected Macrophage using bespoke glycoliposomes. Oral Presentation, Polymers for Advanced Technologies, University of Manchester.

Table of Contents

List of Figures

List of Table

List of Schemes

Abbreviation list

°C	Degrees centigrade
Abs	Absorbance
Con A	Concanavalin A
CRP	Controlled radical polymerisation techniques
CTA	Chain Transfer Agent
Đ	molar-mass dispersity (M_w/M_n)
Da	Dalton
DCM	Dichloromethane
DDS	Drug Delivery System
DLS	Dynamic light scattering
DMEM	Dulbecco's Modified Eagles Medium
DMF	*N,N*-Dimethylformamide
DMSO	Dimethylsulfoxide
DP	Degree of polymerisation
EDTA	Ethylenediaminetetraacetic acid
EE	Encapsulation efficiency
EPR	Enhanced permeation and retention
ESI-TOF	Electrospray ionization - Time-of-Flight
FBS	Fetal Bovine Serum
GPC	Gel permeation chromatography
HBSS	Hank's balanced salt solution
HMDS	hexamethyldisilane
I	Initiator
LB broth	Luria-Bertani broth
MALDI-TOF	Matrix-assisted laser desorption/ionization - Time-of-Flight
M_n	Number average molecular weight
MR	Mannose Receptor
M_w	Weight average molecular weight
NMR	Nuclear Magnetic Resonance
PBS	Phosphate buffered saline

PEG	Polyethylene glycol
RAFT	Reversible addition–fragmentation chain transfer
RES	Reticuloendothelial system
TEG	Tetraethylene glycol
SCV	Salmonella containing vacuole
SEC	Size exclusion chromatography

CHAPTER 1

Glycocode for intracellular delivery

1.1 Glycocode

Glycosylation is a feature encountered in all living organisms (Ito 1974), (Costerton and Irvin 1981). All prokaryotic and eukaryotic cells and viruses present a complex layer of glycans on their membrane surface termed glycocalyx (Varki *et al.* 2009). Glycolipids and glycoproteins contribute to the formation of this carbohydrate coating, with 70% of known eukaryotic proteins being glycosylated (Apweiler *et al.* 1999). Once considered a simple physical barrier (Bennett 1963), the glycocalyx actually represents a sophisticated coding system, essential to allow cells to communicate (Yarema and Bertozzi 2001). To decipher sugar-encoded biological language, cell membranes display carbohydrate-binding proteins, known collectively as lectins, which are able to selectively recognise specific sugar ligands (Maupin *et al.* 2012). The interactions between glycans and lectins mediate a plethora of biological events, including fertilisation (Florman and Wassarman 1985), (Pang *et al.* 2011), (Raj *et al.* 2017), implantation (Feng *et al.* 2017), cell adhesion (Varki 1993), cell communication (Scheiffele *et al.* 1995), and even cell death (Hernandez and Baum 2002). Glycan-lectin interactions also play a key role in the control of innate and adaptive immune responses (van Kooyk and Rabinovich 2008), host-pathogen recognition (Cambi and Figdor 2005), (Sequeira 1978) and pathogen invasion (Kwon *et al.* 2002). Furthermore,

carbohydrates also have a role during inflammation for leucocyte extravasation (Lowe 2003) and in specific pathological conditions - *e.g.* membrane sugar patterns of cancer cells are altered compared to healthy cells (Hakomori 1985), (Zhao *et al.* 2008).

The human glycans are built primarily from only 9 monosaccharides (Schnaar 2016). However, carbohydrate-oligomers meet all the structural requirements to organise such a minimal system for performing all the aforementioned functions (Gabius *et al.* 2004). Unlike proteins and nucleic acids, carbohydrates are capable of forming many different combinatorial structures, and this is because each monomeric unit presents multiple functional groups (most commonly hydroxyl groups) (Schnaar 2016), (Lee and Lee 1995). When aminoacids combine together to form proteins, or nucleotides for nucleic acids, each individual unit can only combine in linear sequences to one other using a single type of intersubunit bond. Monosaccharides bind to one another in 2 possible configurations (α or β) at any of the 3-4 hydroxyl groups on each monomer in linear or branched groupings. This means that while 3 different aminoacids (or nucleotides) can generate 6 distinct structures, 3 different sugars can combine to make more than 1000 distinct structures (Schnaar 2016). As the possibilities increase exponentially, one calculation of possible distinct hexasaccharides estimated the number at 10^{12} (Laine 1994). However, many theoretical combinations may not be synthesised by the mammalian glycosylation machinery due to lack of some of the required enzymes, and it has been calculated that there are possibly ~7000 glycan determinants in the human glycome (Cummings 2009).

1.1.1 Cluster Glycoside Effect

Although the wide range of biological functions mediate by glycan-lectin (coding-decoding) system, surprisingly monosaccharide-lectin interactions are relatively weak. The affinity of binding (K_a) is typically in the millimolar range (10^3-10^6 M^{-1}) (Lis and Sharon 1998). The driving force of these interactions is a favourable enthalpy offset by the multiple contact points (hydrogen bonds, van der Waals' interactions and hydrophobic stacking) between the carbohydrate and the protein. However, this favourable enthalpy is counteracted by an entropy reduction as each carbohydrate unit loses flexibility upon binding the receptor (Holgersson *et al.* 2005). Enthalpy–entropy compensations are a characteristic of weak chemical interactions and are especially common in interactions involving water molecules (Dunitz 1995). Indeed the hydrophilic surfaces of both proteins and carbohydrates are engaged in hydrogen bonds with water molecules. Accordingly, dehydration of the ligand and the receptor followed by rehydration of the formed complex between the two contributes to the overall binding affinity with enthalpy/entropy gains and penalties that seem to be individual for each ligand/receptor involved (Swaminathan *et al.* 1998), (Holgersson *et al.* 2005). In Nature, this low affinity is compensated by the architecture of the lectin itself, containing typically two or more carbohydrate binding sites, and by the host presenting the oligosaccharide ligands multivalently or as clusters on the cell surface (Mammen *et al.* 1998). Indeed multivalency is a hallmark of many protein–carbohydrate interactions (Figure 1). Multivalent interactions occur when multiple copies of ligands on a surface or macromolecule simultaneously bind multicentre receptors or groups of receptors.

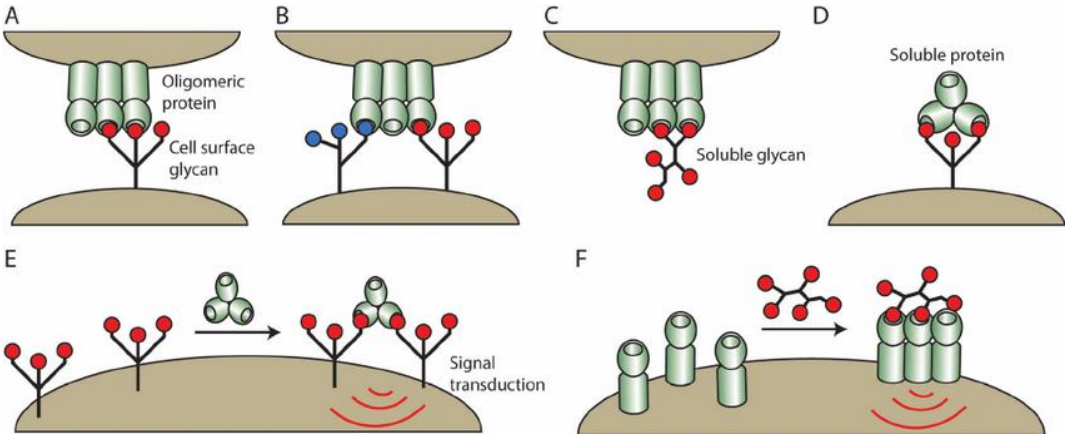

Figure 1 – Schematic representation of carbohydrate-binding proteins-glycans possible interaction mechanisms. (A) An oligomeric protein interacts with an individual cell-surface glycan. (B) An oligomeric protein interacts with multiple different cell-surface glycans simultaneously. (C) Oligomeric proteins interact with soluble glycans. (D) Soluble oligomeric lectins interact with cell surface glycans. (E) Soluble proteins cluster cell-surface glycoproteins to mediate signal transduction. (F) Soluble glycans cluster cell-surface receptors to mediate signal transduction (Kiessling and Grim 2013).

The overall magnitude of these interactions (avidity) is typically stronger than the sum of the corresponding individual interactions (Mammen *et al.* 1998). For lectin-carbohydrate recognition this phenomenon is known as cluster glycoside effect (Lundquist and Toone 2002).

After the first ligand-receptor interaction takes place between two bivalent species, the subsequent intramolecular interactions occur with less translational and rotational entropic cost (Reynolds and Pérez 2011). In addition, the entropy cost is usually smaller than monovalent interactions as restriction of carbohydrate flexibility has already been imposed beforehand partly by backbone carrier (Mammen *et al.* 1998). Therefore the bivalent interactions would occur with a greater change in free energy compared to that generated from two separate monovalent interactions (Mammen *et al.* 1998).

The summation of multiple high affinity interactions would render binding irreversible, while low affinity multivalent interactions are kinetically labile. Therefore they provide

the means to capture a cell of interest while still allowing for reversibility if the wrong cell type binds initially (Kiessling and Grim 2013).

1.1.2 Lectins

Carbohydrate-binding proteins were named lectins from the Latin *legere,* meaning to select, for their remarkable specificity in binding sugars (Boyd and Shapleigh 1954), (Goldstein *et al.* 1980). Lectins were originally found in extracts of plants at the end of 19th century, these proteins showed the ability to agglutinate erythrocytes (Sharon and Lis 2004). Since then, lectins have been the subject of extensive research (Elgavish and Shaanan 1997), (Lis and Sharon 1991) and they have been identified in most living organisms, ranging from viruses and bacteria to animals (Taylor and Drickamer 2014), (Ambrosi *et al.* 2005). In humans, there are about a dozen different structural families with more than 80 lectins (Schnaar 2016). Despite the enormous diversity of lectins, the sugar-binding activity can be ascribed to a limited portion of most lectin molecules, typically a globular carbohydrate-recognition domain (CRD) of less than 200 amino acids (Weis and Drickamer 1996). At present, there are no single universally accepted classifications of lectins (Varki *et al.* 2009). Drickamer identified two main groups of lectins; one group which require calcium for recognition, which are therefore called C-type lectins; and the other group which require free thiols for stability and the members are termed S-type lectins (later renamed the galectins, as not all of them were thiol-dependent, but generally bind β-galactosides) (Drickamer 1995). Lectins can also be grouped according to their localisation, *i.e.* intracellular or extracellular. Intracellular lectins are located in luminal compartments and are involved in the trafficking, sorting and targeting of glycoproteins to the endosomal compartments or other secretory

pathways. Extracellular lectins are either secreted into extracellular matrix or body fluids, or localised to plasma membrane, and mediate a range of functions including cell adhesion, cell signalling, glycoprotein clearance and pathogen recognition (Varki *et al.* 2009).

1.2 From glycocode to glycocoded liposomes

This multitude of biological functions mediated by carbohydrate-lectin interactions makes endogenous lectins an attractive target for drug delivery (Yamazaki *et al.* 2000). Drug Delivery Systems (DDS) are routinely developed and clinically utilised to overcome limitations of new and existing drugs, such as poor water solubility, low permeability, unsatisfactory bioavailability, non-specific targeting, high toxicity and side effects (Pelaz *et al.* 2017). Current drug nanocarriers are often classified according to the material used to assemble them - *e.g.* polymers, lipids, virus, organometallic compounds - and methods of preparation (Figure 2) (Mishra *et al.* 2010), (Rawat *et al.* 2006).

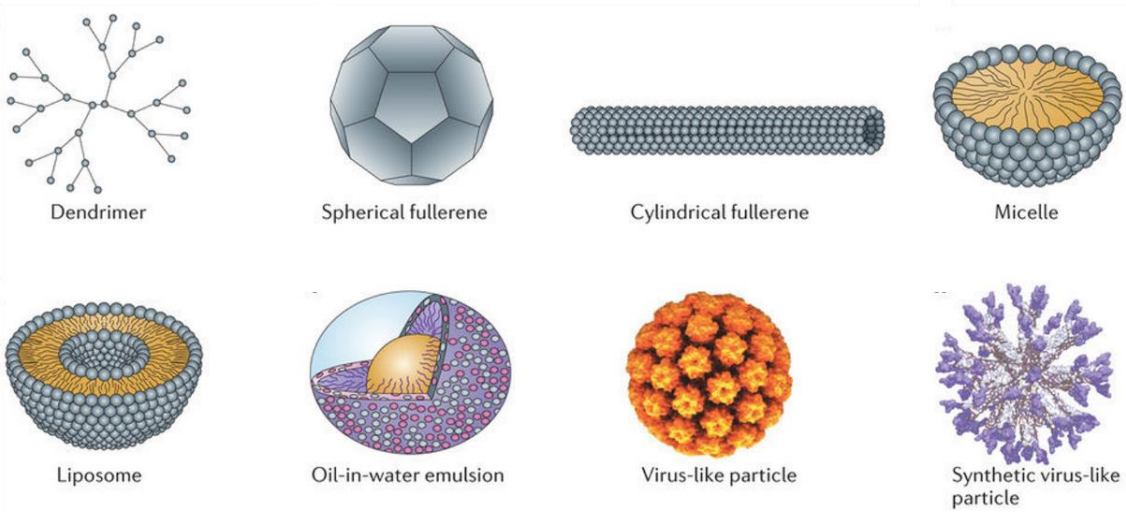

Figure 2 – Examples of nanoparticles commonly used as drug delivery carriers (Smith, Simon, and Baker 2013).

Many ligand-modified drug carriers have been investigated for active cell-selective drug delivery by receptor-mediated endocytosis (Sheikhpour *et al.* 2017). Similarly, a broad range of ligands have been explored for targeted drug delivery systems, including antibodies, peptides, small molecules and carbohydrates (Nicolas *et al.* 2013).

Antibodies have been the first class of tumour targeting ligands used to deliver drugs encapsulated in micelles (Kabanov *et al.* 1989). They represent one of the most efficient class of ligands due to their high affinities and specificity of binding their target (Muro 2012). However, the hydrodynamic radius of an antibody is in the range of 15-20 nm, which can impede the effective conjugation with a drug carrier and significantly increase the diameter of the targeted delivery system. Moreover, the high cost/efficiency ratio of the preparation restricts their applications (Bertrand *et al.* 2014). Small molecules, such as folic acid (vitamin B_9), and biotin (vitamin B_7) have been widely used for targeting cancer cells (Byrne *et al.* 2008) for their very high affinity for folate and biotin receptors, respectively, which are frequently overexpressed on the tumor cell surface (Chen *et al.* 2010). Peptides represent another promising class of targeting ligands. The tripeptide Arginine-Glycine-Aspartic acid (RGD) is a cell recognition and attachment site for a number of extracellular matrix proteins as well as blood and cell surface proteins, and appears extremely attractive as tumor and vascular targeting ligand (Danhier, Breton, and Préat 2012). Indeed, RGD-based nanoparticles have shown the ability to bind to the $\alpha_v\beta_3$ integrin receptor, which is highly expressed at the surface of malignant cells (Desgrosellier and Cheresh 2010). Although these classes of ligands are some of the most promising strategies for targeted nanocarriers, their main downside comes from their relatively non-selective interactions with non-target tissues (Allen 2002).

In addition to the aforementioned classes of targeting agents, carbohydrate ligands constitute a powerful tool for targeted drug delivery. Glycotargeting exploits the highly specific interactions of endogenous lectins with carbohydrates, in some cases this specificity of binding can be higher than in many other ligand-binding systems; such is

the enormous density of information that sugars can convey (Davis and Robinson 2002). Moreover, glycosylation of drug carrier is an other promising route to provide different beneficial properties in the field of drug delivery, including stability and stealth characteristics (Jain *et al.* 2012).

Therefore the use of carbohydrate-ligands is an attractive strategy to selectively (or preferentially) deliver therapeutic agents to target sites, simultaneously reducing potential off-target effects (Jain *et al.* 2012), (Allen 2002).

Some examples of glycosylated carriers and their potential applications in pharmaceutical field are reported in Table 1.

Table 1 - Summary of therapeutic applications of glycosylated carriers (Jain *et al.* 2012).

Therapeutic application	Ligand	Carrier	Active ingredient	References
Enhanced cellular uptake	Galactose	Liposomes	Azidothymidine	(Garg *et al.* 2007)
	Mannose	Dendrimers	Efavirenz	(Dutta *et al.* 2007)
Delivery of anticancer agent	Galactose	Nanoparticles	Paclitaxel	(Jeong *et al.* 2005)
Selective delivery to liver cells	Galactose	Microcapsules	Aciclovir	(F. Zhang *et al.* 2008)
	Galactose	Liposomes	Doxorubicin	(Wang *et al.* 2010)
Targeted delivery to alveolar macrophage	Mannose	Dendrimers	Rifampicin	(Kumar *et al.* 2006)
	Mannose	Liposomes	-	(Chono *et al.* 2010)
Gene transfection	Mannose	Cationic Liposomes	Plasmid DNA (luciferase gene)	(S Kawakami *et al.* 2000)
Reduction in toxicity of drug and carrier	Galactose	Nanoparticles	DNA	(X. Q. Zhang *et al.* 2005)
	Galactose	Dendrimers	Chloroquine phosphate	(Agrawal *et al.* 2007)
	Galactose	Liposomes	Azidothymidine	(Garg *et al.* 2007)
	Mannose	Dendrimers	Efavirenz	(Dutta *et al.* 2007)

Different drug delivery systems have been investigated: dendrimers, polymer conjugate, liposomes and nanoparticles (Shigeru *et al.* 2014), (Jain *et al.* 2012). For the aim of this work, particular emphasis will be given to the use of liposomes as drug delivery systems.

1.2.1 Liposomes

Among all drug delivery systems, liposome-based formulations are arguably one of the most widespread, with many available on the market and several currently at different stages of clinical trials (Bulbake *et al.* 2017), (Chang and Yeh 2012), (Lian and Ho 2001). In general, liposomes are biocompatible, biodegradable and non-immunogenic, which are key prerequisites for a successful drug carrier (Allen 1997).

Liposomes are self-assembled phospholipid vesicles with spherical shape. Due to the amphiphilic nature of the molecules forming their lipid bilayers, they can home hydrophobic drugs within the lipophilic layers of their membrane, whilst hydrophilic drugs can be encapsulated in their aqueous lumen (Sharma and Sharma 1997). Liposomes are often classified according to their size – from 20-30 nanometres to several micrometres - and number of bilayers (uni- and multi-lamellar) (Figure 3) (Immordino *et al.* 2006).

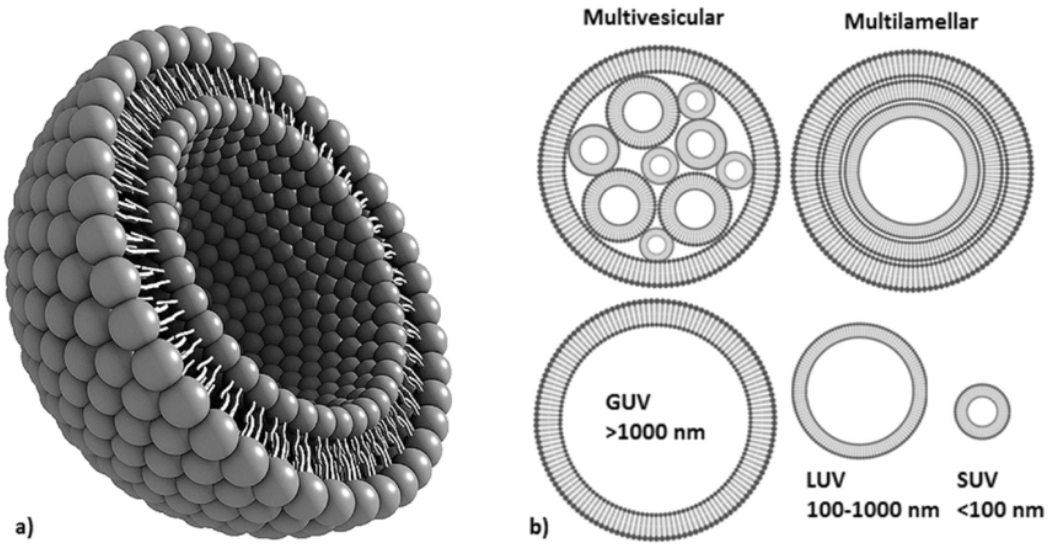

Figure 3 - Schematic representation of (a) 3D-unilamellar liposome. (b) various forms of lamellar and sizes; small unilamellar vesicles (SUVs), large unilamellar vesicles (LUVs), giant unilamellar vesicles (GUVs), multilamella and multivesicular (Brako *et al.* 2017).

In general, the size of nanoparticles can directly affect the efficiency of drug delivery. In anticancer therapy, liposomes with an average diameter of 50-100 nm are able to penetrate tumour tissues passing through fenestrated tumour blood vessels whilst being still small enough to avoid capture by macrophages located in the reticuloendothelial system (RES) in the liver or in the spleen (Perche and Torchilin 2013), (Moghimi *et al.* 2001).

Therefore, liposomes can allow for passive targeting, where their accumulation at the intended site of action is only dependent on physiology and anatomy of both healthy and disease tissues (Nam *et al.* 2013).

1.2.2 Engineered liposomes

Since their discovery by Bangham in 1965 (Bangham *et al.* 1965), increasingly sophisticated liposomes have been developed to control and optimise small drug, protein or gene delivery. First generation liposomes were assembled from natural phospholipids such as phosphatidylcholine and phosphatidylglycerol, with cholesterol entrapped within (Drummond *et al.* 1999). Although conceptually simple, these nanocarrier models provided solutions to many of the therapeutic challenges previously discussed - *i.e.* poor drug solubility, stability and side effects. However, the circulation half-life of these liposomes was often limited by rapid elimination by the RES (Immordino *et al.* 2006).

One successful strategy to overcome this delivery hurdle involves coating the outer surface of liposomes with hydrophilic polymers such as poly(ethylene glycol), PEG (Blume *et al.* 1993), (Klibanov *et al.* 1990), which protect the lipid vesicles from opsonisation by repelling plasma proteins (Torchilin and Papisov 1994) and improve

stability by shielding the liposome surface, avoiding colloidal aggregation (Bakowsky *et al.* 2008).

Further development of liposome technology led to the development of targeted lipid vesicles (Allen and Cullis 2013), (van der Meel *et al.* 2013). Active targeting, also known as "ligand-based targeting", requires the presence of ligands at the liposome surface which can be selectively recognised by specific receptors overexpressed by target cancer cells.

Ligands investigated include monoclonal antibodies (Weissmann *et al.* 1975), proteins (Kobayashi *et al.* 2007), peptides (Santos *et al.* 2010) and carbohydrates (Kawakami and Hashida 2014). Although active drug delivery systems are yet to reach the market, at present at least 5 targeted liposome formulations are undergoing clinical trials (Bertrand *et al.* 2014), with many more expected to follow.

1.2.3 Glycosylated liposomes

Several carbohydrate ligands - *e.g.* glucose, fucose, and lactose - have been utilised to engineer liposomes for active targeting of lectin receptors (Kawakami and Hashida 2014). In particular, several studies have investigated the ability of mannosylated liposomes to target Mannose Receptor-positive cells (Kelly *et al.* 2011), (Ahsan *et al.* 2002), (Kawakami *et al.* 2000), as well as other important Man-recognising lectins such as Mannan Binding Lectin (MBL), key for innate immunity, and plant lectins, *e.g.* Concanavalin A (Opanasopit *et al.* 2001) both *in vitro* and *in vivo.* Mannosylated liposomes represent therefore an ideal suitable platform to investigate liposome-cell membrane interactions.

1.2.3.1 A receptor model: concanavalin A

Concanavalin A (Con A) is a C-type lectin - a protein which requires Ca^{2+} ions to bind carbohydrate - widely used in biology and biochemistry as model lectin to bind glycoproteins and other sugar-containing entities on the surface of various cells (McMorran *et al.* 2017), (Toye *et al.* 2016), (Qin *et al.* 2014). Relevant to this present work, Con A has been often used to probe the binding properties of glycosylated liposomes (Sandoval-Altamirano *et al.* 2017), (Mauceri *et al.* 2015), (Mauceri *et al.* 2014). Con A binds selectively D-manno- and D-gluco-pyranoside residues, which, unlike other monosaccharide ligands such as D-galactose, possess an equatorial-equatorial trans configuration of hydroxyl groups at C3 and C4 of the pyranose ring, required for Con A recognition (Figure 4) (Williams *et al.* 1981).

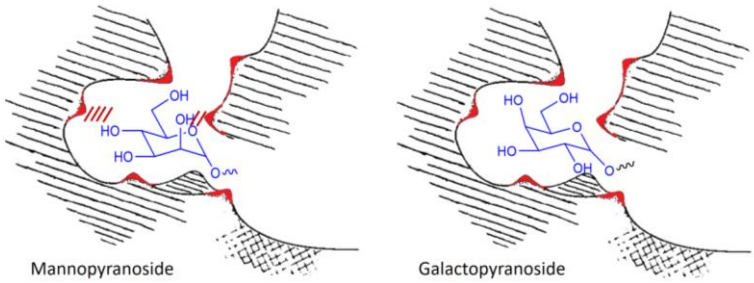

Figure 4 - Pictorial representation of mannopyranoside and galactopyranoside fitting into the carbohydrate binding pocket of Concanavalin A, binding sites highlighted in red. [adapted from (Williams *et al.* 1981)].

Con A has a pH-dependent structure, being tetrameric at pH 7 and mostly dimeric at more acidic conditions. For carbohydrate binding, Ca^{2+} and Mn^{2+} ions are required in each domain (Dimick *et al.* 1999). In its tetrameric form Con A is able to crosslink

liposomes presenting D-mannopyranosyl ligands. In binding studies, both quantification of crosslinked assemblies and rate of aggregation have been utilised to measure ligand accessibility and affinity for Con A model lectin (Goldstein *et al.* 1965).

1.2.4 Mimicking multivalency

As previously discussed, multivalency is a hallmark in carbohydrate-lectin interactions. Liposomal systems can mimic this property by displaying multiple copies of ligands on the membrane surface. Chemical synthesis provides access to designed compounds that can be used to explore the role of molecular interactions. The structural architecture of the ligand can vary from monovalent ligand (where the multivalent effect can be achieved by spatial proximity of contiguous individual sugar ligands on the liposomal surface) to multivalent ligand (cluster of ligands grouped in macromolecular structures). Recent advances in polymer chemistry have made possible the synthesis of glycopolymers with well-defined architecture (Kiessling and Grim 2013).

1.2.4.1 Controlled radical polymerisations

Materials design is a subtle balance between simplicity and complexity (Lutz *et al.* 2016). For the synthesis of polymeric ligands, recent development in the field of polymer chemistry allowed for the synthesis of well-defined macromolecules with controlled composition, chain ends, chain lengths, molecular-weight distribution and topology (Matyjaszewski 2011). Since the early days of polymer science (Carothers 1931), synthetic polymers are prepared using two main mechanisms: step-growth and chain-growth polymerisations (Figure 5).

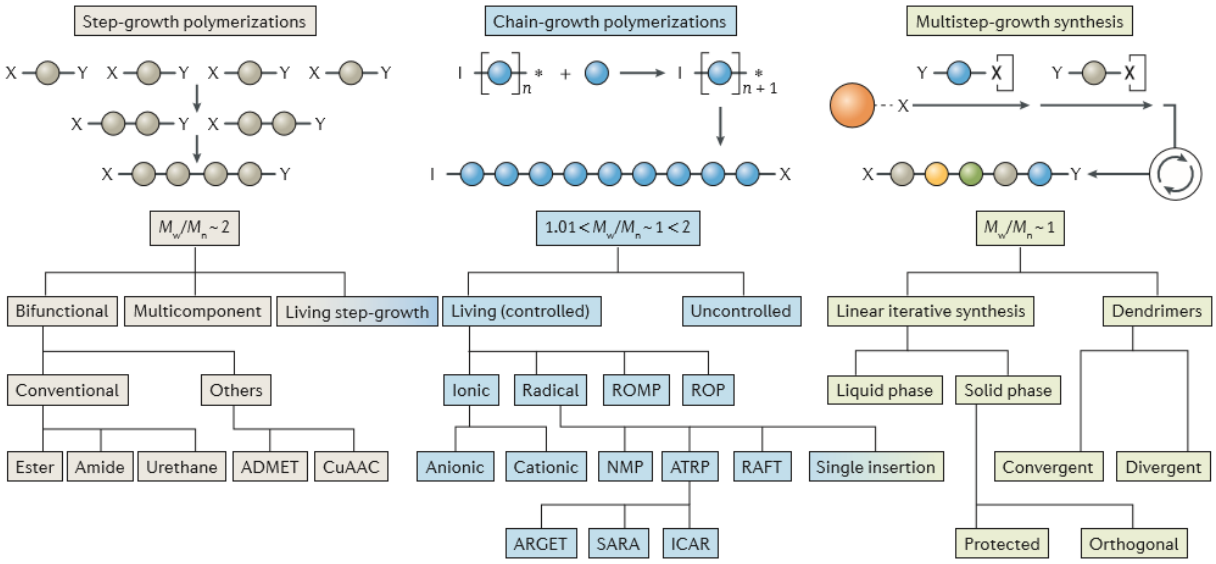

Figure 5 - Classification of the main approaches for polymer synthesis (Lutz *et al.* 2016). Abbreviations: ADMET (Acyclic diene metathesis), ARGET (activators regenerated by electron transfer), ATRP (atom transfer radical polymerisation), CuAAC (copper(I)-catalysed azide alkyne cycloaddition), ICAR (Initiators for continuous activator regeneration), NMP (nitroxide-mediated radical polymerisation), RAFT (reversible addition-fragmentation chain transfer), ROMP (ring-opening metathesis polymerisation), ROP (ring-opening polymerisation), SARA (supplemental activator and reducing agent).

Briefly, a step-growth polymerisation proceeds by individual reactions of difunctional monomers and the molecular weight of the polymer chain builds up slowly (Stille 1981). Conversely, in a chain polymerisation each polymer chain grows rapidly, producing a high molecular weight polymer and the process starts by a free radical initiator or a cationic/anionic catalyst. Moreover initiation, propagation and termination steps are distinct events of the polymerisation process (McGrath 1981). However, through these two conventional mechanisms, polymers are often generated with high polydispersity. To overcome this limitation, various refined and optimised polymerisation approaches have been developed. These advances began during the 1950s with the discovery of living polymers through living anionic chain-growth polymerisations (Szwarc 1956). A living polymerisation is a chain polymerisation in which a chain could only propagate and not undergo chain transfer or irreversible termination (Szwarc 1956). A further improvement of living polymerisation came with the development of controlled radical polymerisation techniques (CRP), so defined because allowed control over the polymer architecture, which includes molecular weight, molecular weight distribution (polydispersity), functionality, and composition. A number of CRP methods have been developed and the three most promising are:

i. stable free radical polymerisation (SFRP), most commonly nitroxide mediated polymerisation (NMP);
ii. transition-metal-catalysed atom transfer radical polymerisation (ATRP);
iii. reversible addition- fragmentation chain transfer polymerisation (RAFT).

In order to extend the lifetime of the propagating chains, each of these methods relies on establishing a dynamic equilibrium between a low concentration of active

propagating chains and a predominant amount of dormant chains that are unable to propagate or terminate (Matyjaszewski and Spanswick 2005).

CRPs allow the synthesis of well-defined macromolecules with controlled chain lengths and a narrow molecular weight distribution, and also provide fine control of molecular parameters, such as chain composition (Lutz *et al.* 2016), (Lutz *et al.* 2013).

Similarly, the aforementioned techniques have enabled the synthesis of glycopolymers featuring a wide range of controlled architectures and functionalities (Vázquez-Dorbatt *et al.* 2012), (Ladmiral *et al.* 2004).

Among the living radical polymerisation techniques, reversible addition–fragmentation chain transfer (RAFT), appears one of the most convenient and versatile (Perrier and Takolpuckdee 2005). RAFT polymerisation does not require a transition metal and tolerates a wide range of functional groups, temperatures, and solvents (Moad *et al.* 2005). Since the first report in 1998 by Rizzardo and co-workers (Chiefari *et al.* 1998), further significant achievements over the past few years have greatly expanded the versatility of the approach for both the synthesis of new materials and the preparation of previously accessible materials in a more efficient, faster, or convenient manner (Hill *et al.* 2015). In this work, we exploited a newly developed *ultrafast* version of RAFT radical polymerisation technique (Gody *et al.* 2015) which allows the synthesis of well-defined polymers within minutes (discuss in Chapter 2.4.3).

1.3 Salmonella infection

Salmonella is a Gram-negative bacterium of the *Enterobacteriaceae* family (Blaser and Newman 1982). *Salmonella* is divided into two species: *Salmonella bongori* and *Salmonella enterica* (de Jong *et al.* 2012). *S. bongori* is considered a bacterium of cold-blooded animals and is most frequently associated with reptiles (Garai *et al.* 2012). *Salmonella enterica* is further divided into six subspecies with over 2,500 serotypes (Figure 6) (Jacobsen *et al.* 2011). A number of these serovars are serious human pathogens (Ibarra and Steele-mortimer 2009).

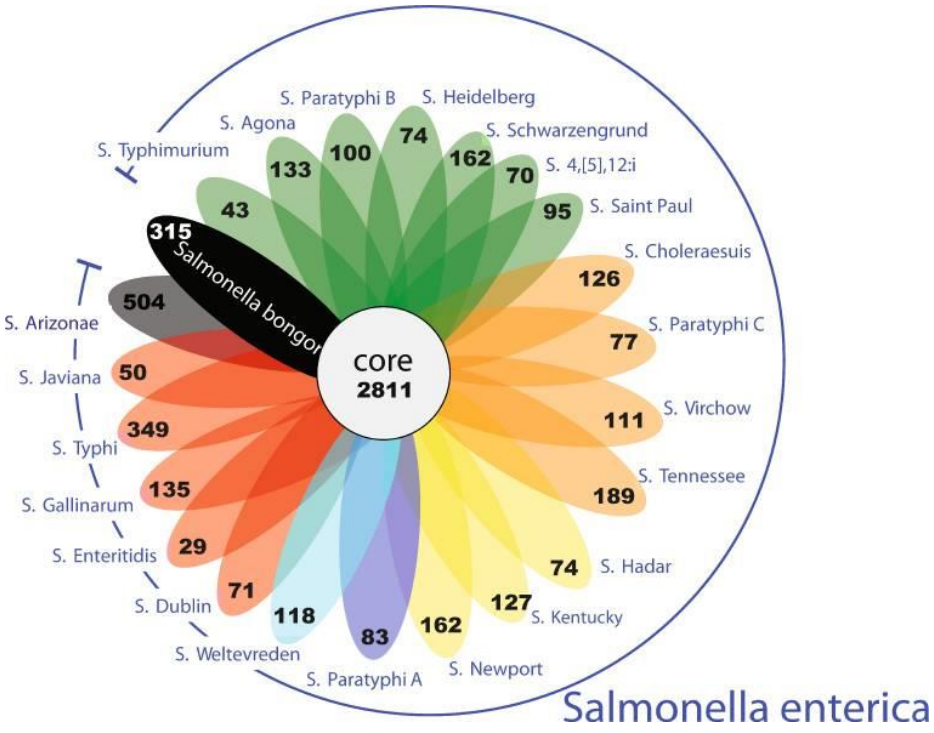

Figure 6 - Flowerplot of unique gene families in each *Salmonella* serovar. The figure presents the average number of gene families found in each genome as being unique to the serovar. Also given is the size of the core genome. The colour of the petals represents the different *S. enterica* serogroups (Jacobsen *et al.* 2011).

1.3.1 Salmonella invasion mechanism

In general, *Salmonella enterica* infections are acquired through the oral route, after ingestion of food or beverages contaminated with bacteria (Figure 7). Although the gastric pH helps to reduce the infectious dose of the bacterium, salmonella have an adaptive acid-tolerance response and can survive the passage through the stomach environment (Lawrence 1998). After reaching the gut lumen, salmonella can cross the apical side of the epithelial barrier either by passive mechanisms facilitated by dendritic cells or by active invasion of the cells in the ileal portion of the small intestine. This latter invasion strategy requires the delivery of distinct effector proteins injected directly into host cells (*Salmonella* pathogenicity island-1) (Velge *et al.* 2012). In the subepithelial location, *Salmonella* spp. are taken-up by phagocytic cells such as macrophages that transport the bacteria into the lymphatic system and disseminate the infection systematically (mainly liver, spleen and lymph nodes) (Mastroeni *et al.* 2009).

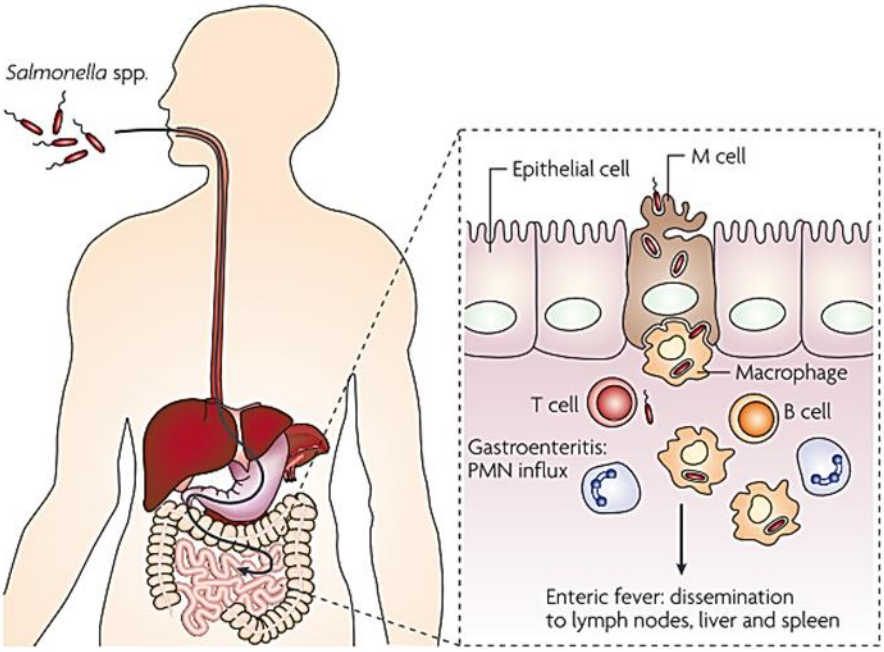

Figure 7 – *Salmonella* infection scheme (Haraga *et al.* 2008).

1.3.2 Same species, different diseases

Salmonella enterica subspecies *enterica* serovar Typhimurium and Typhi are the subspecies responsible for most salmonella infections in humans (Darwin and Miller 1999). Although sharing more than 96% of genes (McClelland *et al.* 2001), *S*. Typhimurium and *S*. Typhi elicit very different diseases and distinct immune responses in humans. *S*. Typhi is responsible for inducing enteric fever, a potentially fatal multisystemic illness, which differs dramatically from the gastroenteritis associated with *S*. Typhimurium. Normally *S*. Typhimurium infections in humans induce localised gastroenteritis and just 5% of cases evolve in extraintestinal disease leading to bacteraemia and systemic infection, or sepsis (Gal-Mor *et al.* 2014). *S*. Typhimurium is typically associated with acute diarrhea and with a strong influx of neutrophils into the intestinal lumen during the invasion process. On the contrary, S. Typhi does not induce inflammatory responses during the initial invasion of the intestinal mucosa, indeed it is not associated with diarrheal symptoms. The lack of intestinal inflammation allows *S*. Typhi to invade the deeper tissues of the gut and disseminate to systemic sites (Garai *et al.* 2012).

1.3.3 Intracellular survival of Salmonella

Salmonella enterica is a facultative intracellular pathogen and, after crossing the epithelial barrier, the bacteria can enter intestinal macrophage cells by inducing macropinocytosis (Alpuche-Aranda *et al.* 1994). Within the intracellular environment salmonella are contained in salmonella containing vacuole (SCV), which allows bacterial survival and replication (Haraga *et al.* 2008). The interaction of *Salmonella* with macrophages is a complex process (Gog *et al.* 2012). *Salmonella* has developed a variety of mechanisms to evade and survive intra-phagosomal killing and establish a replicative intracellular niche

within macrophages (Steele-Mortimer 2008). Some studies have demonstrated that *Salmonella* can inhibit phagolysosomal fusion (Ribet and Cossart 2015), other researchers have shown that the SCV fuses with lysosomes but *Salmonella* can survive this process (Haraga *et al.* 2008), (Knodler and Steele-Mortimer 2003), whereas others showed that infected host cells simply do not have a sufficient quantity of lysosomes to target SCV (Eswarappa *et al.* 2010). After replication, *Salmonella* can induce macrophage death and escape from the intracellular environment, enabling further systemic dissemination of the bacteria via the blood- stream (Mastroeni *et al.* 2009).

1.3.4 Salmonella infection treatments

Typhoid fever is a global health problem. Since 1972, strains of *S*. Typhi from many parts of the world have developed multidrug-resistance (MDR) against ampicillin, chloramphenicol, sulfonamide, trimethoprim, streptomycin and tetracycline (WHO 2003). At the moment, fluoroquinolones are the treatment of choice for typhoid fever in adults. Fluoroquinolones attain excellent tissue penetration and therefore these antibiotics can reach the intracellular infection site (WHO 2003). Aminoglycosides are a different class of antibiotic active against this infection, but due to their high hydrophilicity, cell membranes are poorly permeative to these molecules (Lo *et al.* 2014). Importantly in the context of this thesis, it is this class of antibiotics which would benefit most from the development of targeted liposomal system for intracellular delivery to infected macrophage cells (Abed and Couvreur 2014), (Huh and Kwon 2011).

1.4 Targeting (infected) macrophages

Macrophages are migratory cells deriving from bone marrow precursors and are found in most tissues of the body. Together with other mononuclear phagocytic cells, such as monocytes and dendritic cells, macrophages constitute an important front line of host defence involved in innate immunity, and, through their role as antigen-presenting cells, key effector cells in adaptive immunity (Janeway *et al.* 2001).

However as previously described, some pathogens like salmonella are able to survive inside macrophage cells (Haraga *et al.* 2008). Therefore infected macrophages are an important target for drug delivery to treat intracellular infections (Ranjan *et al.* 2012). Although parenterally administered liposomes are naturally cleared by macrophage cells (Kelly *et al.*2011), controlling of the physicochemical properties of liposome and ligand-functionalisation can enhance uptake by target cells. Mannosylated liposomes (as discussed in section 1.2.3) appear a promising strategy for targeting the MR in macrophage cells. However, it should be noted that there are a wide variety of lectins with mannose affinity including MR, Dendritic Cell-Specific Intercellular adhesion molecule-3-Grabbing Non-integrin (DC-SIGN) and Endo 180 (Irache *et al.* 2008), and this poses serious risks of getting off-site effects *in vivo*. Thus delivery strategies must be optimised on a case-by-case basis, to minimise potential side effects.

1.4.1 Targeted receptor: CD206

Receptor CD206, also known as Mannose Receptor (MR), is a transmembrane C-type lectin receptor (Figure 8) expressed by selected populations of macrophages and dendritic cells (DCs) and nonvascular endothelium (Martinez-Pomares 2012). MR is a highly effective endocytic receptor that recycles constantly between the plasma

membrane and the early endosomal compartment (Gazi and Martinez-Pomares 2009). It contains three types of domains at its extracellular region, an *N*-terminal cysteine-rich (CR) domain capable of Ca^{2+}-independent binding to sulfated sugars terminated in SO_4-3-Gal or SO_4-3/4-GalNAc (P. R. Taylor, Gordon, and Martinez-Pomares 2005), a fibronectin type II (FN II) domain involved in collagen binding (Martinez-Pomares 2012) and eight tandemly arranged C-type lectin-like carbohydrate recognition domains (CTLD) responsible for Ca^{2+}-dependent binding to sugars terminated in D-mannose, L-fucose or N-acetyl glucosamine (P. R. Taylor, Gordon, and Martinez-Pomares 2005).

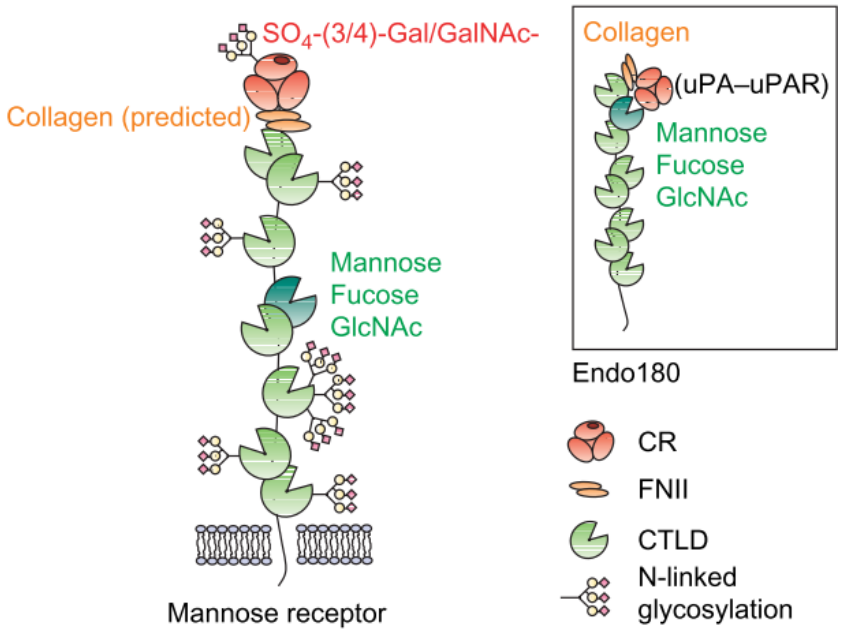

Figure 8 Schematic structure of the mannose receptor (MR) (P. R. Taylor, Gordon, and Martinez-Pomares 2005). Abbreviations: CR (cysteine-rich domain), CTLD (C-type lectin-like carbohydrate recognition domain), FNII (fibronectin type two repeats domain), uPA–uPAR (urokinase plasminogen activator–uPA receptor complex).

1.5 Project aims

This project aims to investigate how the glycan structural features, comparing monovalent glycoligands and multivalent polyglycosides, affect the interactions between glycotargeted liposomes and specific cells. To identify the key structural parameters for efficient delivery of therapeutic payloads to selected target cells, a range of liposomes with 100-170 nm diameter and with variable lipid composition and carbohydrate ligands have been engineered and screened.

To investigate how both the chemical nature of individual sugar binding units and their spatial distribution affects binding and selectivity towards lectin receptors, different liposome glycosylated ligands have been synthesised. Initially relatively simple monosaccharide ligands have been utilised (galactose- , mannose-), whilst more complex ligands (gycopolymers) have been evaluated at a later stage.

The targeted liposomes have been assembled using the Bangham method (thin-film hydration method) and characterised in terms of size and ability to target isolated model lectins. Lectins, such as Concavanalin A, are often used as model systems for initial screenings of protein-carbohydrate interactions (Cairo *et al.* 2002), (Del Carmen Luzardo *et al.* 2002). Cell uptake studies have been carried out, utilising fluorescent probes.

Lectin carbohydrate-binding protein Con A was initially utilised as model mannose-binding lectin. A potential application of the developed systems was the delivery of antimicrobials for intracellular infection (*e.g.* salmonella intracellular infection). Biological responses *in vitro* have been evaluated to better understand the relationship liposome structure-cell uptake.

The above aim will be achieved through the delivery of the following objectives:

1. Design and synthesis of membrane-inserting glycoligands with variable molecular topology (Chapter 2). These glycoligands will be able to fit into liposomal membranes and therefore the liposome surface will be functionalised with different glycosylation patterns by using monovalent glycoligands or multivalent polyglycosides.

2. Engineering of libraries of liposome nanovectors where both chemistry and density of the membrane recognition elements will be systematically varied (Chapter 3). An initial screening will explore how densities of different carbohydrate residues (mannose and galactose), the spatial distribution of these glycoligands (monovalent and multivalent glycoligands) and the lipidic composition of the liposomal membrane affect the rate of lectin clustering.

3. Incorporation and *in vitro* delivery of low molecular weight drugs (*e.g.* gentamicin) to intracellulary infected cells (Chapter 4). This part of the work will investigate the Mannose Receptor dependent internalisation and antibiotics delivery efficacy of the different glycosylated liposome systems.

1.6 References

Abed, Nadia, and Patrick Couvreur. 2014. "Nanocarriers for Antibiotics: A Promising Solution to Treat Intracellular Bacterial Infections." *International Journal of Antimicrobial Agents* 43 (6). Elsevier B.V.: 485–96.

Agrawal, Payal, Umesh Gupta, and N. K. Jain. 2007. "Glycoconjugated Peptide Dendrimers-Based Nanoparticulate System for the Delivery of Chloroquine Phosphate." *Biomaterials* 28 (22): 3349–59.

Ahsan, Fakhrul, Isabel P. Rivas, Mansoor a. Khan, and Ana I. Torres Suárez. 2002. "Targeting to Macrophages: Role of Physicochemical Properties of Particulate Carriers - Liposomes and Microspheres - On the Phagocytosis by Macrophages." *Journal of Controlled Release* 79 (1–3): 29–40.

Allen, Theresa M. 1997. "Liposomes." *Drugs* 54 (Supplement 4): 8–14.

Allen, Theresa M. 2002. "Ligand-Targeted Therapeutics in Anticancer Therapy." *Nature Reviews Cancer* 2 (10): 750–63.

Allen, Theresa M., and Pieter R. Cullis. 2013. "Liposomal Drug Delivery Systems: From Concept to Clinical Applications." *Advanced Drug Delivery Reviews* 65 (1). Elsevier B.V.: 36–48. 7.

Alpuche-Aranda, Celia M, L Racoosin, Esther, Joel A Swanson, and Samuel I Miller. 1994. "Salmonella Stimulate Macrophage Macropinocytosis and Persist within Spacious Phagosomes." *The Journal of Experimental Medicine:* 179: 601–8.

Ambrosi, Moira, Neil R Cameron, and Benjamin G Davis. 2005. "Lectins: Tools for the Molecular Understanding of the Glycocode." *Organic & Biomolecular Chemistry* 3: 1593–1608.

Apweiler, Rolf, Henning Hermjakob, and Nathan Sharon. 1999. "On the Frequency of Protein Glycosylation, as Deduced from Analysis of the SWISS-PROT Database." *Biochimica et Biophysica Acta - General Subjects* 1473 (1): 4–8.

Bakowsky, Heike, Thomas Richter, Carsten Kneuer, Dick Hoekstra, Ulrich Rothe, Gerd Bendas, Carsten Ehrhardt, and Udo Bakowsky. 2008. "Adhesion Characteristics and Stability Assessment of Lectin-Modified Liposomes for Site-

Specific Drug Delivery." *Biochimica et Biophysica Acta* 1778 (1): 242–49.

Bangham, A. D., M. M. Standish, and J. C. Watkins. 1965. "Diffusion of Univalent Ions across the Lamellae of Swollen Phospholipids." *Journal of Molecular Biology* 13 (1). Academic Press Inc. (London) Ltd.: IN26-IN27.

Bennett, Stanley H. 1963. "Morphological Aspects of Extracellular Polysaccharides." *J. Histochem. Cytochem.* 11 (1): 14–23.

Bertrand, Nicolas, Jun Wu, Xiaoyang Xu, Nazila Kamaly, and Omid C. Farokhzad. 2014. "Cancer Nanotechnology: The Impact of Passive and Active Targeting in the Era of Modern Cancer Biology." *Advanced Drug Delivery Reviews* 66. Elsevier B.V.: 2–25.

Blaser, Martin J., and Lee S. Newman. 1982. "A Review of Human Salmonellosis: I . Infective Dose." *Oxford Journals* 4 (6): 1096–1106.

Blume, G, G Cevc, M D Crommelin, I a Bakker-Woudenberg, C Kluft, and G Storm. 1993. "Specific Targeting with Poly(ethylene Glycol)-Modified Liposomes: Coupling of Homing Devices to the Ends of the Polymeric Chains Combines Effective Target Binding with Long Circulation Times." *Biochimica et Biophysica Acta* 1149 (1): 180–84.

Boyd, William C, and Elizabeth Shapleigh. 1954. "Specific Precipitating Activity of Plant Agglutinins (Lectins)." *Science* 119: 419.

Brako, Francis, Suntharavathanan Mahalingam, Bahijja Rami-Abraham, Duncan Q M Craig, and Mohan Edirisinghe. 2017. "Application of Nanotechnology for the Development of Microbicides." *Nanotechnology* 28 (5). IOP Publishing: 52001.

Bulbake, Upendra, Sindhu Doppalapudi, Nagavendra Kommineni, and Wahid Khan. 2017. "Liposomal Formulations in Clinical Use: An Updated Review." *Pharmaceutics* 9 (2): 1–33.

Byrne, James D., Tania Betancourt, and Lisa Brannon-Peppas. 2008. "Active Targeting Schemes for Nanoparticle Systems in Cancer Therapeutics." *Advanced Drug Delivery Reviews* 60 (15). Elsevier B.V.: 1615–26.

Cairo, Christopher W., Jason E. Gestwicki, Motomu Kanai, and Laura L. Kiessling.

2002. "Control of Multivalent Interactions by Binding Epitope Density." *Journal of the American Chemical Society* 124 (8): 1615–19.

Cambi, Alessandra, and Carl G. Figdor. 2005. "Levels of Complexity in Pathogen Recognition by C-Type Lectins." *Current Opinion in Immunology* 17 (4 SPEC. ISS.): 345–51.

Carothers, Wallace H. 1931. "Polymerization." *Chemical Reviews* 8 (3): 353–426.

Chang, Hsin I., and Ming Kung Yeh. 2012. "Clinical Development of Liposome-Based Drugs: Formulation, Characterization, and Therapeutic Efficacy." *International Journal of Nanomedicine* 7: 49–60.

Chen, Shuyi, Xianrui Zhao, Jingyi Chen, Jin Chen, Larisa Kuznetsova, Stanislaus S. Wong, and Iwao Ojima. 2010. "Mechanism-Based Tumor-Targeting Drug Delivery System. Validation of Efficient Vitamin Receptor-Mediated Endocytosis and Drug Release." *Bioconjug Chem.* 21 (5): 979–87.

Chiefari, John, Y K Bill Chong, Frances Ercole, Julia Krstina, Justine Jeffery, Tam P T Le, Roshan T A Mayadunne, *et al.* 1998. "Living Free-Radical Polymerization by Reversible Addition - Fragmentation Chain Transfer : The RAFT Process." *Macromilecules* 31: 5559–62.

Chono, Sumio, Keita Kaneko, Eri Yamamoto, Kohei Togami, and Kazuhiro Morimoto. 2010. "Effect of Surface-Mannose Modification on Aerosolized Liposomal Delivery to Alveolar Macrophages." *Drug Development and Industrial Pharmacy* 36 (361): 102–7.

Costerton, J W, and R T Irvin. 1981. "The bacterial glycocalyx in nature and disease." *Ann. Rev. Microbiol.*, no. 35: 299–324.

Cummings, Richard D. 2009. "The Repertoire of Glycan Determinants in the Human Glycome." *Molecular bBoSystems* 5 (10): 1087–1104.

Danhier, Fabienne, Aude Le Breton, and Véronique Préat. 2012. "RGD-Based Strategies to Target Alpha(v) beta(3) Integrin in Cancer Therapy and Diagnosis." *Molecular Pharmaceutics* 9 (11): 2961–73.

Darwin, K H, and V L Miller. 1999. "Molecular Basis of the Interaction of Salmonella

with the Intestinal Mucosa." *Clinical Microbiology Reviews* 12 (3): 405–28.

Davis, Benjamin G, and Mark A Robinson. 2002. "Drug Delivery Systems Based on Sugar-Macromolecule Conjugates." *Current Opinion in Drug Discovery and Development* 5 (2): 279–88.

de Jong, Hanna K., Chris M. Parry, Tom van der Poll, and W. Joost Wiersinga. 2012. "Host-Pathogen Interaction in Invasive Salmonellosis." *PLoS Pathogens* 8 (10): 1–10.

Del Carmen Luzardo, Mariá, Mariá Eliana Lanio, Carlos Alvarez, I. F. Pazos, Santiago Figueroa, Vicente Vérez, and E. A. Disalvo. 2002. "Aggregation Induced by Concanavalin A of Lipid Vesicles Containing Neoglycolipids." *Colloids and Surfaces B: Biointerfaces* 26 (3): 281–89.

Desgrosellier, Jay S., and David A. Cheresh. 2010. "Integrins in Cancer: Biological Implications and Therapeutic Opportunities." *Nature Reviews Cancer* 10 (1). Nature Publishing Group: 9–22.

Dimick, Sarah M., Steven C. Powell, Stephen a. McMahon, Davina N. Moothoo, James H. Naismith, and Eric J. Toone. 1999. "On the Meaning of Affinity: Cluster Glycoside Effects and Concanavalin A." *Journal of the American Chemical Society* 121 (44): 10286–96.

Drickamer, Kurt. 1995. "Multiplicity of Lectin-Carbohydrate Interactions." *Nature Structural & Molecular Biology* 2 (6): 437–439.

Drummond, D C, O Meyer, K Hong, D B Kirpotin, and D Papahadjopoulos. 1999. "Optimizing Liposomes for Delivery of Chemotherapeutic Agents to Solid Tumors." *Pharmacological Reviews* 51 (4): 691–743.

Dunitz, Jack D. 1995. "Win Some, Lose Some: Enthalpy-Entropy Compensation in Weak Intermolecular Interactions." *Chemistry and Biology* 2 (11): 709–12.

Dutta, Tathagata, Hrushikesh B. Agashe, Minakshi Garg, Prahlad Balasubramanium, Madhulika Kabra, and Narendra K. Jain. 2007. "Poly (Propyleneimine) Dendrimer Based Nanocontainers for Targeting of Efavirenz to Human Monocytes/macrophages in Vitro." *Journal of Drug Targeting* 15 (1): 89–98.

Elgavish, Sharona, and Boaz Shaanan. 1997. "Lectin-Carbohydrate Interactions: Different Folds, Common Recognition Principles." *Trends in Biochemical Sciences* 22 (12): 462–67.

Eswarappa, Sandeepa M., Vidya Devi Negi, Sangeeta Chakraborty, B. K Chandrasekhar Sagar, and Dipshikha Chakravortty. 2010. "Division of the Salmonella-Containing Vacuole and Depletion of Acidic Lysosomes in Salmonella-Infected Host Cells Are Novel Strategies of Salmonella Enterica to Avoid Lysosomes." *Infection and Immunity* 78 (1): 68–79.

Feng, Ying, Xue Ma, Liwen Deng, Bin Yao, Ying Xiong, Yilun Wu, Lin Wang, Qianhong Ma, and Fang Ma. 2017. "Role of Selectins and Their Ligands in Human Implantation Stage." *Glycobiology* 27 (5): 385–91.

Florman, Harvey M., and Paul M. Wassarman. 1985. "O-Linked Oligosaccharides of Mouse Egg ZP3 Account for Its Sperm Receptor Activity." *Cell* 41 (1): 313–24.

Gabius, Hans Joachim, Hans Christian Siebert, Sabine André, Jesus Jiménez-Barbero, and Harold Rüdiger. 2004. "Chemical Biology of the Sugar Code." *ChemBioChem* 5 (6): 740–64.

Gal-Mor, Ohad, Erin C. Boyle, and Guntram A. Grassl. 2014. "Same Species, Different Diseases: How and Why Typhoidal and Non-Typhoidal Salmonella Enterica Serovars Differ." *Frontiers in Microbiology* 5 (AUG): 1–10.

Garai, Preeti, Divya Prakash Gnanadhas, and Dipshikha Chakravortty. 2012. "Salmonella Enterica Serovars Typhimurium and Typhi as Model Organisms: Revealing Paradigm of Host-Pathogen Interactions." *Virulence* 3 (4): 377–88.

Garg, Minakshi, Tathagata Dutta, and Narendra Kumar Jain. 2007. "Reduced Hepatic Toxicity, Enhanced Cellular Uptake and Altered Pharmacokinetics of Stavudine Loaded Galactosylated Liposomes." *European Journal of Pharmaceutics and Biopharmaceutics* 67 (1): 76–85.

Gazi, Umut, and Luisa Martinez-Pomares. 2009. "Influence of the Mannose Receptor in Host Immune Responses." *Immunobiology* 214 (7). Elsevier: 554–61.

Gody, Guillaume, Raphael Barbey, Maarten Danial, and Sébastien Perrier. 2015. "Ultrafast RAFT Polymerization: Multiblock Copolymers within Minutes." *Polym.*

Chem. 6 (9): 1502–11.

Gog, Julia R., Alicia Murcia, Natan Osterman, Olivier Restif, Trevelyan J. McKinley, Mmark Sheppard, Sarra Achouri, *et al.* 2012. "Dynamics of Salmonella Infection of Macrophages at the Single Cell Level." *Journal of The Royal Society Interface* 9 (75): 2696–2707.

Goldstein, I J, C E Hollerman, and E E Smith. 1965. "Protein-Carbohydrate Interaction. II. Inhibition Studies on the Interaction of Concanavalin a With Polysaccharides." *Biochemistry* 4: 876–83.

Goldstein, Irwin J, Colin R Hughes, Michel Monsigny, Toshiaki Osawa, and Nathan Sharon. 1980. "What Should Be Called a Lectin?" *Nature Correspondence* 285: 66.

Hakomori, Sen-itiroh. 1985. "Aberrant Glycosylation in Cancer Cell Membranes as Focused on Glycolipids : Overview and Perspectives Aberrant Glycosylation in Cancer Cell Membranes as Focused on Glycolipids :" *Cancer Research*, 2405–14.

Haraga, Andrea, Maikke B. Ohlson, and Samuel I. Miller. 2008. "Salmonellae Interplay with Host Cells." *Nature Reviews Microbiology* 6 (1): 53–66.

Hernandez, Joseph D, and Linda G Baum. 2002. "Ah, Sweet Mystery of Death! Galectins and Control of Cell Fate." *Glycobiology* 12 (10): 127R–36R.

Hill, Megan R., R. Nicholas Carmean, and Brent S. Sumerlin. 2015. "Expanding the Scope of RAFT Polymerization: Recent Advances and New Horizons." *Macromolecules* 48 (16): 5459–69.

Holgersson, Jan, Anki Gustafsson, and Michael E. Breimer. 2005. "Characteristics of Protein-Carbohydrate Interactions as a Basis for Developing Novel Carbohydrate-Based Antirejection Therapies." *Immunology and Cell Biology* 83 (6): 694–708.

Huh, Ae Jung, and Young Jik Kwon. 2011. "'Nanoantibiotics': A New Paradigm for Treating Infectious Diseases Using Nanomaterials in the Antibiotics Resistant Era." *Journal of Controlled Release* 156 (2). Elsevier B.V.: 128–45.

Ibarra, J Antonio, and Olivia Steele-mortimer. 2009. "Salmonella – the Ultimate Insider. Salmonella Virulence Factors That Modulate Intracellular Survival."

Cellular Microbiology (2009) 11 (11): 1579–86.

Immordino, Maria Laura, Franco Dosio, and Luigi Cattel. 2006. "Stealth Liposomes: Review of the Basic Science, Rationale, and Clinical Applications, Existing and Potential." *International Journal of Nanomedicine* 1 (13): 297–315.

Irache, Juan M, Hesham H Salman, Carlos Gamazo, and Socorro Espuelas. 2008. "Mannose-Targeted Systems for the Delivery of Therapeutics." *Expert Opinion on Drug Delivery* 5 (6): 703–24.

Ito, S. 1974. "Form and Function of the Glycocalyx on Free Cell Surfaces." *Phil. Trans. R. Soc. Lond.* 268: 55–66.

Jacobsen, Annika, Rene S. Hendriksen, Frank M. Aaresturp, David W. Ussery, and Carsten Friis. 2011. "The Salmonella Enterica Pan-Genome." *Microbial Ecology* 62 (3): 487–504.

Jain, Keerti, Prashant Kesharwani, Umesh Gupta, and Narendra K. Jain. 2012. "A Review of Glycosylated Carriers for Drug Delivery." *Biomaterials* 33 (16). Elsevier Ltd: 4166–86.

Janeway, CA Jr, P Travers, M Walport, and *Et al.* 2001. "The Front Line of Host Defense." In *Immunobiology: The Immune System in Health and Disease. 5th Edition.*

Jeong, Young Il, Seog Jin Seo, In Kyu Park, Hyun Chul Lee, In Chul Kang, Toshihiro Akaike, and Chong Su Cho. 2005. "Cellular Recognition of Paclitaxel-Loaded Polymeric Nanoparticles Composed of Poly(benzyl L-Glutamate) and Poly(ethylene Glycol) Diblock Copolymer Endcapped with Galactose Moiety." *International Journal of Pharmaceutics* 296 (1–2): 151–61.

Kabanov, A. V., V. P. Chekhonin, V. Yu Alakhov, E. V. Batrakova, A. S. Lebedev, N. S. Melik-Nubarov, S. A. Arzhakov, *et al.* 1989. "The Neuroleptic Activity of Haloperidol Increases after Its Solubilization in Surfactant Micelles. Micelles as Microcontainers for Drug Targeting." *FEBS Letters* 258 (2): 343–45.

Kawakami, S, A Sato, M Nishikawa, F Yamashita, and M Hashida. 2000. "Mannose Receptor-Mediated Gene Transfer into Macrophages Using Novel Mannosylated Cationic Liposomes." *Gene Therapy* 7 (4): 292–99.

Kawakami, Shigeru, and Mitsuru Hashida. 2014. "Glycosylation-Mediated Targeting of Carriers." *Journal of Controlled Release : Official Journal of the Controlled Release Society* 190 (September). Elsevier B.V.: 542–55.

Kawakami, Shigeru, Joseph Wong, Ayumi Sato, Yoshiyuki Hattori, Fumiyoshi Yamashita, and Mitsuru Hashida. 2000. "Biodistribution Characteristics of Mannosylated, Fucosylated, and Galactosylated Liposomes in Mice." *Biochimica et Biophysica Acta - General Subjects* 1524 (2–3): 258–65.

Kelly, Ciara, Caroline Jefferies, and Sally-Ann Cryan. 2011. "Targeted Liposomal Drug Delivery to Monocytes and Macrophages." *Journal of Drug Delivery* 11 (January): 1–12.

Kiessling, Laura L, and Joseph C Grim. 2013. "Glycopolymer Probes of Signal Transduction." *Chemical Society Reviews* 42 (10): 4476–91.

Klibanov, Alexander L, Kazuo K Maruyama, VladimirP Torchilin, and Leaf Huang. 1990. "Amphipathic Polyethyleneglycols Effectively Prolong the Circulation Time of Liposomes." *FEBS Letters* 268 (1): 235–37.

Knodler, L A, and O Steele-Mortimer. 2003. "Taking Possession: Biogenesis of the Salmonella-Containing Vacuole." *Traffic* 4 (9): 587–99.

Kobayashi, Tomotaka, Tatsuhiro Ishida, Yurie Okada, Saori Ise, Hideyoshi Harashima, and Hiroshi Kiwada. 2007. "Effect of Transferrin Receptor-Targeted Liposomal Doxorubicin in P-Glycoprotein-Mediated Drug Resistant Tumor Cells." *International Journal of Pharmaceutics* 329 (1–2): 94–102.

Kumar, Palanirajan Vijayaraj, Abhay Asthana, Tathagata Dutta, and Narendra K. Jain. 2006. "Intracellular Macrophage Uptake of Rifampicin Loaded Mannosylated Dendrimers." *Journal of Drug Targeting* 14 (8): 546–56.

Kwon, Douglas S., Glenn Gregorio, Natacha Bitton, Wayne A. Hendrickson, and Dan R. Littman. 2002. "DC-SIGN-Mediated Internalization of HIV Is Required for Trans-Enhancement of T Cell Infection." *Immunity* 16 (1): 135–44.

Ladmiral, Vincent, Emma Melia, and David M. Haddleton. 2004. "Synthetic Glycopolymers: An Overview." *European Polymer Journal* 40 (3): 431–49.

Laine, Roger A. 1994. "A Calculation of All Possible Oligosaccharide Isomers Both Branched and Linear Yields 1.05 X 10e12 Structures for a Reducing Hexasaccharide: The Isomer Barrier to Development of Single-Method Saccharide Sequencing or Synthesis Systems." *Glycobiology* 4 (6): 759–67.

Lawrence, Eleanor. 1998. "How Salmonella Survive the Stomach." *Nature News*, no. October.

Lee, Y. C., and R. T. Lee. 1995. "Carbohydrate-Protein Interactions: Basis of Glycobiology." *Accounts of Chemical Research* 28 (8): 321–27.

Lian, T, and R J Ho. 2001. "Trends and Developments in Liposome Drug Delivery Systems." *Journal of Pharmaceutical Sciences* 90 (6): 667–80.

Lis, Halina, and Nathan Sharon. 1991. "Lectin-Carbohydrate Interactions." *Current Opinion in Structural Biology* 1 (5): 741–749.

Lis, Halina, and Nathan Sharon. 1998. "Lectins: Carbohydrate-Specific Proteins That Mediate Cellular Recognition." *Chemical Reviews* 98 (2): 637–74.

Lo, Jung Hsin, Samuel K. Kulp, B. Ching Shih Chen, and Hao Chieh Chiua. 2014. "Sensitization of Intracellular Salmonella Enterica Serovar Typhimurium to Aminoglycosides in Vitro and in Vivo by a Host-Targeted Antimicrobial Agent." *Antimicrobial Agents and Chemotherapy* 58 (12): 7375–82.

Lowe, John B. 2003. "Glycan-Dependent Leukocyte Adhesion and Recruitment in Inflammation." *Current Opinion in Cell Biology* 15 (5): 531–38.

Lundquist, Joseph J., and Eric J. Toone. 2002. "The Cluster Glycoside Effect." *Chemical Reviews* 102 (2): 555–78.

Lutz, Jean-François, Jean-Marie Lehn, E. W. Meijer, and Krzysztof Matyjaszewski. 2016. "From Precision Polymers to Complex Materials and Systems." *Nature Reviews Materials* 1: 1–14.

Lutz, Jean-François, Makoto Ouchi, David R Liu, and Mitsuo Sawamoto. 2013. "Sequence-Controlled Polymers." *Science* 341: 628-.

Mammen, Mathai, Seok-Ki Choi, and George M. Whitesides. 1998. "Polyvalent Interactions in Biological Systems: Implications for Design and Use of

Multivalent Ligands and Inhibitors." *Angew. Chem. Int. Ed.* 37 (June): 2754–94.

Martinez-Pomares, Luisa. 2012. "The Mannose Receptor." *Journal of Leukocyte Biology* 92 (6): 1177–86.

Mastroeni, Pietro, Andrew Grant, Olivier Restif, and Duncan Maskell. 2009. "A Dynamic View of the Spread and Intracellular Distribution of Salmonella Enterica." *Naure Reviews Microbiology* 7 (January): 73–80.

Matyjaszewski, K. 2011. "Architecturally Complex Polymers with Controlled Heterogeneity." *Science* 333 (6046): 1104–5.

Matyjaszewski, Krzysztof, and James Spanswick. 2005. "Controlled/living Radical Polymerization." *Materials Today* 8 (3). Elsevier Ltd: 26–33.

Mauceri, Alessandro, Stefano Borocci, Luciano Galantini, Luisa Giansanti, Giovanna Mancini, Antonio Martino, Livia Salvati Manni, and Claudio Sperduto. 2014. "Recognition of Concanavalin a by Cationic Glucosylated Liposomes." *Langmuir* 30 (38): 11301–6.

Mauceri, Alessandro, Alessandro Fracassi, Marco D'Abramo, Stefano Borocci, Luisa Giansanti, Antonella Piozzi, Luciano Galantini, Antonio Martino, Virginia D'Aiuto, and Giovanna Mancini. 2015. "Role of the Hydrophilic Spacer of Glucosylated Amphiphiles Included in Liposome Formulations in the Recognition of Concanavalin A." *Colloids and Surfaces B: Biointerfaces* 136. Elsevier B.V.: 232–39.

Maupin, Kevin a., Daniel Liden, and Brian B. Haab. 2012. "The Fine Specificity of Mannose-Binding and Galactose-Binding Lectins Revealed Using Outlier Motif Analysis of Glycan Array Data." *Glycobiology* 22 (1): 160–69.

McClelland, M, K E Sanderson, J Spieth, S W Clifton, P Latreille, L Courtney, S Porwollik, *et al.* 2001. "Complete Genome Sequence of Salmonella Enterica Serovar Typhimurium LT2." *Nature* 413 (6858): 852–56.

McGrath, James E. 1981. "Chain Reaction Polymerization." *Journal of Chemical Education* 58: 844–61.

McMorran, Brian, Carrie M. Miceli, and Linda G. Baum. 2017. "Lectin Binding

Characterizes the Healthy Human Skeletal Muscle Glycophenotype and Identifies Disease Specific Changes in Dystrophic Muscle." *Glycobiology - Oxford University Press*.

Mishra, B., Bhavesh B. Patel, and Sanjay Tiwari. 2010. "Colloidal Nanocarriers: A Review on Formulation Technology, Types and Applications toward Targeted Drug Delivery." *Nanomedicine: Nanotechnology, Biology, and Medicine* 6 (1). Elsevier Inc.: 9–24.

Moad, Graeme, Ezio Rizzardo, and San H. Thang. 2005. "Living Radical Polymerization by the RAFT Process." *Australian Journal of Chemistry* 58 (6): 379–410.

Moghimi, Moein S, Christy A Hunter, and Clifford J Murray. 2001. "Long-Circulating and Target-Specific Nanoparticles: Theory to Practice." *Pharmacological Reviews* 53 (2): 283–318.

Muro, Silvia. 2012. "Challenges in Design and Characterization of Ligand-Targeted Drug Delivery Systems." *Journal of Controlled Release* 164 (2): 125–37.

Nam, Jutaek, Yeong Su Ha, Sekyu Hwang, Woonghee Lee, Jaejung Song, Jeongsoo Yoo, and Sungjee Kim. 2013. "pH-Responsive Gold Nanoparticles-in-Liposome Hybrid Nanostructures for Enhanced Systemic Tumor Delivery." *Nanoscale*, 3–6.

Nicolas, Julien, Simona Mura, Davide Brambilla, Nicolas Mackiewicz, and Patrick Couvreur. 2013. "Design, Functionalization Strategies and Biomedical Applications of Targeted Biodegradable/biocompatible Polymer-Based Nanocarriers for Drug Delivery." *Chem. Soc. Rev.* 42: 1147–1235.

Opanasopit, P, Y Higuchi, S Kawakami, F Yamashita, M Nishikawa, and M Hashida. 2001. "Involvement of Serum Mannan Binding Proteins and Mannose Receptors in Uptake of Mannosylated Liposomes by Macrophages." *Biochimica et Biophysica Acta* 1511 (1): 134–45.

Pang, Poh-Choo, Philip C N Chiu, Cheuk-Lun Lee, Lan-Yi Chang, Maria Panico, Howard R Morris, Stuart M Haslam, *et al.* 2011. "Human Sperm Binding Is Mediated by the Sialyl-Lewisx Oligosaccharide on the Zona Pellucida." *Science* 333 (6050): 1761–64.

Pelaz, Beatriz, Christoph Alexiou, Ramon A. Alvarez-Puebla, Frauke Alves, Anne M. Andrews, Sumaira Ashraf, Lajos P. Balogh, *et al.* 2017. "Diverse Applications of Nanomedicine." *ACS Nanoano* 11 (3): 2313–81.

Perche, Federico, and Vladimir P Torchilin. 2013. "Recent Trends in Multifunctional Liposomal Nanocarriers for Enhanced Tumor Targeting." *Journal of Drug Delivery* 2013 (January): 705265.

Perrier, Sebastien, and Pittaya Takolpuckdee. 2005. "Macromolecular Design via Reversible Addition-Fragmentation Chain Transfer (RAFT)/xanthates (MADIX) Polymerization." *Journal of Polymer Science, Part A: Polymer Chemistry* 43 (22): 5347–93.

Qin, Yannan, Yaogang Zhong, Ganglong Yang, Tianran Ma, Liyuan Jia, Chen Huang, and Zheng Li. 2014. "Profiling of Concanavalin A-Binding Glycoproteins in Human Hepatic Stellate Cells Activated with Transforming Growth Factor-beta1." *Molecules* 19 (12): 19845–67.

Raj, Isha, Hamed Sadat Al Hosseini, Elisa Dioguardi, Kaoru Nishimura, Ling Han, Alessandra Villa, Daniele de Sanctis, and Luca Jovine. 2017. "Structural Basis of Egg Coat-Sperm Recognition at Fertilization." *Cell* 169 (7). Elsevier: 1315–1326.

Ranjan, Ashish, Nikorn Pothayee, Mohamed N. Seleem, Stephen M. Boyle, Ramanathan Kasimanickam, Judy S. Riffle, and Nammalwar Sriranganathan. 2012. "Nanomedicine for Intracellular Therapy." *FEMS Microbiology Letters* 332 (1): 1–9.

Rawat, Manju, Deependra Singh, Swarnlata Saraf, and Swarnlata Saraf. 2006. "Nanocarriers: Promising Vehicle for Bioactive Drugs." *Biological & Pharmaceutical Bulletin* 29 (9): 1790–98.

Reynolds, Michael, and Serge Pérez. 2011. "Thermodynamics and Chemical Characterization of Protein-Carbohydrate Interactions: The Multivalency Issue." *Comptes Rendus Chimie* 14 (1): 74–95.

Ribet, David, and Pascale Cossart. 2015. "How Bacterial Pathogens Colonize Their Hosts and Invade Deeper Tissues." *Microbes and Infection* 17 (3). Elsevier Masson SAS: 173–83.

Sandoval-Altamirano, Catalina, Susana A. Sanchez, Nancy F. Ferreyra, and German Gunther. 2017. "Understanding the Interaction of Concanavalin a with Mannosyl Glycoliposomes: A Surface Plasmon Resonance and Fluorescence Study." *Colloids and Surfaces B: Biointerfaces* 158. Elsevier B.V.: 539–46.

Santos, Adriana O, Lígia C Gomes da Silva, Luís M Bimbo, Maria C Pedroso de Lima, Sérgio Simões, and João N Moreira. 2010. "Design of Peptide-Targeted Liposomes Containing Nucleic Acids." *Biochimica et Biophysica Acta* 1798 (3). Elsevier B.V.: 433–41.

Scheiffele, P, J Peränen, and K Simons. 1995. "N-Glycans as Apical Sorting Signals in Epithelial Cells." *Nature* 378 (6552): 96–98.

Schnaar, R. L. 2016. "Glycobiology Simplified: Diverse Roles of Glycan Recognition in Inflammation." *Journal of Leukocyte Biology* 99 (June): 1–14.

Sequeira, Luis. 1978. "Lectins and Their Role in Host-Pathogen Specificity." *Ann. Rev. Phytopathol.*, no. 16: 453–81.

Sharma, Amarnath, and Uma S Sharma. 1997. "Liposomes in Drug Delivery: Progress and Limitations." *International Journal of Pharmaceutics* 154: 123–40.

Sharon, Nathan, and Halina Lis. 2004. "History of Lectins: From Hemagglutinins to Biological Recognition Molecules." *Glycobiology* 14 (11): 53–62.

Sheikhpour, Mojgan, Leila Barani, and Alibakhsh Kasaeian. 2017. "Biomimetics in Drug Delivery Systems: A Critical Review." *Journal of Controlled Release* 253. Elsevier B.V.: 97–109.

Smith, Douglas M., Jakub K. Simon, and James R. Baker. 2013. "Applications of Nanotechnology for Immunology." *Nature Reviews Immunology* 13 (8): 592–605.

Steele-Mortimer, Olivia. 2008. "The Salmonella-Containing Vacuole-Moving with the Times." *Current Opinion in Microbiology* 11 (1): 38–45.

Stille, J. K. 1981. "Step-Growth Polymerization." *Journal of Chemical Education* 58 (11): 862–66.

Swaminathan, Chittoor P., Namita Surolia, and Avadhesha Surolia. 1998. "Role of Water in the Specific Binding of Mannose and Mannooligosaccharides to

Concanavalin A." *Journal of the American Chemical Society* 120 (21): 5153–59.

Szwarc, M. 1956. "'Living' Polymers." *Nature* 4543: 1168–69.

Taylor, Maureen E., and Kurt Drickamer. 2014. "Convergent and Divergent Mechanisms of Sugar Recognition across Kingdoms." *Current Opinion in Structural Biology* 28 (1). Elsevier Ltd: 14–22.

Taylor, Philip R., Siamon Gordon, and Luisa Martinez-Pomares. 2005. "The Mannose Receptor: Linking Homeostasis and Immunity through Sugar Recognition." *Trends in Immunology* 26 (2): 104–10.

Torchilin, Vladimir P., and M. I. Papisov. 1994. "Why Do Polyethylene Glycol-Coated Liposomes Circulate So Long?" *Journal of Liposome Research* 4 (1): 725–39.

Toye, Ashley M, Steve F Parsons, David J Anstee, and Jan Frayne. 2016. "Evidence for Differential Glycosylation of Human Trophoblast Cell Types." *The American Society for Biochemistry and Molecular Biology* 1 (514): 1–28.

van der Meel, Roy, Laurens J C Vehmeijer, Robbert J. Kok, Gert Storm, and Ethlinn V B van Gaal. 2013. "Ligand-Targeted Particulate Nanomedicines Undergoing Clinical Evaluation: Current Status." *Advanced Drug Delivery Reviews* 65 (10). Elsevier B.V.: 1284–98.

van Kooyk, Y, and G A Rabinovich. 2008. "Protein-Glycan Interactions in the Control of Innate and Adaptive Immune Responses." *Nature Immunoly* 9 (6): 593–601.

Varki, A. 1993. "Biological Roles of Oligosaccharides: All of the Theories Are Correct." *Glycobiology* 3 (2): 97–130.

Varki, Ajit, Marilynn E Etzler, Richard D Cummings, and Jeffrey D Esko. 2009. "Discovery and Classification of Glycan-Binding Proteins." *Essentials of Glycobiology* Chapter 26.

Varki A., Esko D. J., Colley J. K. 2009. "Cellular Organization of Glycosylation." *Essentials of Glycobiology, 2nd Edition*.

Vázquez-Dorbatt, Vimary, Juneyoung Lee, En Wei Lin, and Heather D. Maynard. 2012. "Synthesis of Glycopolymers by Controlled Radical Polymerization Techniques and Their Applications." *ChemBioChem* 13 (17): 2478–87.

Velge, P., A. Wiedemann, M. Rosselin, N. Abed, Z. Boumart, A. M. Chaussé, O. Grépinet, *et al.* 2012. "Multiplicity of Salmonella Entry Mechanisms, a New Paradigm for Salmonella Pathogenesis." *MicrobiologyOpen* 1 (3): 243–58.

Wang, Shaoning, Hui Xu, Jinghua Xu, Ying Zhang, Yingchun Liu, Yi-hui Deng, and Dawei Chen. 2010. "Sustained Liver Targeting and Improved Antiproliferative Effect of Doxorubicin Liposomes Modified with Galactosylated Lipid and PEG-Lipid." *AAPS PharmSciTech* 11 (2): 870–77.

Weis, William I, and Kurt Drickamer. 1996. "Structural Basis of Lectin-Carbohydrate Recognition." *Annual Review of Biochemistry* 65: 441–73.

Weissmann, G, D Bloomgarden, R Kaplan, C Cohen, S Hoffstein, T Collins, a Gotlieb, and D Nagle. 1975. "A General Method for the Introduction of Enzymes, by Means of Immunoglobulin-Coated Liposomes, into Lysosomes of Deficient Cells." *Proceedings of the National Academy of Sciences of the United States of America* 72 (1): 88–92.

WHO. 2003. "Background Document : The Diagnosis, Treatment and Prevention of Typhoid Fever." *Communicable Disease Surveillance and Response Vaccines and Biologicals*, 2–48.

Williams, Taffy J, Louis D Homer, Jules A Shafer, Irwin J Goldstein, Per J Garegg, Hans Hultberg, Tommy Iversen, and Rolf Johansson. 1981. "Characterization of the Extended Carbohydrate Binding Site of Concanavalin A." *Archives of Biochemistry and Biophysics* 209 (2): 555–64.

Yamazaki, N., S. Kojima, N. V. Bovin, S. André, S. Gabius, and H. J. Gabius. 2000. "Endogenous Lectins as Targets for Drug Delivery." *Advanced Drug Delivery Reviews* 43 (2–3): 225–44.

Yarema, K J, and C R Bertozzi. 2001. "Characterizing Glycosylation Pathways." *Genome Biology* 2: 1–10.

Zhang, Fu, Qi Wu, Zhi Chun Chen, Ming Zhang, and Xian Fu Lin. 2008. "Hepatic-Targeting Microcapsules Construction by Self-Assembly of Bioactive Galactose-Branched Polyelectrolyte for Controlled Drug Release System." *Journal of Colloid and Interface Science* 317 (2): 477–84.

Zhang, Xue Qing, Xu Li Wang, Peng Chi Zhang, Zhi Lan Liu, Ren Xi Zhuo, Hai Quan Mao, and Kam W. Leong. 2005. "Galactosylated Ternary DNA/polyphosphoramidate Nanoparticles Mediate High Gene Transfection Efficiency in Hepatocytes." *Journal of Controlled Release* 102 (3): 749–63.

Zhao, Yan-Yang, Motoko Takahashi, Jian-Guo Gu, Eiji Miyoshi, Akio Matsumoto, Shinobu Kitazume, and Naoyuki Taniguchi. 2008. "Functional Roles of N-Glycans in Cell Signaling and Cell Adhesion in Cancer." *Cancer Science* 99 (7): 1304–10.

CHAPTER 2

Design and synthesis of membrane-inserting glycoligands

The synthesis of glycoligands possessing membrane-inserting lipidic functionalities requires the modular assembly of several chemical components. In this chapter, the convergent synthetic strategies utilised to chemically assemble these ligands are presented. Two set of monovalent glycoligands and two set of multivalent polyglycosides - synthetic lipid-terminated glycopolymers - bearing a range of membrane-inserting anchors were designed and synthesised.

2.1 Introduction

Liposomal membranes can be functionalised with the insertion of specific glycoligands for delivering active molecules to target sites *in vivo* (Noble *et al.* 2014), (van der Meel *et al.* 2013), (Lian and Ho 2001), (Forssen and Willis 1998). Depending on the nature of the glycoligand, several categories of carbohydrate-coated liposomes - *e.g.* glycolipid-bearing liposomes, glycoprotein-bearing liposomes, glycopeptide-bearing liposomes and polysaccharide-bearing liposomes - have been identified (Jayaraman *et al.* 2013), (Jayaraman 2009), (Jones 1994).

2.1.1 Glycoligand-liposome conjugation

Ligands can be conjugated to liposomal lipids through two strategies: covalent and non-covalent coupling (Mobed and Chang 1998), (Iwamoto and Sunamoto 1982). Covalent conjugation requires coupling of a ligand to a membrane-inserting hydrophobic residue, and is generally preferred due to increased efficiency of conjugation and stability of the resulting targeted assemblies. Typically this hydrophobic residue (often called 'anchor') is a phospholipid - *e.g.* phosphatidylethanolamine, phosphatidylinositol - which presents a chemical handle suitable for coupling with the chosen ligand (Nobs *et al.* 2004).

The attachment of the ligand to the hydrophobic anchor can occur before or after the assembly of the liposome vesicle (Jayaraman *et al.* 2013). In the first case, the ligand is conjugated to the anchor, and the resulting amphiphilic conjugate is mixed with the other phospholipids and utilised to assemble the desired targeted liposomes (Figure 9). In the latter strategy, the ligands are conjugated to reactive anchors present at the

surface of preformed liposome membranes (Figure 9) (Vabbilisetty and Sun 2015), (Hassane *et al.* 2006). One potential drawback of this second approach is that estimation of the efficiency of the ligand grafting reaction, and consequently the quantification of ligand effectively present at the liposomal membrane can be very challenging. Thus, in this thesis work the first strategy was chosen.

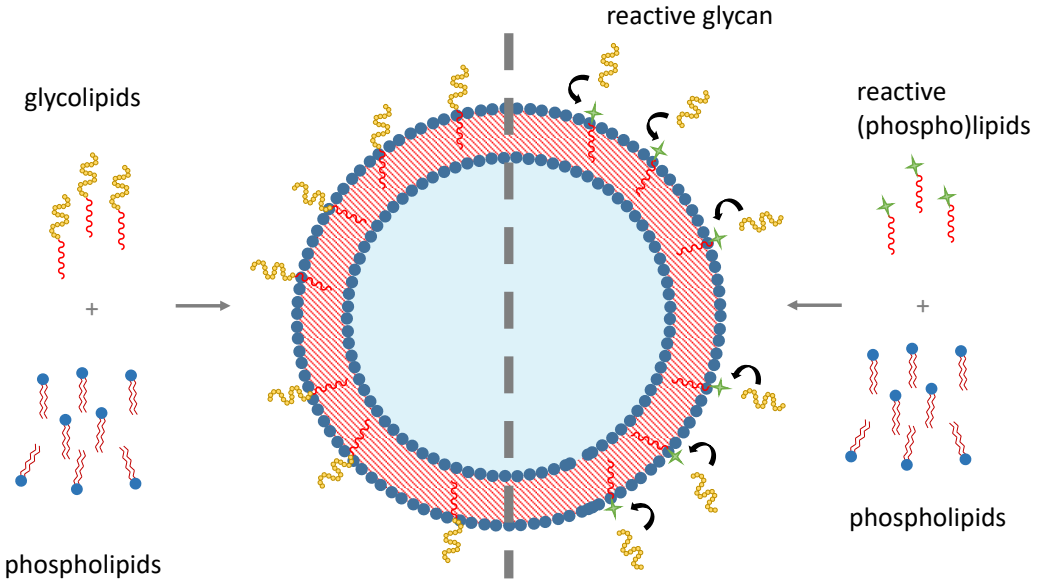

Figure 9 - Strategies for assembling glycosylated liposomes. (left) Assembly of preformed glycolipids: glycosylated ligands are first chemically linked to hydrophobic anchors, then targeted liposomes are assembled using these amphiphilic molecules mixed with other phospholipids. (right) Glycosylation of pre-formed functionalised membrane: liposomes are assembled using lipids which contain reactive polar heads. These are subsequently utilised as "chemical handles" onto which glycosylated ligands can be grafted.

2.1.2 Glycoligand design

A variety of glycoligands have been investigated for liposomal surface glycosylation (Noble *et al.* 2014), (Kelly *et al.* 2011). Among them, the use of glycolipids seems a promising and efficacy strategy to graft sugar-ligands on liposomal membrane (Kawakami and Hashida 2014), (Hashida *et al.* 2001). The overall structure of the anchoring lipids can affect liposome chemical-physical properties, the ligand grafting density and stability, the surface glycofunctionalisation and the interaction with lectin receptor (Vabbilisetty and Sun 2015), (Chen *et al.* 2014).

Therefore, the structural design of a membrane inserting glycolipids should be considered in a comprehensive way merging together three main parameters (Figure 10):

i) The sugar head group - which can consist of individual sugar-units, or cluster of sugars (*e.g.* linear or branched glycopolymers).

ii) The presence and nature of a spacer between the sugar-head and the hydrophobic anchor.

iii) The nature of the anchor. For example, short hydrophobic alkyl chains can enhance surface exposure of the sugars heads, compared to longer alkyl chains. The use of the latter can result in thicker and less flexible lipid bilayers, and consequently reduced ligand exposure and less effective interaction with target lectin receptors (Jayaraman *et al.* 2013). Increase in lipophilicity can also be achieved by using cholesterol derivatives as the hydrophobic anchor.

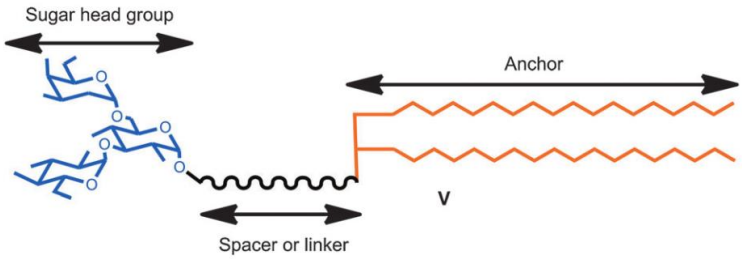

Figure 10 - Example of membrane-inserting glycoligand (Jayaraman *et al.* 2013).

To elucidate how these structural parameters could affect the ability of targeted liposomes to bind to model lectins and enhance uptake in selected cell lines, in this work two set of monovalent glycoligands and two set of multivalent polyglycosides - synthetic lipid-terminated glycopolymers - bearing a range of membrane-inserting anchors were designed and synthesised (Figure 11).

Two different anchor moieties, palmitoyl (Figure 11a and 3c) and cholesterol (Figure 11b and 3d), were selected for the synthesis of our glycoligands. Cholesterol derivatives are not capable of forming lipid bilayers on their own, but are extremely efficient in intercalating within lipid bilayers (in lipid membranes cholesterol : phospholipids molar ratio can be as high as 2:1(Szoka 1980), (Lundberg 1977)), thus they offered great potential to act as anchors for the decoration of liposomes with glycosylated ligands. In addition, in this study we aimed at investigating the effect of the carbohydrate patterns - that is, the spatial distribution of the sugar ligands – at the liposome membrane, on their ability to recognise lectin receptors and promote cell uptake into selected cell lines. For this aim, monovalent (Figure 11a and 11b) and polyvalent ligands (Figure 11c and 11d) were designed and synthesised.

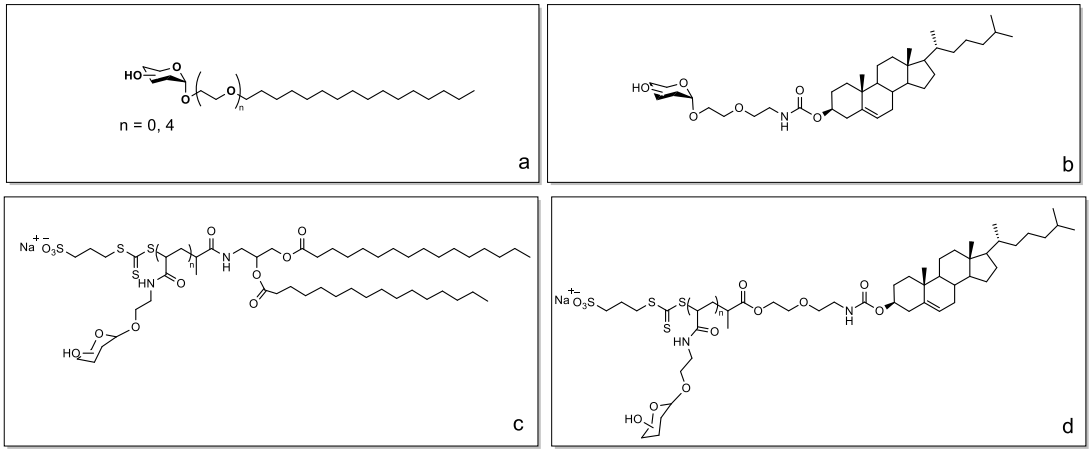

Figure 11 - The four different families of glycoligands (Man/Gal) designed in this work: a) monoglycosides with a palmitoyl anchor; b) monoglycosides with a cholesterol anchor; c) polyglycoside with a dipalmitoyl anchor and d) polyglycoside with a cholesterol anchor.

The structure of palmitoyl-terminated glycopolymers is shown in Figure 11c as these materials were part of the ligands we initially intended to utilise in this thesis work. Although several intermediates were prepared, due to time constraint the synthesis of the final glycoligands was not completed, thus their synthesis is not reported in this chapter.

2.2 Materials and Methods

2.2.1 Materials

All the solvents were purchased from Fischer Chemicals and were of analytical grade. All chemicals were purchased from Sigma-Aldrich Company, Alfa Aesar or Fisher Scientific and utilised without further purification unless otherwise stated.

Azoinitiator 2,2'-azobis[2- (2-imidazolin-2-yl)propane]dihydrochloride (VA-044) was purchased from Wako.

2.2.2 Methods

Thin layer chromatography (TLC) was performed using pre-coated silica gel 60 ALUGRAM SIL G/UV254 and developed in the solvent system indicated. Compounds were visualised by use of UV light (254 nm) or a basic solution (10% w/w K_2CO_3 in water) of $KMnO_4$. ACROS ORGANIC 60Å (0.035-0.070 mm) silica gel was used for column chromatography.

Agilent 971-FP Flash Purification System was used to perform flash column chromatography on SiO_2.

^{1}H and ^{13}C NMR spectra were recorded on a Bruker DPX400 UltraShield™ Spectrometer and processed with MestReNova 6.0.2© 2009 Mestrelab Research S.L. All chemical shifts are reported in ppm (δ) relative to tetramethylsilane or referenced to the chemical shifts of residual solvent resonances. The following abbreviations were used to explain the multiplicities: s = singlet, bs = broad singlet. d = doublet, t = triplet, q= quartet, m = multiplet.

ESI TOF Mass Spectrometry measurements were carried out using a Bruker MicroTOF spectrometer (LC-TOF instrument equipped with an ESI source).

MALDI-TOF Mass Spectrometry measurement was carried out using a Bruker UltraflexIII. The sample was prepared by dissolution in DMSO to a final concentration of 10 mg/mL. The matrix was α-cyano-4-hydroxycinnamic acid dissolved in MeOH (20 mg/mL.).

The polymer molecular weights were determined by size exclusion chromatography (SEC) performed on a Polymer Laboratories GPC 50 system (Polymer Laboratories) equipped with refractive index (RI) detector. Separations were performed on a pair of Agilent PLgel 5 μm Mixed D columns (7.5 x 300 mm, 5 μm bead size, Polymer Labs UK), eluting with DMF + 0.1% w/w LiBr at flow rate of 1 mL min^{-1} and injection volume of 100 μL. Samples were prepared at 5 mg mL^{-1} concentration. The molecular weights and dispersities of the polymers were calculated according to a standard calibration method using PMMA narrow standards (500-450,000 g mol^{-1}). Data were elaborated with Polymer Labs Cirrus 3.0 Software.

2.3 Experimental section

Detailed peak assignment and corresponding chemical structures are reported in Appendix 6.1.

2.3.1 Synthesis of 1,2,3,4,6 Penta-O-acetyl-α-D-mannopyranoside **(1)**

This procedure was adapted from the protocol described by Field and co-workers (Mukhopadhyay *et al.* 2004), (Kartha and Field 1997). D-(+)-Mannose (17.50 g, 97.14 mmol) was suspended in acetic anhydride (50.44 g, 46.70 mL, 494.0 mmol) in a 500 mL beaker. Solid I_2 (0.124 g, 0.488 mmol) was added, and the mixture was allowed to stir at room temperature for 30 min, during which time the reaction mixture turned from a white suspension to a dark brown solution, in a very exothermic process. Upon cooling to ambient temperature, aqueous sodium thiosulfate ($Na_2S_2O_3$, 3.00 g in 100 mL of water) was added to reduce I_2 giving a colourless solution, then aqueous $NaHCO_3$ was added to neutralise the acetic acid formed in the acetylation reaction. The mixture was stirred for 10 min, then extracted with Et_2O (250 mL) and the organic phase washed 3 times with water. The solvent was evaporated under reduced pressure, and the oily residue was dried by codistillation with toluene under reduced pressure, to remove traces of water. The crude product was then purified by column chromatography on SiO_2 (40% EtOAc in petroleum ether) to give pure mannose pentaacetate **(1)** (30.37 g, 77.80 mmol, 80.09%.) as a mixture of α and β anomers (α:β = 70:30 mol:mol).

^{1}H NMR (400 MHz, $CDCl_3$) δ 6.00 (d, *J* = 1.9 Hz, 1H, CH α-*anomeric* 70%), 5.81 (d, *J* = 1.14 Hz, 1H, CH β-*anomeric* 30%), 5.28-5.06 (m, 2H, CH), 4.20-4.18 (m, 2H,

CH_2OAc), 4.06-4.00 (m, 1H, CH), 2.10 (s, 3H, CH_3), 2.09 (d, 3H, CH_3), 1.98 (s, 3H, CH_3), 1.96 (s, 3H, CH_3), 1.93 (s, 3H, CH_3).

^{13}C {^{1}H} NMR (101 MHz, $CDCl_3$) δ 170.52 (1C, CO β-anomer), 170.50 (1C, CO α -anomer), 170.09 (1C, CO β-anomer), 169.87 (1C, CO α-anomer), 169.67 (1C, CO β-anomer), 169.27 (1C, CO α-anomer), 169.50 (1C, CO β-anomer), 169.44 (1C, CO α-anomer), 168.27 (1C, CO β-anomer), 167.97 (1C, CO α-anomer), 90.58 (1C, *a anomeric*), 90.42 (1C, *β-anomeric*), 73.22 (1C β-anomer), 70.59 (1C α/β-anomer), 68.73 (1C α/β-anomer), 68.32 (1C α-anomer), 68.20 (1C β-anomer), 65.53 (1C α-anomer), 65.45 (1C β-anomer), 62.07 (1C α/β-anomer), 20.78 (1C, CH_3), 20.67 (1C, CH_3), 20.6 (1C, CH_3), 20.6 (1C, CH_3), 20.6 (1C, CH_3).

ESI-TOF Mass spectrometry: expected m/z $[M+Na]^+$ 413.11, found 413.11 u.m.a. (100%).

2.3.2 Synthesis of 1-palmitoyl-tetraethylene glycol **(2)**

In a 500 mL round bottom flask, tetra(ethylene glycol) (TEG, 100.00 g, 514.85 mmol) was dissolved in toluene (100 mL) and the solvent was removed under reduced pressure at 60 °C. This procedure was repeated further 5 times to remove any traces of water in the TEG starting material. TEG was left to cool down at room temperature and then further cooled down to 0 °C using an ice bath. NaH 60% dispersion in mineral oil (8.00 g, 200 mmol) was added in small portions at 0 °C under stirring, then the ice bath was removed and the mixture was left to warm up to room temperature. 1-Bromo-hexadecane (39.00 mL, 127.7 mmol) was slowly added using a pipette, and the flask was heated to 90 °C and left under stirring overnight.

The reaction was then cooled down to room temperature, stopped by slow addition of water (100 mL) and then diluted with 100 mL of EtOAc. After separation of the two phases, the organic layer was washed 3 times with water. The organic layer was then dried over $MgSO_4$. After filtration over a sintered glass filter, the solvent was removed under reduced pressure and the residue purified by flash column chromatography on SiO_2 using EtOAc as the eluent, to give, after evaporation of solvent from the relevant fractions under reduced pressure, pure **(2)** (29.1 g, 69.4 mmol, 54.3%) as a colourless oil.

^{1}H NMR (400 MHz, CD_3OD) δ 3.69-3.64 (m, 12H, CH_2O), 3.61-3.57 (m, 4H, OCH_2CH_2O), 3.49 (t, J = 6.6 Hz, 2H, $OCH_2CH_2CH_2$), 1.63-1.56 (m, 2H, $OCH_2CH_2CH_2$), 1.32 (m, 26H, $CH_2(CH_2)_{13}CH_3$), 0.93 (t, J = 6.9 Hz, 3H, CH_2CH_3).

^{13}C {^{1}H} NMR (101 MHz, CD_3OD) δ 73.69, 72.38, 71.62, 71.57, 71.55, 71.42, 71.16 (8C, CH_2O), 62.24 (1C, CH_2OH), 33.07 (1C, $CH_2CH_2CH_2$), 30.77-27.29 (12C, CH_2), 23.65 (1C, CH_2CH_3), 14.44 (1C, CH_3).

ESI-TOF Mass spectrometry: expected m/z $[M+Na]^+$ 441.36, found 441.35 u.m.a. (100%).

2.3.3 Synthesis of alkyl monoglycosides - General procedure

In a 250 mL round bottom flask, the pyranoside pentacetate and desired alkyl alcohol (exact quantities and characterisation of each glycoside are reported below) were dissolved in 40 mL of CH_2Cl_2. When 1-hexadecanol was used, the suspension was sonicated for 40 min at room temperature to allow complete dissolution. The solution was cooled down to 0 °C using an ice bath before dropwise addition of $BF_3{\cdot}Et_2O$. After 1 h the ice bath was removed and the reaction left to proceed under stirring at

room temperature overnight. The reaction was monitored by ^{13}C NMR, following the shift of the anomeric peak from ~90 to 101-105 ppm. After complete conversion of sugar pentaacetate into the desired alkyl glycoside, the reaction solution was diluted with CH_2Cl_2 (60 mL), washed 3 times with a saturated aqueous solution of $NaHCO_3$ (100 mL) and finally dried over $MgSO_4$. After filtrationover a sintered glass filter and solvent removal under reduced pressure, purity was assessed by ^{1}H and ^{13}C NMR. Compounds **3, 5, 7, 9** were used for the subsequent step without further purification. Crude intermediates **3, 5, 7, 9** were separately dissolved in a solution of K_2CO_3 in CH_3OH. The reaction mixture was left under stirring for 2 hours at room temperature. The reaction was monitored by TLC (10% CH_3OH in EtOAc). During the reaction, the formation of a white precipitate was observed. The reaction mixture was neutralised by adding Amberlite IR120-H^+. The resin was filtered off and the solvent was removed under reduced pressure to give residues that were purified by flash column chromatography on SiO_2 (5%-10% CH_3OH in EtOAc). Products were isolated by removal of the solvent from the relevant fractions.

Details:

β-O-palmitoyl galactose **(4)**: Galactose pentacetate (7.42 g, 27.2 mmol), 1-hexadecanol (13.82, 57.00 mmol), $BF_3{\cdot}Et_2O$ (5.00 mL, 36.0 mmol). For deprotection of intermediate **(3)**: K_2CO_3 (0.50 g, 3.6 mmol) in CH_3OH (20.0 mL). Due to time constraint compound **4** was not utilised in subsequent binding studies, thus the crude product was not further purified. However, ^{13}C NMR and ESI-TOF mass spectrometry confirmed the formation of the expected *O*-alkyl glycoside **(4)**.

^{13}C {^{1}H} NMR (101 MHz, $CDCl_3$) δ 103.44 (1C, CH β-*anomeric*), 74.47, 73.52, 71.22, 68.70, 67.89, 62.73, 53.44, 32.57 (1C, CH_2), 31.84-29.34 (10C, CH_2), 22.54(1C, CH_2CH_3), 14.03 (1C, CH_3).

ESI-TOF Mass spectrometry: expected m/z $[M+Na]^+$ 427.30, found 427.30 u.m.a. (100%).

α-O-palmitoyl mannose **(6)**: Mannose pentacetate (10.00 g, 25.62 mmol), 1-hexadecanol (18.76 g, 77.38 mmol), $BF_3{\cdot}Et_2O$ (6.50 mL, 347 mmol). For deprotection of intermediate **(5)**: K_2CO_3 (0.50 g, 3.6 mmol) in CH_3OH (20 mL). Pure compound: white waxy solid (1.48 g, 3.66 mmol, 14.3%).

^{1}H NMR (400 MHz, CD_3OD) δ 4.74 (d, *J* = 1.6 Hz, 1H, CH *anomeric*), 3.85-3.59 (m, 6H, CH [mannose] and CH_2OH [mannose]), 3.57-3.39 (m, 2H, OCH_2CH_2), 1.64-1.52 (m, 2H, $OCH_2CH_2CH_2$), 1.30 (m, 26H, $CH_2(CH_2)_{12}CH_3$), 0.91 (t, *J* = 6.9, 3H, CH_3).

^{13}C {^{1}H} NMR (101 MHz, CD_3OD) δ 101.6 (1C, CH *anomeric*), 74.6, 72.70, 72.3, 68.7, 68.6, 63.0, 33.1 (1C, CH_2), 30.8-30.5 (10C, CH_2), 23.72 (1C, CH_2CH_3), 14.4 (1C, CH_3).

ESI-TOF Mass spectrometry: expected m/z $[M+Na]^+$ 427.30, found 427.30 u.m.a. (99%).

β-O-tetra(ethylene glycol) palmitoyl galactose **(8)**: Galactose pentacetate (10.45 g, 26.70 mmol), TEG-Palmitoyl **(2)** (7.47 g, 17.8 mmol), $BF_3{\cdot}Et_2O$ (5.00 mL, 36.0 mmol). For deprotection of intermediate **(7)**: K_2CO_3 (0.50 g, 3.6 mmol) in CH_3OH (20 mL). Pure compound: white waxy solid (4.56 g, 7.85 mmol, 29.4%).

^{1}H NMR (400 MHz, CD_3OD) δ 4.29 (d, *J* = 7.5 Hz, 1H, CH *anomeric*), 3.85-3.84 (m, 1H, CH [galactose]), 3.78-3.71 (m, 5H, CH [galactose] and CH_2OH [galactose]), 3.69-

3.58, (m, 12H, CH_2 [TEG]), 3.52-3.51 (m, 4H, OCH_2CH_2O), 3.47 (t, 2H, J = 6.5 Hz, $OCH_2CH_2CH_2$), 1.61-1.56 (m, 2H, $OCH_2CH_2CH_2$), 1.31 (m, 26H, $CH_2(CH_2)_{13}CH_3$), 0.93 (t, J = 6.9 Hz, 3H, CH_3).

^{13}C {^{1}H} NMR (101 MHz, CD_3OD) δ 105.09 (1C, CH *anomeric*), 76.69, 74.90, 72.52, 72.38, 71.57, 71.56, 71.51, 71.50, 71.16, 70.28, 69.58, 62.52, 61.52, 33.06 (1C, CH_2), 30.77-27.21 (12C, CH_2), 23.72 (1C, CH_2CH_3), 14.44 (1C, CH_3).

ESI-TOF Mass spectrometry: expected m/z $[M+Na]^+$ 603.41, found 603.41 u.m.a. (100%).

α-O-(tetraethylglycol) palmitoyl mannose **(10)**: Mannose pentacetate (10.61 g, 27.18 mmol), TEG-Palmitoyl (2) (7.59 g, 18.1 mmol), $BF_3{\cdot}Et_2O$ (5.00 mL, 36.0 mmol). For deprotection of intermediate (9): K_2CO_3 (0.50 g, 3.6 mmol) in CH_3OH (20 mL). Pure compound: white waxy solid (2.2 g, 3.8 mmol, 14%).

^{1}H NMR (400 MHz, CD_3OD) δ 4.82 (d, J = 1.7 Hz, 1H, CH *anomeric*), 3.89-3.82 (m, 3H, CH [mannose]), 3.75-3.70 (m, 3H, CH [mannose], 3.69-3.57(m, 12H, CH_2 [TEG]), 3.61-3.57 (m, 4H, OCH_2CH_2O), 3.49 (t, J = 6.6 Hz, 2H, $OCH_2CH_2CH_2$), 1.63-1.59 (m, 2H, OCH_2CH_2), 1.32 (m, 24H, $CH_2(CH_2)_{13}CH_3$), 0.93 (t, J = 6.8 Hz, 3H, CH_3).

^{13}C {^{1}H} NMR (101 MHz, CD_3OD) δ 101.76 (1C, CH *anomeric*), 74.60, 72.57, 72.38, 72.12, 71.62, 71.59, 71.55, 71.40, 71.15, 68.63, 67.68, 62.96, 61.51, 33.07 (1C, CH_2), 30.78-27.21 (12C, CH_2), 23.73 (1C, CH_2CH_3), 14.44 (1C, CH_3).

ESI-TOF Mass spectrometry: expected m/z $[M+Na]^+$ 603.41, found 603.41 u.m.a. (100%).

2.3.4 Synthesis of Cholesterol ethylethoxycarbamate **(11)**

Cholesteryl chloroformate (9.08 g, 20.2 mmol) was dissolved in of CH_2Cl_2 (25.0 mL). The solution was cooled down to 0 °C and Et_3N (3.37 mL, 24.3 mmol) was added. 2-(2-aminoethoxy)ethanol (2.23 mL, 22.2 mmol) was then added dropwise, and the resulting mixture was left to react at room temperature for 2 hours, and finally diluted with CH_2Cl_2 (300 mL). The organic phase was washed 3 times with 300 mL of diluted aqueous H_2SO_4 (pH=3). The organic layer was dried over $MgSO_4$ and, after filtration, the solvent was evaporated under reduced pressure. Removal of the solvent under reduced pressure gave **(11)** (8.90 g, 17.2 mmol, 85.0%) as a white solid.

^{1}H NMR (400 MHz, $CDCl_3$) δ 5.37 (d, *J* = 5.45 Hz, 1H, C=CH), 5.03 (s, 1H, OCONH), 4.50 (m, 1H, OCH), 3.74 (t, *J* = 4.1 Hz, 2H, OCH_2CH_2OH), 3.57 (q, *J* = 4.6 Hz, 4H, CH_2OCH_2), 3.38 (t, *J* = 5.1 Hz, 2H, $NHCH_2CH_2O$), 2.38-2.24 (m, 2H), 2.18 (m, 1H), 2.02-1.79 (m, 5H), 1.60-1.05 (m, 19H), 1.00 (s, 3H, CH_3[23]), 0.98-0.94 (m, 2H), 0.92-0.90 (d, *J* = 6.6 Hz, 3H, CH_3[8]), 0.87-0.85 (dd, *J* = 6.6 Hz, 6H, 1.6 Hz, CH_3[1/3]), 0.68 (s, 3H, CH_3[14]).

^{13}C {^{1}H} NMR (101 MHz, CDCl3) δ 156.41 (1C, OC[28]), 139.95 (1C, C[21]), 122.65 (1C, C[20]), 74.61 (1C, C[25]), 72.33 (1C, C[32]), 70.36 (1C, C[31]), 61.95 (1C, C[33]), 56.90 (1C, C[9]), 56.29 (1C, C[12]), 50.17 (1C, C[16]), 42.47 (1C, C[13]), 40.84 (1C, C[30]), 39.89 (1C, C[4]), 39.67 (2C, C[24/18]), 38.71 (1C, C[22]), 37.14 (1C, C[27]), 36.72 (1C, C[6]), 36.34 (1C, C[7]), 35.95 (1C, C[15]), 32.03 (1C, C[19]), 28.38 (1C, C[26]), 28.32 (1C, C[3]), 28.16 (1C, C[10]), 24.44 (1C, C[11]), 23.98 (1C, C[5]), 22.97 (1C, C[1]), 22.68 (1C, C[2]), 21.20 (1C, C[17]), 19.57 (1C, C[23]), 18.87 (1C, C[8]), 12.01 (1C, C[14]). **ESI-TOF** Mass spectrometry: expected m/z $[M+Na]^+$ 540.39, found 540.40 u.m.a. (50.9%).

2.3.5 Synthesis of 2,3,4,6 tetra-O-acetyl-α-D-mannose-I **(12)**

D-(+)-Mannose (5.00 g, 27.8 mmol) was suspended in acetic anhydride (13.5 ml, 143 mmol) in a 1 L beaker. Solid I_2 (0.051 g, 0.20 mmol) was slowly added and the mixture was allowed to stir at room temperature for 1 hour, during which time solid I_2 catalyst slowly went in solution, starting a very hexotermic acetylation reaction. The reaction was monitored by TLC (Pet. Ether/EtOAc = 6:4). At completion, the reaction mixture was diluted with CH_2Cl_2, and I_2 (4.3 g, 17 mmol) and hexamethyldisilane (HMDS) (2.46 g, 16.8 mmol) were added. The reaction mixture was stirred for 3 hours, and then with 10% $Na_2S_2O_3$ aqueous solution (20 mL) for further 10 min. The organic layer was washed with saturated $NaHCO_3$ aqueous solution (50 mL) and then with water (50 mL). The organic phase was dried over $MgSO_4$, the solvent was evaporated under reduced pressure and the resulting residue was purified by flash chromatography (40% EtOAc in petroleum ether), to give pure **(12)** as a α-anomer(1.57 g, 3.44 mmol, 12.4%) as a colourless oil.

^{1}H NMR (400 MHz, $CDCl_3$) δ 6.68 (s, 1H, CH *anomeric*), 5.78-5.75 (dd, *J* = 10.2, 3.4 Hz, 1H, CH), 5.45 (m, *J* = 3.3 Hz, 1.3 Hz, 1H, ,CH), 5.36 (t, *J* = 10.2 Hz, 1H, CH), 4.32 (dd, *J* = 12.6, 5.0 Hz, 1H, CH_2OAc), 4.12–4.08 (dd, *J* = 12.6 Hz, 2.2 Hz, 1H, CH), 3.95 – 3.91 (m, 1H,) 2.15 (s, 3H, CH_3), 2.08 (s, 3H, CH_3), 2.06 (s, 3H, CH_3), 1.98 (s, 3H, CH_3).

^{13}C {^{1}H} NMR (101 MHz, $CDCl_3$) δ 170.55 (1C, CO), 169.75 (1C, CO), 169.62 (1C, CO), 169.57 (1C, CO), 75.39 (1C, C[4]), 73.43 (1C, C[6]), 68.65 (1C, C[3]), 66.28 (1C, C[5]), 65.46 (1C, C[7]), 61.39 (1C, C[10]), 20.83 (1C, CH_3), 20.75 (1C, CH_3), 20.75 (1C, CH_3), 20.65 (1C, CH_3).

ESI-TOF Mass spectrometry: expected m/z $[M-I]^+$ 331.09, found 331.10 u.m.a. (14%), m/z $[M-I+H+K]^+$ 371.08, found 371.09 u.m.a. (72%).

2.3.6 Synthesis of tetraacetate mannosylated-ethylethoxycarbamate cholesterol **(13)**

Cholesterol alcohol **(11)** (8.90 g, 17.2 mmol) was dissolved in anhydrous CH_2Cl_2 (20 mL). Ag_2CO_3 was added, and the mixture was protected from light, degassed by N_2 bubbling for 20 min, and then stirred protected for 30 min at room temperature. Tetra-*O*-acetyl-α-D-mannosepyranosyl iodide **(2)** (1.60 g, 3.44 mmol) was dissolved in 20 mL of anhydrous CH_2Cl_2 (20 mL), 3Å molecular sieves (pellets, 1 g) were added, and the mixture was stirred under N_2 for 30 minutes, then it was transferred via cannula to the solution containing cholesterol alcohol **(11)** and $AgCO_3$, and the resulting mixture stirred overnight under N_2. The precipitate was filtrated, and the volatiles were removed from filtrate under reduced pressure. The resulting residue was purified by flash column chromatography on SiO_2 (40% EtOAc in Petroleum Ether) to give, after removal of solvent under reduce pressure, **(13)** (2.42 g, 2.86 mmol, 83%) as a pale yellow waxy solid.

^{1}H NMR (400 MHz, $CDCl_3$) δ 5.49-5.48 (d, *J* = 2.4 Hz, 1H, CH *anomeric*), 5.37(d, 1H, *J* = 4.96 Hz, C=CH), 5.29 (t, *J* = 9.7 Hz, 1H, CH [mannose]), 5.15-5.11 (m, 1H, CH, [mannose]), 5.04 (s, 1H, OCONH), 4.62 (t, *J* = 2.9Hz, 1H, CH [mannose]), 4.49 (m, 1H, OCH), 4.23 (dd, 1H, *J* = 12.6 Hz, 4.9 Hz, CH [mannose]), 4.13 (dd, *J* = 12.1 Hz, 2.4 Hz, 1H, CH [mannose]), 3.74 (q, *J* = 9.0 Hz, 4.8 Hz, 2H, OCH_2CH_2O), 3.70-3.60 (m, 1H, CH [mannose]), 3.57 (q, *J* = 4.6 Hz, 4H, CH_2OCH_2), 3.38 (m, 2H, $NHCH_2CH_2O$), 2.38-2.15 (m, 2H), 2.06 (s, 3H, $COCH_3$ [mannose]), 2.04 (s, 3H, COH_3 [mannose]), 2.01 (s, 3H, $COCH_3$ [mannose]), 2.00-1.77 (m, 5H), 1.76 (s, 3H, $COCH_3$

[mannose]), 1.59-1.03 (m, 19H), 1.00 (s, 3H, CH_3[23]), 0.97-0.93 (m, 2H,), 0.91-0.90 (d, J = 6.5 Hz, 3H, CH_3[8]), 0.86-0.85 (dd, J = 6.6 Hz, 1.6 Hz, 6H, CH_3[1/2]), 0.67(s, 3H, CH_3[14]).

^{13}C {^{1}H} NMR (101 MHz, $CDCl_3$) δ 170.76 (1C, CO), 170.52 (2C, CO), 169.53 (1C, CO), 156.41 (1C, OC(O)NH[28]), 139.93 (1C, C[21]), 122.63 (1C, C[20]), 97.50 (1C, C[34 *anomeric*]), 76.42 (1C, C[42]), 74.61 (1C, C[25]), 72.33 (1C, C[32]), 71.54 (1C, C[35]), 70.73/70.34 (1C, C[31]), 69.77 (1C, C[2]), 65.65 1C, C[36], 62.49 (1C, C[43]), 61.91 (1C, C[33]),56.83 (1C, C[9]), 56.27 (1C, C[12]), 50.15 (1C, C[16]), 42.45 (1C, C[9]) 40.82 (1C, C[30]), 39.88 (1C, C[4]), 39.65 (2C, C[18/24]), 38.70 (1C, C[22]), 37.13 (1C, C[27]), 36.70 (1C, C[6]), 36.32 (1C, C[7]), 35.93 (1C, C[15]), 32.01 (1C, C[19]), 28.36 (1C, C[26]), 28.30(1C, C[3]), 28.14 (1C, C[10]), 24.42 (1C, C[11]), 23.97 (1C, C[5]), 22.95 (1C, C[1]), 22.70(1C, C[2]), 21.18 (1C, C[17]), 20.89 (1C, CO*C*H_3), 20.85 (2C, CO*C*H_3), 20.80 (1C, CO*C*H_3), 19.47 (1C, C[23]), 18.85 (1C, C[8]), 11.99 (1C, C[14]).

ESI-TOF Mass spectrometry: fragment [$CONHCH_2CH_2OCH_2CH_2$-mannose tetraacetate] $^+$, expected m/z 462.16, found 462.16 u.m.a. (28%), m/z.

2.3.7 Synthesis of mannosylated-ethylethoxycarbamate cholesterol **(14)**

(13) (2.42 g, 2.86 mmol) was dissolved in CH_3OH (10.0 mL). K_2CO_3 (0.50 g, 3.6 mmol) was added, and the reaction mixture was left under stirring for 2 hours at room temperature. The reaction was monitored by TLC (EtOAc/CH_3OH 9 : 1). During the reaction the formation of a white precipitated was observed. The reaction mixture was neutralised adding Amberlite IR120-H^+. The resin was filtered off and the solvent was removed under reduced pressure. The crude of reaction was purified by flash column chromatography on SiO_2 (10% CH_3OH in EtOAc) to give, after removal of solvent

under reduce pressure, pure **(14)** (0.612 g, 0.900 mmol, 31.5%) as a pale yellow waxy solid.

^{1}H NMR (400 MHz, $CDCl_3$) δ 5.78 (d, *J* = 5.9 Hz, 1H, CH, β-*anomeric*), 5.49 (s, 1H, CH, α-*anomeric*), 5.37 (d, *J* = 4.6 Hz, 1H, C=CH), 5.29 (t, *J* = 9.7 Hz, 1H, CH [mannose]), 5.15-5.11 (m, 1H, CH [mannose]), 4.49(m, 1H, OCH), 4.48-4.42 (m, 1H, CH [mannose]), 3.74 (t, *J* = 4.2 Hz, 2H, OCH_2CH_2O), 3.70-3.60 (m, 1H, CH [mannose]), 3.57 (q, *J* = 4.6 Hz, 4H, CH_2OCH_2), 3.38 (m, 2H, $NHCH_2CH_2O$), 2.38-2.15 (m, 2H), 2.00-1.76 (m, 5H), 1.59-1.03 (m, 19H), 1.00 (s, 3H, CH_3[17]), 0.97-0.93 (m, 2H), 0.91-0.90 (d, *J* = 6.5 Hz, 3H, CH_3[8]), 0.86-0.85 (dd, *J* = 6.6 Hz, 1.6 Hz, 6H, CH_3[1/2]), 0.67(s, 3H, CH_3[14]).

^{3}C {^{1}H} NMR (101 MHz, $CDCl_3$) δ 156.54 (1C, OC[28]), 139.90 (1C, C[20]), 123.11/122.55 (1C, C[21]), 100.03/97.50 (1C, C[34 *anomeric*]), 79.82 (1C, C[39]), 74.66 (1C, C[25]), 72.15 (1C, C[32]), 71.00 (1C, C[35]), 70.17 (1C, C[31]), 69.68 (1C, C[36]), 68.11 (1C, C[37]), 61.76 (1C, C[33]), 56.83 (1C, C[9]), 56.21 (1C, C[12]), 50.16 (1C, C[16]), 42.61 (1C, C[13]) 40.82 (1C, C[30]), 39.8 (1C, C[4]), 39.76 (2C, C[18/24]), 38.69 (1C, C[22]), 37.12 (1C, C[27]), 36.83 (1C, C[6]), 36.33 (1C, C[7]), 35.87 (1C, C[15]), 32.04 (1C, C[19]), 28.37 (1C, C[26]), 28.30(1C, C[3]), 28.16 (1C, C[10]), 24.39 (1C, C[11]), 24.03 (1C, C[4]), 23.08 (1C, C[1]), 22.71 (1C, C[2]), 21.10 (1C, C[17]), 19.43 (1C, C[23]), 18.86 (1C, C[8]), 12.11 (1C, C[14]).

2.3.8 Cholesterol-(2-ethylethoxycarbamate) 2-bromopropionyl ester **(15)**

A solution of alcohol **(11)** (7.43 g, 13.0 mmol) and Et_3N (2.20 ml, 15.6 mmol) in CH_2Cl_2 (30 mL) was cooled down to 0 °C and 2-bromo propionyl bromide (1.06 mL, 15.0 mmol) was added dropwise. The mixture was left to react at room temperature

under stirring overnight, then quenched with CH_3OH (5 mL). The solvents were removed under reduced pressure, and the residue was dissolved in Et_2O (200 mL). The organic phase was washed 3 times with diluted aqueous H_2SO_4 (3 x 200 mL pH=3). The organic layer was dried over $MgSO_4$ and, after filtration, the solvent was evaporated under reduced pressure. The crude was purified by flah column chromatography on SiO_2 (10% Et_2O in petroleum ether) to give pure **(15)** (6.46 g, 9.90 mmol, 76.2%) as a colorless oil.

^{1}H NMR (400 MHz, $CDCl_3$) δ 5.37 (d, *J* = 5.1 Hz, 1H, C=CH), 5.01 (s, 1H, OCONH), .49 (m, 1H, OCH), 4.43-4.38 (q, *J* = 6.9 Hz, 1H, CHBr), 4.27 (m, 2H, OCH_2CH_2O), 3.69 (t, *J* = 4.7 Hz, 2H, CH_2OCH_2), 3.56 (t, *J* = 5.0 Hz, 2H, CH_2OCH_2), 3.38 (q, *J* =4.7 Hz, 2H, $NHCH_2CH_2O$), 2.38-2.24 (m, 2H), 2.02-1.92 (m, 2H), 1.91-1.78 (m, 2H, including at 1.82-1.80 d, 3H, *J* = 6.9 Hz, CH_3CHBr), 1.68-1.04 (m, 19H,), 1.01 (s, 3H, CH_3[23]), 0.98-0.94 (m, 2H), 0.92-0.90 (d, 3H, *J* = 6.6 Hz, CH_3[8]), 0.87- 0.85 (dd, 6H, *J* = 6.6 Hz, 1.6 Hz, CH_3[1/2]), 0.67 (s, 3H, CH_3[14]).

^{13}C {^{1}H} NMR (101 MHz, $CDCl_3$) δ 170.42 (1C, OC[34]), 156.25 (1C, OC[28]), 140.06 (1C, C[21]), 122.62 (1C, C[20]), 74.57 (1C, C[25]), 70.31 (1C, C[32]), 68.68 (1C, C[31]), 64.91 (1C, C[33]), 56.84 (1C, C[9]), 56.29 (1C, C[12]), 50.17 (1C, C[16]), 42.47 (1C, C[13]), 40.76 (1C, C[30]), 39.93 (1C, C[4]), 39.89 (2C, C[18/24]), 39.67 (1C, C[35]) 38.72 (1C, C[22]), 37.14 (1C, C[27]), 36.72 (1C, C[6]), 36.33 (1C, C[7]), 35.94 (1C, C[15]), 32.06 (1C, C[19]), 28.38 (1C, C[26]), 28.32 (1C, C[3]), 28.16 (1C, C[10]), 24.44 (1C, C[11]), 23.98 (1C, C[5]), 22.97 (1C, C[1]), 22.71 (1C, C[2]), 21.73 (1C, C[36]), 21.19 (1C, C[17]), 19.48 (1C, C[23]), 18.87 (1C, C[8]), 12.01 (1C, C[14]).

ESI-TOF Mass spectrometry: expected m/z $[M+Na]^+$ 674.34, found 674.34 (14.5%), 676.33 (15.1%) u.m.a.

2.3.9 Cholesterol-10-methyl-1,9-dioxo-12-thioxo-5,8-dioxa-15,16-dihydroxy-11,13-dithia-2-azahexadecane **(16)**

Trithiocarbonylglycerol sodium salt was kindly gifted by Dr. Francesca Mastrotto. Compound **(15)** (1.39 g, 2.14 mmol) was dissolved in acetone (10 mL). Separately, trithiocarbonlylglycerol sodium (0.530 g, 2.57 mol) was dissolved in acetone (2 mL) and 15-crown-5 (0.51 mL, 2.57 mmol) was added to improve its solubility. This solution was added to the cholesterol bromide solution, and the resulting mixture was left to react at room temperature for 4 hours. The solvent was evaporated under reduced pressure, and the crude misture was purified by column chromatography on SiO_2 (Et_2O) to give pure **(16)**, (0.50 g, 0.66 mmol, 31%) as a yellow oil.

^{1}H NMR (400 MHz, Acetone-d_6) δ 6.06 (s, 1H, OCONH), 5.39 (d, *J* = 4.7 Hz, 1H, C=CH), 4.85 (q, *J* = 7.3 Hz, 1H, CH[35]), 4.42 (m, 1H, CH[25]), 4.29 (m, 2H, CH_2[33]), 3.98-3.88 (m, 2H, CH_2[40]), 3.79-3.74 (m, 1H, CH[39]), 3.70 (t, *J* = 4.7 Hz, 2H, CH_2[38]), 3.60 (t, 2H, *J* = 5.6 Hz, CH_2[33]), 3.55 (t, 2H, *J* = 5.6 Hz, CH_2[31]), 3.30 (m, 2H, CH_2[30]), 2.40-2.30 (m, 2H), 2.38-2.24 (m, 4H), 2.04-1.80 (m, 5H), 1.61 (d, *J* = 6.9 Hz, 3H, C*H*$_3$CH [36]), 1.60-1.02 (m, 19H), 1.03 (s, 3H, CH_3[23]), 1.01-0.93 (m, 2H), 0.92-0.90 (d, *J* = 6.6 Hz, 3H, CH_3[8]), 0.87-0.85 (dd, *J* = 6.6 Hz, 1.6 Hz, 6H, CH_3[1/2]), 0.68 (s, 3H, CH[14]).

^{13}C {^{1}H} NMR (101 MHz, Acetone-d_6) δ 223.85 (1C, SCS[37]), 171.53 (1C, OC[34]), 156. 99 (1C, OC[28], 140.23 (1C, C[21], 123.05 (1C, C[20]), 74.60 (1C, C[25]), 71.00 (1C, C[39]), 70.73 1C, C[32]), 69.34 (1C, C[31]), 66.10 (1C, C[40] 57.76 (1C, C[33]), 57.21 (1C, C[12]), 51.23, 49.06 (1C, C[16]), 43.32 (1C, C[38]), 41.98 (1C, C[13]), 41.47 (1C, C[30]), 40.85 (1C, C[4]), 40.43 (2C, C[18,24]), 39.90 (1C, C[35]), 39.62 (1C, C[22]), 38.08 (1C, C[27]), 37.52 (1C, C[6]), 37.14(1C, C[7]), 36.79 (1C, C[15]), 32.79 (1C, C[19]),

29.15(1C, C[26]), 29.10(1C, C[3]), 28.86 (1C, C[10]), 25.11 (1C, C[11]), 23.27 (1C, C[5]), 23.02 (1C, C[1]), 22.00 (1C, C[2]), 19.89 1C, C[17]), 19.27 (1C, C[23]), 17.32 1C, C[8]), 15.85 (1C, C[36]), 12.39 (1C, C[14]).

2.3.10 Synthesis of sodium 3-(trithiocarboxyl)propane-1-sulfonate **(17)**

In a 500 mL round bottom flask, sodium 3-mercapto-1-propanesulfonate (10.18 g, 57.10 mmol) was dissolved in acetonitrile (100 mL). The solution was cooled down to 0 °C, and NaH (60% w/w in mineral oil, 1.370 g, 57.10 mmol) was slowly added portionwise. CS_2 (17.40 g, 13.74 mL, 228.9 mmol) was then added dropwise, and the reaction solution turned bright yellow almost instantaneously. The reaction was left under stirring overnight at room temperature. The reaction solution was then added to Et_2O (200 mL) under stirring to precipitate compound **(17)**, which was isolated as a yellow-orange solid by filtration (15.12 g, 54.72 mmol, 96%), and used for the subsequent step without further purification.

^{1}H NMR (400 MHz, D_2O) δ 3.32 (t, J = 7.2 Hz, 2H, $CH_2CH_2CH_2SC(S)$), 3.03 (m, 2H, $CH_2CH_2CH_2SC(S)$), 2.13 (m, 2H, $CH_2CH_2CH_2SC(S)$).

^{13}C {^{1}H} NMR (101 MHz, D_2O) δ 246.72 (1C, SC(S)S), 50.00 (1C, $SCH_2CH_2CH_2SC(S)$), 39.55 (1C, $CH_2CH_2CH_2SC(S)$), 23.49 (1C, $SCH_2CH_2CH_2S(S)$).

2.3.11 Sodium 1-(cholesterol)-10-methyl-1,9-dioxo-12-thioxo-5,8-dioxa-11,13-dithia-2-azahexadecane-16-sulfonate **(18)**

Compound **(15)** (1.63 g, 2.50 mmol) was dissolved in acetone (10 mL). Separately, compound **(17)** (0.83 g, 3.0 mol) was dissolved in acetone (5 mL) and 15-crown-5 (1.4

mL, 7.2 mmol) was added to improve its solubility. This solution was transferred in the cholesterol bromide **(15)** solution, and the resulting mixture was left to react at room temperature for 4 hours. The solvent was evaporated under reduced pressure and the residue was purified by flash column chromatography on SiO_2 (20% CH_3OH in EtOAc) to give, after removal of solvent under reduce pressure, pure **(18)** (1.48 g, 1.41 mmol, 57%) as a yellow waxy solid.

^{1}H NMR (400 MHz, $CDCl_3$) δ 5.37 (t, *J* = 4.7 Hz, 1H, C=CH), 5.09 (s, 1H, OCONH), 4.85-4.79 (q, *J* = 6.9 Hz, 1H, CHS), 4.49 (m, 1H, OCH), 4.29 (t, *J* = 4.7 Hz, 2H, OCH_2CH_2O), 3.67 (t, *J* = 5.0 Hz, 2H, OCH_2CH_2O), 3.55 (m, 4H, CH_2OCH_2 and (S)SCSCH_2), 3.36 (q, *J* =4.8 Hz, 2H, $NHCH_2CH_2O$), 2.97 (t, *J* = 7.2 Hz, 2H, CH_2[40]), 2.40-2.30 (m 2H), 2.38-2.24 (m, 4H), 2.04-1.80 (m, 5H), 1.82 (d, *J* = 6.9 Hz, 3H, C[36]), 1.60-1.02 (m, 19H), 1.03 (s, 3H, CH_3[23]), 1.01-0.93 (m, 2H), 0.92-0.90 (d, *J* = 6.6 Hz, 3H, CH_3[8]), 0.87-0.85 (dd, *J* = 1.6 Hz, 6.6 Hz, 6H, CH_3[1/2]), 0.68 (3H, s, CH_3[14]). (3.07 crown ether).

^{13}C {^{1}H} NMR (101 MHz, $CDCl_3$) δ 221.73 (1C, SCS[37]), 171.16 (1C, OC[34]), 156.35 (1C, OC[29], 140.01 (1C, C[21]), 122.54 (1C, C[20]), 74.46 (1C, C[25]), 70.22(1C, C[32]), 68.73 (1C, C[31]), 64.78 (1C, C[33]), 56.79 (1C, C[9]), 56.30 (1C, C[12]), 50.18 (1C, C[16]), 49.92 (1C, C[40]), 48.14 (1C, C[38], 42.41 (1C, C[13]), 40.72 (1C, C[30]), 39.92 (1C, C[4]), 39.61 (2C, C[18/24]), 38.84 (1C, C[35]), 38.59 (1C, C[22]), 37.10 (1C, C[27]), 36.67 (1C, C[6]), 36.28 (1C, C[7]), 35.89 (1C, C[15]), 31.97 (1C, C[19]), 29.38 (1C, C[26]), 28.33 (1C, C[3]), 28.00 (1C, C[10]), 24.47 (1C, C[11]), 24.09 (1C, C[39]), 23.94 (1C, C[5]), 22.92 (1C, C[1]), 22.62 (1C, C[2]), 21.15 1C, C[17]), 19.45 (1C, C[23]), 18.87 (1C, C[8]), 16.94 (1C, C[36]), 11.97 (1C, C[14]). [69.06 crown ether]

2.3.12 2'-acrylamidoethyl-2,3,4,6-tetra-O-acetyl-β-D-galactopyranoside **(19)**

In a 250 ml flask, β-D-galactose pentaacetate (10.00 g, 25.62 mmol) and *N*-hydroxyethyl acrylamide (4.42 g, 38.0 mmol) were mixed together, and chloroform (50.0 mL) was added to completely dissolve the mixture. Using a dropping funnel, $BF_3{\cdot}Et_2O$ (5.45 g, 4.90 mL, 38.4 mmol) was added dropwise to the reaction mixture to give a biphasic mixture which was ultrasonicated for 1 hour, then left under stirring at room temperature. The reaction was monitored by ^{13}C NMR, by following the disappearance of the anomeric carbon of β-D-Galactose pentaacetate starting material at 92 ppm, and the appearance of that of the desired 2'-acrylamidoethyl-galactopyranoside product at 99.7 ppm. Over the following 2 days, 1.5 eq (5ml) + 1 eq (3ml) + 1eq (3ml) of $BF_3{\cdot}Et_2O$ were sequentially added to push the reaction to 100% conversion. The reaction mixture eventually became dark brown and monophasic, and galactose pentaacetate starting material could no longer be detected by ^{13}C NMR. Chloroform (50 mL) was added to the reaction mixture and the organic phase was washed 3 times with 100 ml of aqueous $NaHCO_3$. The organic layer was dried over $MgSO_4$ and, after filtration, the solvent was evaporated under reduce pressure. The crude yellow oily residue was purified by flash chromatography on SiO_2 (50-100% Et_2O in petroleum) to give pure **(19)**, (7.28 g, 16.3 mmol, 63%) as a pale yellow oil.

^{1}H NMR (400 MHz, DMSO) δ 8.11 (t, *J* = 5.4 Hz, 1H, NH), 6.26- 6.19 (dd, *J* = 10.1 Hz, 1H, 17.1 Hz, C*H*=CH_2), 6.09-6.04 (dd, *J* = 17.1, 2.3 Hz, 1H, CH=C*H*$_2$ [*trans*]), 5.59-5.56 (dd, *J* = 10.0, 2.3 Hz, 1H, Hz, CH=CH_2 [*cis*]), 5.25-5.24 (d, *J* = 3.8 Hz, 1H, CH), 5.16-5.13 (dd, *J* = 10.4, 3.6 Hz, 1H, CH), 4.95-4.91(dd, *J* = 10.4, 8.0 Hz, 1H, CH), 4.73-4.71 (d, *J* = 8.0 Hz, 1H, CH *anomeric*), 4.19 (t, *J* = 6.4 Hz, 1H, $CHOCH_2$), 4.05-4.03 (m, 2H, CH_2OAc), 3.76-3.55 (m, 2H, OC*H*$_2$$CH_2NH$), 3.29 (m, 2H,

OCH_2CH_2NH), 2.11 (s, 3H, CH_3), 2.00 (s, 3H, CH_3), 1.99 (s, 3H, CH_3), 1.91 (s, 3H, CH_3).

^{13}C {^{1}H} NMR (101 MHz, DMSO) δ 169.91 (1C, CO), 169.87 (1C, CO), 169.47 (1C, CO), 169.12 (1C, CO), 164.74 (1C, CONH), 131.62 (1C, $CH=CH_2$), 125.09 (1C, $CH=CH_2$), 99.98 (1C, CH *anomeric*), 70.27 (1C, CH), 69.89 (1C, CH), 68.53 (1C, OCH_2CH_2N) 67.65, (1C, CH), 67.39 (1C, CH), 61.27 (1C, CH_2OAc), 38.67 (1C, CH_2NH), 20.47 (2C, CH_3), 20.38 (1C, CH_3), 20.31 (1C, CH_3).

ESI-TOF Mass spectrometry: expected m/z $[M+Na]^+$ 468.15, found 468.15 (100%).

2.3.13 2'-acrylamidoethyl -β-D-galactopyranoside **(20)**

Compound **(19)** (3.64 g, 8.17 mmol) was dissolved in CH_3OH (50.0 mL) and solid KOH (0.050 g, 0.891 mmol) was added. The reaction mixture was left under stirring overnight at room temperature, then solvent was removed under reduced pressure. The crude yellow oil residue was purified by flash chromatography on SiO_2 (25% CH_3OH in EtOAc), to give pure monomer (20) (1.89 g, 6.80 mmol, 83.2%) as a pail yellow oil.

^{1}H NMR (400 MHz, DMSO-d_6) δ 8.11 (t, J = 5.5 Hz, 1H, NH), 6.28-6.21 (dd, J = 17.1, 10.1 Hz, 1H, $CH=CH_2$), 6.10-6.05 (dd, J = 17.1, 2.3 Hz, 1H, $CH=CH_2$ [*trans*]), 5.60-5.57 (dd, J = 10.1, 2.2 Hz, 1H, $CH=CH_2$ [*cis*]), 4.87 (d, J = 2.6 Hz, 1H, OH) 4.75 (s, 1H, OH), 4.62 (t, J = 5.4 Hz, 1H, CH_2OH), 4.39 (d, J = 4.4 Hz, 1H, OH), 4.09 (d, J = 7.0 Hz, 1H, CH *anomeric*), 3.77-3.72 (m, 1H), 3.62 (s, 1H), 3.54-3.46 (m, 3H), 3.37-3.25 (m, 5H).

^{13}C {^{1}H} NMR (101 MHz, DMSO-d_6) δ 164.76 (1C, CONH), 131.71 (1C, $CH=CH_2$), 125.27 (1C, $CH=CH_2$), 103.79 (1C, CH *anomeric*), 75.31 (1C, CH), 73.33 (1C, CH), 70.61

(1C, CH), 68.20 (1C, O*C*H$_2$CH$_2$N), 67.76 (1C, CH), 60.55 (1C, CH$_2$), 38.96 (1C, *C*H$_2$NH).

ESI-TOF Mass spectrometry: expected m/z $[M+Na]^+$ 300.10, found 300.10 (100%).

2.3.14 2'-acrylamidoethyl-2,3,4,6-tetra-O-acetyl-α-D-mannopyranoside **(21)**

In a 250 ml flask, α-D-mannose pentaacetate (5.00 g, 12.8 mmol) and *N*-hydroxyethyl acrylamide (1.85 g, 15.6 mmol) were mixed together, and anhydrous acetonitrile (50.0 mL) was added to completely dissolve the mixture. Using a dropping funnel, $BF_3{\cdot}Et_2O$ (11.1 g, 9.80 mL, 78.2 mmol) was added dropwise to the reaction mixture, then left under stirring at room temperature. The reaction was monitored by ^{13}C NMR ($CDCl_3$) by following the disappearance of the anomeric carbon of α-D-mannose pentaacetate starting material at 90.7 ppm, and the appearance of that of the desired 2'-acrylamidoethyl-galactopyranoside product at 97.9 ppm. Dichloromethane (100 mL) was added to the reaction mixture and the organic phase was washed 3 times with 100 mL of aqueous $NaHCO_3$. The organic layer was dried over $MgSO_4$ and, after filtration, the solvent was evaporated under reduce pressure. The crude yellow oil residue was purified by flash chromatography on SiO_2 (20%-60% EtOAc in petroleum), to give pure **(21)** (4.60 g, 10.3 mmol, 80.5%), as a colorless oil.

^{1}H NMR (400 MHz, DMSO) δ 8.30 (t, *J* = 5.5 Hz, 1H, NH), 6.28-6.21 (dd, *J* = 17.1, 10.1 Hz, 1H, C*H*=CH$_2$), 6.11-6.06 (dd, *J* = 17.1, 2.3 Hz, 1H, CH=C*H*$_2$ [*trans*]), 5.61-5.58 (1H, *J* = 10.1, 2.3 Hz, dd, CH=CH$_2$ [*cis*]), 5.15-5.09 (m, 3H, CH), 4.88 (d, *J* = 1.4 Hz, 1H, CH *anomeric*), 4.14 (dd, *J* = 12.3, 5.4 Hz, 1H, CH), 4.03-3.96 (m, 2H, CH$_2$OAc), 3.70–3.51 (m, 2H, OC*H*$_2$CH$_2$NH), 3.37-3.34 (m, 2H, OCH$_2$C*H*$_2$NH), 2.11 (s, 3H, CH$_3$), 2.02 (s, 3H, CH$_3$), 2.01 (s, 3H, CH$_3$), 1.94 (s, 3H, CH$_3$).

^{13}C {^{1}H} NMR (101 MHz, DMSO) δ 170.02 (1C, CO), 169.60 (1C, CO), 169.56 (1C, CO), 169.47 (1C, CO), 164.79 (1C, CONH), 131.57 (1C, *C*H=CH$_2$), 125.17 (1C, CH=*C*H$_2$), 99.66 (1C, CH *anomeric*), 68.68 (1C, CH), 68.66 (1C, CH), 67.85 (1C, O*C*H$_2$CH$_2$N), 65.41(1C, CH), 61.83 (1C, CH$_2$OAc), 38.35 (1C, *C*H$_2$NH), 20.59 (1C, CH$_3$), 20.47 (1C, CH$_3$), 20.44 (1C, CH$_3$), 20.40 (1C, CH$_3$).

ESI-TOF Mass spectrometry: expected m/z [M+Na]$^+$ 468.15, found 468.15 (100%).

2.3.15 2'-acrylamidoethyl-α-D-mannopyranoside **(22)**

Compound **(21)** (4.60 g, 10.3 mmol) was dissolved in CH$_3$OH (20.0 mL) and KOH (0.120 g, 2.14 mmol) was added. The reaction mixture was left under stirring overnight at room temperature. The solvent was removed under reduced pressure, and the crude yellow oil residue was purified by flash chromatography on SiO$_2$ (25% CH$_3$OH in EtOAc) to give pure monomer **(22)** (2.12 g, 7.64 mmol, 74.3%) as a colorless oil.

^{1}H NMR (400 MHz, DMSO-d$_6$) δ 8.14 (t, *J* = 5.4 Hz, 1H, NH), 6.27-6.20 (dd, *J* = 17.1 Hz, 10.1 Hz, 1H, C*H*=CH$_2$), 6.10-6.05 (dd, *J* = 17.1, 2.3 Hz, 1H, CH=C*H*$_2$ [*trans*]), 5.59-5.56 (dd, *J* = 10.1, 2.3 Hz, 1H, CH=CH$_2$ [*cis*]), 4.70–4.69 (2 s, 2H, 2 x OH), 4.62 (d, *J* = 1.5 Hz, 1H, CH *anomeric*), 4.55 (s, 1H, OH), 4.48 (t, *J* = 5.8 Hz, 1H, CH$_2$O*H*), 4.67-3.57 (m, 3H), 3.62 (s, 1H), 3.47-3.26 (m, 7H – overlapping H$_2$O signal).

^{13}C {^{1}H} NMR (101 MHz, DMSO-d$_6$) δ 164.71 (1C, CONH), 131.69 (1C, *C*H=CH$_2$), 125.13 (1C, CH=*C*H$_2$), 100.00 (1C, CH *anomeric*), 74.04 (1C, CH), 70.90 (1C, CH), 70.25 (1C, CH), 66.98 (1C, O*C*H$_2$CH$_2$N), 65.36 (1C, CH), 61.24 (1C, CH$_2$), 38.55 (1C, *C*H$_2$NH).

ESI-TOF Mass spectrometry: expected m/z [M+Na]$^+$ 300.10, found 300.10 (100%).

2.3.16 RAFT polymerisation of cholesterol-$(HEAm)_{25}$ **(23)**

HEAm (0.143 g, 1.25 mmol), cholesterol RAFT agent **(18)** (47 mg, 0.057 mmol) and 2,2'-azobis[2-(2-imidazolin-2-yl)propane] dihydrochloride (VA-044) (0.2 mg, 0.6 μmol, added as an aliquot taken from a stock solution 2 mg/mL in water) were dissolved in H_2O (494 μL) and toluene (494 μL), and the resulting solution was added to a Schlenk tube, which was then sealed with a rubber septum. The mixture was degassed by Ar bubbling for 30 minutes, after which the Schlenk tube was placed in an oil bath at 100 °C under stirring. The reaction was stopped after 15 min, when 70% monomer conversion, as determined by ^{1}H NMR, was reached. The solution was diluted with CH_3OH and the polymer precipitated in THF. The solid was filtered and dried under vacuum, to yield 41 mg (0.02 mmol, 66% yield) for cholesterol-$(HEAm)_{25}$ **(23)** as a yellow waxy solid. $M_{n(NMR)}$ was calculated by comparing the area of the peak at 0.64 ppm of the three methyl protons of cholesterol chain-end and that of the amide protons peak at 8.28-7.20 ppm of the polymer repeating units.

^{1}H NMR (400 MHz, DMSO) δ 7.62 (br s, 25H, N*H*CH_2CH_2OH), 4.96 (br s, 25H, O*H*), 0.64 (s, 3H, CH_3[Cholesterol]). $M_{n(Theor)}$ = 3.2 kDa, $M_{n(NMR)}$ = 3.7 kDa.

$SEC_{(DMF)}$: M_n = 5.9 kDa; Đ = 1.06.

2.3.17 RAFT polymerisation of glycopolymers

General procedure

Cholesterol RAFT agent **(18)** and desired carbohydrate-containing monomer were dissolved in a mixture of H_2O and toluene (ratio 1 : 2 vol:vol) in a Schlenk tube equipped with a magnetic stirrer. The biphasic solution obtained was sonicated for 5 seconds in order to form an homogeneus dispersion. 2,2'-Azobis[2-(2-imidazolin-2-yl)propane] dihydrochloride (VA-044) in H_2O was added, and the reactor was sealed with a rubber septum. The mixture was degassed by Ar bubbling for 20 minutes at 0 °C using an ice bath, then the Schlenk tube was placed in an pre-heated oil bath at 100 °C under stirring. The reaction was stopped after 20 min. Monomer conversions (p) were calculated from ^{1}H NMR data using the following equation: $p = 1 - (\int I_v / \int I_a / DP_{targeted})$, where $\int I_v$ is the integral of the three vinyl protons from the monomer, $\int I_a$ is the integral of the three methyl protons at 0.64 ppm belonging to the R group of the cholesterol RAFT agent, and $DP_{targeted}$ is the average degree of polymerisation targeted ($DP=[M]_0/[CTA]_0$).

The solution was diluted with a mixure $CHCl_3/CH_3OH$ (1:1 vol/vol ratio) and precipitated twice in THF. The precipitate was then redissolved in water and the solution was purified by dialysis (MWCO: 1 kDa) against water for 6 hours, with two water changes, followed by lyophilisation.

Cholesterol-Gal$_7$ **(24):** 2'-acrylamidoethyl-β-D-galactopyranoside **(20)** (40 mg, 0.14 mmol), Cholesterol RAFT agent **(18)** (15 mg, 0.018 mmol), VA-044 (117 µg, 0.400 µmol, added as an aliquot taken from a stock solution 4 mg/mL in water). H_2O: 72.0 µL, Toluene: 144 µL. (34 mg, 62%).

^{1}H NMR (400 MHz, DMSO-d_6) δ 8.28-7.31 (br s, 7H, N*H*CO), 7.06 (s, 1H, NH [cholesterol]), 5.34 (s, 1H, CH=C [cholesterol]), 5.40–4.21 (4 bs, 28H, O*H*), 4.12 (bs, 7H, CH anomeric), 0.64 (s, 3H, CH_3 [cholesterol]). $M_{n(Theor)}$ = 2.8 kDa, $M_{n(NMR)}$ = 2.7 kDa.

SEC$_{(DMF)}$: M_n = 4.2 kDa; Đ = 1.11.

Cholesterol-Gal$_{14}$ **(25):** 2'-acrylamidoethyl-β-D-galactopyranoside **(20)** (73 mg, 0.26 mmol), Cholesterol RAFT agent **(18)** (16 mg, 0.019 mmol), VA-044 (122 µg, 0.400 µmol added as an aliquot taken from a stock solution 4 mg/mL in water). H_2O: 132 µL, Toluene: 264 µL. (62 mg, 70%).

^{1}H NMR (400 MHz, DMSO-d_6) δ 8.28-7.31 (br s, 14H, N*H*CO), 7.06 (s, 1H, NH [cholesterol]), 5.34 (s, 1H, CH=C [cholesterol]), 5.40 – 4.21 (4 bs, 64H, O*H*), 4.12 (bs, 14H, CH anomeric), 0.64 (s, 3H, CH_3 [cholesterol]). $M_{n(Theor)}$ = 4.7 kDa, $M_{n(NMR)}$ = 4.7 kDa.

SEC$_{(DMF)}$: M_n = 5.4 kDa; Đ = 1.11.

Cholesterol-Man$_7$ **(26):** 2'-acrylamidoethyl-α-D-mannopyranoside **(22)** (94 mg, 0.34 mmol), cholesterol RAFT agent **(18)** (56 mg, 0.067 mmol), VA-044 (436 µg, 1.30 µmol added as an aliquot taken from a stock solution 4 mg/mL in water). H_2O: 168 µL, Toluene: 337 µL. (52 mg, 35%).

^{1}H NMR (400 MHz, DMSO-d_6) δ 7.89-7.22 (br s, 7H, N*H*CO), 7.06 (s, 1H, NH [cholesterol]), 5.34 (s, 1H, CH=C [cholesterol]), 4.76–4.53 (4 bs, 35H, OH and CH *anomeric*), 0.64 (s, 3H, CH_3 [cholesterol]). $M_{n(Theor)}$ = 2.8 kDa $M_{n(NMR)}$ = 2.7 kDa.

SEC$_{(DMF)}$: M_n = 3.9 kDa; Đ = 1.10

MALDI-TOF: expected m/z $[M+Na]^+$ 2791.2, found 2791.3 (100%), (Appendix Figure S50).

Cholesterol-Man14 **(27)**: 2'-acrylamidoethyl-α-D-mannopyranoside **(22)** (98 mg, 0.35 mmol), Cholesterol RAFT agent **(18)** (19 mg, 0.024 mmol), VA-044 (152 µg, 0.500 µmol added as an aliquot taken from a stock solution 4 mg/mL in water). H_2O: 177 µL, Toluene: 353 µL. (39 mg, 27%).

^{1}H NMR (400 MHz, DMSO-d_6) δ 7.89-7.12 (br s, 14H, N*H*CO), 6.90 (s, 1H, NH [cholesterol]), 5.34 (s, 1H, CH=C [cholesterol]), 4.93–4.32 (4 bs, 70H, OH and CH *anomeric*), 0.64 (s, 3H, CH_3 [cholesterol]). $M_{n(Theor)}$ = 4.7 kDa, $M_{n(NMR)}$ = 4.7 kDa.

SEC$_{(DMF)}$: M_n = n.d.; Đ = n.d.

2.4 Results and Discussion

2.4.1 Synthesis of linear aliphatic monoglycosides

In the initial part of this work, four different alkyl glycoside amphiphilic molecules (Scheme 1) were designed and synthesised to investigate how the presence of a spacer between a carbohydrate moiety and the liposome surface would affect the affinity of mannosylated liposomes with a model mannose-binding lectin, concanavalin A (Con A) (results discussed in Chapter 3.4.1). Our working hypothesis, supported by early works of Engel *et al.* (Engel *et al.* 2003), (Engel *et al.* 2003) was that the presence of a spacer would improve exposure of the carbohydrate ligands at the outer surface of liposomes (Figure 12), facilitating their interaction with sugar-binding proteins (lectins).

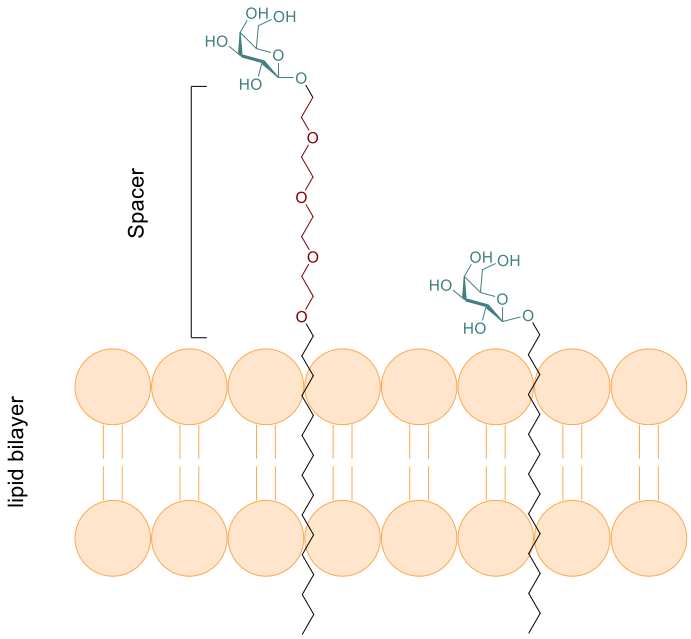

Figure 12 – Membrane exposure of different monoglycoside ligands: (left) ligand with tetraethylglycol spacer separating the sugar from the membrane; (right) ligand laying at the surface of liposomal membrane.

The alkyl glycoside molecules were designed to incorporate a hydrophilic carbohydrate head and a membrane-inserting hydrophobic palmitoyl chain (C16) to anchor the

chosen glycoligand to the liposomal phospholipid bilayer. The hydrophilic head included two different sugars, α-mannose (Man) and β-galactose (Gal), with the latter that was used as a negative control for all the binding studies due to its inability to bind the mannose-binding model lectin (Con A) utilised for this part of our study (discussed in Chapter 1.2.3.1).

The synthetic strategy utilised to prepare the required monovalent glycolipids is illustrated in Scheme 1.

Pentaacetate galactose and mannose starting materials are both commercially available. However, due to its excessive cost, at this stage of the work mannose pentaacetate **(1)** was synthesised from D-mannose and acetic anhydride, using I_2 as a catalyst, as described by Field and co-workers (Mukhopadhyay *et al.* 2004), (Kartha and Field 1997).

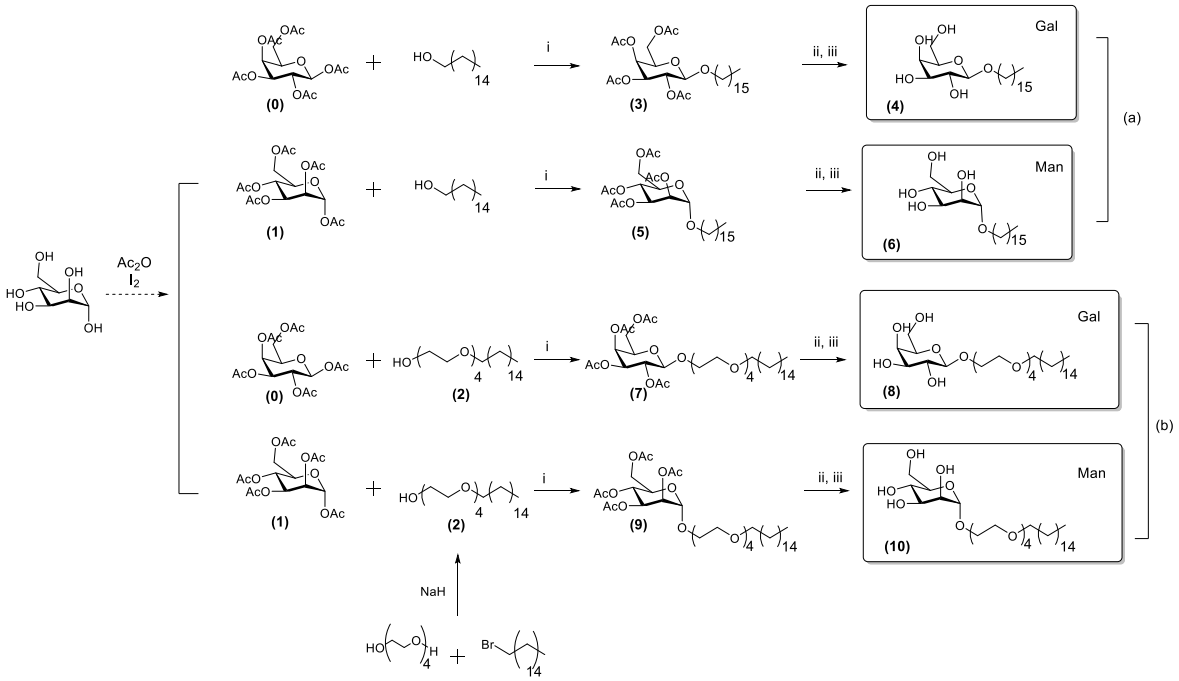

Scheme 1 - Synthetic routes to alkyl monoglycosides **(4)**, **(6)**, **(8)** and **(10)**. Reagents and Conditions: (i) $BF_3{\cdot}Et_2O$, CH_2Cl_2 0°C to RT; (ii) K_2CO_3, CH_3OH: (iii) Amberlite IR120-H^+.

From galactose- **(0)** and mannose-pentaacetate **(1)**, a range of alkyl glycosides were prepared by reaction with an appropriate alkyl alcohol, and $BF_3{\cdot}OEt_2$ as a Lewis acid. Gal and Man glycosides **(3)** and **(5)**, with monosaccharides directly linked to the lipid anchor, were prepared from sugar pentaacetate and 1-hexadecanol, followed by K_2CO_3/CH_3OH-catalysed removal of the acetate protecting groups.

For the synthesis of Gal and Man glycosides **(7)** and **(9)**, which present a hydrophilic tetra(ethylene glycol) (TEG) spacer between the sugar unit and the hydrophilic anchor, TEG-palmitoyl alcohol **(2)** was first prepared by reaction of tetra(ethylene glycol) with NaH and hexadecyl bromide, under solvent-free conditions, followed by purification by SiO_2 flash chromatography, to remove traces of bis-alkylated side-product and residual TEG starting material. The subsequent steps were analogous to those

optimised for the synthesis of glycosydes **(3)** and **(5)**, that is, glycosylation followed by base-catalysed deprotection of the acetate protecting groups.

For all four $BF_3{\cdot}OEt_2$ mediated glycosylation reactions, a near-perfect control over the stereochemistry of the anomeric centre of the desired glycosides was observed. This is believed to occur via anchimeric assistance (participation by neighbouring group) of the acetyl group in C2 position, which by coordinating a carbocationic anomeric intermediate, reduces the accessibility of one of the two faces of the anomeric centre, leading to selective formation of α mannose and β galactose alkylglycosides (Wang *et al.* 2010). The reactions were monitored by ^{13}C NMR, by following the shifting of the anomeric signals from ~ 90 ppm to ~100-110 ppm.

The intermediate compounds **(3)**, **(5)**, **(7)** and **(9)** were used directly for the subsequent deacetylation reactions without further purification. Following deprotection, purification by flash chromatography on SiO_2 afforded final glycosides **(6)**, **(8)** and **(10)** which were characterised and utilised to engineer carbohydrate-targeted glycoliposomes, as shown in Chapter 3.

2.4.2 Synthesis of cholesterol-based mannose monoglycoside **(14)**

It has been proved that a minimum spacer length of 2 ethylene glycol units is required to achieve detectable binding between liposomal mannose ligands and Con A (Jones 1994). Thus, compound **(11)** (shared intermediate for the synthesis of cholesterol derivate **(15)**, **(16)** and **(18),** Scheme 4) was specifically designed with an ethylethoxy spacer (Scheme 2). Compound **(11)** was synthesised by conjugation of commercially available cholesteryl chloroformate with 2-(2-aminoethoxy) ethanol. The reaction was conducted in CH_2Cl_2 at 0 °C in the presence of Et_3N and the resulting cholesteryl alcohol intermediate **(11)** was used directly for the next step without further purification.

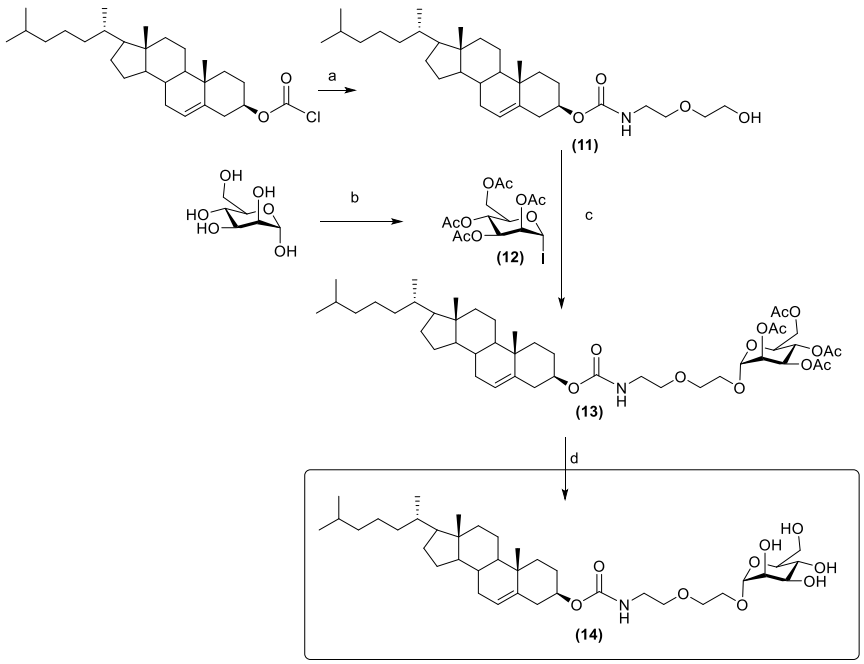

Scheme 2 - Synthesis cholesterol-based mannose monoglycoside **(14)**. *Reagents and Conditions*: a) 2-(2-aminoethoxy)ethanol, CH_2Cl_2, Et_3N, 0°C to RT; b) i: Ac_2O, I_2, ii: CH_2Cl_2, I_2, HMDS; c) anhydrous CH_2Cl_2, Ag_2CO_3; d) K_2CO_3, CH_3OH.

For the synthesis of mannosylated cholesterol **(14)**, a synthetic strategy involving a $BF_3{\cdot}OEt_2$ mediated condensation, under conditions previously utilised for the synthesis of the *O*-alkyl glycosydes prepared in this study, was initially attempted (Scheme 3).

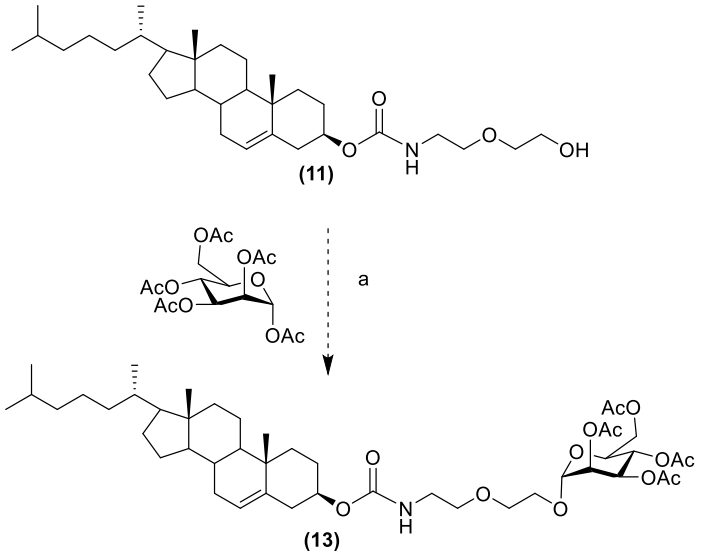

Scheme 3 – Attempted synthetic route to cholesterol-based monoglycoside **(13)**. *Reagents and Conditions:* a) $BF_3{\cdot}Et_2O$, CH_2Cl_2 0°C to RT.

Mannose pentaacetate **(1)** and cholesterol alcohol **(11)** were dissolved in CH_2Cl_2, $BF_3{\cdot}OEt_2$ Lewis acid was added and the mixture was let to react for 2 days. Interestingly, although this synthetic approach successfully allowed to synthesise the palmitoyl monoglycosides (Scheme 1), in this case cholesterol-based monoglycoside **(13)** could not be detected. Therefore a different synthetic approach was carried out via a Koenigs-Knorr reaction, where glycosyl halides are used as glycosyl donors. For this purpose, tetraacetate mannose iodide **(12)** was synthesised in two steps (Scheme 2). Firstly, mannose pentaacetate was generated from D-mannose and acetic anhydride, using I_2 as a catalyst, as described by Field and co-workers (Kartha and Field 1997),

(Mukhopadhyay *et al.* 2004) and the reaction was monitored by TLC. At full completion, additional I_2 and hexamethyldisilane (HMDS) - believed to generate trimethylsilyl iodide activator *in situ*, were added in CH_2Cl_2 and the conversion to 1-iodo-α-D-mannose tetraacetate was found to be complete within 3 hours. The reaction was monitored by ^{13}C NMR following the shifting of the anomeric C signal from 92 to 66.3 ppm. The upfield shift of the anomeric carbon resonance was expected, as it is in agreement with literature data (Gervay-Hague 2016). Compound **(11)** was then dissolved in anhydrous CH_2Cl_2, and Ag_2CO_3 and **(12)** were subsequently added, and the resulting mixture was let to react at room temperature for 24 hours. The presence of a iodide group in position C1 of the protected mannose increases the reactivity of this electrophilic centre, as iodine is a better leaving group than the OAc residue of mannose pentaacetate. Insoluble AgI precipitates in the process, thus shifting the equilibrium of the reaction towards the desired *O*-alkyl glycoside **(13)**. The reaction was monitored by ^{13}C NMR, by following the shifting of the anomeric signal from 62 to ~100 ppm. The intermediate acetylated compound **(13)** was purified by flash chromatography on SiO_2, and isolated in 83% yield. Deacetylation of **(13)** was conducted with K_2CO_3 in CH_3OH. Following deprotection, purification by flash chromatography on SiO_2 afforded the final mannose cholesterol glycoside **(14)**.

2.4.3 Synthesis of cholesterol-based polyglycosides

In this work, short oligosaccharide mimics were synthesised using RAFT (Reversible Addition Fragmentation chain Transfer) polymerisation. This technique is a radical polymerisation reaction which involves an additional component, a chain-transfer agent (CTA, also called RAFT agent) and where irreversible termination reactions directly correspond to the number of radicals initially introduced in the system, hence allowing to produce synthetic polymers with narrow molecular weight distribution, and to control the polymer molecular weight (Boyer *et al.* 2009), (Moad *et al.* 2008), (Perrier 2017).

In this chapter, we exploited a newly developed *ultrafast* version of RAFT radical polymerisation technique (Gody *et al.* 2013), (Gody *et al.* 2014a), (Gody *et al.* 2014b) to precisely control the number of polymer repeating units whilst performing the polymerisation within minutes (Gody *et al.* 2015).

In typical chain growth radical polymerisation, the rate of propagation (R_p) follows the equation $R_p = k_p[M][P\bullet]$, where k_p is the propagation rate coefficient of the monomer, and [M] and [P•] are the concentrations of the monomer and of propagating radicals, respectively. Performing the polymerisation at high temperature and in very polar solvents increases k_p and thus the overall rate of polymerisation. Likewise, when azoinitiators are used as the source of radical species, higher temperatures also increase the concentration of propagating species [P•], thus further accelerating the propagation process. However, this would also increase the rate of termination (R_t), according to the equation $R_t = 2k_t[P\bullet]^2$ resulting in faster bimolecular termination. Perrier's strategy overcomes this limitation by dramatically reducing the proportion of radical initiators, thus increasing the CTA/initiator ratio, and using a thermal initiator which

decomposes very quickly at the polymerisation temperature (azoinitiator VA-044, half-life of 77s at 100 °C). In RAFT polymerisation, which is degenerative transfer (DT) system, the number of dead chains is only governed by the number of radicals generated throughout the polymerisation. Increasing the rate of radical generation will increase the polymerisation rate without affecting the livingness (Gody *et al.* 2014b).

2.4.3.1 Design and synthesis of cholesterol RAFT agents

A RAFT agent is usually a thiocarbonylthio compound (Figure 13). Following reaction with radical species, the R· group can leave the resulting adduct and start the growth of polymeric chains. The Z group activates the thiocarbonyl bond towards radical addition and then stabilises the resultant radical adduct (Moad *et al.* 2008), (Boyer *et al.* 2009). One important feature of RAFT agents is that they dictate the nature of the chemical groups present at the α and ω chain-ends of polymers prepared by RAFT polymerisation, with the R group at one end of the polymer, and the thiocarbonyl-Z residue at the other.

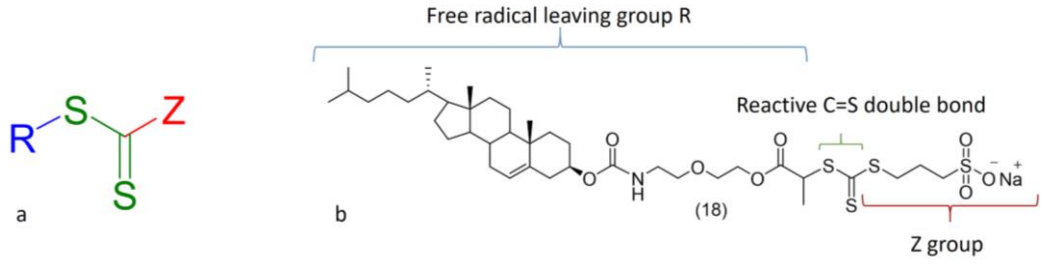

Figure 13 - a) General structure of a RAFT agent; b) structure of cholesterol RAFT agent **(18)**.

In this work, we intended to anchor the glycopolymers (Man/Gal) to the liposomal membrane by using a cholesterol anchor. To this aim, the latter was incorporated in the R group of our RAFT agent (Figure 13b). Accordingly, a synthetic route to a novel RAFT agent **(18)** with the required cholesterol anchor was identified (Scheme 4).

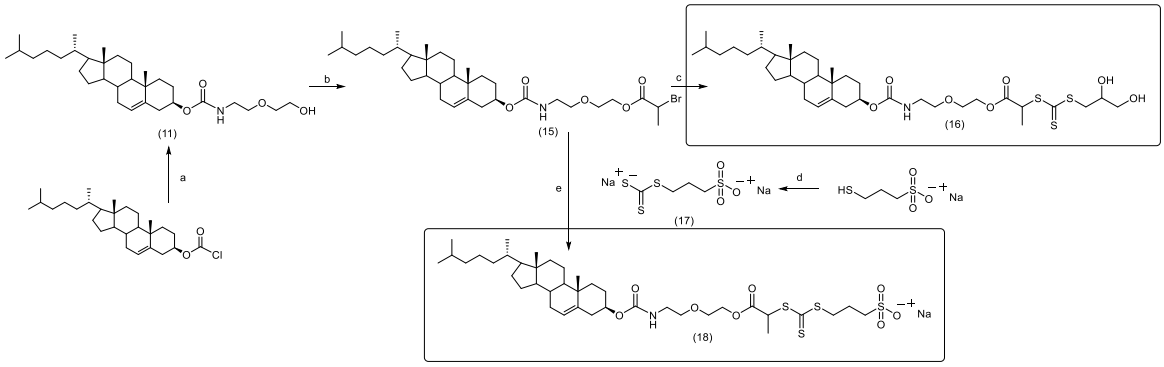

Scheme 4. Synthesis of cholesterol RAFT agents **(16)** and **(18)**. Reagents and Conditions: a) 2-(2-aminoethoxy)ethanol, CH_2Cl_2, Et_3N, 0°C to RT; b) 2-bromo propionyl bromide, CH_2Cl_2, Et_3N, 0°C to RT; c) trithiocarbonylglycerol sodium salt, acetone, 15-crown-5; d) NaH, acetonitrile, CS_2; e) sodium 3-(trithiocarboxyl)propane-1-sulfonate **(17)**, acetone, 15-crown-5.

The *ultrafast* RAFT polymerisation described by Perrier and co-workers is carried out in very polar media, typically in water or water-containing homogeneous mixture of solvents (Gody *et al.* 2015). This technique can allow excellent control over polymer molecular weight, distribution, and chain-end fidelity, even at virtually quantitative monomer conversion. Thus it appeared to be particular suited for the synthesis of the oligomeric carbohydrate ligands required for this study. As cholesterol is known for being very hydrophobic, to ensure a certain level of water solubility to our cholesterol-containing RAFT agents, very hydrophilic Z groups were identified.

From a synthetic perspective, the preparation of amphiphilic molecules is not always trivial, as it involves the conjugation of very hydrophilic species to very hydrophobic

ones. This makes the indentification of reaction media where all these species are sufficiently soluble to allow them to react with each other, very challenging. In this work, in many cases a series of trial-and-error attempts were made to optimise the synthesis of functional CTAs and sugar ligands.

Initial experiments focussed on a thioglycerol Z group. Accordingly, cholesterolpropionyl bromide was synthesised from cholesterol and 2-bromo propionyl bromide. Reaction of the resulting adduct with trithiocarbonylglycerol sodium salt was attempted (Scheme 5).

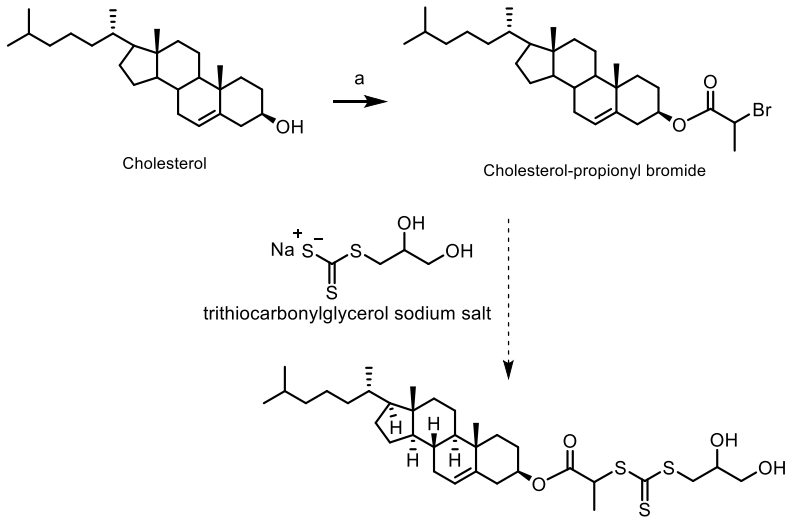

Scheme 5. Attempted synthetic route to cholesterolpropionyl trithioglycerol RAFT agent.

The reactions were conducted in CH_2Cl_2/CH_3OH, but failed to afford the desired RAFT agent. The stability of the trithiocarbonylglycerol sodium salt was investigated in CH_3OH. Surprisingly, we found that trithiocarbonylglycerol sodium salt in CH_3OH led to the formation of two possible degradation products: a dithiocarbamate derivative (degradation product 1, Figure 14) by oxidation induced by the presence of air or a

disulfide derivative (degradation product 2, Figure 14) presumably through initial decomposition of the thrithiocarbonate salt, followed by dimerisation of the resulting thiol by oxidation. This important side reaction may explain the poor success of conjugation under those conditions.

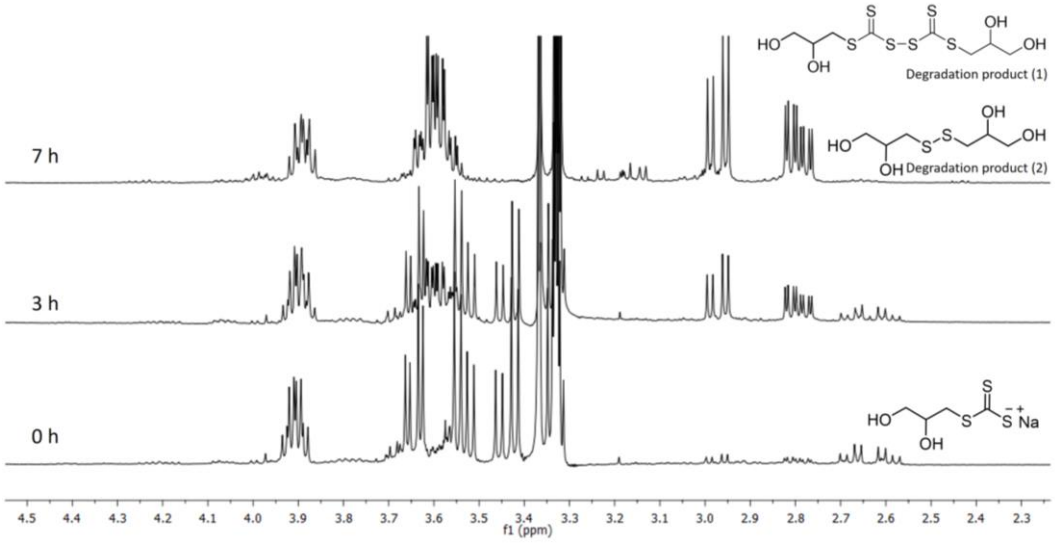

Figure 14 - ^{1}H-NMR spectra showing the time-dependent degradation of trithiocarbonylglycerol sodium salt in CD_3OD, with consequent formation of a dithiocarbamate derivative (degradation product 1) or disulfide derivative (degradation product 2) in 7 hours. Trithiocarbonylglycerol sodium salt was dissolved in CD_3OD and checked by ^{1}H-NMR every hour. The same stability test was carried out dissolving trithiocarbonylglycerol sodium in $(CD_3)_2CO$. Under these conditions trithiocarbonyl-glycerol sodium salt was found stable (data not shown).

Attempts using other solvents - DMSO, THF, acetonitrile, acetone - were carried out, with no success, possibly due to poor solubility of at least one of the two reagents involved in these solvents. Therefore, a new cholesterol alcohol intermediate with better solubility in polar organic solvents was synthesised. Accordingly, compound **(11)** where a polar spacer was introduced in order to reduce the hydrophobicity of the

cholesterol moiety, was prepared from commercially available cholesteryl chloroformate and 2-(2-aminoethoxy)ethanol. **(11)** was then reacted with 2-bromo-proprionyl bromide in the presence of Et_3N, in CH_2Cl_2 to give, after purification, the bromoester **(15)** in 76% yield. Several attempts of conjugation in acetone of compound 15 with trithiocarbonlylglycerol sodium salt were unsuccessful, most likely due to the poor solubility of the sodium salt in acetone. However, the latter issue could be circumvented by using 15-crown-5, which by complexing the Na^+ counterion, increased the solubility of the trithiocarbonylglycerol sodium salt starting material. Under these conditions, cholesterol RAFT Agent **(16)** could be successfully synthesised. The reaction was monitored by ^{1}H NMR following the disappearance of the quartet of the -CHBr residue at 4.44 ppm in the starting material (15), and the appearance of that of the corresponding –CHSC(S)S trithiocarbonyl group at 4.86 ppm. Trithiocarbonyl salt **(17)** was prepared by treating sodium 3-mercapto-1-propanesulfonate with NaH in acetonitrile, followed by addition of CS_2. Compound **(17)** was purified by precipitation in Et_2O since it was found to rapidly degrade under the conditions employed for flash chromatography purification on SiO_2. Reagents **(15)** and **(17)** were separately dissolved in acetone. 15-crown-5 crown ether was added to the reaction mixture of **(17)** to improve its solubility in the organic solvent, then the solution was slowly added to that of the cholesterol bromide **(15)**, and the mixture left under stirring at room temperature for 4 hours.

As for the synthesis of RAFT agent **(16)**, the reaction was monitored by ^{1}H NMR following the shif of the quartet of –CHBr group. The final compound **(18)** was isolated and characterised, with only residual traces of 15-crown-5 left as impurities in

the final RAFT agent, which were still found in the final RAFT agent **(18)** after several purification cycles.

2.4.3.2 Synthesis of carbohydrate-containing monomers

For this work acrylamide-based monomers, a monomer family with high k_p (high $k_p/(k_t)^{1/2}$, where k_p and k_t are the propagation and termination rate coefficients, respectively) (Moad *et al.* 2008), were found to be particularly suited for the chosen *ultrafast* RAFT protocol. The synthesis of the required carbohydrate-containing monomers was carried out following a strategy analogous to that utilised for the synthesis of the monovalent alkyl glycosides. Accordingly, this involved a $BF_3{\cdot}OEt_2$-mediated condensation of either galactose or mannose pentaacetate and *N*-hydroxyethyl acrylamide, followed by base-catalysed deprotection with KOH in CH_3OH.

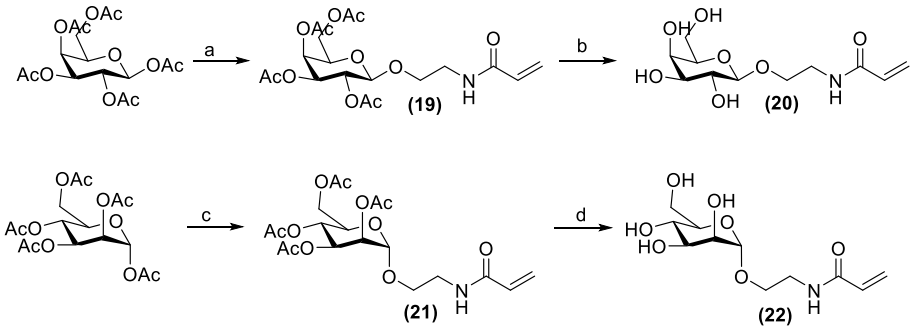

Scheme 6 - Synthesis of galactose **(20)** and mannose **(22)** monomers. *Reagents and Conditions*: a) (i) $BF_3{\cdot}Et_2O$, $CHCl_3$, 1 hour sonication; b) KOH, CH_3OH; c) $BF_3{\cdot}Et_2O$, acetonitrile; d) KOH, CH_3OH.

The synthesis of these carbohydrate-containing monomers was optimised in order to obtain higher yields compared to those of the monovalent alkyl glycosides. Purification of protected acetylated intermediates **(19)** and **(21)** was found to be key to achieve final

overall yields of over 50% for the two steps. The main side-reaction observed in the first step was a transesterification reaction which occurs between the acetate group at the sugar C1 anomeric position, and the hydroxyl functionality of HEAm. The resulting side-products HEAm acetate and mannose/galactose tetraacetate (which were isolated and characterised) and the desired acetylated glycomonomers (Scheme 7) could be separated by flash chromatography whereas utilising the reaction mixture containing the monomer intermediates **(19)** and **(21)** and impurities for the deprotection step led to a mixture of products from which isolation of final monomers **(20)** and **(22)** was found to be particularly challenging.

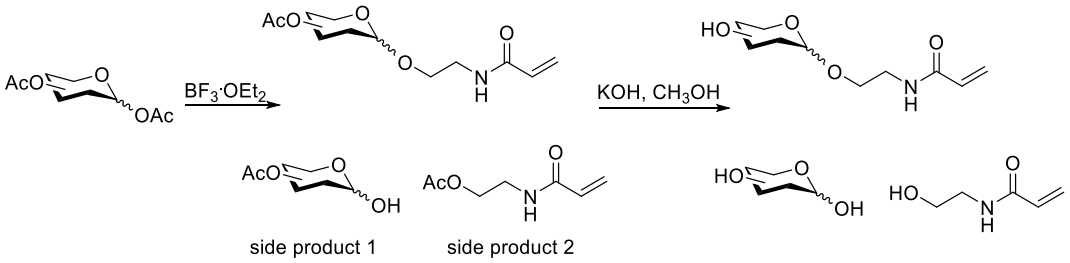

Scheme 7- General synthesis of carbohydrate-containing monomers showing the formation of side products

2.4.3.3 Biphasic ultrafast RAFT polymerisation

An initial series of experiments were required to verify the ability of thiocarbonylthio derivative **(18)** to act as a RAFT chain transfer agent under *ultrafast* RAFT polymerisation, and to identify suitable reaction conditions (*i.e.* monomer concentration and [CTA]/[I] molar ratio) which would allow to reach near-quantitative monomer conversion. Firstly, RAFT polymerisation was performed using

commercially available monomer *N*-hydroxyethyl acrylamide (HEAm). HEAm was dissolved in H_2O and VA-044 initiator was added (Scheme 8).

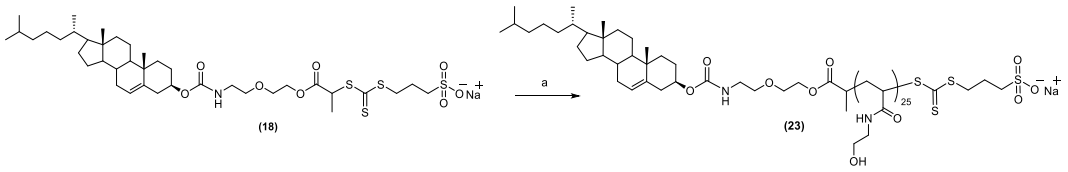

Scheme 8 - Synthesis of cholesterol-terminated $(HEAm)_{25}$. *Reagents and Conditions* a) VA-044, HEAm, H_2O, toluene, 100°C, 15 min.

In a separate vial, cholesterol RAFT agent **(18)** was dissolved in toluene, and the two solutions mixed in a 1:1 vol/vol ratio. The final monomer concentration in water was [HEAm] = 2.0 M (volume of the monomer was taken into account). The biphasic solution was degassed in ice bath by bubbling Argon for 20 minutes. *Ultrafast* RAFT polymerisation was carried out at 100°C in 15 minutes, after which time 70% conversion was reached, as determined by ^{1}H NMR. Polymer **(23)** was recovered by precipitation in THF and analysed by SEC using DMF + 0.1% LiBr as the mobile phase. M_n (SEC): 5.85 kDa and a $Đ$ of 1.05. The theoretical Mn calculated from the initial [monomer]:[RAFT agent] ratio and the reaction conversion, was 2.21 kDa.

Sligthly different conditions were optimised for the *ultrafast* RAFT polymerisation using carbohydrate monomers **(20)** and **(22)** (Scheme 9).

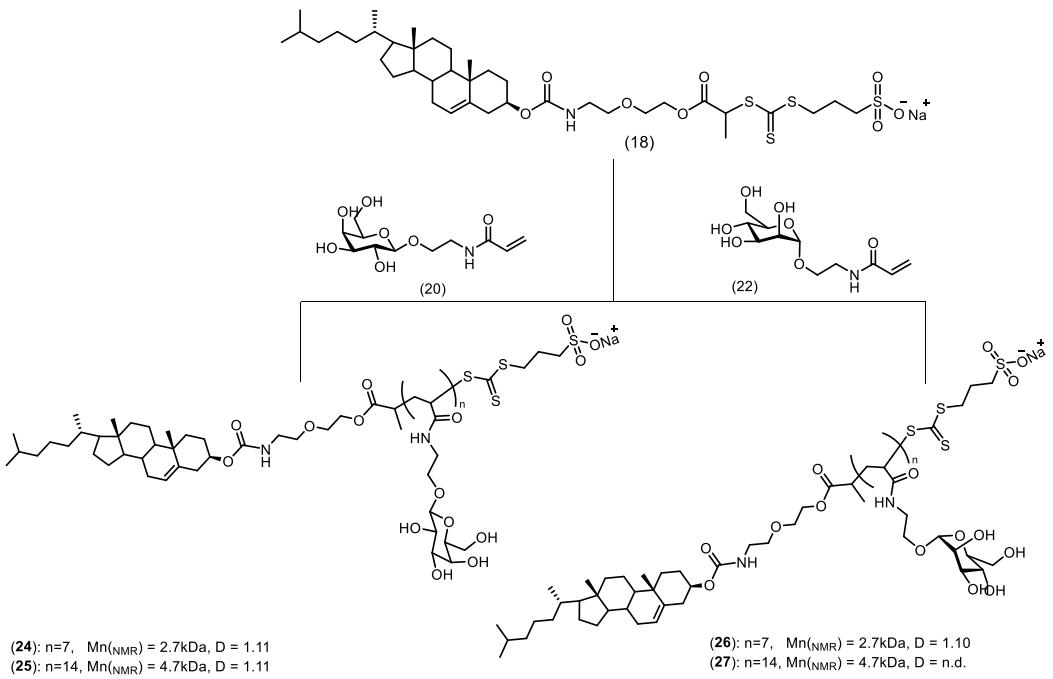

Scheme 9 - Synthesis of cholesterol-terminated galactose **(23)** and **(24)** and mannose **(25)** and **(26)** polyacrylamide glycopolymers. *Reagents and Conditions* a) VA-044, H_2O, toluene, 100°C, 20 min.

Due to the high viscosity of the carbohydrate-monomer, which made it very difficult to accurately measure their volume, the monomer volume was not included for the final monomer concentration, [M] = 2 M. The water/toluene ratio was reduced to 1:2 to allow completely dissolution of cholesterol RAFT agent (18) in the organic phase. The suspension was sonicated for few seconds to allow formation of a more homogeneus dispersion, then the VA-044 in water was added. [CTA]/[I] was reduced to 50, the polymerisation was carried out at 100°C for 20 min. Conversion and SEC analysis data are reported in Table 2.

Table 2 Characterisation and [M]/[CTA]/[I] ratios utilised for the synthesis of cholesterol-terminated galactose and mannose polymers.

Polymer	Code	[M]/[CTA]/[I]	Conversion	$Mn,_{NMR}$[a] (kDa)	$Mn,_{SEC}$[b] (kDa)	Đ
Chol-Gal$_7$	**24**	8 : 1 : 0.02	91%	2.7	4.2	1.11
Chol-Gal$_{14}$	**25**	14 : 1 : 0.02	99%	4.7	5.4	1.11
Chol-Man$_7$	**26**	8 : 1 : 0.02	90%	2.7	3.9	1.10
Chol-Man$_{14}$	**27**	14 : 1 : 0.02	99%	4.7	n.d.	n.d.

[a] calculated by comparing the integrals of the amide protons peak of the sugar repeating unit at 8.28-7.20 ppm, and the methyl peak of cholesterol at 0.64 ppm set as 3; [b] SEC measurents were carried out using DMF + 0.1% LiBr as the mobile phase, and PMMA narrow standards as calibrants.

Glycopolymers **(24)**, **(25)**, **(26)** and **(27)** were precipitated in THF to remove any potentially unreacted cholesterol RAFT agent **(18)**. Residual monomer was removed by dialisys against water.

SEC analysis (Table 1 and Figure S51 in Appendix 6.2) showed that very well-defined glycopolymers were synthesised, indicating good control over the polymerisation process.

2.5 Conclusions

In this chapter, the synthesis of membrane inserting monovalent and multivalent glycoligands has been described. Four monovalent galactose- and mannose- ligands with palmitoyl membrane-inserting moieties, and one monovalent mannose ligand with a cholesterol anchor were successfully synthesised and characterised.

New amphiphilic trithiocarbonyl cholesterol-based RAFT agents were synthesised and successfully utilised to synthesise multivalent cholesterol-terminated mannose and galactose glycopolymers with narrow molecular weight distributions at very high monomer conversion, using adapted Perrier's conditions for *ultrafast* RAFT polymerisation.

2.6 References

Boyer, Cyrille, Volga Bulmus, Thomas P. Davis, Vincent Ladmiral, Jingquan Liu, and Sébastien Perrier. 2009. "Bioapplications of RAFT Polymerization." *Chemical Reviews* 109 (11): 5402–36.

Chen, Peiming, Xiaoping Zhang, Lee Jia, Robert K Prud, Zoltan Szekely, and Patrick J Sinko. 2014. "Optimal Structural Design of Mannosylated Nanocarriers for Macrophage Targeting." *Journal of Controlled Release* 194. Elsevier B.V.: 341–49.

Engel, Andreas, Swapan K. Chatterjee, Ali Al-Arifi, and Peter Nuhn. 2003. "Influence of Spacer Length on the Agglutination of Glycolipid-Incorporated Liposomes by ConA as Model Membrane." *Journal of Pharmaceutical Sciences* 92 (11): 2229–35.

Engel, Andreas, Swapan Kumar Chatterjee, Ali Al-arifi, Dagmar Riemann, Jürgen Langner, and Peter Nuhn. 2003. "Influence of Spacer Length on Interaction of Mannosylated Liposomes with Human Phagocytic Cells." *Pharmaceutical Research* 20 (1): 51–57.

Forssen, Eric, and Michael Willis. 1998. "Ligand-Targeted Liposomes." *Advanced Drug Delivery Reviews* 29 (3): 249–71.

Gervay-Hague, Jacquelyn. 2016. "Taming the Reactivity of Glycosyl Iodides to Achieve Stereoselective Glycosidation." *Accounts of Chemical Research* 49 (1): 35–47.

Gody, Guillaume, Raphael Barbey, Maarten Danial, and Sébastien Perrier. 2015. "Ultrafast RAFT Polymerization: Multiblock Copolymers within Minutes." *Polym. Chem.* 6 (9): 1502–11.

Gody, Guillaume, Thomas Maschmeyer, Per B Zetterlund, and Sébastien Perrier. 2013. "Rapid and Quantitative One-Pot Synthesis of Sequence-Controlled Polymers by Radical Polymerization." *Nature Communications*, 1–9.

Gody, Guillaume, Thomas Maschmeyer, Per B Zetterlund, and Sébastien Perrier. 2014a. "Exploitation of the Degenerative Transfer Mechanism in RAFT Polymerization for Synthesis of Polymer of High Livingness at Full Monomer Conversion." *Macromolecules* 47: 639–49.

Gody, Guillaume, Thomas Maschmeyer, Per B Zetterlund, and Sébastien Perrier. 2014b. "Pushing the Limit of the RAFT Process: Multiblock Copolymers by One-Pot Rapid Multiple Chain Extensions at Full Monomer Conversion." *Macromolecules* 47: 3451–60.

Hashida, Mitsuru, Makiya Nishikawa, Fumiyoshi Yamashita, and Yoshinobu Takakura. 2001. "Cell-Specific Delivery of Genes with Glycosylated Carriers." *Advanced Drug Delivery Reviews* 52 (3): 187–96.

Hassane, Fatouma Said, Benoit Frisch, and Francis Schuber. 2006. "Targeted Liposomes : Convenient Coupling of Ligands to Preformed Vesicles." *BioconjugateChem.* 17: 849–54.

Iwamoto, Kiyoshi, and Junzo Sunamoto. 1982. "Adsorption Oof Polysaccharides on Liposomal Membranes as Monitored by Fluorescence Depolarization." *J. Biochem.* 91 (589012): 975–79.

Jayaraman, Narayanaswamy. 2009. "Multivalent Ligand Presentation as a Central Concept to Study Intricate Carbohydrate-Protein Interactions." *Chemical Society Reviews* 38 (12): 3463–83.

Jayaraman, Narayanaswamy, Krishnagopal Maiti, and Kottari Naresh. 2013. "Multivalent Glycoliposomes and Micelles to Study Carbohydrate-Protein and Carbohydrate-Carbohydrate Interactions." *Chemical Society Reviews* 42 (11): 4640–56.

Jones, Malcom N. 1994. "Carbohydrate-Mediated Liposomal Targeting and Drug Delivery." *Advanced Drug Delivery Reviews* 13: 215–49.

Kartha, K P Ravindranathan, and Robert A Field. 1997. "Iodine: A Versatile Reagent in Carbohydrate Chemistry IV. Per-O-Acetylation, Regioselective Acylation and Acetolysis." *Tetrahedon* 53 (34): 11753–66.

Kawakami, Shigeru, and Mitsuru Hashida. 2014. "Glycosylation-Mediated Targeting of Carriers." *Journal of Controlled Release*, 190 (June): 542-55.

Kelly, Ciara, Caroline Jefferies, and Sally-Ann Cryan. 2011. "Targeted Liposomal Drug Delivery to Monocytes and Macrophages." *Journal of Drug Delivery* 11 (January): 1–

12.

Lian, T, and R J Ho. 2001. "Trends and Developments in Liposome Drug Delivery Systems." *Journal of Pharmaceutical Sciences* 90 (6): 667–80.

Lundberg, B. 1977. "Properties of Mixed Vesicle of Lecitin: Cholesterol up to 1:2 Molar Ratio." *Chemistry and Physics of Lipids* 18: 212–20.

Moad, Graeme, Ezio Rizzardo, and San H. Thang. 2008. "Radical Addition-Fragmentation Chemistry in Polymer Synthesis." *Polymer* 49 (5): 1079–1131.

Mobed, M., and T. M S Chang. 1998. "Comparison of Polymerically Stabilized PEG-Grafted Liposomes and Physically Adsorbed Carboxymethylchitin and Carboxymethyl/glycolchitin Liposomes for Biological Applications." *Biomaterials* 19 (13): 1167–77.

Mukhopadhyay, Balaram, K P Ravindranathan Kartha, David a Russell, and Robert a Field. 2004. "Streamlined Synthesis of Per- O -Acetylated Sugars , Glycosyl Iodides , or Thioglycosides from Unprotected Reducing Sugars 1 Unprotected Reducing Sugars Would Be Useful . as a Promoter for Sugar per- O -Acetylation , 10 That Sugar per- O -Acetates Can Be." *The Journal of Organic Chemistry*, no. 6: 7758–60.

Noble, Gavin T, Jared F Stefanick, Jonathan D Ashley, Tanyel Kiziltepe, and Basar Bilgicer. 2014. "Ligand-Targeted Liposome Design: Challenges and Fundamental Considerations." *Trends in Biotechnology* 32 (1). Elsevier Ltd: 32–45.

Nobs, Leila, Franz Buchegger, Robert Gurny, and Eric Allémann. 2004. "Current Methods for Attaching Targeting Ligands to Liposomes and Nanoparticles." *Journal of Pharmaceutical Sciences* 93 (8): 1980–92.

Perrier, Sébastien. 2017. "50th Anniversary Perspective: RAFT Polymerization - A User Guide." *Macromolecules* 50 (19): 7433–47.

Szoka, Francis Jr. 1980. "Comparative Properties and Methods of Preparation of Lipid Vesicles (Liposomes)." *Annual Review of Biophysics and Bioengineering* 9: 467–508.

Vabbilisetty, Pratima, and Xue-Long Sun. 2015. "Liposome Surface Functionalization Based on Different Anchoring Lipids via Staudinger Ligation." *Org Biomol Chem*

12 (8): 1237–44.

van der Meel, Roy, Laurens J C Vehmeijer, Robbert J. Kok, Gert Storm, and Ethlinn V B van Gaal. 2013. "Ligand-Targeted Particulate Nanomedicines Undergoing Clinical Evaluation: Current Status." *Advanced Drug Delivery Reviews* 65 (10). Elsevier B.V.: 1284–98.

Wang, Zerong Daniel, Yirong Mo, Chiao-lun Chiou, and Minghong Liu. 2010. "A Simple Preparation of 2,3,4,6-Tetra-O-Acyl-Gluco-, Galacto- and Mannopyranoses and Relevant Theoretical Study," 374–84.

CHAPTER 3

Design and formulation of glycosylated liposomes

In nature, carbohydrate-binding cell receptors mediate a plethora of key biological events – *e.g.* fecundation and the mounting of immune responses (van Kooyk and Rabinovich 2008). Liposomes functionalised with simple monosaccharide ligands have been employed to selectively deliver a number of drugs and antigens to target cells *in vitro* and *in vivo* (Xie *et al.* 2014), (Unger *et al.* 2012). However, despite of these initial studies, the understanding of the function of structural and chemical patterns of membrane ligands - their spatial distribution, presentation modalities and density, and how the lipid composition of the membranes can affect these parameters– is still largely lacking.

In this chapter, we describe an investigation on the role of the liposome structural components on their ability to target selected lectins, with the aim to identify optimal liposomal formulations for the *in vitro* studies presented in Chapter 4. Con A was used as a model carbohydrate-binding protein (Ladmiral *et al.* 2006) - to investigate how

i. membrane concentration (density) of different sugars residues (mannose and galactose),
ii. ligand exposure – *e.g.* the physical distance between the sugar ligands and the liposome bilayer.
iii. the nature of the membrane-inserting hydrophobic anchor of the sugar ligands, and
iv. the lipid composition of the liposomal membrane

affect the rate of binding to Con A model lectin, which in this part of our study was used as a convenient readout to compare all the different liposomal formulations investigated.

3.1 Introduction

Liposomes are a widely explored platform technology for drug delivery. Liposomes for passive targeting have already showed valid results - with notable examples that include the recent seminal work by Sahin and co-workers on cancer vaccination (Kranz *et al.* 2016) - and further improvements have been achieved by surface coating (Noble *et al.* 2014), (Mody *et al.* 2014). The way ligands are presented on the liposomal membrane can profoundly affect the efficacy of targeted nanocarriers (Espuelas *et al.* 2008), (Jayaraman *et al.* 2013), (Jayaraman 2009). In Nature multivalent interactions are used to enhance ligand-receptor low binding affinity and to increase binding selectivity (as discussed in Chapter 1.1.1) The same strategy can be transposed to glycosylated liposomes, where multivalent binding can be modulated by varying the surface density of glycosylated ligands at the liposome surface (Kingery-Wood *et al.* 1992), (Spevak *et al.* 1993), (Mammen *et al.* 1998).

However, the relationship between liposomal ligand density and binding affinity is not linear and greater ligand density does not necessarily lead to a higher cellular uptake (Sanna *et al.* 2014), (Bertrand *et al.* 2014). For example, high ligand density can affect the ligand molecular orientation - thus its ability to bind its intended biological target - due to steric hindrance of neighbouring molecules, moreover excessive competition for the binding site can sometimes interfere with ligand-receptor binding (Nobs *et al.* 2004). In addition, high membrane density of hydrophobic ligands on liposomes can lead to decreased circulation half-life due to internalisation by macrophages (Valencia *et al.* 2011). Furthermore, high density of ligands on liposome surface can negatively

affect biodistribution and half-life *in vivo* due to increased immunogenicity and consequent antibody-mediated elimination (Li *et al.* 2002).

Liposomes functionalised with monosaccharide ligands have been employed to deliver a number of drugs and antigens to target cells (Johannssen and Lepenies 2017), (Jain *et al.* 2012). Although targeted liposomes have been widely investigated, the performance of these nanocarriers both *in vitro* and *in vivo* still needs improvements (Sipai Altaf Bhai *et al.* 2012), and a better understanding of the function of their structural and chemical patterns - the spatial distribution and density of the ligands, and lipid composition - is much needed.

This part of the project aimed at understanding how the ligand presentation on the surface of liposome affects binding to mannose-binding lectin Con A. In this contest, three models of liposomes with different ligand presentation modalities were utilised.

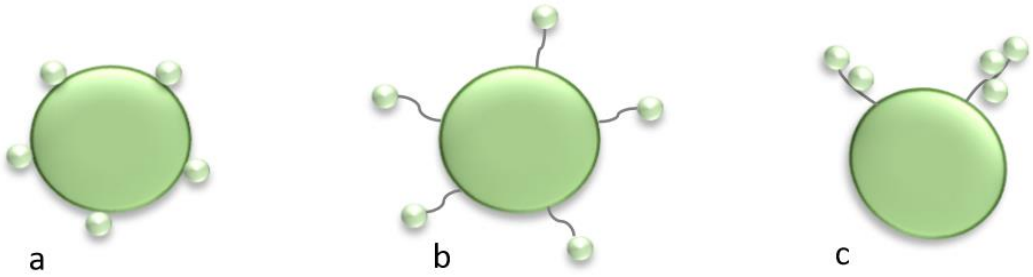

Figure 15 - Schematic representation of the three different glycosylated liposome models investigated in our work: a) glycoside lipid heads laying at the surface of liposomal membrane. b) liposomes with spacers separating the sugar ligand from the membrane. c) glycosides presented as ligand clusters.

In the first liposome pattern (Figure 15a), carbohydrate ligand molecules are displayed in very close vicinity of the lipid membrane, and are therefore surrounded by the

hydrophilic heads of the membrane phospholipids. In the second model (Figure 15b), a spacer is introduced between the hydrophobic anchor inserted in the membrane bilayer and the sugar moieties, to potentially improve the accessibility of individual carbohydrate ligands to lectin receptor binding pockets. In both models, carbohydrate ligands are presented as individual units at the liposomal membrane, and multivalent effect can be achieved due to spatial proximity of contiguous individual sugar ligands. In the third model (Figure 15c) glycoside ligands are presented as clusters, as part of short oligosaccharide sequences (discussed in chapter 4.4.2). *Engel* and co-workers have investigated the influence of spacer length on Con A binding, and found that a minimum spacer length of 2 ethylene glycol units is required to achieve detectable binding (Engel *et al.* 2003). The initial part of this work aimed at validating these findings, and further show how the liposomal lipid composition, in addition to the length of the spacer, can affect liposomal binding to Con A. The synthesis of the glycoligands used in this chapter (compounds **6**, **8**, **10**, **14**) has been reported and discussed in detail in Chapter 2.

3.2 Materials and Methods

3.2.1 Materials

Dioleoyl-sn-glycero-3-phospho-L-serine sodium salt, sphingomyelin and 1-palmitoyl-2-oleoyl-sn-glycero-3-phosphocholine were purchased from NOF Europe Corporation. Cholesterol, methyl-α-D-mannopyranoside, concanavalin A and all other chemicals were purchased from Sigma-Aldrich. Acetone, chloroform and methanol were purchased from Fischer Chemicals and were of analytical grade. Glycolipid ligands were prepared as described in Chapter 2.

3.2.2 Methods

The mean diameter and size distribution of liposomes were measured using Zetasizer 2000, Malvern Instruments, UK (Measurement angle: 173° Backscatter), and disposable ZEN0040 cuvettes. Results are the mean of eleven measurements, performed at 25°C.

UV-vis measurements were recorded with a PerkinElmer UV/Vis spectrophotometer, using quartz microcells (Path Length: 10 mm, Inside Width 2 mm, Volume 1.5 ml).

Sonicator used was Ultrasonic Bath Branson 5510. Avanti Mini Extruder was used for liposomes extrusion.

Best fitting nonlinear regression and rate constant (K) were determined by GraphPad Prism 7.03©, using nonlinear regression, one phase association analysis.

3.3 Experimental section

3.3.1 Liposome assembling

Stock solutions of phospholipids, cholesterol, glycoligands (compounds **6, 8, 10, 14**), Con A and methyl α-D-mannopyranoside were all prepared at a concentration of 1.0 mg/mL unless otherwise stated (Table 3). The lipid composition of the liposomes was controlled by varying the molar ratio of the phospholipids utilised in this study. Liposome formulations were prepared by the Bangham Method (hydration of a thin lipid film). The required amount of each lipid stock solution was mixed in a round-bottomed flask and the organic solvent was evaporated under reduced pressure to form a lipid film. The round bottom flask was then left under a stream of nitrogen to dry for two hours to ensure that any residual solvent was removed. After suspension of the lipid film with DI water - total lipid concentration was 1.0 mM in all formulations - the mixture was sonicated and extruded at 20°C through a polycarbonate membrane with 0.1 μm pore size. After 21 cycles through the extrusion device, the resulting liposomal formulation was analysed by dynamic light scattering to characterise the vesicle size and polydispersity.

Table 3- Stock solutions: concentration and solvents.

Solute	Code	Conc mg/mL	Solvent
1-palmitoyl-2-oleoyl-sn-glycero-3-phosphocholine	POPC	1.0	$CHCl_3$
Cholesterol	Chol	1.0	$CHCl_3$
Sphingomyelin	SM	1.0	$CHCl_3$/MeOH (9:1)
1,2-dioleoyl-sn-glycero-3-phospho-l-serine, sodium salt	PS	1.0	$CHCl_3$
Glycoligands (**6**, **8**, **10**, **14**)	-	0.1	$CHCl_3$/MeOH (9:1)
Concanavalin A	Con A	4.56 uM[1]	HEPES Buffer[2]
Methyl α-D-mannopyranoside	-	54 mM	HEPES Buffer[2]

[1]Con A concentration was derived by measuring the absorbance at λ = 280 nm and applying the formula [A_{280}=1.37 x (mg/mL Con A)] (Gou *et al.* 2013)

[2]0.10 M HEPES buffer containing 0.90 M NaCl, 1.0 mM $CaCl_2$, 1.0 mM $MgCl_2$ – pH 7.4.

3.3.2 Con A lectin binding studies

Muller and Schuber's method (Muller and Schuber 1989) was followed to carry out the agglutination assay. Briefly, 500 μL of liposome sample (1.0 mM of total lipid concentration) were introduced in a quartz microcell, which was then placed in a UV-vis spectrophotometer. Con A stock solution (500 μL) was added. The change in absorbance (due to light scattering) at λ=550 nm was measured over 5 minutes, at 25°C, with acquisition of data every 0.2 sec.

Espuelas' method (Espuelas *et al.* 2003) was followed to carry out the disaggregation assay, where the stability of glycosylated liposomes-Con A clusters over time in the presence of an excess of a monovalent competitive ligand (α-methyl-D-mannopyranoside) was investigated. Briefly, 500 μL of the aggregated liposome-Con A suspension was diluted fourfold with milliQ water. 900 μL of the resulting diluted suspension were introduced in a quartz cuvette and placed into a UV-vis spectrophotometer. 100 μL of the 54 mM α-methyl-D-mannopyranoside stock solution were added to the suspension. The change in light scattering (absorbance, or optical density, OD) at λ=550 nm and was monitored over a period of 5 minutes at 25°C, with acquisition of data every 0.2 sec.

All tests were repeated at least twice, data reported are the average of all absorbance readings. The error shown is the standard deviation. Some error bars are smaller than the symbols. Controls used in these experiments are *i)* galactose containing liposomes (Gal-TEG-liposomes, unable to bind Con A), *ii)* blank liposomes without ligands, and *iii)* mannosylated liposomes (Man-TEG-liposomes) without Con A, were used as negative controls.

3.4 Results and Discussion

The aim of this part of the project was to investigate the influence of the density of carbohydrate ligands at the liposome membrane and lipid composition on binding to Con A model lectin.

As discussed in the introduction, in this part of our study, we investigated

i. how the liposome structural components – lipids and carbohydrate ligands - affect the lipid vesicle size,
ii. how the nature of the sugar molecules, mannose vs. galactose, and their membrane concentration affected the rate of lectin binding,
iii. the effect of liposome lipid composition on lectin binding,
iv. the anchoring lipid effects on liposome surface glycosylation and their lectin binding activity.

The ligands (**6**), (**8**), (**10**) and (**14**) were utilised along cholesterol and phospholipids - 1-palmitoyl-2-oleoyl-sn-glycero-3-phosphocholine (PC), sphingomyelin (SM), 1,2-dioleoyl-sn-glycero-3-phospho-L-serine, sodium salt (DOPS-Na) - to prepare a library of different liposome formulations using the Bangham Method (hydration of a thin lipid film). The latter involved suspension of the lipid films with DI water, ultrasonication of the resulting mixture to reduce the size and produce mostly unilamellar vesicles, and then extrusion at 20°C through a polycarbonate membrane with 0.1 μm pore size to give liposome with average diameter of around 100 nm. The rate of binding between the glycosylated liposomes and Concanavalin A (Con A) model lectin was assessed by a turbidimetry assay (tetrameric Con A induces clustering of mannosylated liposomes, which over time results in the formation of a visible

precipitate), whilst the stability of resulting liposome-Con A aggregates in the presence of carbohydrate competitive ligands was investigated by a reversal aggregation assay using an excess of methyl-α-D-mannopyranoside monovalent ligand. Liposome size distribution and stability analysis were performed by dynamic light scattering (DLS) measurements.

3.4.1 Influence of carbohydrate ligand accessibility and membrane density on Con A binding

In order to investigate how the density of liposome membrane sugar ligands affects the rate of clustering with Con A, a set of glycosylated liposomes with different ligand membrane densities were prepared.

0-30% of α-O-(tetra(ethyleneglycol)) palmitoyl mannose (**10**) with respect to the total lipid molar composition was initially utilised. The palmitoyl-TEG-mannoside ligand was mixed with cholesterol (40% of the total lipid molar composition), sphingomyelin (5% of the total lipid molar composition), 1-palmitoyl-2-oleoyl-sn-glycero-3-phosphocholine (55-25% of the total lipid molar composition) – (Table 4, Figure 16). After extrusion, the mean diameters of the Man-TEG-liposome formulations produced were in the 102-118 nm range (Appendix 6.3, Table S1, Figure S54) which suggests that no liposome aggregation/merging occurred following liposome extrusion. This indicated that within the range of compositions investigated, the physical stability of liposomes was not affected by the presence of Man-glycolipids within the liposomal membrane.

Table 4 - Lipid composition of Man-TEG liposome formulations.

	Molar Ratio %					
Formulation	Man-TEG (**10**)	Chol	SM	POPC	Z-Average[a] (d. nm) ± S.D.	PdI[a] ± S.D.
Liposome-0	0	40	5	55.0	82.68 ± 0.22	0.154 ± 0.07
Man-TEG Liposome-2.5	2.5	40	5	52.5	102.2 ± 0.55	0.163 ± 0.02
Man-TEG Liposome -5	5	40	5	50.0	99.75 ± 0.63	0.101 ± 0.01
Man-TEG Liposome -7.5	7.5	40	5	47.5	112.2 ± 0.99	0.123 ± 0.64
Man-TEG Liposome -10	10	40	5	45	103.3 ± 0.68	0.234 ± 0.09
Man-TEG Liposome -15	15	40	5	40.0	105.8 ± 0.28	0.172 ± 0.02
Man-TEG Liposome -20	20	40	5	35.0	108.1 ± 0.64	0.180 ± 0.01
Man-TEG Liposome -30	30	40	5	25.0	117.7± 0.67	0.148± 0.09

Man-TEG: α-O-(tetra(ethyleneglycol)) palmitoyl mannose; Chol: cholesterol; SM: sphingomyelin; POPC: palmitoyl-2-oleoyl-sn-glycero-3-phosphocholine. [a]Average values ± S.D. (n=3).

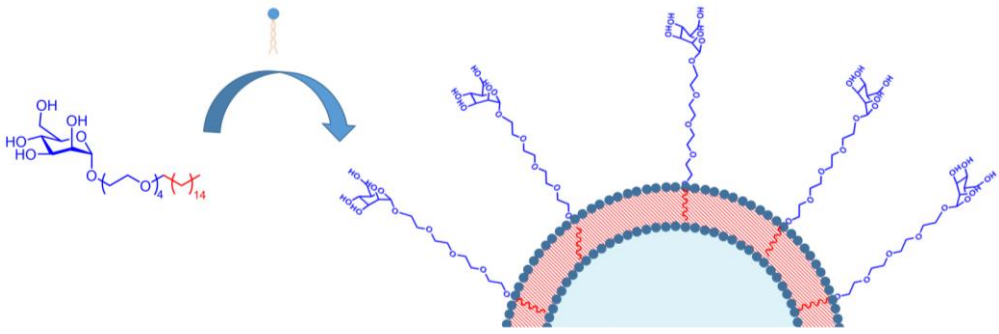

Figure 16 – Targeted liposomes formed from Mannose ligand (**10**), where a tetra(ethylene glycol) TEG spacer was employed to improve exposure of Man carbohydrate moieties to Con A model lectin.

In biology, the rate at which lectin receptors interact with their carbohydrate ligands can range from less than a second to several hours (Gestwicki *et al.* 2002). Although not strictly a direct measure of strength of binding, for which techniques like isothermal titration calorimetry (ITC) are more appropriate, the rate at which multivalent ligands and lectins form insoluble aggregates is commonly utilised as a rapid test to screen libraries of novel multivalent carbohydrate ligands (Ladmiral *et al.* 2006), (Cairo *et al.* 2002). Typically this is carried out by turbidimetry, by measuring the change of absorbance, here a measure of light scattering, which occurs following the mixing of multivalent ligands and lectins. Being tetrameric at pH ~ 7, Con A is particularly suited for the clustering of multivalent mannosylated ligands.

In this study a turbidimetric assay was carried out to evaluate the relative rate of clustering in function of the glycosylation ratio on a set of 7 formulations, where the Man-TEG-ligand content was respectively 0%, 2.5%, 5%, 7.5%, 10%, 15%, 20% and 30% of the total lipid molar composition (Table 4). Here the molar proportion of cholesterol and sphingomyelin were kept constant at 40 % and 5 %, respectively, and the concentration of POPC was used to balance the variation of Man-TEG-ligand. A solution of Con A in 0.10 M HEPES buffer (also containing 0.90 M NaCl, 1.0 mM $CaCl_2$, 1.0 mM $MgCl_2$ – pH 7.4) was added to the glycosylated liposome formulations and the rate of aggregation was measured as a function of the increase in the light scattering (absorbance) at $\lambda = 550$ nm (Figure 17).

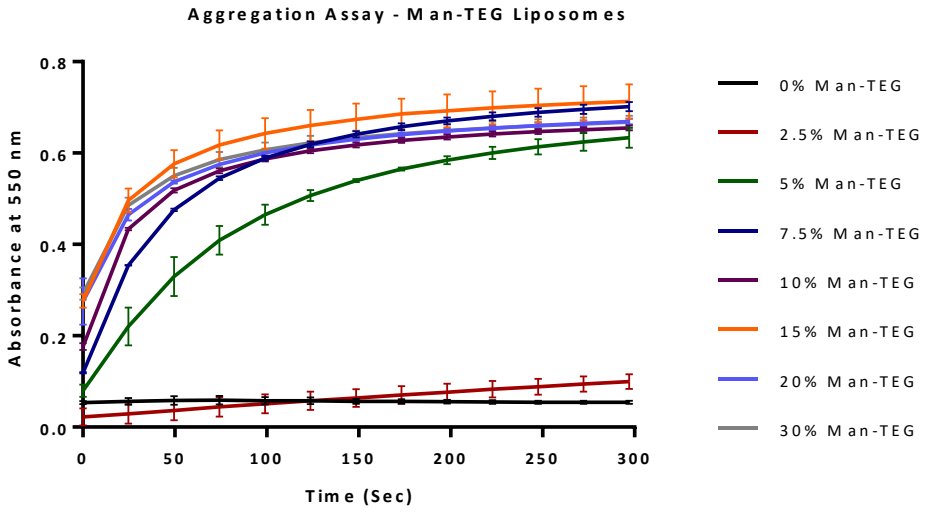

Figure 17 - Aggregation assay conducted on Man-TEG liposomes where Man-TEG-ligand content was increased from 0% to 30% of the total lipid molar composition. Con A in 0.10 M HEPES buffer (0.90 M NaCl, 1.0m M $CaCl_2$, 1.0 mM $MgCl_2$ - pH7.4) was added to each formulation. N=2. The data set shows groups of continuous data acquired every 0.2 sec. For more convenient data visualisation, standard deviations are shown for every 25 sec recorded data points

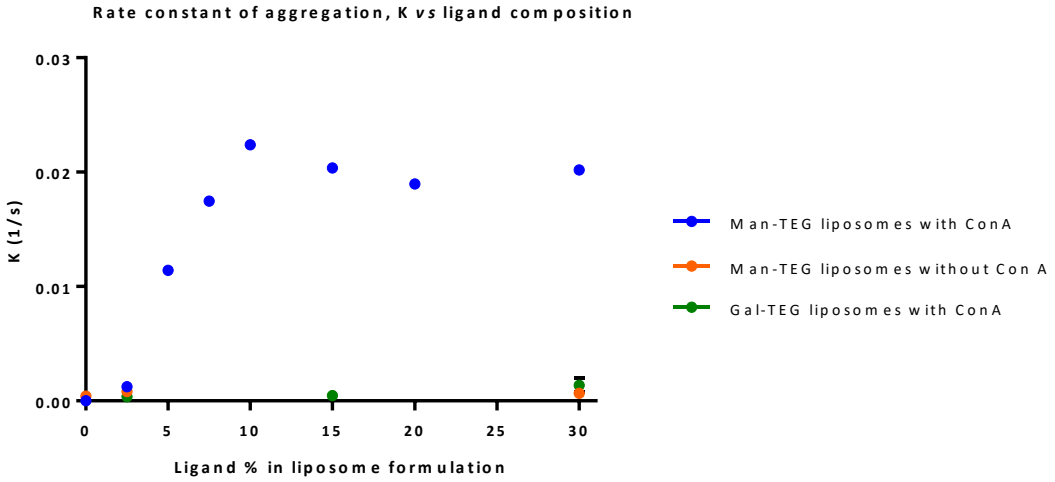

Figure 18 - Rate constant of aggregation Con A-Man-TEG liposome against ligand composition. For each Man-TEG liposome formulation, the rate constant (K) from nonlinear regression best fitting the entire aggregation curve was plotted vs. Man-TEG ligand (%), N=2. Gal-TEG-liposomes (unable to bind Con A) and Man-TEG liposomes in HEPES buffer without Con A were used as controls, N=2. The error shown is the standard error. Some error bars are smaller than the symbols.

Two distinct events in the clustering experiments can be identified. Firstly, tetravalent Con A clusters mannosylated-TEG-liposomes, resulting in the formation of insoluble aggregates and consequently inducing an increase in the absorbance (initial aggregation). Subsequently, secondary aggregation events can start occurring, where these Con A-liposome clusters will start to aggregate together. The second order aggregates do not provide any useful information in term of kinetic of binding between Con A and glycoliposomes, hence typically only the first few seconds of the kinetic curves are utilised to estimate the rate of binding (Gou *et al.* 2013). In our experiments, however, these higher-order aggregation phenomena seemed to be less evident than what observed in studies where synthetic glycopolymers were employed (Ladmiral *et al.* 2006), (Cairo *et al.* 2002). Indeed, after an initial steep increase of scattering, virtually all samples almost plateaued towards the end of each kinetic run.

A nonlinear regression best fitting the aggregation curve was calculated for each mannosylated liposome formulation, and its rate constant (K) (data reported in Appendix 6.3, Table S2) was used to estimate the aggregation rate against glycoligands % composition (Figure 18). The change of observed absorbance at t = 0 in Figure 17, and to an extent was found to be dependent on the ligand concentration, is due to the fact that measurements start a fraction of a second after the addition of Con A to the liposome samples, when some minimal, but detectable aggregation has already started. As the rate is calculated from the rate constant (K) of the entire aggregation curve, the small initial delay in starting the measurement (in a first approximation approximately the same for all samples) will not affect significantly the measurements. This is a qualitative assay, and can be used to screen libraries of polymers, liposomes, by providing a relative (not absolute) comparison of aggregation rates. Up to 10% Man

ligand content, the rate of clustering was found to be directly proportional to the density of Man-TEG-ligands on the liposome membrane and this trend is in agreement with other lectin induced aggregation studies (Curatolo *et al.* 1978), (Kitano *et al.* 2001), (Thomas *et al.* 2009). The formulation of plain liposomes without Man-TEG-ligands on the surface was used as control and, as expected, no Con A-mediated liposome clustering could be observed (Figure 17).

The lack of aggregation for the 2.5% Man-TEG liposome formulation and Con A might be attributed to a low density of Man-TEG ligand on the liposomal membrane. The mannose ligand units are too spaced apart to allow Con A tetramer to crosslink bilayer membranes (Figure 19a), thus the lower binding rate. Increasing the amount of Man-TEG content corresponds to increased ligand surface density. The distance between mannose ligands is reduced, allowing sufficient lateral diffusion for aggregation and also increasing the chances of effective collision between two glycoligands and two sugar binding sites on Con A (Figure 19b) (Mammen *et al.* 1998). Maximum aggregation rate was achieved with 10% Man-TEG content, suggesting the distance between mannose ligands is such as to match the binding site separation distance in tetrameric Con A, allowing strong binding during each collision between Con A and Man-TEG liposomes. After 10% Man vs. total lipid molar composition, a plateau in clustering rate was observed showing that at around this ligand density maximal Con A binding was achieved and further increase in ligand concentration did not affect lectin binding. This might be attributed to high glycoligand density steric effects may hamper further Con A binding, or simply steric encumbrance provided by large Con A tetramers at the liposomal membrane which may prevent access of

additional Con A molecules to membrane glycoligands, resulting in constant binding rate (Figure 19c) (Bakowsky *et al.*, 2000), Ladmiral *et al.*, 2006).

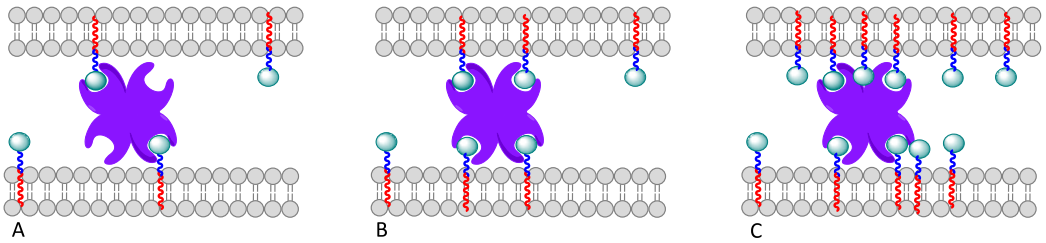

Figure 19 - Schematic representation of Con A clustering by different Man-TEG content in Man-TEG liposomes. (A) Low-density Man-TEG ligand; (B) Optimum-density ligand; (C) High-density ligand.

The stability of the Con A-liposome clusters in the presence of mannosylated competitive ligands was assessed by a reversal aggregation assay. The aggregated suspensions from the previous set of experiments were diluted 4-fold. Then, a solution of methyl-α-D-mannopyranoside (54 mM, this concentration was chosen after different trials aimed at optimising the rate of disaggregation) was added and the decrease in turbidity was measured. Methyl-α-D-mannopyranoside acted as a competitive monovalent ligand which at high concentration can displace Con A from the targeted mannosylated liposomes (Figure 20).

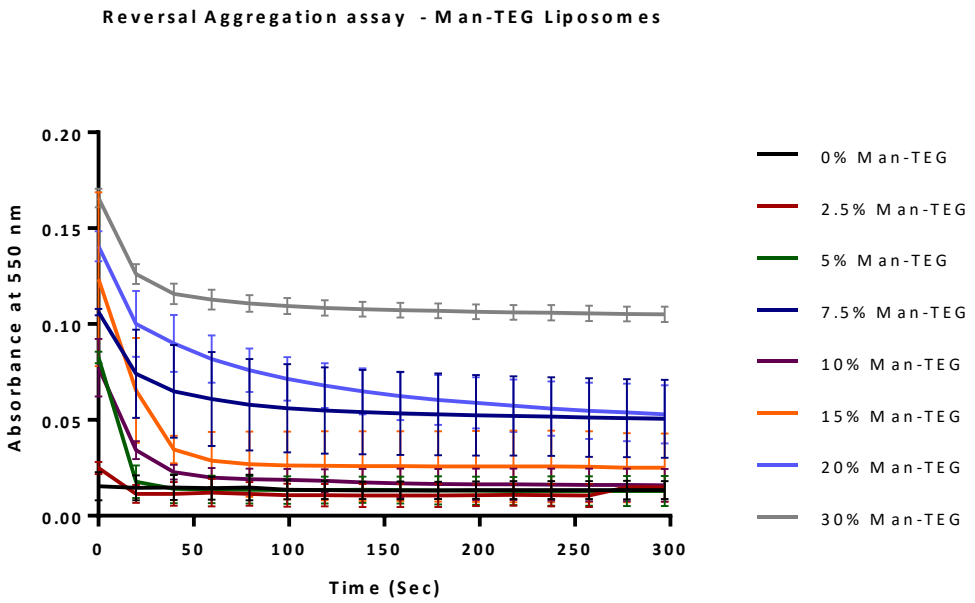

Figure 20 Reversal aggregation assay conducted on aggregated Man-TEG liposome formulations. After addition of a 54 mM α-methyl-D-mannopyranoside in 0.10 M HEPES buffer containing 0.90 M NaCl, 1.0 mM $CaCl_2$, 1.0 mM $MgCl_2$ – pH 7.4. Disaggregation of Man-TEG **(10)**-liposome-Con A clusters was monitored as a function of a decrease light scattering at λ=550 nm. N=2. The data set shows groups of continuous data acquired every 0.2 sec. For more convenient data visualisation, standard deviations are shown for every 25 sec recorded data points.

In order to further confirm that the observed clustering was indeed mannose-dependent, three galactosylated liposome formulations were prepared using 2.5%, 15%, or 30% of galacto-TEG-ligand (**8**), with 5% sphingomyelin, 40% cholesterol and respectively 52.5%, 40% and 25% of POPC (Table 5).

The average diameter of this set of liposome formulations was in the 87–93 nm range (Appendix 6.3, Figure S55). A stereoisomer of mannose, galactose has identical molecular weight (thus similar size) than mannose, but is unable to bind to Con A, is an ideal non-binding control ligand for this study. The aggregation assay was carried out following the same procedure of the Man-TEG **(10)** liposome, and as expected no

increase in light scattering was observed (Figure 21). This confirmed the specificity of binding to Con A for the mannosylated liposome formulations.

Table 5 – Lipid compositions of Gal-TEG liposome formulations.

	Molar Ratio %					
Formulation	Gal-TEG (**8**)	Chol	SM	POPC	Z-Average[a] (d. nm) ± S.D.	PdI[a] ± S.D.
Gal-TEG Liposome-2.5	2.5	40	5	52.5	87.06 ± 0.62	0.177 ± 0.01
Gal-TEG Liposome-15	15	40	5	40.0	96.21 ± 0.65	0.178 ± 0.08
Gal-TEG Liposome -30	30	40	5	25.0	94.22 ± 0.14	0.142 ± 0.03

Man-TEG: α-O-(tetra(ethyleneglycol)) palmitoyl mannose; Chol: cholesterol; SM: sphingomyelin; POPC: palmitoyl-2-oleoyl-sn-glycero-3-phosphocholine. [a]Average values ± S.D. (n=3).

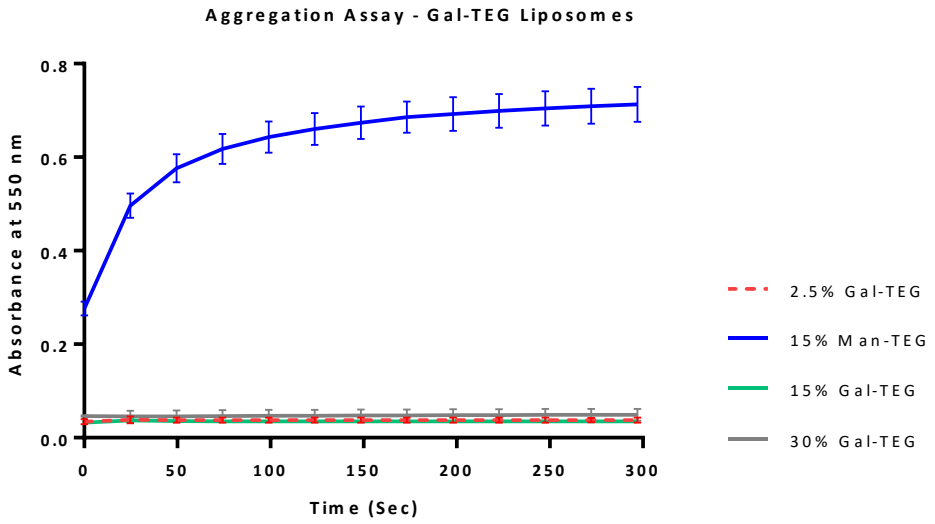

Figure 21 - Aggregation assay conducted on Gal-TEG liposomes where Gal-TEG-ligand content was varied from 2.5%, 15% and 30% of the total lipid molar composition. Aggregation plot for 15% Man-TEG liposome formulations is shown for comparisons. Con A in 0.10 M HEPES buffer (0.90 M NaCl, 1.0 mM $CaCl_2$, 1.0 mM $MgCl_2$ - pH7.4) was added to each liposomal formulation. N=2. The data set shows groups of continuous data acquired every 0.2 sec. For more convenient data visualisation, standard deviations are shown for every 25 sec recorded data points.

To investigate how the accessibility of sugar ligands at the liposomal membrane affects the binding with Con A, an additional family of liposomes incorporating mannosylated lipids lacking the TEG spacer (compound **6**), was prepared (Figure 22). A liposomal formulation was prepared with 10% mannose ligand (**6**), 5% of sphingomyelin, 40% of cholesterol and 45% of POPC. After extrusion through a 0.1 μm membrane, the average diameter D_h was found to be ~ 130 nm. The slight difference in diameter of this mannosylated liposome without TEG spacer, compared with both galactose and mannose TEG-liposomes is difficult to explain, and it could be speculated that this could be due to an increase of steric hindrance on the liposome surface among polar heads of the phospholipids and the carbohydrate units.

Again, aggregation assays were carried out comparing 10% Man-TEG liposome with 10% Man liposome, and showed that in the absence of a spacer lifting mannose ligands sufficiently above the liposomal membrane to allow lectin binding, no Con A-mediated liposome clustering occurred (Figure 23). These results are in line with analogous previous studies by Engel *et al* (Engel *et al.* 2003a), (Engel *et al.* 2003b).

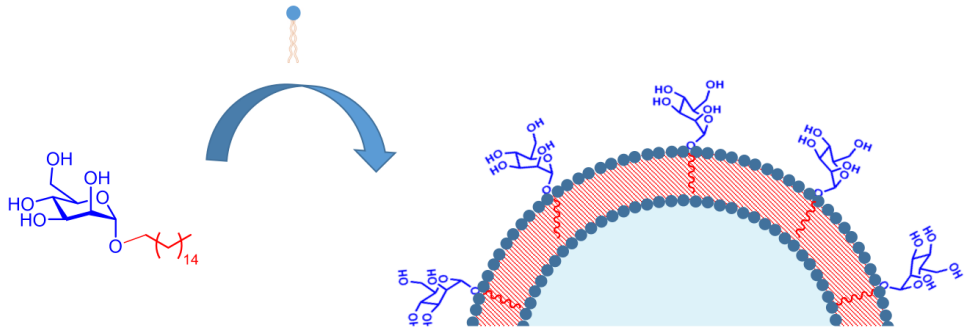

Figure 22 - Targeted liposomes formed from Mannose ligand (**6**).

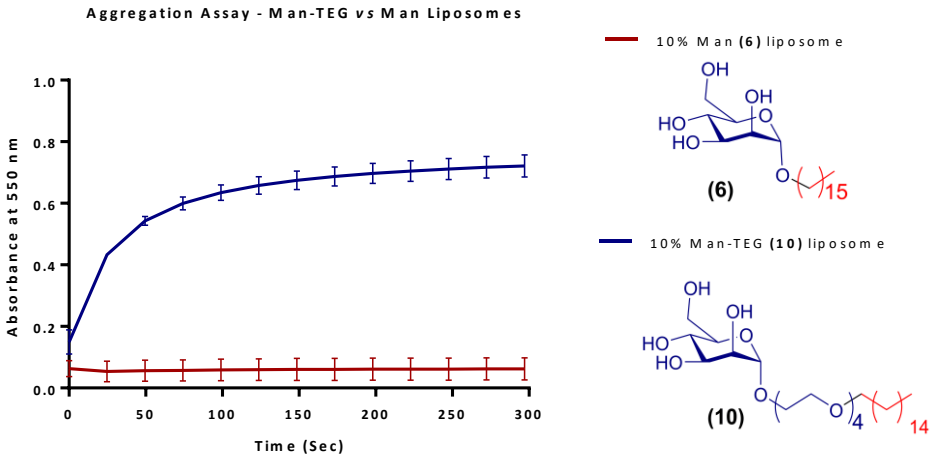

Figure 23 - Effect of TEG spacer on Con A-mediated liposome aggregation: Man-TEG **(10)** liposome vs Man liposome **(6)**, 10 % ligand content on the liposome membrane. Con A in 0.10 M HEPES buffer (0.90 M NaCl, 1.0 mM $CaCl_2$, 1.0 mM $MgCl_2$ - pH7.4) was added to each formulation to induce liposome clustering. N=2. The data set shows groups of continuous data acquired every 0.2 sec. For more convenient data visualisation standard deviations are shown for every 25 sec recorded data points.

3.4.2 Influence of lipid composition on liposome binding to Con A lectin

This part of the study focused mainly on two lipids, cholesterol and DOPS-Na.

Cholesterol is an essential component in the cells membranes and plays a crucial role in membrane organisation, dynamics, function and sorting (Ikonen 2008). Cholesterol regulates membrane fluidity and contributes to generate a semipermeable barrier between cellular compartments (van Meer *et al.* 2008). Similarly, cholesterol incorporation in liposomal membrane increases the packing of phospholipid molecules and reduces bilayer permeability (Szoka 1980), and typically makes them more rigid (Liu *et al.* 2000) and increases their stability (Briuglia *et al.* 2015). Altough in lipid membranes cholesterol:phospholipids molar ratio can be as high as 2:1 (Lundberg 1977), (Szoka 1980), the amount of cholesterol usually incorpored in liposomal

membrane is ~ 30 mol% (Lian and Ho 2001). However optimum lipids:cholesterol ratio needs to be determined for each specific application on a case by case basis (Sorkin *et al.* 2017), (Bunker *et al.* 2016). In this part of the project we investigated the effect of different cholesterol content in liposomal formulations on liposome binding to Con A lectin. Firstly, a set of six formulations with variable cholesterol content were prepared. Each sample was formulated with 10% palmitoyl-TEG-mannoside ligand and 10% SM. The content of cholesterol was increased from 0 to 50% of total lipid molar composition and POPC was decreased accordingly from 80% to 30%, to compensate the change in composition of cholesterol (Table 6). As expected, following sonication and extrusion through a 0.1 μm membrane, the average size for all liposome formulation as measured by DLS was close to 100 nm for all formulations investigated (Appendix 6.3, Table S1, Figure S56).

Table 6 – Lipid composition of Man-TEG liposome formulations with variable cholesterol content.

	Molar Ratio %					
Formulation	Man-TEG (**10**)	Chol	SM	POPC	Z-Average[a] (d. nm) ± S.D.	PdI[a] ± S.D.
Man-TEG Chol-0	10	0	10	80	105.2 ± 0.46	0.079 ± 0.02
Man-TEG Chol-10	10	10	10	70	93.23 ± 0.47	0.180 ± 0.01
Man-TEG Chol-20	10	20	10	60	95.37 ± 0.81	0.116 ± 0.01
Man-TEG Chol-30	10	30	10	50	111.4 ± 0.60	0.095 ± 0.01
Man-TEG Chol-40	10	40	10	40	120.7± 0.67	0.148 ± 0.10
Man-TEG Chol-50	10	50	10	30	136.4 ± 1.18	0.079 ± 0.01

Man-TEG: α-O-(tetra(ethyleneglycol)) palmitoyl mannose; Chol: cholesterol; SM: sphingomyelin; POPC: palmitoyl-2-oleoyl-sn-glycero-3-phosphocholine. [a]Average values ± S.D. (n=3).

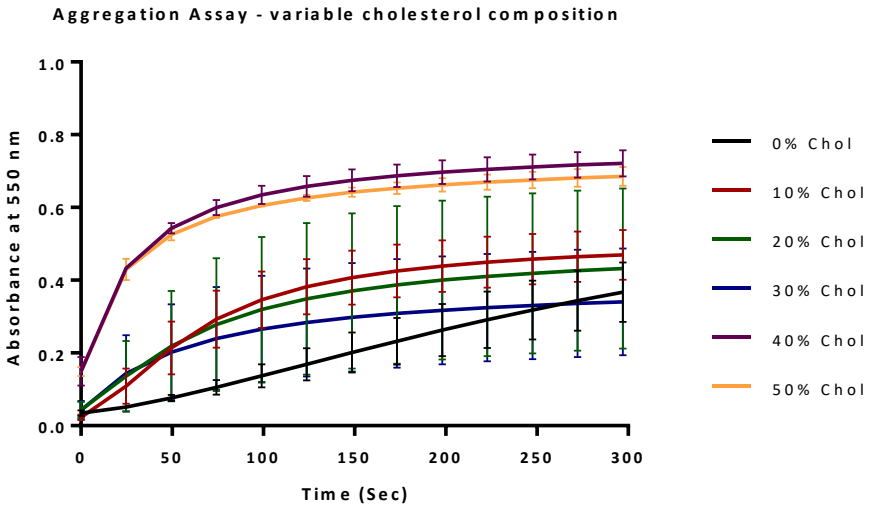

Figure 24 - Aggregation assay conducted on Man-TEG liposomes where cholesterol content was increased from 0 to 50% of the total lipid molar composition. Con A in 0.10 M HEPES buffer (0.90 M NaCl, 1.0 mM $CaCl_2$, 1.0 mM $MgCl_2$ – pH 7.4) was added to each formulation. N=2. The data set shows groups of continuous data acquired every 0.2 sec. For more convenient data visualisation, standard deviations are shown for every 25 sec recorded data points.

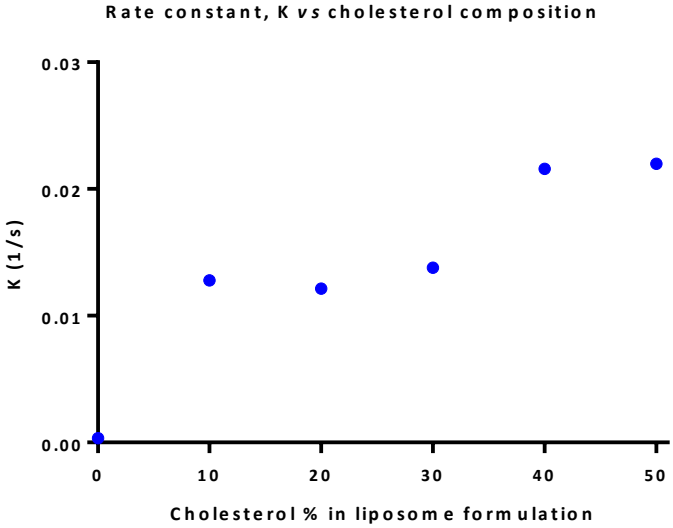

Figure 25 – Rate constant of Con A-mediated aggregation of Man-TEG liposomes with different cholesterol content. For each formulation, the rate constant (K) from nonlinear regression line best fitting the entire aggregation curve was plotted vs cholesterol % composition. N=2. The error shown is the standard deviation. Some error bars are smaller than the symbols.

Aggregation assay clearly showed that under the range of concentrations investigated, an increase of cholesterol content induced an increase in the rate of clustering (Figure 24). A nonlinear regression fitting the aggregation curve was calculated for each Man-TEG Chol liposome formulations, and its rate constant (K) (data reported in Appendix 6.3, Table S2) was used to evaluate the aggregation rate against glycoligands % composition (Figure 25). In the range of concentrations investigated, the rate of clustering increased with the concentration of cholesterol in the liposome membrane, up to ca. 40% cholesterol content.

Again, at this stage it was quite difficult to rationalise these results. It is well known that within cell membranes, lipid raft regions are enriched in cholesterol (Simons and Toomre 2000). These lipid domains are more ordered and tightly packed than the surrounding bilayer and usually entrapped transmembrane proteins (Lingwood and Simons 2010). These domains containing mixtures of different phospholipids-cholesterol can exist in liposomal membranes (Brown and London 2000). High concentration of cholesterol in lipid membrane results in the formation of the liquid-ordered (I_o) phase which is a liquid from the point of view of the translational degrees of freedom (lateral diffusion) but otherwise regarded as rigid in terms as acyl chain order (Mouritsen 1991), (Jacobson *et al.* 2007). Alkyl chain of lipids in the I_o phase are extended and tightly packed but have a high degree of lateral mobility (Brown and London 1998),(Brown and London 2000). Therefore, one could hypothesise that increasing the cholesterol content, increases the lateral mobility of Man-TEG ligand, hence the faster Con A aggregation.

An analogous set of experiments were carried out with liposomal formulations where the phosphatidyl-L-serine (DOPS-Na) content was systematically varied (Table 7). Negatively charged lipids like DOPS-Na are of particular interested in liposome formulations. The negative charge helps in stabilising the lipid vesicles avoiding colloidal aggregation (Lian and Ho 2001). In addition, it is hypothesised that the inner negatively charged heads repelling each other create a larger water core, that allows enhanced hydrophilic drug encapsulation (Sipai Altaf Bhai *et al.* 2012). As expected, following sonication and extrusion through a 0.1 μm membrane, the average size for all liposome formulation as measured by DLS was close to 100 nm for all formulations investigated (Appendix 6.3, Figure S57)

Table 7 - Lipid composition of Man-TEG liposome formulations with variable PS content.

	Molar Ratio %					
Formulation	Man-TEG (**10**)	Chol	PS	POPC	Z-Average[a] d. nm	PdI[a]
Man-TEG PS-0	10	10	0	80	111.6	0.075
Man-TEG PS-5	10	10	5	75	114.2	0.117
Man-TEG PS-10	10	10	10	70	132.7	0.163
Man-TEG PS-15	10	10	15	65	131.1	0.205

Man-TEG: α-O-(tetra(ethyleneglycol)) palmitoyl mannose; Chol: cholesterol; SM: sphingomyelin; POPC: palmitoyl-2-oleoyl-sn-glycero-3-phosphocholine. [a]Diameter and polydispersity index as assessed by DLS, n=1 due to time constraint.

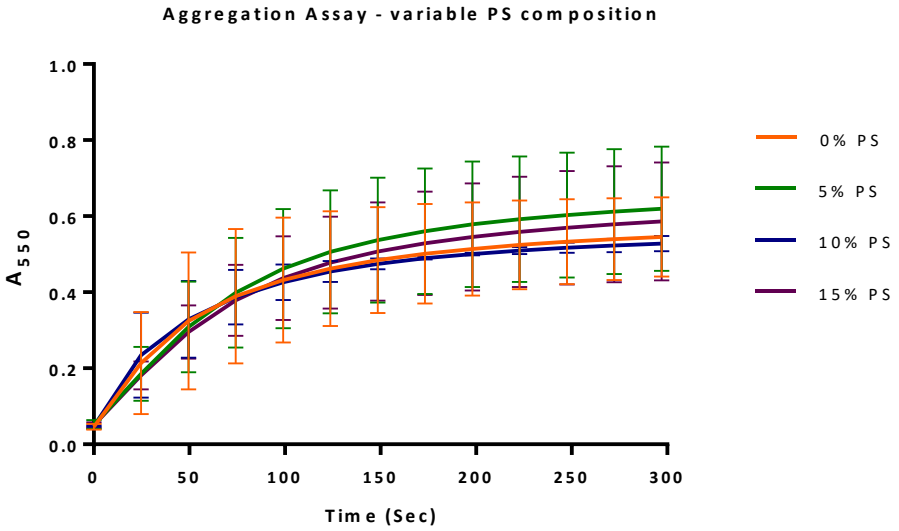

Figure 26 - Aggregation assay conducted on Man-TEG Liposomes where phosphatidylserine (PS) content was increased from 0 to 15% of the total lipid molar composition. Con A in 0.10 M HEPES buffer (0.90 M NaCl, 1.0 mM $CaCl_2$, 1.0 mM $MgCl_2$ - pH7.4) was added to each formulation. The data set shows groups of continuous data acquired every 0.2 sec. For more convenient data visualisation, standard deviations are shown for every 25 sec recorded data points

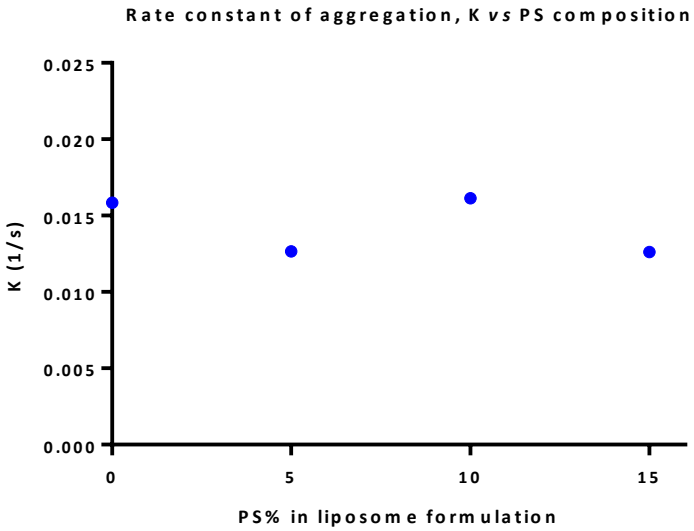

Figure 27 - Rate constant of aggregation Con A-Man-TEG Liposomes with different PS content against PS composition. For each formulation, the rate constant (K) from nonlinear regression best fitting the entire aggregation curve was plotted vs PS % composition. N=2. The error shown is the standard deviation. Some error bars are smaller than the symbols.

In our study changing DOPS-Na content did not have any significant impact on Con A-liposome clustering rate (Figure 26 and Figure 27), (data reported in Appendix 6.3, Table S2). This result may suggest that the content of negatively charged DOPS-Na could be increased to reduce the natural tendency of liposomes to aggregate, without detrimental effects on lectin binding.

3.4.3 Influence of ligand anchors on liposome lectin binding

For targeted liposomes, the role of the lipid anchor on the liposome binding properties is still largely unexplored (Vabbilisetty and Sun 2015). We hypothesised that both the overall membrane lipid composition and the chemical nature of the chemical anchor of the carbohydrate ligands could affect how the sugar ligands are spatially distributed within the membranes – *i.e.* randomly distributed vs. clustered ligands. In order to investigate the effect of the two anchor systems developed in this work (glycolicands **10** and **14**, Figure 28) on Con A binding, a liposomal formulation was prepared with 10% mannose-cholesterol ligand (**14**), 10% of sphingomyelin, 30% of cholesterol and 50% of POPC (Table 8, Figure 29). After extrusion through a 0.1 μm membrane, the average diameter D_h was found to be ~ 110 nm (Appendix 6.3, Figure S58). For comparion purposes, a 10% Man-TEG liposomal formulation with similar composition was prepared (Table 8).

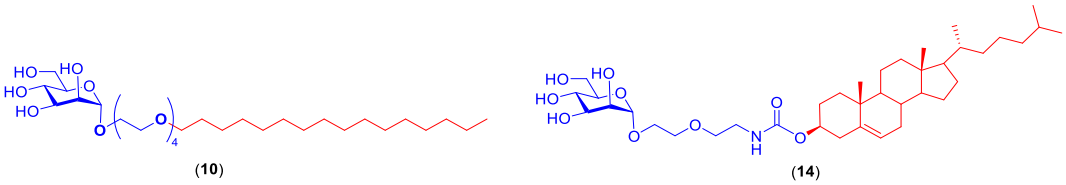

Figure 28 – Chemical structures of glycoligands with different hydrophobic anchors: (**10**) Man-TEG palmitoyl ligand, (**14**) Man-Cholesterol ligand.

Table 8 - Lipid composition of Man-Chol liposome and Man-TEG liposome formulations.

	Molar Ratio %					
Formulation	Glyco-ligand	Chol	SM	POPC	Z-Average [c] (d. nm) ± S.D.	PdI[c] ± S.D.
Man-Chol Liposome	10[a]	30	10	50	109.9 ± 0.10	0.088± 0.01
Man-TEG Liposome	10[b]	40	10	40	113.6 ± 0.80	0.085± 0.01

[a]Glycoligand (**14**); [b]glycoligand (**10**). Man-TEG: α-O-(tetra(ethyleneglycol)) palmitoyl mannose; Chol: cholesterol; SM: sphingomyelin; POPC: palmitoyl-2-oleoyl-sn-glycero-3-phosphocholine. [c]Average values ± S.D. (n=3).

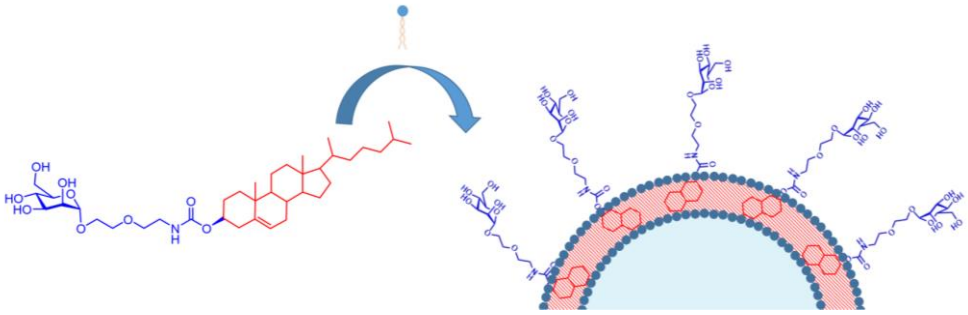

Figure 29 - Targeted liposomes formed from Mannose ligand (**14**), where a cholesterol anchor was employed to insert Man ligand in the liposomal membrane.

Aggregation assay were carried out comparing 10% Man-Chol liposome with 10% Man-TEG liposome. Surprisingly, for the 10% Man-Chol liposome formulation no Con A-mediated liposome clustering could be observed (Figure 30). As previously discussed, when membranes are rich in cholesterol, some of their components can segregate with the formation of lipid rafts (Lingwood and Simons 2010), (Hayden *et al.* 2009). Noble and coworkers showed that mannosylated ligands with a hydrophobic perfluoroalkyl pyrene anchor, when inserted into vesicles, can phase-separate into artificial lipid rafts (Noble *et al.* 2009) and bind Con A in a monovalent manner.

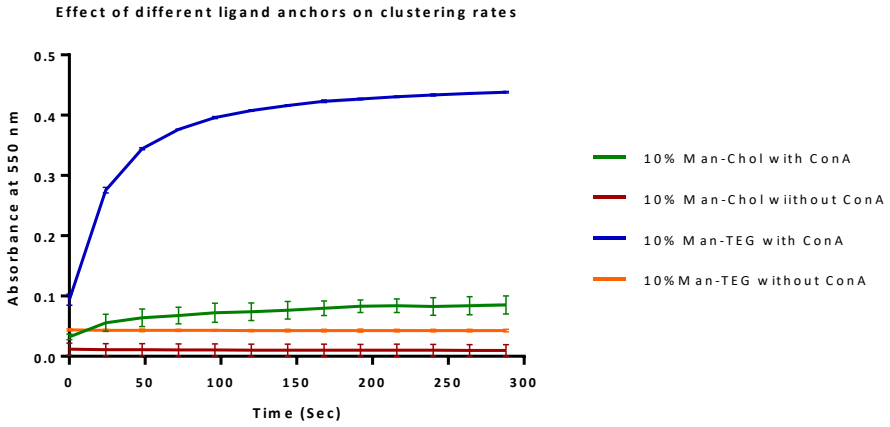

Figure 30 - Effect of lipid anchor on Con A-liposome aggregation using 10 % mannosylated ligands - Man-TEG palmitoyl **(10)** and Man-cholesterol **(14)** ligands - on the liposome membrane. Con A in 0.10 M HEPES buffer (0.90 M NaCl, 1.0 mM $CaCl_2$, 1.0 mM $MgCl_2$ - pH7.4) was added to each formulation to induce liposomal aggregation. The data set shows groups of continuous data acquired every 0.2 sec. For more convenient data visualisation, standard deviations are shown for every 25 sec recorded data points.

The lack of any significant lectin binding shows that the mannose groups are less available, which could be due to the lack of tetravalent interactions between Con A and liposomal membranes (Figure 31a) or to steric crowding of the mannose groups in the lipid rafts (Figure 31b) (Noble *et al.* 2009).

Another possible explanation of the poor ligand membrane exposure is related to the location of cholesterol in the membrane (Marquardt *et al.* 2016) which could reduce the ligand exposure at the surface for effective interaction with lectin binding pockets with deeper embedding of the Man-TEG ligand in the membrane (Figure 31c).

For time restrictions, these hypotheses have not been further investigated in this thesis work, and will be the subject of future work within our group.

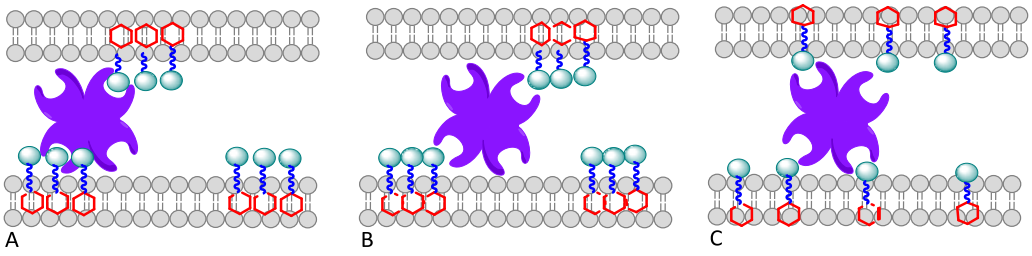

Figure 31 - Schematic representation of Con A clustering by Man-ligand with cholesterol anchor in Man-liposomes. (A) Binding of Con A to mannosylated ligands that are in artificial "lipid rafts"; (B) Clustering of mannosyl ligands causes steric congestion for efficient Con A binding; (C) deeper embedding of the Man-TEG ligand in the membrane causes poor mannose ligand membrane exposure.

3.5 Conclusions

In this chapter, the role of the liposome structural components on binding to Con A model binding was investigated. Four glycosylated lipids (**6**, **8**, **10** and **14**) - with and without tetraethyleneglycol spacer and with different anchors - have been used to formulate targeted glycoliposomes. Following sonication and extrusion, all formulations investigated were found to be stable and with an average size around 0.1 μm. Con A was used as a model lectin to investigate how densities of different sugars residues (mannose and galactose), the spatial distribution of these ligands and the lipid composition of the liposomal membrane affect the rate of lectin binding. At this point in the work, glycopolymer ligands were not yet available, therefore aggregation studies were carried out only on monovalent ligands. Our results indicated that the binding kinetics can be strongly affected by these parameters. The presence of sugar ligands on the surface of liposomal membrane is not sufficient *per se* to achieve efficient binding; the way they are displayed is equally important. Both the surface density of glycosilated-lipids and the lipidic composition of the liposomal membrane were found to affect the rate of lectin binding. The cholesterol content was found to increase the binding rate, whilst within the range of concentrations investigated (0-15% of the total lipid molar composition) the effect of PS was significantly less marked. The rate of Con A-mediated liposome clustering was found to be directly proportional to the density of Man-TEG ligand (**10**) on the liposome membrane, up to10% Man *vs.* total lipid molar composition. After this limit a plateau in clustering rate was observed. Surprisingly Man-Chol ligand (**14**) showed poor ligand exposure compare with Man-TEG ligand palmitoyl anchored. We hypothesised that the lack of binding between Con A and

Man-Chol liposome may be due to a lack of cluster glycoside effect caused by the segregation of Man-Chol ligand (**14**) in lipid-rafts or due to the poor ligand membrane exposure for the deeper embedding of the cholesterol anchor.

3.6 References

Bertrand, Nicolas, Jun Wu, Xiaoyang Xu, Nazila Kamaly, and Omid C. Farokhzad. 2014. "Cancer Nanotechnology: The Impact of Passive and Active Targeting in the Era of Modern Cancer Biology." *Advanced Drug Delivery Reviews* 66. Elsevier B.V.: 2–25.

Briuglia, Maria Lucia, Chiara Rotella, Amber McFarlane, and Dimitrios A. Lamprou. 2015. "Influence of Cholesterol on Liposome Stability and on in Vitro Drug Release." *Drug Delivery and Translational Research* 5 (3): 231–42.

Brown, D. A., and E. London. 1998. "Structure and Origin of Ordered Lipid Domains in Biological Membranes." *The Journal of Membrane Biology* 164 (2): 103–14.

Brown, Deborah A, and Erwin London. 2000. "Structure and Function of Sphingolipid- and Cholesterol-Rich Membrane Rafts." *Journal of Biological Chemistry* 275 (23): 17221–24.

Bunker, Alex, Aniket Magarkar, and Tapani Viitala. 2016. "Rational Design of Liposomal Drug Delivery Systems, a Review: Combined Experimental and Computational Studies of Lipid Membranes, Liposomes and Their PEGylation." *Biochimica et Biophysica Acta (BBA) - Biomembranes* 1858 (10). Elsevier B.V.: 2334–52.

Cairo, Christopher W., Jason E. Gestwicki, Motomu Kanai, and Laura L. Kiessling. 2002. "Control of Multivalent Interactions by Binding Epitope Density." *Journal of the American Chemical Society* 124 (8): 1615–19.

Curatolo, William, Annie O Yau, Donald M Small, and Barry Sears. 1978. "Lectin-Induced Agglutination of Phospholipid/Glycolipid Vesicles." *Biochemistry* 17 (26): 5740–44.

Engel, Andreas, Swapan K. Chatterjee, Ali Al-Arifi, and Peter Nuhn. 2003a. "Influence of Spacer Length on the Agglutination of Glycolipid-Incorporated Liposomes by Con A as Model Membrane." *Journal of Pharmaceutical Sciences* 92 (11): 2229–35.

Engel, Andreas, Swapan Kumar Chatterjee, Ali Al-arifi, Dagmar Riemann, Jürgen

Langner, and Peter Nuhn. 2003b. "Influence of Spacer Length on Interaction of Mannosylated Liposomes with Human Phagocytic Cells." *Pharmaceutical Research* 20 (1): 51–57.

Espuelas, Socorro, Philippe Haller, Francis Schuber, and Benoît Frisch. 2003. "Synthesis of an Amphiphilic Tetraantennary Mannosyl Conjugate and Incorporation into Liposome Carriers." *Bioorganic and Medicinal Chemistry Letters* 13 (15): 2557–60.

Espuelas, Socorro, Christine Thumann, Béatrice Heurtault, Francis Schuber, and Benoît Frisch. 2008. "Influence of Ligand Valency on the Targeting of Immature Human Dendritic Cells by Mannosylated Liposomes." *Bioconjugate Chemistry* 19 (12): 2385–93.

Gestwicki, Jason E., Christopher W. Cairo, Laura E. Strong, Karolyn A. Oetjen, and Laura L. Kiessling. 2002. "Influencing Receptor-Ligand Binding Mechanisms with Multivalent Ligand Architecture." *Journal of the American Chemical Society* 124 (50): 14922–33.

Gou, Yanzi, Jin Geng, Sarah Jane Richards, James Burns, C. Remzi Becer, and D. M. Haddleton. 2013. "A Detailed Study on Understanding Glycopolymer Library and Con A Interactions." *Journal of Polymer Science, Part A: Polymer Chemistry* 51 (12): 2588–97.

Hayden, Carl C., Jane S. Hwang, Elisa A. Abate, Michael S. Kent, and Darryl Y. Sasaki. 2009. "Directed Formation of Lipid Membrane Microdomains as High Affinity Sites for His-Tagged Proteins." *Journal of the American Chemical Society* 131 (25): 8728–29.

Ikonen, Elina. 2008. "Cellular Cholesterol Trafficking and Compartmentalization." *Nature Reviews. Molecular Cell Biology* 9 (2): 125–38.

Jacobson, Ken, Ole G Mouritsen, and Richard G W Anderson. 2007. "Lipid Rafts: At a Crossroad between Cell Biology and Physics." *Nature Cell Biol* 9 (1): 7–14.

Jain, Keerti, Prashant Kesharwani, Umesh Gupta, and Narendra K. Jain. 2012. "A Review of Glycosylated Carriers for Drug Delivery." *Biomaterials* 33 (16). Elsevier

Ltd: 4166–86.

Jayaraman, Narayanaswamy. 2009. "Multivalent Ligand Presentation as a Central Concept to Study Intricate Carbohydrate-Protein Interactions." *Chemical Society Reviews* 38 (12): 3463–83.

Jayaraman, Narayanaswamy, Krishnagopal Maiti, and Kottari Naresh. 2013. "Multivalent Glycoliposomes and Micelles to Study Carbohydrate-Protein and Carbohydrate-Carbohydrate Interactions." *Chemical Society Reviews* 42 (11): 4640–56.

Johannssen, Timo, and Bernd Lepenies. 2017. "Glycan-Based Cell Targeting To Modulate Immune Responses." *Trends in Biotechnology* 35 (4). Elsevier Ltd: 334–46.

Kingery-Wood, Jill E, Kevin W Williams, George B Sigal, and George M Whiteside. 1992. "The Agglutination of Erythrocytes by Influenz Virus Is Strongly Inhibited by Liposomes Incorpoprating an Analog of Sialyl Gangliosides." *Journal of the American Chemical Society* 114 (18): 7303–5.

Kitano, H., Y. Sumi, and K. Tagawa. 2001. "Recognition of Novel Lipopolypeptides with Many Pendent Sugar Residues by Lectin." *Bioconjugate Chemistry* 12 (1): 56–61.

Kranz, Lena M, Mustafa Diken, Heinrich Haas, Sebastian Kreiter, Carmen Loquai, Kerstin C Reuter, Martin Meng, *et al.* 2016. "Systemic RNA Delivery to Dendritic Cells Exploits Antiviral Defence for Cancer Immunotherapy." *Nature Letter* 0 (0). Nature Publishing Group: 1–6.

Ladmiral, Vincent, Giuseppe Mantovani, Guy J Clarkson, Solene Cauet, Jacob L Irwin, and David M Haddleton. 2006. "Synthesis of Neoglycopolymers by a Combination of 'Click Chemistry' and Living Radical Polymerization." *Journal of the American Chemical Society* 128 (14): 4823–30.

Li, Wai Ming, Lawrence D Mayer, and Marcel B Bally. 2002. "Prevention of Antibody-Mediated Elimination of Ligand-Targeted Liposomes by Using Poly(ethylene Glycol)-Modified Lipids." *The Journal of Pharmacology and Experimental Therapeutics* 300 (3): 976–83.

Lian, T, and R J Ho. 2001. "Trends and Developments in Liposome Drug Delivery Systems." *Journal of Pharmaceutical Sciences* 90 (6): 667–80.

Lingwood, Daniel, and Kai Simons. 2010. "Lipid Rafts as a Membrane-Organizing Principle." *Science* 327 (5961): 46–50.

Liu, Der Zen, Wen Yih Chen, Li Min Tasi, and Shu Ping Yang. 2000. "Microcalorimetric and Shear Studies on the Effects of Cholesterol on the Physical Stability of Lipid Vesicles." *Colloids and Surfaces A: Physicochemical and Engineering Aspects* 172 (1–3): 57–67.

Mammen, Mathai, Seok-Ki Choi, and George M. Whitesides. 1998. "Polyvalent Interactions in Biological Systems: Implications for Design and Use of Multivalent Ligands and Inhibitors." *Angew. Chem. Int. Ed.* 37 (June): 2754–94.

Marquardt, Drew, Norbert Kucerka, Stephen R Wassall, Thad A Harroun, and John Katsaras. 2016. "Cholesterol's Location in Lipid Bilayers." *Chemistry and Physics of Lipids* 199: 17–25.

Mody, Nishi, Rakesh Kumar Tekade, Neelesh Kumar Mehra, Prashant Chopdey, and Narendra Kumar Jain. 2014. "Dendrimer, Liposomes, Carbon Nanotubes and PLGA Nanoparticles: One Platform Assessment of Drug Delivery Potential." *AAPS PharmSciTech* 15 (2): 388–99.

Mouritsen, O. G. 1991. "Theoretical Models of Phospholipid Phase Transitions." *Chemistry and Physics of Lipids* 57: 179–94.

Muller, C.D., and F. Schuber. 1989. "Neo-Mannosylated Liposomes: Synthesis and Interaction with Mouse Kupffer Cells and Resident Peritoneal Macrophages." *Biochimica et Biophysica Acta (BBA) - Biomembranes* 986 (1): 97–105.

Noble, Gavin T, Sabine L Flitsch, Kwan Ping Liem, and Simon J Webb. 2009. "Assessing the Cluster Glycoside Effect during the Binding of Concanavalin A to Mannosylated Artificial Lipid Rafts." *Organic & Biomolecular Chemistry* 7 (24): 5245–54.

Noble, Gavin T, Jared F Stefanick, Jonathan D Ashley, Tanyel Kiziltepe, and Basar Bilgicer. 2014. "Ligand-Targeted Liposome Design: Challenges and Fundamental

Considerations." *Trends in Biotechnology* 32 (1). Elsevier Ltd: 32–45.

Nobs, Leila, Franz Buchegger, Robert Gurny, and Eric Allémann. 2004. "Current Methods for Attaching Targeting Ligands to Liposomes and Nanoparticles." *Journal of Pharmaceutical Sciences* 93 (8): 1980–92.

Sanna, Vanna, Nicolino Pala, and Mario Sechi. 2014. "Targeted Therapy Using Nanotechnology: Focus on Cancer." *International Journal of Nanomedicine* 9 (1): 467–83.

Simons, K, and D Toomre. 2000. "Lipid Rafts and Signal Transduction." *Nature Reviews. Molecular Cell Biology* 1 (1): 31–39.

Sipai Altaf Bhai, M, Vandana Y, Y Mamatha, and V Prasanth. 2012. "Liposomes: An Overview." *Journal of Pharmaceutical and Scientific Innovation* 1 (1): 13–21.

Sorkin, Raya, Nir Kampf, and Jacob Klein. 2017. "Effect of Cholesterol on the Stability and Lubrication Efficiency of Phosphatidylcholine Surface Layers." *Langmuir* 33 (30): 7459–67.

Spevak, Wayne, Jon O Nagy, Deborah H Charych, Mary E Schaefer, James H Gilbert, and Mark D Bednarski. 1993. "Polymerized Liposomes Containing C-Glycosides of Sialic Acid: Potent Inhibitors of Influenza Virus in Vitro Infectivity." *Journal of the American Chemical Society* 115 (3): 1146–47.

Szoka, Francis Jr. 1980. "Comparative Properties and Methods of Preparation of Lipid Vesicles (Liposomes)." *Annual Review of Biophysics and Bioengineering* 9: 467–508.

Thomas, Glen B, Lenea H Rader, Juhee Park, Ludmila Abezgauz, Dganit Danino, Philip DeShong, and Douglas S English. 2009. "Carbohydrate Modified Catanionic Vesicles: Probing Multivalent Binding at the Bilayer Interface." *Journal of the American Chemical Society* 131 (15): 5471–77.

Unger, Wendy W J, Astrid J. Van Beelen, Sven C. Bruijns, Medha Joshi, Cynthia M. Fehres, Louis Van Bloois, Marleen I. Verstege, *et al.* 2012. "Glycan-Modified Liposomes Boost CD4 + and CD8 + T-Cell Responses by Targeting DC-SIGN on Dendritic Cells." *Journal of Controlled Release* 160 (1). Elsevier B.V.: 88–95.

Vabbilisetty, Pratima, and Xue-Long Sun. 2015. "Liposome Surface Functionalization

Based on Different Anchoring Lipids via Staudinger Ligation." *Org Biomol Chem* 12 (8): 1237–44.

Valencia, Pedro M., Mikhail H. Hanewich-Hollatz, Weiwei Gao, Fawziya Karim, Robert Langer, Rohit Karnik, and Omid C. Farokhzad. 2011. "Effects of Ligands with Different Water Solubilities on Self-Assembly and Properties of Targeted Nanoparticles." *Biomaterials* 32 (26). Elsevier Ltd: 6226–33.

van Kooyk, Y, and G A Rabinovich. 2008. "Protein-Glycan Interactions in the Control of Innate and Adaptive Immune Responses." *Nature Immunoly* 9 (6): 593–601.

van Meer, Gerrit, Dennis R. Voelker, and Gerald W. Feigenson. 2008. "Membrane Lipids: Where They Are and How They Behave." *Nature Reviews. Molecular Cell Biology* 9 (2): 112–24.

Xie, Ran, Lu Dong, Rongbing Huang, Senlian Hong, Ruoxing Lei, and Xing Chen. 2014. "Targeted Imaging and Proteomic Analysis of Tumor-Associated Glycans in Living Animals." *Angewandte Chemie - International Edition* 125 (53): 14306–14310.

CHAPTER 4

Bespoke glycoliposomes for *Salmonella* intracellular infection *in vitro* model

Intracellular infections caused by pathogens such as *Salmonella, Listeria*, and *Mycobacterium* species, constitute a challenge for antimicrobial treatment (Ranjan *et al.* 2012). As discussed in Chapter 1.3.3, in such infections bacteria are protected inside the host cells, thus to eradicate them antibiotics need to cross the host-cell membrane and reach the intracellular site at a sufficient therapeutic level. Therefore the discovery of new antibiotics *per se* is not sufficient for the treatment of these pathogens (Huh and Kwon 2011). Antibiotic-loaded carriers have been investigated to improve the delivery of drugs to bacteria-infected cells (Pinto-Alphandary *et al.* 2000). Mannose Receptor (MR, CD206) a carbohydrate endocytic receptor present on immature dendritic cells, macrophages, and selected endothelial cells, is a potential access gate to *Salmonella*-infected macrophages which could be selectively targeted with mannosylated-decorated liposomes.

Chapter 4: Bespoke glycoliposomes for *Salmonella* intracellular infection *in vitro* model

Liposomes are the most employed nanodevices to encapsulate antibiotics for treating intracellular infections (Velge *et al.* 2012) and they have been used in several *Salmonella* intracellular infection studies both *in vitro* (Lutwyche *et al.* 1998) and *in vivo* (Fierer *et al.* 1990), thus they were utilised in this work as the drug delivery carrier of choice. In this chapter we describe the design, the development and investigation of liposomal systems to delivery antimicrobials into *Salmonella*-infected macrophages. The hereby presented preliminary results of liposome internalisation and bacterial killing efficacy will require further investigation (discuss in Chapter 5.2).

4.1 Introduction

As discussed in Chapter 1.3, *Salmonella enterica* subspecies *enterica* serovar Typhi and Typhimurium (hereafter referred to as *S*. Typhi and *S*. Typhimurium, respectively) are the subspecies responsible for most *Salmonella* infections in humans (Darwin and Miller 1999). *S*. Typhi is an exclusive human pathogen (Parry *et al.* 2002) and it is responsible for an invasive, life-threatening, systemic disease, known as typhoid fever, where the bacteria enter, survive and replicate within macrophages (Finlay and Brumell 2000). It has been estimated that there are over 16 million cases of typhoid fever per year worldwide, with more than 600,000 deaths (Crumpi *et al.* 2004). *S*. Typhimurium usually causes gastroenteritis in human with 93.8 million cases per year (Crump *et al.* 2004). *S*. Typhimurium, as its name murine-Typhi suggests, induces a systemic disease in mice similar to human typhoid fever, and therefore provides a valid model to study *Salmonella* intracellular infection in macrophages (Mackaness *et al.* 1966). A key parameter in *Salmonella* intracellular infection of macrophage cells is the average number of bacteria inside each infected cell. Counts of bacteria in patients with acute typhoid fever indicated that not all phagocytic cells are infected (Mastroeni *et al.* 2009), and showed a median concentration of 1.3 organisms per phagocytic cell (Rubin *et al.* 1990), (Wain *et al.* 1998), (Wain *et al.* 2001). Accordingly, in this work we targeted an analogous multiplicity of infection (MOI) in our infection model (Figure 32).

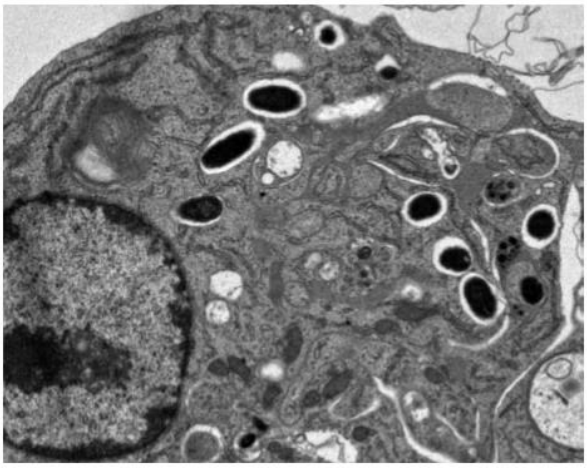

Figure 32 - Transmission electron microscopy image of *Salmonella enterica* subsp. *enterica* serovar Typhimurium growing within a macrophage 22 hours post-infection. (Image of G. M. Barton, University of California, Berkeley, USA.), (Sanchez 2011).

An additional complication in the treatment of *Salmonella* infections is the potential development of antimicrobial resistance which can dramatically reduce the range of effective antibiotics (Levy and Marshall 2004), (Rowe *et al.* 1997). The gold standard antibiotics against serious bacterial pathogens are aminoglycosides, which are very potent, broad-spectrum antibiotics (Magnet and Blanchard 2005). Although aminoglycosides are effective against many bacterial pathogens, including *Salmonella*, they have no activity in treating intracellular bacterial infections (Lo *et al.* 2014), (Holmes *et al.* 1966), as the hydrophilicity of these molecules restricts their permeability through the cell membrane of the host (Magnet and Blanchard 2005). In order to increase the therapeutic index of this class of antibiotics and to reduce their side effects, liposomal formulations incorporating aminoglycoside antibiotics have been investigated both in pre-clinical and clinical studies. For example, amikacin

encapsulated in DPPC and cholesterol liposomes for lung infections treatment is currently in phase III of clinical trials (Bulbake *et al.* 2017), (Schiffelers *et al.* 2002).

A number of *in vitro* studies suggest that liposomes loaded with the aminoglycoside gentamicin (Appendix 6.4, Figure S59) can be potentially effective for the treatment of intracellular infections (Burton *et al.* 2015), (Mugabe *et al.* 2005), (Lutwyche *et al.* 1998). In these studies the effectiveness of these liposomal formulations was ascribed to their ability to prolong the half-life of the drug in systemic circulation, and achieve passive accumulation at a site of infection. Few other studies have utilised pH-sensitive liposomes to induce the gentamicin release in endosomal compartments (Lutwyche *et al.* 1998), (Cordeiro *et al.* 2000). In this part of our work, we aimed at enhancing the antibacterial activity of gentamicin for the treatment of *Salmonella* intracellular infections, by utilising glycosylated liposomes able to target the macrophage Mannose Receptor (Figure 33), and exploit its ability to promote cellular uptake of appropriate glycosylated ligands.

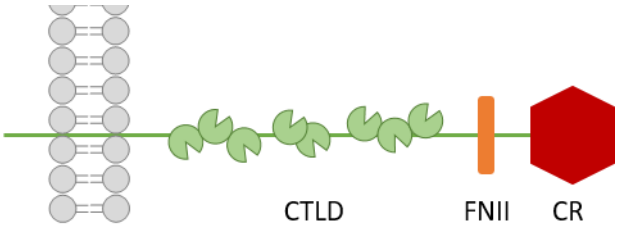

Figure 33 – Schematic representation of the structure of the mannose receptor (MR, CD206). Cysteine rich (CR) domain: binds sulfated glycans containing Gal and GalNAc 3/4 O-sulfated . FNII domain: binds Collagens (I-IV). C type-like domains CTLD: binds to mannose and fucose carbohydrate residues (Martinez-Pomares 2012).

4.2 Materials and Methods

4.2.1 Materials

RAW 264.7 cells obtained from the European Collection of Cell Culture (ECACC 91062702) were kindly gifted by Dr Frankie Rawson (School of Pharmacy, Nottingham) and used between passages 7-20. Gentamicin, Dulbecco's Modified Eagles Medium (DMEM), phosphate buffered saline (PBS), Foetal Bovine Serum (FBS, non-USA origin), 4-(2hydroxyethyl)-1-piperazineethanesulfonic acid (HEPES), Triton X-100, Mueller-Hinton (MH) agar, Luria-Bertani (LB) broth and agar were all obtained from Sigma Aldrich. Antibiotic-antimycotic solution (containing Amphotericin B, Penicillin, Streptomycin) and Hanks Balanced Salt Solution (HBSS) with calcium chloride, magnesium sulfate and glucose, without sodium bicarbonate and phenol red, were obtained from Invitrogen Gibco. Dimethylsulfoxide (DMSO) and cell scrapers (25 cm x 20 mm) were purchased from VWR international. Cell culture dishes (58 cm^2), sterile pipettes, and sterile centrifuge tubes (of 15 mL and 50 mL volume capacity) were purchased from Sarstedt. Black tissue culture 96-well plates were obtained from Thermo Scientific Nunc.

4.2.2 Methods

4.2.2.1 Cell cultures

Cell medium for sub-culturing was supplemented with FBS, HEPES and Amphotericin B/penicillin/streptomycin solution at final concentrations of 10% v/v, 2.4% v/v and 1% v/v respectively. RAW 264.7 cells were routinely cultured in 58 cm^2 dishes at 5% CO_2, 95% relative humidity and 37°C until near-confluence (approximately 70% coverage of the dish surface by cells). Cell growth was monitored regularly by viewing the cells under an optical microscope. Once near-confluent, cells were passaged following ATCC recommendations (ATCC 1997). Cell culture medium was replaced every two - three days by aspirating all but 5 mL of culture medium from the dishes. Cells were dislodged from the dish with a cell scraper, aspirated and appropriate aliquots of the cell suspension was added into new culture vessel in ratio of 1:3 or 1:6 by the addition of 12-15 mL of pre-warmed to 37°C fresh medium. For seeding density, cells were counted using a haemocytometer (Laboratory Supplies) (ATCC 2014). For frozen storage of cells, RAW 264.7 were cultured to confluence and then dislodged from the flask with a cell scraper. Following centrifugation of the cell suspension, the supernatant was aspirated, and the cell pellet was resuspended in 1 mL of complete culture medium containing 10% v/v DMSO. The cell suspension was transferred to a sterile cryovial, which was placed into a Mr Frosty freezing container (Nalgene) at -80°C. Thereafter, cells were transferred into a liquid nitrogen cell storage tank. For thawing the cells, cryovials containing frozen cells were removed from the liquid nitrogen-containing storage tank and thawed by gentle agitation in a 37°C water bath. DMSO-containing medium was removed by transferring the cell suspension into

a centrifuge tube containing approximately 5 mL of warm (37°C) culture medium, centrifuging the resulting suspension at 1500 x g for 5 min and aspirating the supernatant. The cell pellet was thereafter resuspended in approximately 5 mL of culture medium and transferred into a 58 cm^2 flask containing approximately 10 mL of fresh, warmed (37°C) culture medium.

4.2.2.2 Bacterial cultures

Salmonella enterica subsp. e*nterica* serovar Typhimurium DsRed2 (SL1344 transformed with a DsRed2 expression plasmid to facilitate bacterial visualisation) and *Staphylococcus aureus* Newman were kindly made available by Dr Alan Huett (School of Life Sciences, Nottingham). Bacteria were preserved at -80°C in glycerol at a final concentration of 20% (v/v) until use. For bacterial seeding, a small amount of bacteria was scraped off the glycerol stock. The loop was wiped at the top end of a fresh agarose agar plate moving in a zig-zag horizontal pattern until 1/3 of the plate was covered. The plate was rotated about 60 degrees and the bacteria were spread from the end of the first streak into a second area. This procedure was repeated to spread the bacteria in a third area of the plate. The plate was incubated in incubator overnight at 37°C.

4.2.2.3 Statistical Analysis

Data set have been processed by Tukey's method (Hoaglin *et al.* 1986) to identify and remove any outliers. Briefly, using the lower and upper fourths, FL and FU (approximate quartiles), it labels as "outside" any observations below FL - 1.5 (FU - FL) or above FU + 1.5(FU - FL). Data are reported as mean and the error shown is the standard deviation. One-way or two-way analysis of variance (ANOVA) were carried out using GraphPad Prism. In this chapter, N = numbers of replicates (experiment performed in different days, same conditions) and n = numbers of repetition (different measurements during the same experiment).

4.3 Experimental section

All the different cell and bacterial media with the supplemented components utilised in the experimental procedures described in this chapter are summarised in Table 9.

Table 9 – Cell DMEM media and Bacterial growth media.

Media	Antibiotic used	Antibiotic μg/mL	Used for
Cell DMEM Media[1]			
Growth Medium[2]	P/S	100	Normal cell subculturing and cell seeding
Gentamicin Free Medium	-	-	During infection assay, to suspend *Salmonella* for cell infection
Low Gentamicin Medium	G	20	During infection assay, to maintain cells after *Salmonella* internalisation
High Gentamicin Medium	G	100	During infection assay, to kill extracellular *Salmonella*
Bacterial Growth Media			
Luria-Bertani (LB) Broth	A	100	For *Salmonella* overnight culture
Luria-Bertani (LB) Agar	A	100	For *Salmonella* colonies seeding
Luria-Bertani (LB) Broth	-	-	For *S. aureus* overnight culture
Muller- Hinton (MH) Agar	-	-	For *S. aureus* inhibition studies

P: Penicillin, S: Streptomycin, A: Ampicillin, G: Gentamicin.

[1]10% v/v FBS; [2] 2.4% v/v 1 M HEPES solution.

4.3.1 *Salmonella* intracellular infection in RAW 264.7 cells

The day before the infection experiment, RAW 264.7 cells were seeded in a 24 well plate with a density of 5 x 10^4 cells/mL per well and the plate was incubated overnight at 37°C (Figure 34a). In parallel, two - three colonies of SL1344 DsRed2 were scraped off the agar plate of a culture using a disposable sterile loop. The colonies were suspended in 4 mL of LB broth supplemented with 100 µg/mL ampicillin. The culture was incubated overnight in a shaking incubator (250 rpm) at 37°C.

After 16 hours, bacteria were collected by centrifugation (1500 x g for 15 min) and resuspended in 4 mL of PBS. Bacteria were diluted in Gentamicin Free Medium (GFM) with different dilutions in order to test different multiplicity of infection (MOI) ratios. Cultured RAWs 264.7 were infected by the addition of 0.5 mL per well of SL1344 DsRed2 in GFM (Figure 34b). The plate was centrifuged (700 x g for 10 min) and incubated for 20 min at 37°C (Figure 34c). Then, medium was aspirated, each well was rinsed and then incubated with 0.5 mL of High Gentamicin Medium (HGM) for 30 min in order to kill extracellular bacteria (Figure 34d). Thirty minutes later, HGM was replaced with Normal Gentamicin Medium (NGM) and incubated for different durations. At the desired time point, the infected cells were washed three times with PBS, and the surviving intracellular bacteria were harvested by lysing the cells with 1% Triton X-100 in PBS for 10 min at 37°C (Figure 34e). The supernatants were immediately serially diluted with PBS (Figure 34f) and spotted onto LB agar plates (Figure 34g). After incubation for 16 h at 37°C, the numbers of bacterial colonies for each sample were counted and expressed as colony-forming units (CFU) per mL (Figure 34h). For fluorescence cell imaging, a glass coverslip was placed at the bottom of the well and then cells were seeded. After the infection assay and the PBS washes,

cells were fixed with 0.5 mL of 4% formaldehyde in PBS for 15 min. Cells were washed once in PBS and then permeabilised with 1% Triton-X in PBS for 2 min. The solution was then removed and cells were washed once in PBS. DNA staining DAPI and actin-staining Phalloidin were added and the coverslips incubated at room temperature for 20 min in the dark. Coverslips were then washed in PBS, mounted onto a glass slide and sealed with nail polish.

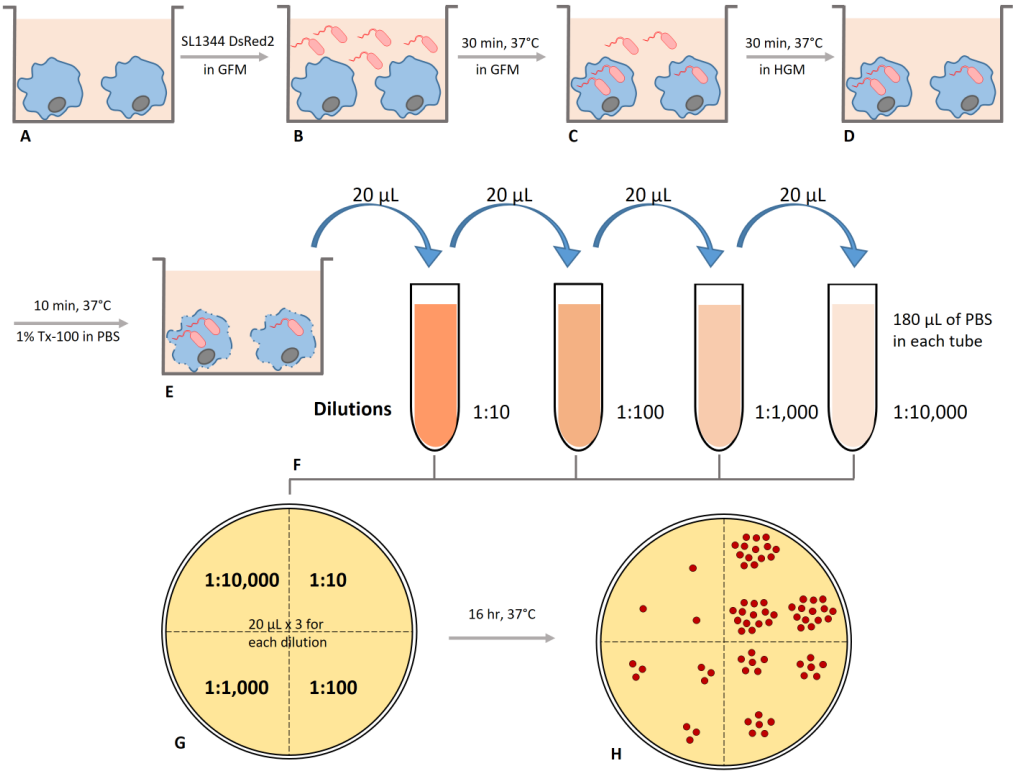

Figure 34 – Schematic representation of *Salmonella* infection assay. A) RAW 264.7 cells are incubated overnight at 37°C. B) After 16 hours, an overnight culture of SL1344 DsRed2 is diluted in Gentamicin Free Medium (GFM) and used to infect RAWs 264.7. C) The plate is centrifuged for 10 min and incubated for 20 min at 37°C. D) Cells are treated with High Gentamicin Medium (HGM) for 30 min to remove extracellular bacteria. E) At the desired time point, the infected cells area washed with PBS, and the surviving intracellular bacteria are harvested by lysis the cells with 1% Triton X-100 in PBS for 10 min at 37°C. F) Supernatants are immediately serially diluted with PBS and G) spotted onto LB agar plates. H) After 16 h of incubation at 37°C, the numbers of bacterial colonies for each sample are counted and expressed as colony-forming units (CFU) per mL.

4.3.2 Fluorescently labelled and gentamicin encapsulated liposomes

Liposomes were prepared similarly as described in Chapter 3.3.1. Briefly, stock solutions of phospholipids, cholesterol, glycoligands (compounds **10, 14, 26**), 1,1'-dioctadecyl-3,3,3',3'-tetramethylindodicarbocyanine 4-chlorobenzenesulfonate salt (DID) were all prepared at a concentration of 1.0 mg/mL unless otherwise stated (Table 10). Liposome formulations were prepared by the Bangham Method (hydration of a thin lipid film). The required amount of each lipid stock solution was mixed in a round-bottomed flask and the organic solvent was evaporated under reduced pressure to form a lipid film. The round bottom flask was then left under a stream of nitrogen to dry for two hours to ensure that any residual solvent was removed. The lipid film was hydrated with HBSS (25.0 mM HEPES, pH 7.4) buffer with total lipid concentration of 5.0 mM in all formulations. The mixture was sonicated and extruded at 20°C through a polycarbonate membrane with 0.1 μm pore size. After 21 cycles through the extrusion device (AvantiPolar Lipid), the resulting liposomal formulation was diluted with HBSS (25.0 mM HEPES) buffer at final lipid concentration of 1.0 mM.

For gentamicin loaded liposomes, the dried lipid films were rehydrated by adding 1.0 mL HBSS (25.0 mM HEPES) containing 5 mg/mL of gentamicin with total lipid concentration of 5.0 mM. Hydration was facilitated by extensive vortexing and by five freeze-thaw cycles using ice bath and oil bath at 60°C. After 21 cycles through the extrusion device, the resulting liposomal formulation was diluted with HBSS (25.0 mM HEPES) buffer at final lipid concentration of 1.0 mM. Unencapsulated gentamicin was removed by 10 cycles of centrifugal ultrafiltration (Centrisart®, MWCO: 20 kDa). The ultrafiltrate containing unloaded gentamicin was removed and replaced with the same

volume of fresh HBSS (25.0 mM HEPES) for each cycle. Encapsulation efficiency of gentamicin was measured by microbiological assay (4.3.5).

Table 10 - Stock solutions: concentration and solvents.

Solute	Code	Conc mg/mL	Solvent
1-palmitoyl-2-oleoyl-sn-glycero-3-phosphocholine	POPC	1.0	$CHCl_3$
Cholesterol	Chol	1.0	$CHCl_3$
Sphingomyelin	SM	1.0	$CHCl_3$/MeOH (9:1)
1'-Dioctadecyl-3,3,3',3'-tetramethyl-indodicarbocyanine, 4-chlorobenzene sulfonate salt	DID	0.1	$CHCl_3$
Glycoligands (**10**, **14, 26**)	-	0.1	$CHCl_3$/MeOH (9:1)
Gentamicin	-	5	HBSS (25.0 mM HEPES)

4.3.3 *In vitro* uptake studies

RAW 264.7 were seeded at a density of 2×10^4 cells/mL in a 96 black well plate with 0.1 mL of growth medium and incubated overnight at 37 °C. Cells were infected with SL1344 DsRed2 with the infection assay described in section 4.3.1. After the incubation with HGM, each well was washed 3 times with 0.1 mL of PBS and then 0.1 mL of the desired liposomal formulation (1.0 mM of total lipids in HBSS, 25 mM HEPES) was applied. The cells were incubated for 2 hours at 37 °C. After this time, the liposomal suspension was removed from each well, cells were washed with PBS 3 times and then were lysed with DMSO. The uptake level was detected via the intensity of DID (Tecan Plate Reader, λ_{ex} 630 nm, λ_{em} 700 nm). Fluorescence data of the lysates

(F_{lysat}) were corrected (F_{corr}) with the DID encapsulation efficiency of the liposomes (EE %) to eliminate alteration of cell uptake data by altered DID encapsulation of each individual liposome preparation. Corrected fluorescence data were used for calculation of cellular uptake. The amount of encapsulated dye was determined by reading fluorescence value of 50 µL of liposomal formulation dissolved in 50 µL of DMSO. The EE% was calculated by dividing the concentration values taken from the encapsulated dye liposomes and initial value of DID added to the initial formulation (Vabbilisetty and Sun 2015).

4.3.4 *Salmonella* killing study

Free gentamicin and two liposomal formulations were tested for their ability to kill intracellular SL1344 infecting RAW 264.7 with validated *in vitro* cell infection model previously described (4.3.1). RAW 264.7 were seeded at a density of 2×10^4 cells/mL in a 96 black well plate with 0.1 mL of growth medium and incubated overnight at 37 °C. Cells were infected with SL1344 DsRed2 with the infection assay described in section 4.3.1. After the incubation with HGM, each well was washed 3 times with 0.1 mL of PBS and then 0.1 mL of the desired gentamicin loaded liposomal formulation (1 mM of total lipids in HBSS, 25 mM HEPES) was applied. The cells were incubated for 2 hours at 37 °C. Then, cells were rinsed with PBS and incubated for 4 additional hours with Normal Gentamicin Medium (NGM). After this time, the cells were washed three times with PBS, and the surviving intracellular bacteria were harvested by lysis of the cells with 1 % Triton X-100 in PBS. The supernatants were immediately serially diluted with PBS and spread onto LB agar plates. After incubation for 16 h at 37°C,

the numbers of bacterial colonies for each sample were counted and expressed as colony-forming units (CFU) per mL.

4.3.5 Microbiological assay

The concentration of antibiotics encapsulated into liposomes was determined by agar diffusion assay. A laboratory strain of *Staphylococcus aureus* Newman was used as indicator organism for gentamicin. Fresh colonies of *S. aureus* were suspended in 3 mL of antibiotic-free LB broth. The culture was incubated overnight in a shaking incubator (250 rpm) at 37°C. The bacterial suspension (containing 1.2 x 10^9 CFU/mL) was then diluted to 8x10^4 CFU/mL in 30 mL of warm (~50°C) MH agar into a falcon tube (Figure 35a). The mixture was poured into a sterile omni tray (128 mm×86 mm) and left to solidify for 30 min at room temperature (Figure 35b). Wells of 5 mm diameter were made with a cork borer (Figure 35c) and were filled with 50 μL of gentamicin solutions or liposomal samples (Figure 35d) in PBS with 0.2% of Triton X-100. The plate was incubated for 16 h at 37°C. The diameter of the zones of inhibition were measured (Figure 35e) and the average of duplicate measurements was used in data analysis. A standard curve was constructed with known concentrations of free gentamicin (Appendix 6.4 Figure S63) and was utilised to calculate concentrations of the entrapped gentamicin that were released from the liposomes by 0.2% Triton X-100. The minimum detection limit of the assay for gentamicin was 7.8 μg/mL.

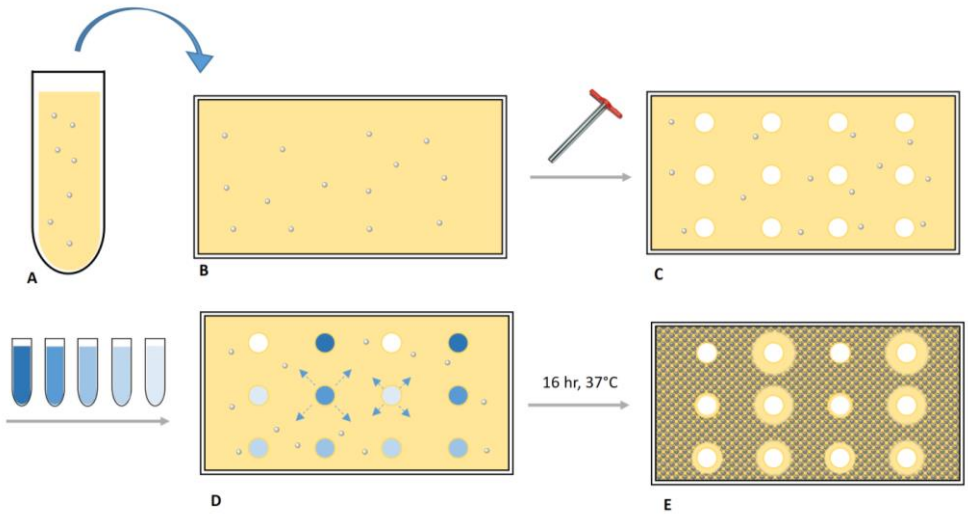

Figure 35 – Schematic representation of *S. aureus* inhibition assay. Colonies of *S. aureus* are suspended in antibiotic-free LB broth and incubated overnight (250 rpm at 37°C). A) The bacteria suspension is diluted to in 30 mL of warm (~50°C) MH agar into a falcon tube. B) The mixture is poured into a sterile omni tray and left to solidify for 30 min at room temperature. C) Wells of 5 mm diameter are made with a cork borer and D) filled with 50 μL of gentamicin solutions or liposomal samples in PBS with 0.2% of Triton X-100. The plate is incubated for 16 h at 37°C. E) The diameter of the zones of inhibition are measured and the average of duplicate measurements is used in data analysis.

4.4 Results and Discussion

4.4.1 *Salmonella* intracellular infection model

The initial aim of this part of the project was to develop an *in vitro* cell culture model to mimic *Salmonella*-infected macrophage cells. Comparative analyses have shown similarities between immunological and genetic mechanisms that regulate the interaction of *S. enterica* and its host in mice, humans and domestic animal species (Mastroeni *et al.* 2009). In the literature, several *in vitro* models have been investigated to study *Salmonella enterica* invasion mechanisms (Velge *et al.* 2012), (Walker *et al.* 2013), virulence (Garai *et al.* 2012) and interaction with macrophages (Ibarra and Steele-mortimer 2009). Murine macrophage-like cell line RAW264.7 has shown high susceptibility to *Salmonella* infection and it is considered the most useful model cell line to study intracellular survival of *Salmonella* within macrophages *in vitro* (Garai *et al.* 2012), (Gog *et al.* 2012). It should be noted that *in vitro Salmonella* infection models are extremely dynamic systems. Once *Salmonella* invades cultured macrophages, it undergoes rapid intracellular growth within a membrane-bound compartment, known as the *Salmonella*-containing vacuole (SCV) and can divide up to 100-fold in less than 24 hours (Tierrez *et al.* 2005). In contrast, in human infection it has been found that four days post-infection, more than 90% of the infected cells contained less than 3 bacteria (Sheppard *et al.* 2003). Furthermore, infecting cultured macrophage cells with high dose of *Salmonella* (MOI 100) can lead to cell apoptosis (Schwan *et al.* 2000). Thus, our initial experiments aimed at identifying the experimental conditions required to establish a controlled and reproducible infection model.

Salmonella enterica subsp. *enterica* serovar Typhimurium (SL1344), expressing a red fluorescent protein (DsRed2), was used to infect mouse macrophage RAW264.7 cells as previously described (4.3.1). In addition to its high susceptibility to infection, this cell line is characterised by a "lag-phase" of 24 hour (Iloki Assanga *et al.* 2013), which means that despite the fast rate of growing, within the first 24 hours following infection the density of cells seeded in a plate will not increase significantly. Two multiplicities of infection (MOI) were tested at ratio 55:1 and 6:1 bacteria per cell, and the infection was monitored over 4 hours. After 0.5, 1, 2 and 4 hours, cells were lysed with 1% Tx-100 in PBS and the cell content was diluted and seeded onto LB agar plates. After overnight incubation of the agar plates, the number of colony-forming units (CFU) was counted and the bacteria content was expressed as CFU/mL (Figure 36).

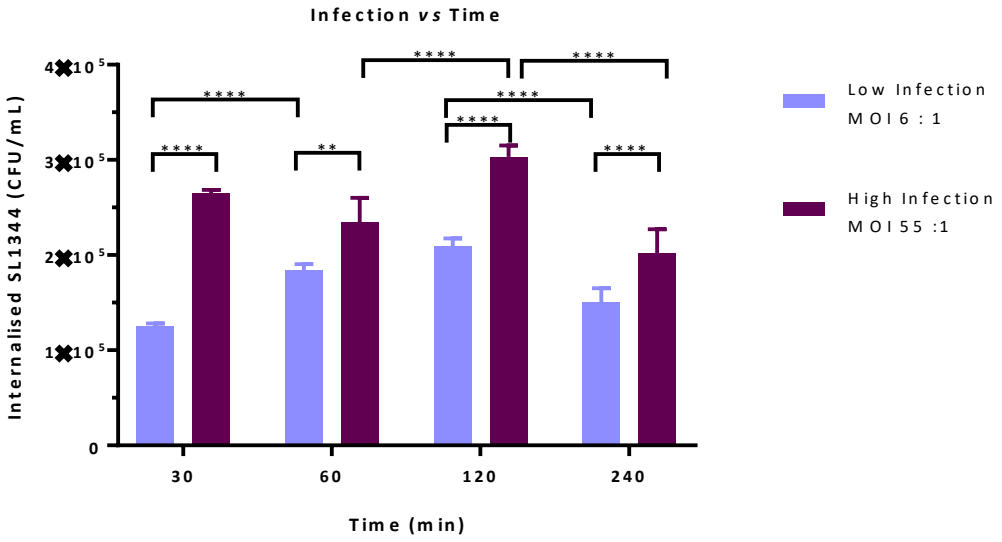

Figure 36 – Colony forming units (CFU) per mL of internalised SL1344 after 30, 60, 120 and 240 min of incubation. Mean and standard deviation are shown N=1, n=6, * $P \leq 0.05$.

For cells infected with MOI 55, the bacterial internalisation was in the order of 10% with an average of 5 internalised bacteria per cell after 30 minutes of infection. For the cells infected with MOI of 6, the bacteria internalisation was in the order of 42% with an average of 2.5 internalised bacteria per cell. For both the infection conditions, the number of internalised bacteria significantly increased within the first 2 hours post-infection, and this may be due to bacterial replication inside macrophage cells. After 4 hours post infection, a significant decrease in colony-forming units (CFU) per mL of internalised bacteria was observed. As the cells die by apoptosis, they become permeable to gentamicin which is dissolved in the medium or cells detach and are washed away by the PBS; both reasons could explain the reduction in bacteria CFU/mL after 4 hours of infection. Figure 37 shows fluorescence micrographs of infected cells. Micrographs A and D show RAW 264.7 after 30 min of infection with MOI 6 and MOI 55 respectively. Micrographs G and J showed that infection levels did not significantly change after 2 hours. The red spots in micrographs B, E, H and K are *Salmonella* bacterial cells inside RAW 264.7 after 30 min (B and E) and after 2 hour (H and K) of infection at the two different MOI. Micrographs C, F, I and L show the nuclei of those cells. 30 min post-infection, at the lower infection dose (MOI 6) not all the cells were found to be infected, and the infected ones only contained a limited number of bacteria (B). These conditions were found to give a level of *Salmonella* infection in macrophage cells similar to that typically found *in vivo* (Mastroeni *et al.* 2009), and this level was maintained for 2 hours (H). In contrast, at 30 min post-infection at the higher infection dose (MOI 55), *Salmonella* appeared to form aggregates inside macrophage cells (E), which increased in size in 2 hours post-infection (K), due to bacterial replication. Moreover, infected macrophage cells showed an irregular

morphological shape (J), which in previous studies has been associated to early stages of apoptosis (Elmore 2007).

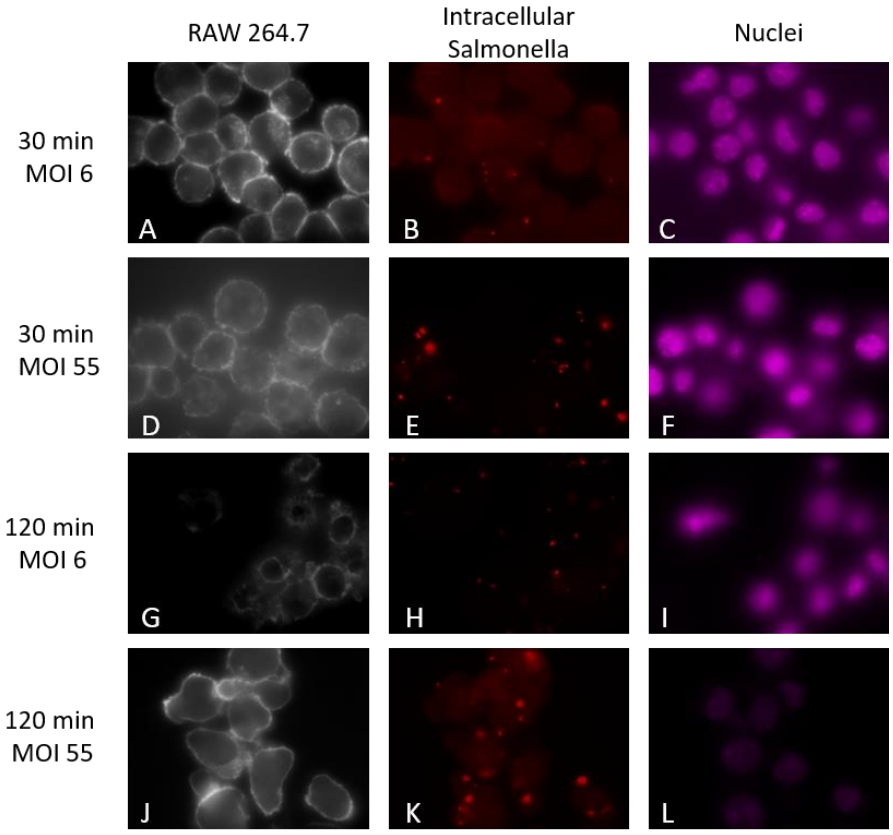

Figure 37 – Fluorescence micrographs of *Salmonella* intracellular infection in RAW 264.7 (actin – white, SL1344 – red, DNA – magenta). Micrographs A, B and C show RAW 264.7 after 30 min of infection with MOI 6. Micrographs C, D and E show RAW 264.7 after 30 min of infection with MOI 55. Micrographs G, H and I and J, K and L show the same infections (MOI 6 and 55) condition after 2 hours.

Subsequently, two more infection conditions were investigated (Figure 38) using infection MOIs of 10 and 1 (bacteria per cell) respectively, with the aim of further reducing the number of bacteria per cell. After 2 hours post-infection, bacteria internalisation was found to be 10% for MOI 10, with an average of 1 bacterium per cell, and 20% for MOI 1 with an average of 0.2 bacteria per cell. These infection conditions were utilised to generate the *Salmonella* infected RAW macrophages used for the liposome uptake studies and *Salmonella* killing study discussed in this chapter.

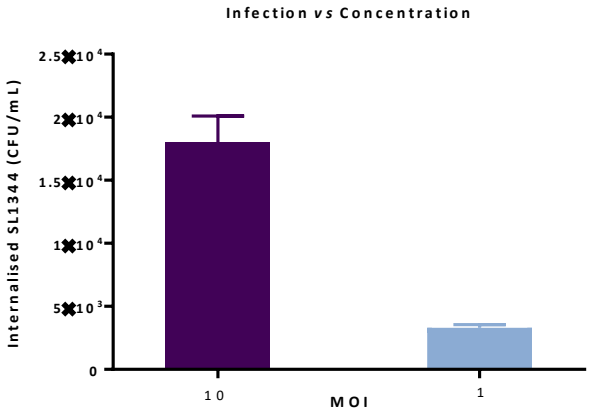

Figure 38 - Colony forming units (CFU) per mL of internalised SL1344 after 2 hours of incubation with different MOIs. Mean and standard deviation are shown. N=2, n=12.

4.4.2 Liposome uptake by MR^+ RAW 264.7 macrophages

To investigate the ability of mannosylated liposomes to target and induce MR-mediated uptake in RAW 264.7 macrophages, and the effect of different glycosylation patterns on the liposomal surface on cell uptake, four different liposomal formulations were assembled (Table 11, Figure 40). To this aim, three glycoligands, (**10**, **14** and **26**, synthesis described in Chapter 2), varying for valency and nature of the membrane-inserting anchor, were utilised (Figure 40).

The (phospho)lipid and glycolipid composition of these formulations was chosen based on the results discussed in Chapter 3. Accordingly, 10% glycoligand molar ratio of total lipids was chosen, as the binding studies with concanavalin A model lectin using Man-TEG liposomes showed that no improvement of the aggregation rate could be observed above this ligand molar content (Chapter 3 - 4.1). As the aggregation rate was found to increase with the cholesterol content (Chapter 3 - 4.2) a concentration of cholesterol of 40 %, towards the upper end of the cholesterol molar ratios explored in Chapter 3, was chosen. Moreover, previous studies have also shown that high cholesterol content could prolong the retention time of gentamicin within liposomal vesicles (Jia, Joly, and Omri 2008), (Cordeiro *et al.* 2000), (Lutwyche *et al.* 1998), (Lutwyche *et al.* 1998). To follow the liposomal cell uptake, a fluorescent hydrophobic dye was also included in the lipid mixture. For these studies, we utilised 1,1'-dioctadecyl–3,3,3',3'-tetramethylindodicarbo-cyanine 4-chlorobenzenesulfonate salt (DID) (0.5 % molar ratio) (Appendix S.4, Figure S60) which is highly retained within liposomal membranes (Snipstad *et al.* 2016).

Table 11 - Lipid composition of mannosylated liposome formulations.

			Molar Ratio %				
Formulation	**Code**	**Ligand Used**	**Ligand**	**Chol**	**SM**	**POPC**	**DID**
Untargeted liposomes	**A**	-	0	40	10	49.5	0.5
Man-TEG liposomes	**B**	**10**	10	40	10	39.5	0.5
Man-Chol liposomes	**C**	**14**	10	30	10	49.5	0.5
Chol-Man_7 liposomes	**D**	**26**	10	30	10	49.5	0.5

Man-TEG: α-O-(tetra(ethyleneglycol)) palmitoyl mannose; Man-Chol: mannosylated-ethylethoxycarbamate cholesterol; Chol-Man_7: glycopolymer $(Mannose)_7$-cholesterol; Chol: cholesterol; SM: sphingomyelin; POPC: palmitoyl-2-oleoyl-sn-glycero-3-phosphocholine; DID: 1,1'-dioctadecyl-3,3,3',3'-tetramethylindodicarbocyanine 4-chlorobenzenesulfonate salt.

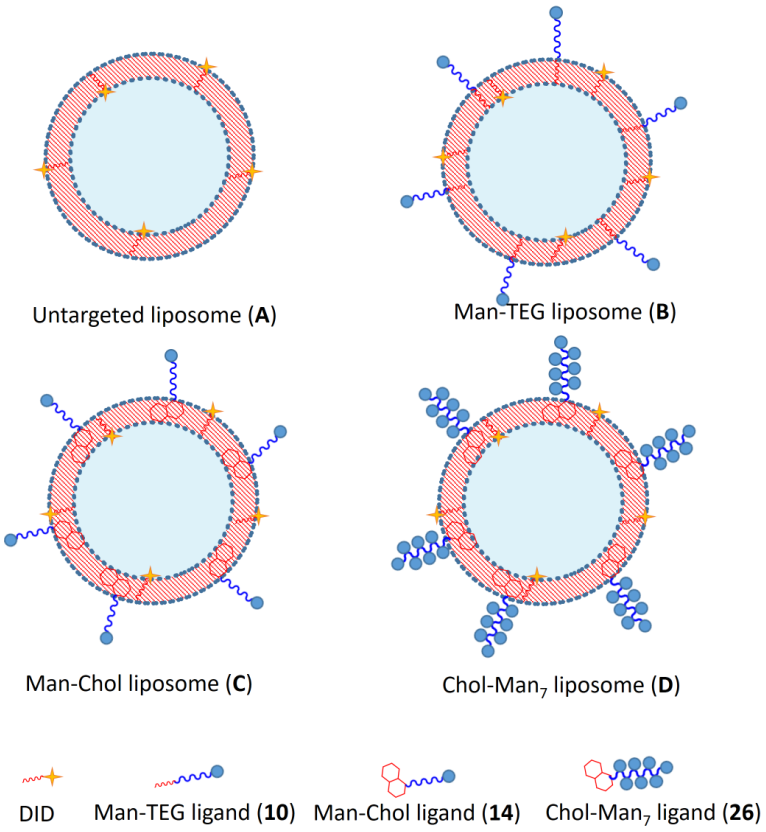

Figure 39 – Schematic representation of liposome formulations tested in *in vitro* studies.

Untargeted liposomes (formulation **A**), with no carbohydrate ligands, were prepared as control liposomal formulations. Both Man-TEG (**B**) and Man-Chol (**C**) liposomes displayed monovalent mannopyranose ligands, linked to their membrane-inserting anchors through short ethylene glycol spacers. In formulation **B** the mannose ligand is anchored to the liposome bilayer membrane by a palmitoyl chain (ligand **10**), while in formulation **C** the linear alkyl anchor was replaced with a cholesterol moiety (ligand **14**). Both the formulation **B** and **C** were previously tested in the aggregation studies with concanavalin A, as described in Chapter 3. Despite the lack of interaction between liposomes in formulation **C** and concanavalin A (Chapter 3 - 4.3), formulation **C** was still included in these *in vitro* studies to validate the reliability of concanavalin A as mannose receptor model for future work within our group. Chol-Man_7 liposome (**D**) was formulated using glycopolymer **26**, with cholesterol anchor chain-end. To maintain the total ratio of cholesterol constant at 40%, for formulations **C** and **D** only 30% of cholesterol was added since glycoligands **14** and **26** are grafted by cholesterol anchors. For formulation **B,** POPC content was decreased accordingly from 49.5% to 39.5% (Table 11).

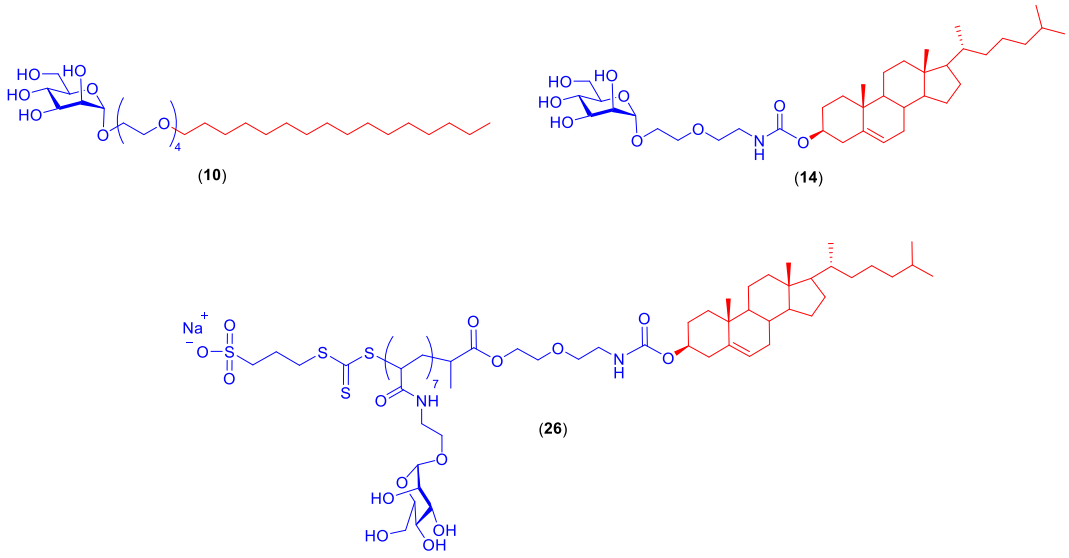

Figure 40 - Chemical structures of glycoligands used for mannosylated liposome formulations: (**10**) Man-TEG palmitoyl ligand, (**14**) Man-Cholesterol ligand, (**26**) Cholesterol-Man$_7$ ligand.

The mannose receptor has been targeted as an endocytic route of entry in studies involving RAW 264.7 macrophages (Chen *et al.* 2016), (Jeong *et al.* 2014). Infected and non-infected RAW 264.7 were used for uptake studies. Infection assay was performed as previously described (Chapter 4 - 3.1) with two infection conditions: an average of 1 bacterium per cell, and an average of 0.2 bacterium per cell. After RAW 264.7 infection (Figure 34d), extracellular *Salmonella* were killed with washes and incubation with High Gentamicin Media (HGM) for 30 min. Then cells were washed with PBS to remove any residual traces of gentamicin. Liposomal formulations were incubated with infected and non-infected cells for 2 hours, at 37°C. Next, the surface of RAW 264.7 cells was washed three times with PBS, finally cells were lysed with DMSO, and the fluorescence of internalised DID was utilised to estimate the extent of liposomal

uptake. In the calculations, fluorescence values were corrected according to the dye encapsulation efficiency (EE%) of each liposomal formulation.

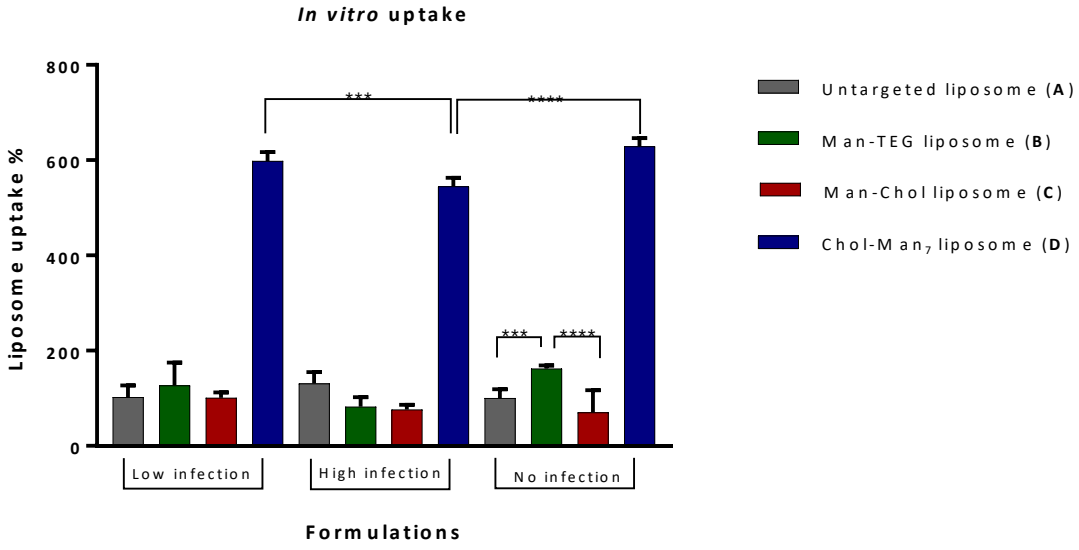

Figure 41 – *In vitro* uptake of untargeted and mannosylated liposomes (1mM total lipid) by RAW264.7 cells. N=2, n=10 for Chol-Man liposome and untargeted liposome; N=1, n=4 for Man-Chol liposome; N=1, n=6 for Man-TEG liposome. Low infection = 0.2 internalised bacteria per cell – High infection = 1 internalised bacteria per cell. Uptake levels are normalised so that the uptake of untargeted liposomes (**A**) in non-infected RAW 264.7 is taken as 100% intensity. * $P \leq 0.05$.

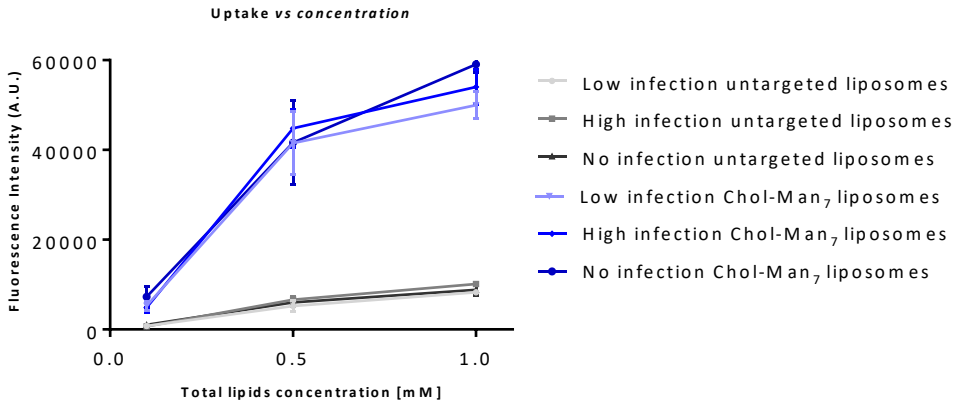

Figure 42 – Effect of liposome concentration (expressed as total lipid concentration) on cellular uptake. N=1, n=4. Low infection = 0.2 internalised bacteria per cell – High infection = 1 internalised bacteria per cell.

Uptake levels were normalised so that the uptake of untargeted liposome (**A**) in non-infected RAW 264.7 was set at 100% intensity. Chol-Man_7 liposome (**D**) was found to be very efficiently internalised by RAW 264.7 in all the conditions tested (infected and non-infected cells) with a significant reduction in uptake by highly infected RAW 264.7 (Figure 9). To the best of our knowledge, the effect of *Salmonella* infection on expression of MR has never been described. Due to time constraint this specific aspect of our uptake experiments was not further investigated, but, along with confocal investigations aimed at elucidating distribution and localisation of the liposomes within infected cells, it will be the subject of future studies within our group (Chapter 5 - 2).

As expected, formulation **C**, displaying monovalent Man-Chol ligands did not show any significant level of uptake, confirming the results previously observed in the concanavalin A (Con A) aggregation studies, which suggested limited accessibility of Man-Chol ligand to lectin binding pockets. Interestingly, Man-TEG liposome (**B**) which was found to be able to efficiently aggregate with Con A (Chapter 3 - 4.1), showed a comparatively small uptake, in the range of 1.5 fold compared to control untargeted formulation (**A**). Whilst further studies will be needed to further rationalise these results, one possibility is that, unlike the binding site of Con A which is shallow and solvent exposed, the mannose-binding CTLD (4-7) domains of the Mannose Receptor (Figure 33) at the cell membrane may not be sufficiently accessible to Man-TEG ligands (Martinez-Pomares 2012). In previous work Engel and co-workers explored different spacer lengths of monovalent mannosylated liposomes for targeting MR in human pericardial monocytes/macrophage cells (Engel *et al.* 2003a), (Engel *et al.* 2003b). In their work, Man-TEG liposomes showed an increased in uptake of 1.5 fold and their longest monovalent ligand with 8 ethylene glycol units spacer

improved the uptake of 2.5 fold, both formulations compared to uncoated liposome (Engel *et al.* 2003a). Our formulation **D** with an oligomeric ligand with 7 mannose units was found to increase the uptake over 6-fold, compared to untargeted liposomes. Some level of non-specific endocytosis by macrophage-like cell line is inevitable, as demonstrated by uptake of untargeted liposome control. Formulations **A** (untargeted control liposomes) and **D**, possessing Chol-Man_7 oligomeric ligands, were further tested at different liposome concentrations, and the uptake by MR^+ RAW 264.7 macrophages of mannose-targeted liposomes **D** was found to increase with the increase of the liposomal concentration (Figure 43).

4.4.3 *Salmonella* killing study

Based on the results obtained in the uptake studies (4- 4.2), Chol-Man_7 liposomes (formulation **D**) and untargeted liposomes (control, formulation **A**) were tested for the delivery of gentamicin to infected RAW 264.7. Infection was carried out to achieve an internalised bacterial rate of 1.8. Liposomes were prepared as described previously with the difference that a solution of gentamicin (5 mg/ mL in HBSS 25mM HEPES, pH 7.4 buffer) was used in the hydration step of the thin lipid layer (4.3.2). To improve gentamicin encapsulation, five freeze–thaw cycles were followed. The freeze–thaw process is a method that helps the encapsulation of hydrophilic drugs (Fujimoto and Isomura 1985), (Ohsawa *et al.* 1985), likely due to a physical disruption of lamellar structure and ice crystals of the drug formed during the freezing process (Mayer *et al.* 1985). After extrusion, unentrapped gentamicin was removed *via* 10 cycles of centrifugal ultrafiltration, and after each cycle the ultrafiltrate (500 µL) was replaced

with an equal volume of fresh HBSS-HEPES buffer, to maintain the total lipid concentration constant at 1.0 mM. The mean diameter (~160 nm) of the two formulations was found to be larger than the mean diameter of analogous formulations which did not contain gentamicin (Appendix 6.4, Table S3, Figure S61).

Gentamicin encapsulation efficiency (EE %) was quantified by microbiological assay using *S. aureus*. Antibiotic diffusion assays are a common method of measuring antibiotic sensitivity using microorganisms. The principle is that the organism is inoculated into a medium containing all the growth factors needed, small holes are created into the solidified medium and these gaps are then filled with the antibiotic to test. If the bacteria are sensitive to the antibiotic, a clear ring, or zone of inhibition, is seen around the holes, indicating poor growth. This method can be used to quantify unknown amount of antibiotics by building a calibration curve of standard solutions of the antibiotic *versus* the inhibition areas, usually measured as diameters (Figure 35). *S. aureus* is commonly used to quantify gentamicin-loaded in liposome due to its high susceptibility to this antibiotic which allows higher resolution of the inhibition zones (Patel *et al.* 2015). To check if all unencapsulated gentamicin was removed from the liposomes, the last wash was analysed by microbiological assay; this indicated that not all the extraliposomal gentamicin had been removed. This means that our liposomal formulations still contained extraliposomal gentamicin. Microbiological assay of liposomal formulations showed a total gentamicin content (intraliposomal + extraliposomal) of 17 μg/mL, for both formulations but due to the presence of extraliposomal gentamicin in the last wash, it was not possible to estimate the encapsulation efficiency of gentamicin in liposomes. Gentamicin, like most aminoglycosides in general, is poorly permeative to cell membrane (Maurin and Raoult

2001). Therefore at this stage we assumed that any extraliposomal gentamicin would not have interfered with the delivery study. Whilst not ideal, this experiment was carried out as first attempt to establish a method for further investigating our liposomal systems. Infected cells were incubated with the liposomal formulations **A** and **D**, while infected cells incubated with 20 μg/mL of gentamicin in medium (Normal Gentamicin Media, NGM) were used as control. Therefore the amount of gentamicin content of the control cells (20 μg/mL) was higher than the total amount of gentamicin content (intraliposomal + extraliposomal content = 17 μg/mL). After 2 hour of incubation at 37°C, the cell medium containing non-internalised liposomal formulations was removed, RAW 264.7 cells were rinsed with PBS, and then incubated for 4 additional hours with Normal Gentamicin Medium (NGM). In our initial experiments this 4-hour incubation was considered to be sufficient to allow the intracellular release of gentamicin from the internalised liposomes. Incubation with Normal Gentamicin Medium ensured the maintenance of infection conditions. If during this 4-hour period a proportion of RAW 264.7 cells died, in the absence of gentamicin in the maintenance medium *Salmonella* released from dead macrophage cells could re-infect other cells, increasing the bacteria/cell count. Although generally regarded as an unlikely event during *Salmonella* infections *in vivo* (Sheppard *et al.* 2003), (Mastroeni *et al.* 2009), this could happen in *in vitro* experiments, thus to prevent it gentamicin was included in the incubation medium.

Finally, the cells were washed three times with PBS and were then lysed in 1% Triton X-100 in PBS. Dilutions of the lysates were grown overnight at 37°C on LB agar. Unloaded formulations **A** and **D** were tested and did not show any antimicrobial

activity. Results of the CFU counting for formulation **A** and **D** and the free gentamicin control, are shown in Figure 43 and Figure 44.

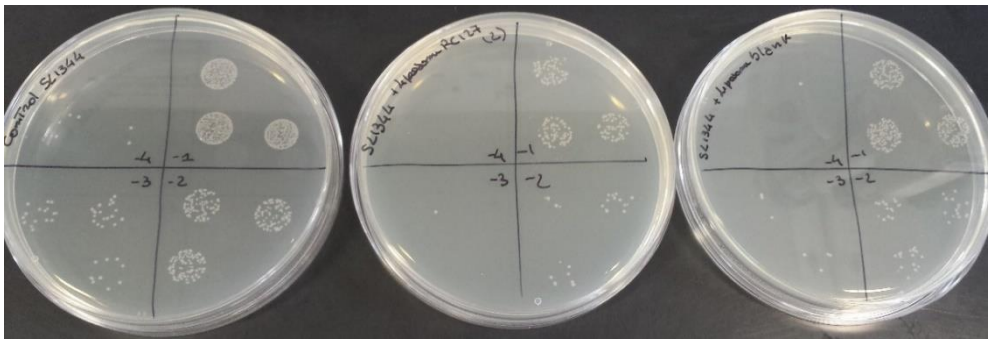

Figure 43 – Agar plates with SL1344 colonies after overnight culture post-treatments. The colonies represent bacteria from lysed cell contents which have survived the gentamicin delivery. Each plates has 4 serial of dilutions of the cell lysates, indicated with -1 (1:10), -2 (1:100), -3 (1:1000), -4(1:10,000). (left) *Salmonella* content of RAW 264.7 incubated with NGM control. (centre) *Salmonella* content of RAW 264.7 incubated with Chol-Man_7 liposome. (right) *Salmonella* content of RAW 264.7 incubated with untargeted liposome. N=1, n=6 for untargeted liposome, n=9 for Chol-Man_7 liposome.

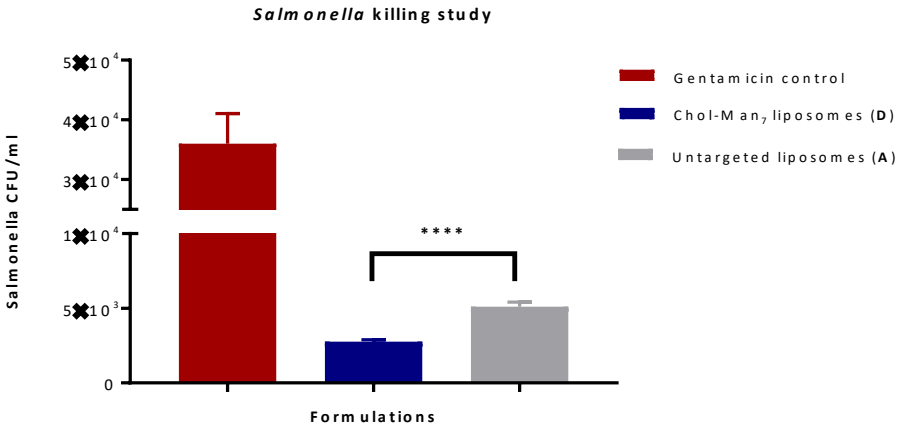

Figure 44 – Colony survival post free gentamicin, and gentamicin-loaded Chol-Man_7 and untargeted liposomes. *= $p<0.05$.

As expected, the free gentamicin control had no effect in reducing intracellular infection which reached 3.6 x 10^4 CFU/mL (1.8 bacteria per cell). Both liposomal formulations showed a significant improvement in killing intracellular *Salmonella*, which was expected due to the poor capacity of free gentamicin to cross the cell membrane. There was one order of magnitude reduction in the number of colonies following treatment with the two liposomal systems. Chol-Man_7 liposome (**D**) showed the best antibacterial activity (survival colonies: 2.9 x 10^3 CFU/mL), with a 40% increase of killing of intracellular *Salmonella* Typhimurium, compared to untargeted liposomal control formulation **A** (survival colonies: 4.8x10^3 CFU/mL), indicating that active targeting of MR resulted in enhanced antibacterial activity.

4.5 Conclusions

In this chapter, an *in vitro* model of *Salmonella* Typhimurium intracellular infection in RAW 264.7 was developed to mimic the same infection rate that occurs during a *Salmonella* Typhi infection in human macrophages. An internalised multiplicity of infection of 1, which means an average of 1 bacterium per cell, was achieved.

This infection model was then used to investigate the mannose receptor (MR, CD206) targeting efficacy of three glycosylated liposomes. Three different glycoligands were used for liposomal formulation conferring different sugar-presentation on the liposomal membrane. Liposome coated with mannosylated-polymer (Chol-Man_7 liposome) resulted in 6-fold increase in uptake compared to untargeted liposome control. At this stage of the project, these preliminary results were further supported by a gentamicin delivery study to *Salmonella* infected cells, where Chol-Man_7 liposome reduced the intracellular infection by 40% compared to analogous uncoated control liposomes. These initial results suggest that receptor-mediated endocytosis of targeted liposomes allows for higher uptake efficiency, while providing the potential advantages of selectivity and specificity. However, further investigations of MR expression and inhibition binding assays will be carried out to support our preliminary findings (discuss in Chapter 5.2).

4.6 References

ATCC. 1997. "RAW 264.7 (ATCC TIB-71)." *American Type Culture Collection Protocolos*, 1–2.

ATCC. 2014. "Animal Cell Culture Guide." *American Type Culture Collection Protocolos* 39 (6).

Brett Finlay, B., and J. H. Brumell. 2000. "Salmonella Interactions with Host Cells: In Vitro to in Vivo." *Philosophical Transactions of the Royal Society B: Biological Sciences* 355 (1397): 623–31.

Bulbake, Upendra, Sindhu Doppalapudi, Nagavendra Kommineni, and Wahid Khan. 2017. "Liposomal Formulations in Clinical Use: An Updated Review." *Pharmaceutics* 9 (2): 1–33.

Burton, Alexandra J., Steeve Giguère, Londa J. Berghaus, Mary K. Hondalus, and Robert D. Arnold. 2015. "Efficacy of Liposomal Gentamicin against Rhodococcus Equi in a Mouse Infection Model and Colocalization with R. Equi in Equine Alveolar Macrophages." *Veterinary Microbiology* 176 (3–4): 292–300.

Chen, Jasmin, Hye Nam Son, John J. Hill, Selvi Srinivasan, Fang Yi Su, Patrick S. Stayton, Anthony J. Convertine, and Daniel M. Ratner. 2016. "Nanostructured Glycopolymer Augmented Liposomes to Elucidate Carbohydrate-Mediated Targeting." *Nanomedicine: Nanotechnology, Biology, and Medicine* 12 (7). Elsevier Inc.: 2031–41.

Cordeiro, Carol, David J. Wiseman, Peter Lutwyche, Mitchell Uh, Jennifer C. Evans, B. Brett Finlay, and Murray S. Webb. 2000. "Antibacterial Efficacy of Gentamicin Encapsulated in pH-Sensitive Liposomes against an in Vivo Salmonella Enterica Serovar Typhimurium Intracellular Infection Model." *Antimicrobial Agents and Chemotherapy* 44 (3): 533–39.

Crump, John, Stephen Luby, and Eric Mintz. 2004. "The Global Burden of Typhoid Fever." *Bulletin of the World Health Organization* | 82 (5): 346–53.

Darwin, K H, and V L Miller. 1999. "Molecular Basis of the Interaction of Salmonella

with the Intestinal Mucosa." *Clinical Microbiology Reviews* 12 (3): 405–28.

Elmore, Susan. 2007. "Apoptosis: A Review of Programmed Cell Death." *Toxicologic Pathology* 35 (4): 495–516.

Engel, Andreas, Swapan K. Chatterjee, Ali Al-Arifi, and Peter Nuhn. 2003. "Influence of Spacer Length on the Agglutination of Glycolipid-Incorporated Liposomes by ConA as Model Membrane." *Journal of Pharmaceutical Sciences* 92 (11): 2229–35.

Engel, Andreas, Swapan Kumar Chatterjee, Ali Al-arifi, Dagmar Riemann, Jürgen Langner, and Peter Nuhn. 2003. "Influence of Spacer Length on Interaction of Mannosylated Liposomes with Human Phagocytic Cells." *Pharmaceutical Research* 20 (1): 51–57.

Fierer, Joshua, Loren Hatlen, Jan-ping Lin, Daniel Estrella, Paul Mihalko, and Annie Yau-young. 1990. "Successful Treatment Using Gentamicin Liposomes of Salmonella Dublin Infections in Mice." *Antimicrobial Agents and Chemotherapy* 34 (2): 343–48.

Garai, Preeti, Divya Prakash Gnanadhas, and Dipshikha Chakravortty. 2012. "Salmonella Enterica Serovars Typhimurium and Typhi as Model Organisms: Revealing Paradigm of Host-Pathogen Interactions." *Virulence* 3 (4): 377–88.

Gog, Julia R., Alicia Murcia, Natan Osterman, Olivier Restif, Trevelyan J. McKinley, Mmark Sheppard, Sarra Achouri, *et al.* 2012. "Dynamics of Salmonella Infection of Macrophages at the Single Cell Level." *Journal of The Royal Society Interface* 9 (75): 2696–2707.

H. Fujimoto, M. Isomura, K. Ajisaka. 1985. "Evaluation of a New Liposome Preparation Technique, the Freeze-Thawing Method, Using L-Asparaginase Ad a Model Drug." *Bioscienci Biotechnology Biochemistry* 33.

Hoaglin, David C, Boris Iglewicz, and John W Tukey. 1986. "Performance of Some Resistant Performance Rules for Labeling Outlier." *Journal of the American Statistical Association* 81 (396): 991–99.

Holmes, Beulah, Paul G. Quie, Dorothy B. Windhorst, Bernard Pollara, and Robert A Good. 1966. "Protection of Phagocytized Bacteria from the Killing Action of

Antibiotics." *Nature* 210 (5033): 309–10.

Huh, Ae Jung, and Young Jik Kwon. 2011. "'Nanoantibiotics': A New Paradigm for Treating Infectious Diseases Using Nanomaterials in the Antibiotics Resistant Era." *Journal of Controlled Release* 156 (2). Elsevier B.V.: 128–45.

Ibarra, J Antonio, and Olivia Steele-mortimer. 2009. "Salmonella – the Ultimate Insider. Salmonella Virulence Factors That Modulate Intracellular Survival." *Cellular Microbiology (2009)* 11 (11): 1579–86.

Iloki Assanga, S. B, A. A Gil-Salido, L. M Lewis Luja, A Rosas-Durazo, A. L Acosta-Silva, E. G Rivera-Castaneda, and J. L Rubio-Pino. 2013. "Cell Growth Curves for Different Cell Lines and Their Relationship with Biological Activities." *International Journal of Biotechnology and Molecular Biology Research* 4 (4): 60–70.

Jeong, Hwan Seok, Kyung Sook Na, Hyosook Hwang, Phil Sun Oh, Dong Hyun Kim, Seok Tae Lim, Myung Hee Sohn, and Hwan Jeong Jeong. 2014. "Effect of Space Length of Mannose Ligand on Uptake of Mannosylated Liposome in RAW 264.7 Cells: In Vitro and in Vivo Studies." *Journal of Biomedical Materials Research - Part A* 102 (12): 4545–53.

Jia, Yimei, Hélène Joly, and Abdelwahab Omri. 2008. "Liposomes as a Carrier for Gentamicin Delivery: Development and Evaluation of the Physicochemical Properties." *International Journal of Pharmaceutics* 359 (1–2): 254–63.

Levy, Stuart B, and Bonnie Marshall. 2004. "Antibacterial Resistance Worldwide: Causes, Challenges and Responses." *Nature Medicine* 10 (1078–8956 (Print)): S122–29.

Lo, Jung Hsin, Samuel K. Kulp, B. Ching Shih Chen, and Hao Chieh Chiua. 2014. "Sensitization of Intracellular Salmonella Enterica Serovar Typhimurium to Aminoglycosides in Vitro and in Vivo by a Host-Targeted Antimicrobial Agent." *Antimicrobial Agents and Chemotherapy* 58 (12): 7375–82.

Lutwyche, Peter, Carol Cordeiro, David J. Wiseman, Maryse St-Louis, Mitchell Uh, Michael J. Hope, Murray S. Webb, and B. Brett Finlay. 1998. "Intracellular Delivery and Antibacterial Activity of Gentamicin Encapsulated in pH-Sensitive

Liposomes." *Antimicrobial Agents and Chemotherapy* 42 (10): 2511–20.

Lutwyche, Peter, Carol Cordeiro, David J Wiseman, Maryse St-louis, Mitchell Uh, Michael J Hope, S Murray, *et al.* 1998. "Intracellular Delivery and Antibacterial Activity of Gentamicin Encapsulated in pH-Sensitive Liposomes." *Antimicrobial Agents and Chemotherapy* 42 (10): 2511–20.

Mackaness, G. B., RV Blanden, and F. M. Collins. 1966. "Host-Parasite Relations in Mouse Typhoid." *The Journal of Experimental Medicine* 124 (4): 573–83.

Magnet, Sophie, and John S. Blanchard. 2005. "Molecular Insights into Aminoglycoside Action and Resistance." *Chemical Reviews* 105 (2): 477–97.

Martinez-Pomares, Luisa. 2012. "The Mannose Receptor." *Journal of Leukocyte Biology* 92 (6): 1177–86.

Mastroeni, Pietro, Andrew Grant, Olivier Restif, and Duncan Maskell. 2009. "A Dynamic View of the Spread and Intracellular Distribution of Salmonella Enterica." *Naure Reviews Microbiology* 7 (January): 73–80.

Maurin, M, and D Raoult. 2001. "Use of Aminoglycosides in Treatment of Infections Due to Intracellular Bacteria MINIREVIEW Use of Aminoglycosides in Treatment of Infections Due to Intracellular Bacteria." *Antimicrobial Agents and Chemotherapy* 45 (11): 2977–86.

Mayer, L. D., M. J. Hope, P. R. Cullis, and A. S. Janoff. 1985. "Solute Distributions and Trapping Efficiencies Observed in Freeze-Thawed Multilamellar Vesicles." *BBA - Biomembranes* 817 (1): 193–96.

Mugabe, Clement, Ali O. Azghani, and Abdelwahab Omri. 2005. "Liposome-Mediated Gentamicin Delivery: Development and Activity against Resistant Strains of Pseudomonas Aeruginosa Isolated from Cystic Fibrosis Patients." *Journal of Antimicrobial Chemotherapy* 55 (2): 269–71.

Ohsawa, Takashi, Hiroshi Miura, and Kiyoshi Harada. 1985. "Improvement of Encapsulation Efficiency of Water-Soluble Drugs in Liposomes Formed by the Freeze-Thawing Method." *Chemical & Pharmaceutical Bulletin* 33 (9): 3945–52.

Parry, Christopher M, Tran Tinh Hien, Gordon Dougan, Nicholas J White, and Jeremy

J Farrar. 2002. "Typhoid Fever." *The New England Journal of Medicine* 347 (22): 1770–82.

Patel, Jean B, Franklin Cockerill, Patricia A. Bradford, and George M. Eliopoulos. 2015. "Performance Standards for Antimicrobial Susceptibility Testing; Twenty-Fith Informational Supplement." *Clinical and Laboratory Standards Institue*.

Pinto-Alphandary, Huguette, Antoine Andremont, and Patrick Couvreur. 2000. "Targeted Delivery of Antibiotics Using Liposomes and Nanoparticles: Research and Applications." *International Journal of Antimicrobial Agents* 13 (3): 155–68.

Ranjan, Ashish, Nikorn Pothayee, Mohamed N. Seleem, Stephen M. Boyle, Ramanathan Kasimanickam, Judy S. Riffle, and Nammalwar Sriranganathan. 2012. "Nanomedicine for Intracellular Therapy." *FEMS Microbiology Letters* 332 (1): 1–9.

Rowe, Bernard, Linda R Ward, and John E. Therlfall. 1997. "Multidrug-Resistant Salmonella Typhi: A Worlwide Epidemic." *Clinical Infectious Diseases* 24 (1): S106-9.

Rubin, F. A., P. D. McWhirter, D. Burr, N. H. Punjabi, E. Lane, S. Kumala, P. Sudarmono, *et al.* 1990. "Rapid Diagnosis of Thypoid Fever through Identification of Salmonella Typhi within 18 Hours of Specimen Acquisition by Culture of the Mononuclear Cell-Platelet Fraction of Blood." *Journal of Clinical Microbiology* 28 (4): 825–27.

Sanchez, Cesar. 2011. "With a Little Help from My Enemies." *Nature Reviews. Microbiology* 9 (5). Nature Publishing Group: 315.

Schiffelers, Raymond, Gert Storm, and Irma Bakker-Woudenberg. 2002. "Liposome-Encapsulated Amicnoglycosides in Pre-Clinical and Clinical Studies." *Journal of Antimicrobial Chemotherapy* 48: 333–44.

Schwan, William R., Xiao Zhe Huang, Lan Hu, and Dennis J. Kopecko. 2000. "Differential Bacterial Survival, Replication, and Apoptosis-Inducing Ability of Salmonella Serovars within Human and Murine Macrophages." *Infection and Immunity* 68 (3): 1005–13.

Sheppard, Mark, Cerian Webb, Fred Heath, Victoria Mallows, Romina Emilianus, Duncan Maskell, and Pietro Mastroeni. 2003. "Dynamics of Bacterial Growth and Distribution within the Liver during Salmonella Infection." *Cellular Microbiology* 5 (9): 593–600.

Snipstad, Sofie, Sjoerd Hak, Habib Baghirov, Einar Sulheim, Yrr MORrch, Sylvie Lelu, Eva Von Haartman, *et al.* 2016. "Labeling Nanoparticles: Dye Leakage and Altered Cellular Uptake." *Cytometry Part A*, 25–29.

Tierrez, Alberto, and Francisco Garcáia-del Portillo. 2005. "New Concepts in Salmonella Virulence: The Importance of Reducing the Intracellular Growth Rate in the Host." *Cellular Microbiology* 7 (7): 901–9.

Vabbilisetty, Pratima, and Xue-Long Sun. 2015. "Liposome Surface Functionalization Based on Different Anchoring Lipids via Staudinger Ligation." *Org Biomol Chem* 12 (8): 1237–44.

Velge, P., A. Wiedemann, M. Rosselin, N. Abed, Z. Boumart, A. M. Chaussé, O. Grépinet, *et al.* 2012. "Multiplicity of Salmonella Entry Mechanisms, a New Paradigm for Salmonella Pathogenesis." *MicrobiologyOpen* 1 (3): 243–58.

Wain, John, Phan Van Be Bay, Ha Vinh, Nguyen M Duong, To Song Diep, Amanda L Walsh, Christopher M Parry, *et al.* 2001. "Quantitation of Bacteria in Bone Marrow from Patients with Typhoid Fever : Relationship between Counts and Clinical Features Quantitation of Bacteria in Bone Marrow from Patients with Typhoid Fever : Relationship between Counts and Clinical Features." *Journal of Clinical Microbiology* 39 (4): 1571–76.

Wain, John, To Song Diep, Vo Anh Ho, Amanda M Walsh, Tuyet Thi Nguyen Hoa, Christopher M Parry, and Nicholas J White. 1998. "Quantitation of Bacteria in Blood of Typhoid Fever Patients and Relationship between Counts and Clinical Features , Transmissibility , and Antibiotic Resistance." *Journal of Clinical Microbiology* 36 (6): 1683–87.

Walker, Dawn M., Steve Oghumu, Gaurav Gupta, Bradford S. McGwire, Mark E. Drew, and Abhay R. Satoskar. 2013. "Mechanisms of Cellular Invasion by

Intracellular Parasites." *Cellular and Molecular Life Sciences* 71 (7): 1245–63.

CHAPTER 5

Glycocoded liposomes: general conclusion and future directions

5.1 General conclusion

This thesis focussed on exploiting glycocode-based recognition to achieve high receptor mediated internalisation and intracellular delivery of antibacterial agent against intracellular pathogen – *e.g. S*. Typhi. Delivering high doses of antibiotic intracellularly to infected cells is crucial to eradicate the infection and to reduce the risk of development of antimicrobial resistances associated with sub-therapeutic doses.

In chapter 1, we introduced the concept of glycocoded liposomes as carriers for antimicrobial delivery. Previous works have shown that mannosylated liposomes improve lectin receptors targeting and this strategy can benefit by using multivalent interactions (discussed in section 1.2.3). Glycosylation of liposomal surface is achieved mainly using glycoproteins or synthetic glycolipids (Kawakami and Hashida 2014). Recent advances in polymer chemistry (Lutz *et al.* 2016) have made possible the

synthesis of glycopolymers with well-defined architecture opening new options for liposome glyco-functionalisation (Jain *et al.* 2012).

In chapter 2, we described the different synthetic strategies for the synthesis of glycoligands designed to insert into liposomal membrane to functionalise the liposome surface. Firstly, five different monovalent ligands (Figure 45) were designed and synthesised with galactose- and mannose- as sugar units. These carbohydrates were conjugated to different membrane-inserting anchors: palmitoyl and cholesterol moieties.

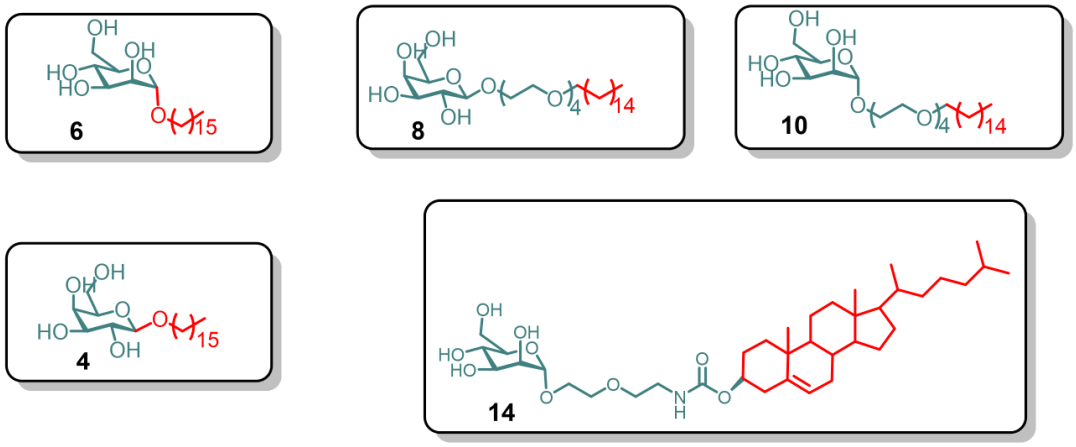

Figure 45 – Monovalent ligands alkyl monoglycosides **(4)**, **(6)**, **(8)** and **(10)** and cholesterol monoglycoside **(14)**.

O-alkyl glycosydes (compounds: β-O-palmitoyl galactose **(4)**, α-O-palmitoyl mannose **(6)**, β-O-tetra(ethylene glycol) palmitoyl galactose **(8)** and α-O-(tetraethylglycol) palmitoyl mannose **(10)** were synthesised by $BF_3{\cdot}OEt_2$ mediated condensation with a near-perfect control over the stereochemistry of the anomeric centre of the desired glycosides. However, the same synthetic approach was unsuccessful for the synthesis of cholesterol-based mannose monoglycoside (mannosylated-ethylethoxycarbamate

cholesterol **(14)**). This problem was circumvented via Koenigs-Knorr reaction, replacing the OAc in C1 of the acetylated mannose with a iodide group, to increase the reactivity of this electrophilic centre.

In the next stage, we designed and synthesised two sets of well-defined cholesterol-terminated mannose and galactose glycopolymers (Figure 46), to increase the sugar exposure at the surface and present ligand as a multivalent structure. Multivalent interactions have been shown to lead to a significant increase in avidity (Cairo *et al.* 2002), (Kiessling *et al.* 2006).

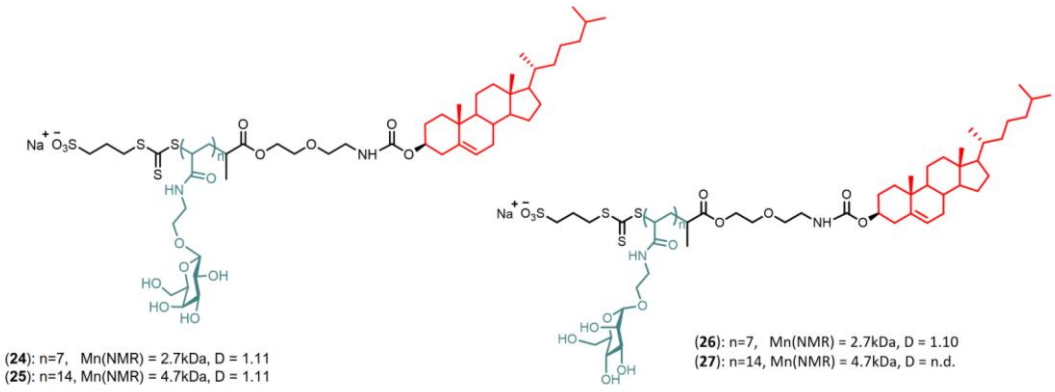

Figure 46 - Cholesterol-terminated galactose **(23)** and **(24)** and mannose **(25)** and **(26)** polyacrylamide-based glycopolymers.

These polyvalent ligands were synthesised using a newly developed *ultrafast* version of RAFT (Reversible Addition Fragmentation chain Transfer) radical polymerisation technique (Gody *et al.* 2015). *Ultrafast* RAFT is a versatile, facile and metal-free procedure for performing polymerisation within minutes using aqueous conditions with excellent control over polymer molecular weight, distribution, and chain-end fidelity. We synthesised new amphiphilic trithiocarbonyl cholesterol-based RAFT agents with a cholesterol moiety incorporated in the R group. To ensure a certain level of water solubility of cholesterol-containing RAFT agents, hydrophilic Z groups were identified – *i.e.* sulfonate salt (Figure 47). A series of trial-and-error attempts were made to identify and optimise the reaction conditions of RAFT agents and sugar ligands. *Ultrafast* RAFT polymerisations for glycopolymer **24**, **25**, **26**, and **27** were carried out in biphasic condition (water/toluene) at 100°C within 20 min. To our knowledge this may be the first synthesis of glycopolymer *via ultrafast* RAFT polymerisation.

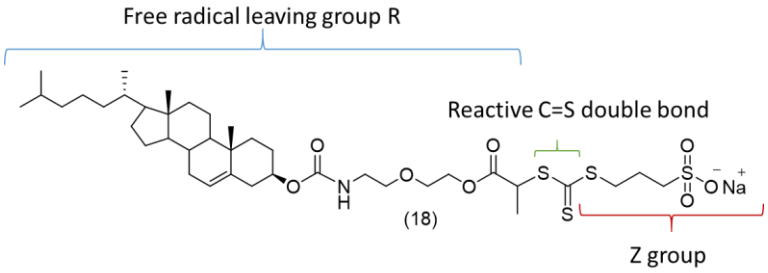

Figure 47 - Structure of cholesterol RAFT agent **(18)**.

In chapter 3, we investigated the interaction between glycosylated liposomes and a model lectin receptor Concanavalin A (Con A). Glycoligand modified liposomes, shown in Figure 48, were formulated with different mannose and galactose ligands, with different spacer length and different hydrophobic anchors, using monovalent ligands (**6**, **8**, **10** and **14,** Figure 46). At this point in the work, glycopolymer ligands were not yet available. Concanavalin A was used as a model lectin to investigate how densities of different sugars residues (mannose and galactose), the effect of the tetraethylenglycol spacer between the sugar ligands and the liposome bilayer, the nature of the membrane-inserting hydrophobic anchor of the sugar ligands, and the lipid composition of the liposomal membrane, affected the rate of lectin induced aggregation of ligand presenting liposomes, as follows.

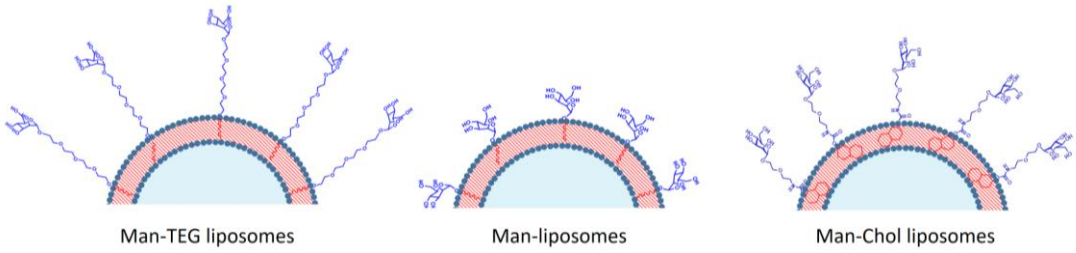

Figure 48 – Schematic representation of the different categories of targeted liposomes glycosylated with monovalent ligands.

The cholesterol content was found to increase the binding rate. The aggregation rate was directly proportional to the density of Man-TEG ligand (**10**) (mannoslylated ligand containing a tetraethylenglycol spacer) on the liposome surface, up to 10 mol % Man-TEG (**10**), after which a plateau was reached, indicating that at high glycoligand density

steric effects may hamper further Con A binding, or simply steric encumbrance provided by large Con A tetramers at the liposomal membrane may prevent access of additional Con A molecules to membrane glycoligands.

Surprisingly Man-Chol ligand (**14**) showed poor ligand exposure, as judged from the lack of Con A induced liposomes aggregation, compare with Man-TEG ligand with palmitoyl anchor. We hypothesised that cholesterol anchor could lead to a deeper embedding of the Man-Chol ligand in the liposomal membrane phospholipid bilayer and thus to 'poor' ligand surface exposure.

Based on the results of this screening, we selected the lipid composition of 40 mol % of cholesterol content and the glycoligand density of 10 mol % for the liposomal formulations to take forward to *in vitro* uptake study on *Salmonella* infected macrophage-like cell RAW 264.7.

In chapter 4, we developed an *in vitro* model of *Salmonella* Typhimurium intracellular infection in MR^+ macrophage-like cell line, RAW 264.7, which aimed to mimic the infection rate that occurs during a *Salmonella* Typhi infection in human macrophages, with an average of 1 bacterium *per* cell. We used this *in vitro* infection model to investigate the Mannose Receptor (MR) dependent internalization and antibiotics delivery efficacy of three glycosylated liposomes (Figure 49).

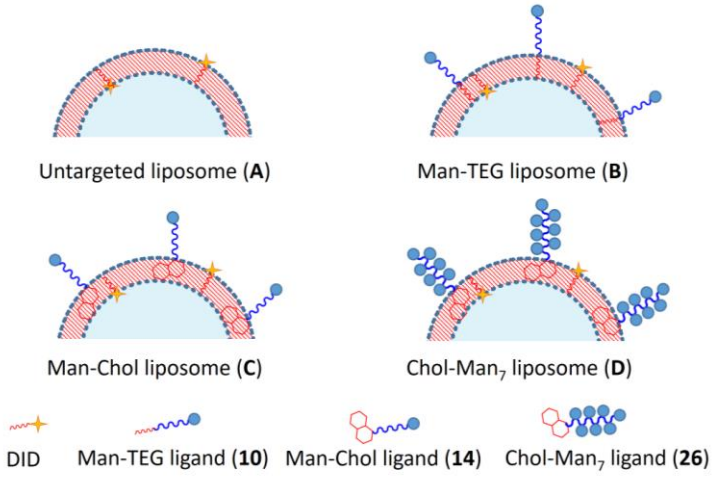

Figure 49 – Schematic representation of liposome formulations tested in uptake *in vitro* studies in Salmonella Typhimurium infected MR^+ macrophage like RAW 264.7.

The glycoligands used for liposome glycosylation were compounds (**10**) [mannose-TEG ligand anchored by palmytoil chain], (**14**) [mannose-cholesterol ligand] (Figure 45) and (**26**) [cholesterol anchored glycopolymer with 7 units of mannose] (Figure 46) to create formulations **B**, **C** and **D** (Figure 49), respectively. For time restriction, glycoligand (**27**) (Figure 46) was not included in these experiments. Studies on RAW 264.7 cells internalisation of liposomes indicated that surface modification with mannose-glycopolymer (**26**) (Chol-Man_7 liposome) had 4-fold higher uptake than liposome coated with monovalent ligand Mon-TEG (**10**) and 6-fold higher uptake than

untargeted liposome control (formulation A, Figure 50). These results indicate that (*i*) the surface ligand presentation promoted the liposomes-cell interactions and mannose receptor mediated endocytosis, as expected from *in vitro* liposomes aggregation studies, whereby (*ii*) the multivalency of the glycopolymer-ligand *i.e.* Chol-Man_7 ligand, further increased avidity for the receptor binding and the liposomal cellular uptake.

Finally, a gentamicin delivering study was performed using ligand modified liposome formulation with mannose-glycopolymer (**26**) (Chol-Man_7 liposome) and unmodifiecd liposomes as control; this made the study relatively small to conduct and still allowed for an essential comparisons to be made. The study measured the killing efficacy of the formulations against internalised *Salmonella* Typhimurium in MR^+ in RAW 264.7 cells. Chol-Man_7 ligand presenting liposomes reduced the intracellular infection by 40%, compared to control liposomes.

In the first instance simple encapsulation of antibiotics into liposomes increased cellular availability of gentamicin, relative to free drug. However liposomes internalisation and bacterial killing was increased when liposomes were coated with mannosepolymer (Chol-Man_7 **26**), whereby the initial test showed that the multivalency of the sugar-ligands, using well-defined Chol-Man_7 glycopolymer (**26**) significantly improved *in vitro* activity of gentamicin against intracellular infection of *S. Typhimurium* in macrophage like cell RAW 264.7.

5.2 Future directions

As anticipated in Chapter 4, further studies are required to validate, improve and expand the work presented within this thesis.

- Determination of MR (CD206) expression in infected *vs* non-infected cells is currently under investigation in our research group to investigate possible effects of *Salmonella* infection in MR expression.

- In order to confirm that the glycoliposome formulations **D** and **B** were selectively taken up via mannose receptor, competitive uptake studies will be performed pretreating the cells with free D-mannose.

- In this work, the liposomal formulations **B** and **D** were formulated with the same molar ratio of ligands (10%). This implies that formulation **D** contains 7 times the amount of mannose-ligands on the liposomal surface than formulation **B**. In order to compare the spatial distribution of the same "sugar-content" on the liposomal membrane, Chol-Man_7 liposomes should be formulated using 7 time less molar ratio of ligands (1.43%).

- Similarly Chol-Man_{14} (**27**) will be tested using half molar ratio Chol-Man_7 (**26**) in order to investigate the effect of different distibuition of the total sugar-content.

- Galactose polymers **24** and **25** can be explored as further ligands for galectin receptors for cancer therapy, since have been demonstrated that galectins trigger tumor angiogenesis (Böcker and Elling 2017).

5.3 References

Böcker, Sophia, and Lothar Elling. 2017. "Binding Characteristics of Galectin-3 Fusion Proteins." *Glycobiology* 27 (5): 457–68.

Cairo, Christopher W., Jason E. Gestwicki, Motomu Kanai, and Laura L. Kiessling. 2002. "Control of Multivalent Interactions by Binding Epitope Density." *Journal of the American Chemical Society* 124 (8): 1615–19.

Gody, Guillaume, Raphael Barbey, Maarten Danial, and Sébastien Perrier. 2015. "Ultrafast RAFT Polymerization: Multiblock Copolymers within Minutes." *Polym. Chem.* 6 (9): 1502–11.

Jain, Keerti, Prashant Kesharwani, Umesh Gupta, and Narendra K. Jain. 2012. "A Review of Glycosylated Carriers for Drug Delivery." *Biomaterials* 33 (16): 4166-86.

Kawakami, Shigeru, and Mitsuru Hashida. 2014. "Glycosylation-Mediated Targeting of Carriers." *Journal of Controlled Release* 190: 542-55.

Kiessling, Laura L., Jason E. Gestwicki, and Laura E. Strong. 2006. "Synthetic Multivalent Ligands as Probes of Signal Transduction." *Angewandte Chemie - International Edition* 45 (15): 2348–68.

Lutz, Jean-François, Jean-Marie Lehn, E. W. Meijer, and Krzysztof Matyjaszewski. 2016. "From Precision Polymers to Complex Materials and Systems." *Nature Reviews Materials* 1: 1–14.

CHAPTER 6 APPENDIX

6.1 Supplementary Information Chapter 2 – NMR and mass spectra

6.1.1 NMR spectra of 1,2,3,4,6 penta-O-acetyl-α-D-mannopyranoside **(1)**

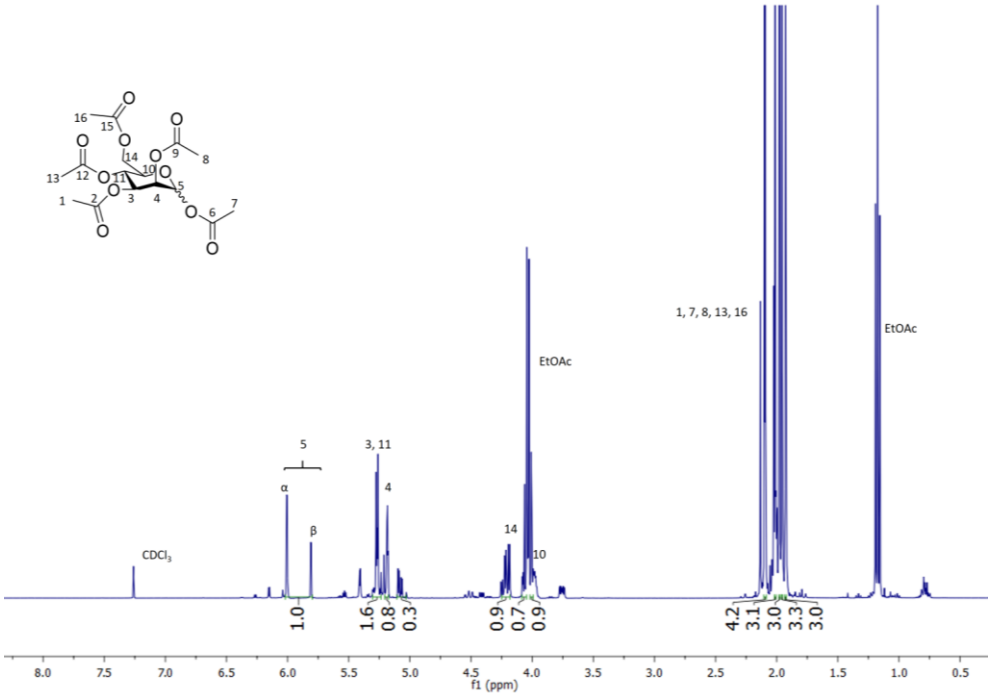

Figure S1 – ^{1}H NMR spectrum of 1,2,3,4,6 penta-O-acetyl-α-D-mannopyranoside **(1)** in $CDCl_3$.

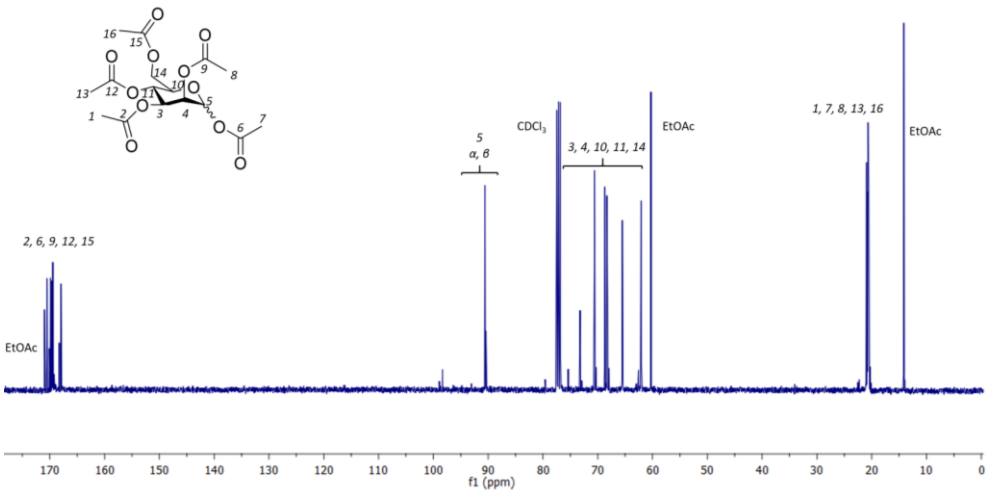

Figure S2 - ^{13}C NMR spectrum of 1,2,3,4,6 penta-O-acetyl-α-D-mannopyranoside **(1)** in $CDCl_3$.

6.1.2 NMR spectra of 1-palmitoyl-tetraethylene glycol **(2)**

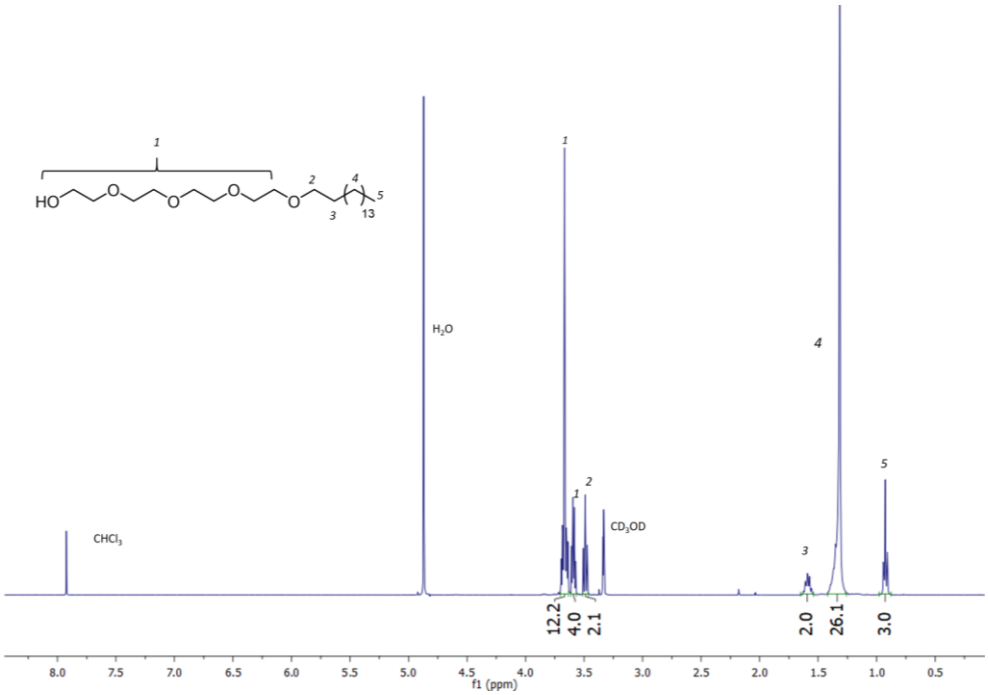

Figure S3 - ^{1}H NMR spectrum of 1-palmitoyl-tetraethylene glycol **(2)** in CD_3OD.

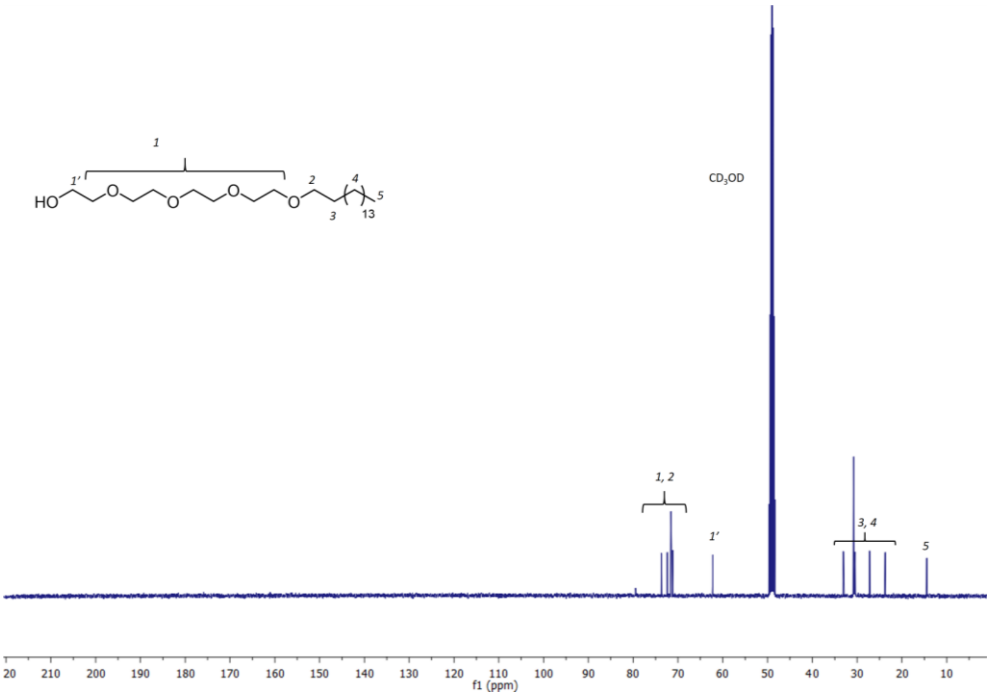

Figure S4 - ^{13}C NMR spectrum of 1-palmitoyl-tetraethylene glycol **(2)** in CD_3OD.

6.1.3 NMR spectra of α-O-palmitoyl mannose **(6)**

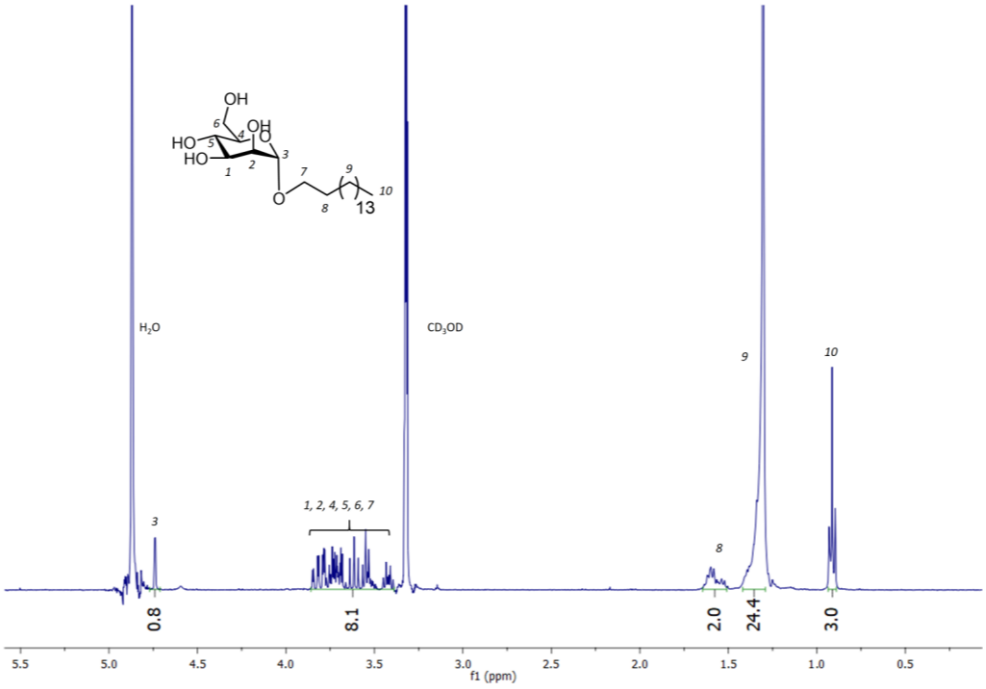

Figure S5 - ^{1}H NMR spectrum α-O-palmitoyl mannose **(6)** in CD_3OD.

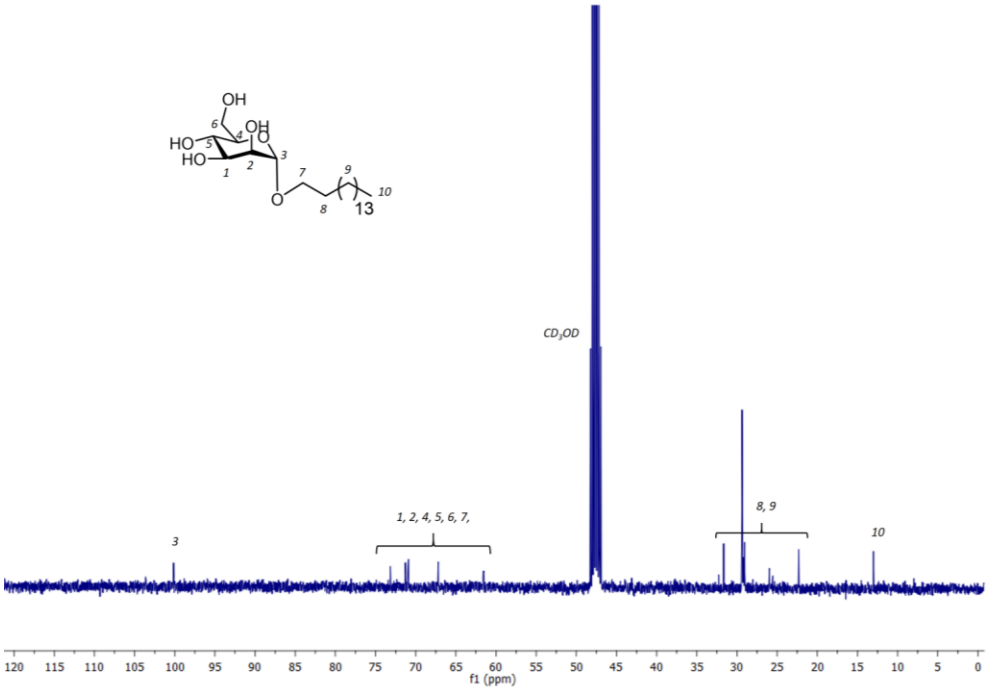

Figure S6 – ^{13}C NMR spectrum α-O-palmitoyl mannose **(6)** in CD_3OD.

6.1.4 NMR spectra of β-O-tetra(ethylene glycol) palmitoyl galactose **(8)**

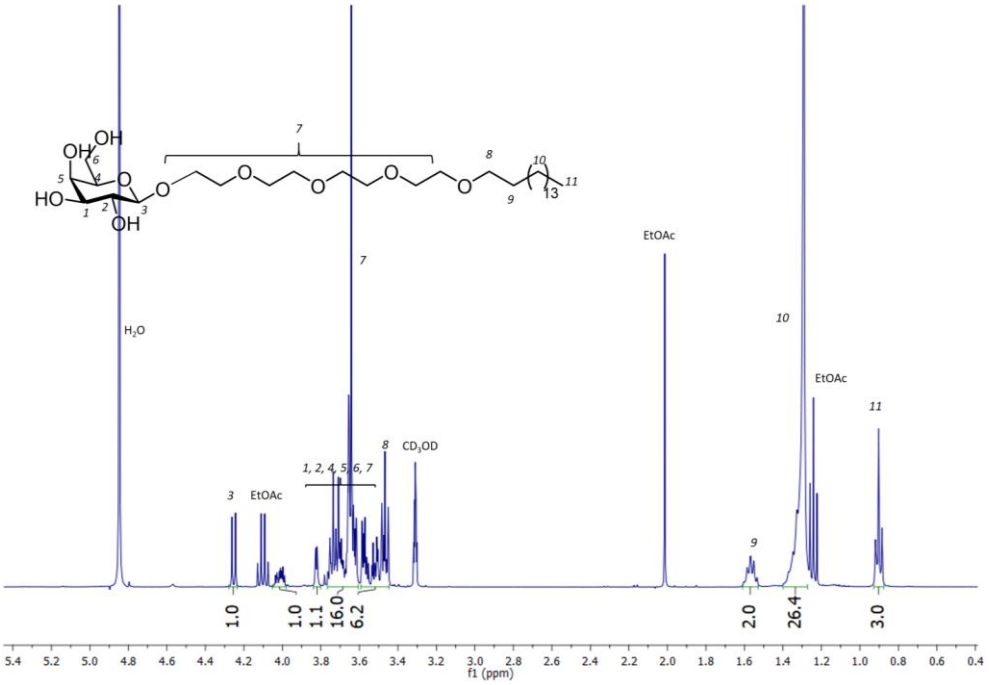

Figure S7 - ^{1}H NMR spectrum of β-O-tetra(ethylene glycol) palmitoyl galactose **(8)** in CD_3OD.

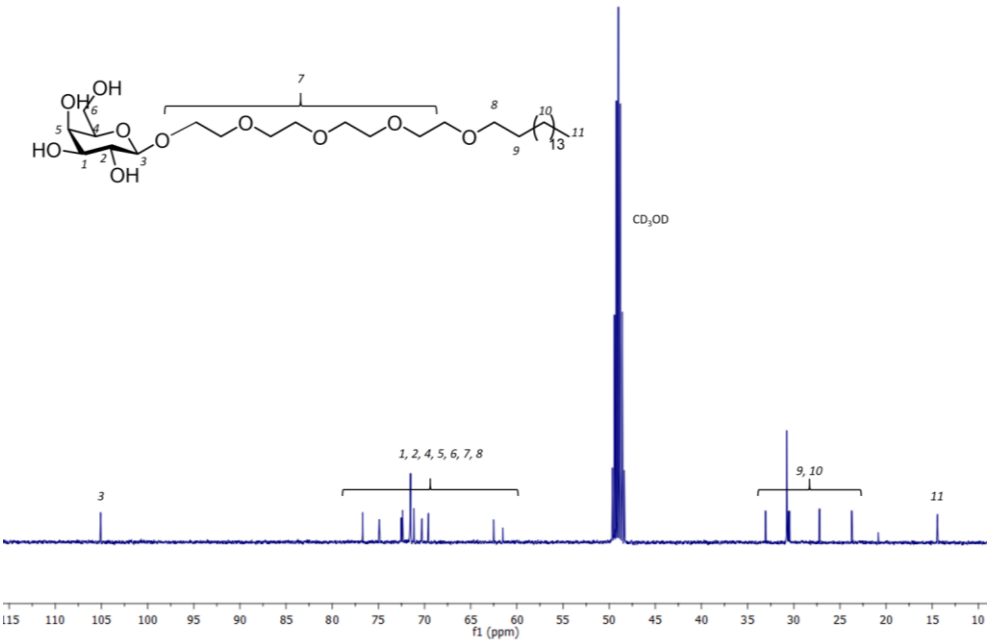

Figure S8 - ^{13}C NMR spectrum of β-O-tetra(ethylene glycol) palmitoyl galactose **(8)** in CD_3OD.

6.1.5 NMR spectra of α-O-(tetraethylglycol) palmitoyl mannose **(10)**

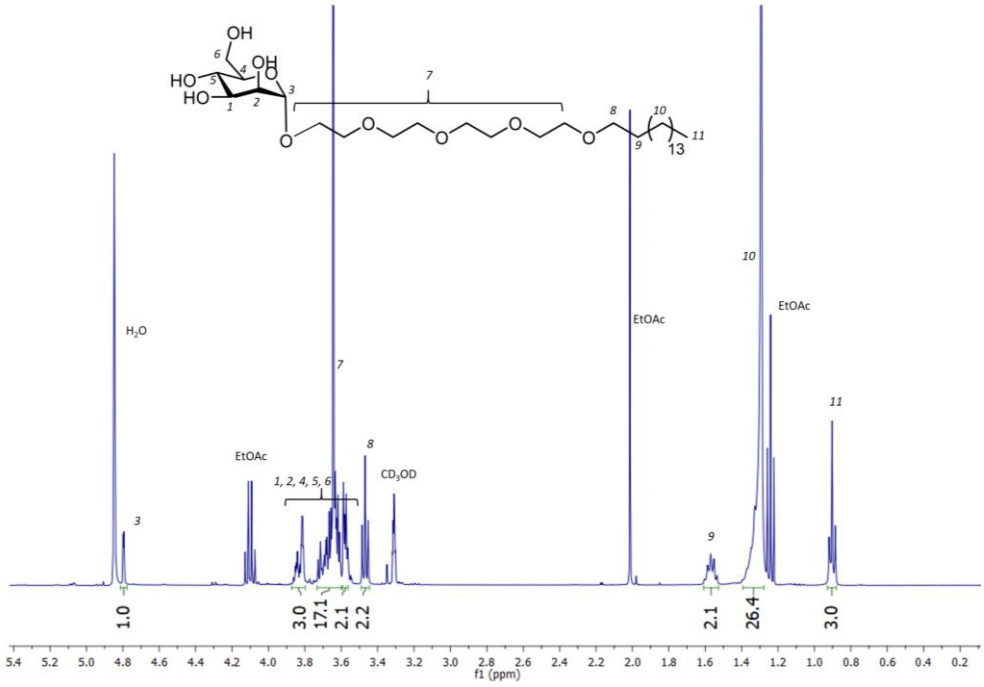

Figure S9 - ^{1}H NMR spectrum of α-O-(tetraethylglycol) palmitoyl mannose **(10)** in CD_3OD.

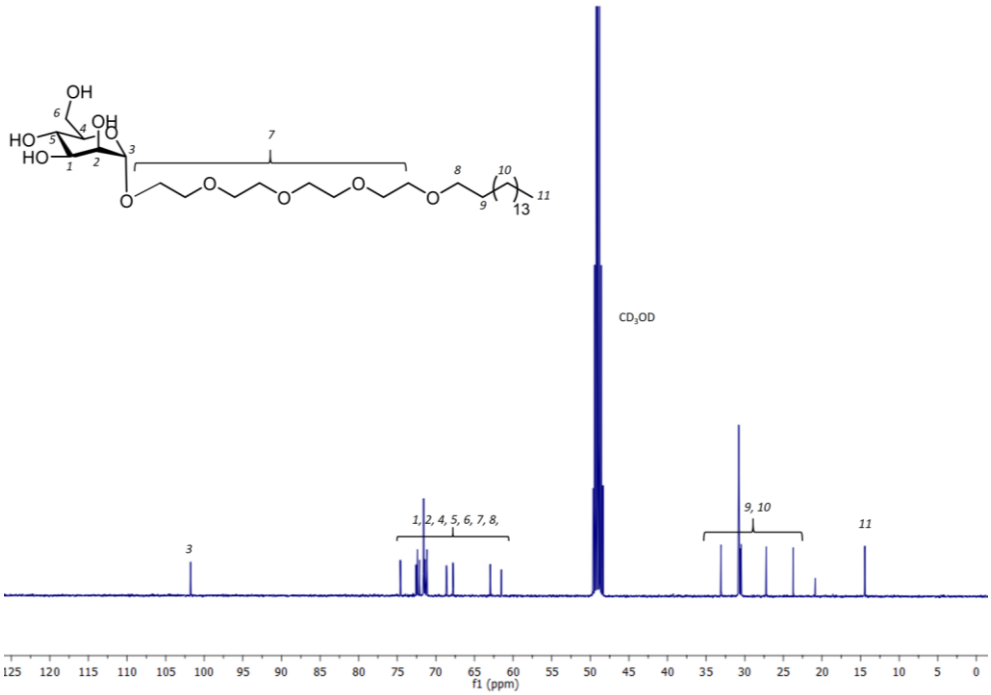

Figure S10 - ^{13}C NMR spectrum of α-O-(tetraethylglycol) palmitoyl mannose **(10)** in CD_3OD.

6.1.6 NMR spectra of cholesterol ethylethoxycarbamate **(11)**

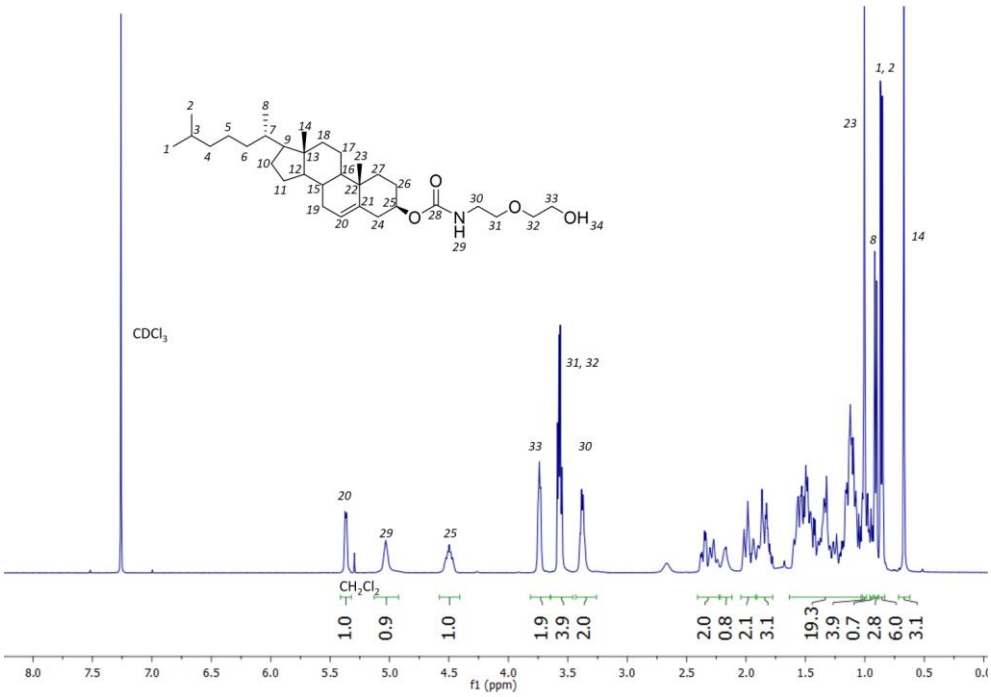

Figure S11 – ^{1}H NMR spectrum of cholesterol ethylethoxycarbamate **(11)** in $CDCl_3$.

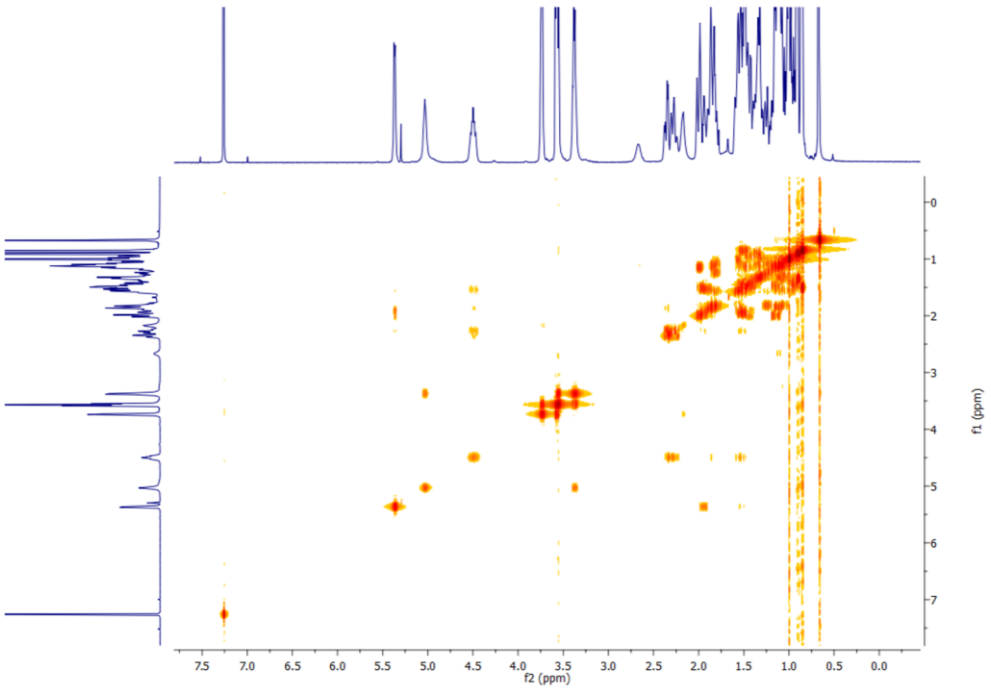

Figure S12 – COSY NMR spectrum of Cholesterol ethylethoxycarbamate **(11)** in $CDCl_3$.

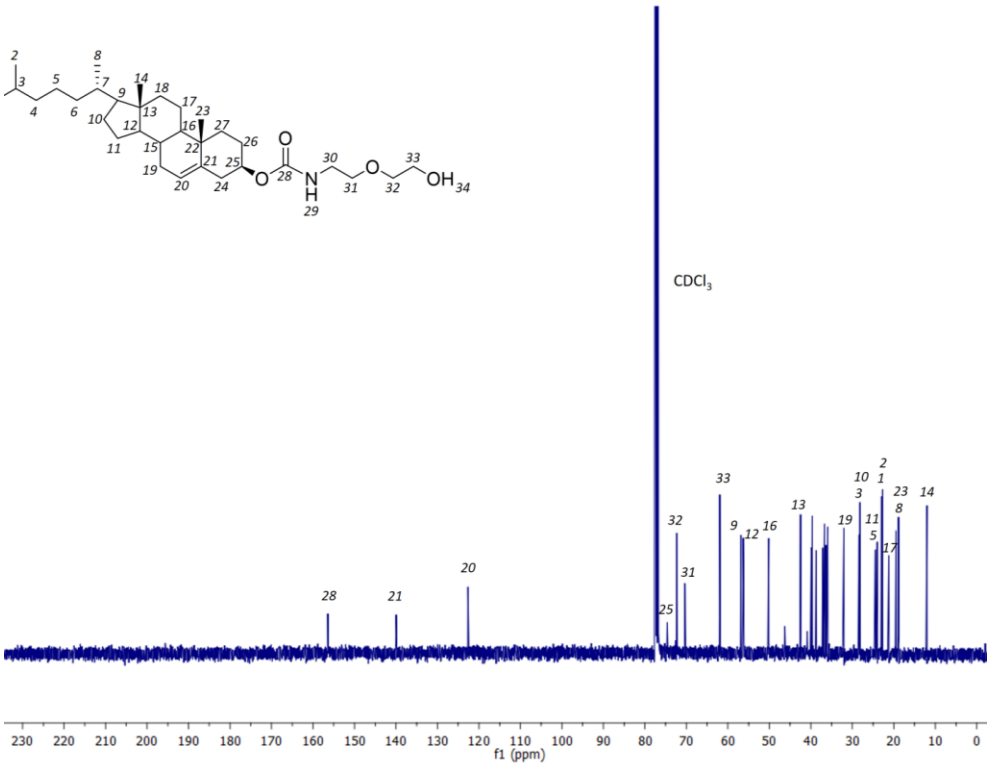

Figure S13 – ^{13}CNMR spectrum of Cholesterol ethylethoxycarbamate **(11)** in $CDCl_3$.

6.1.7 NMR spectra of 2,3,4,6 tetra-O-acetyl-α-D-mannose-I **(12)**

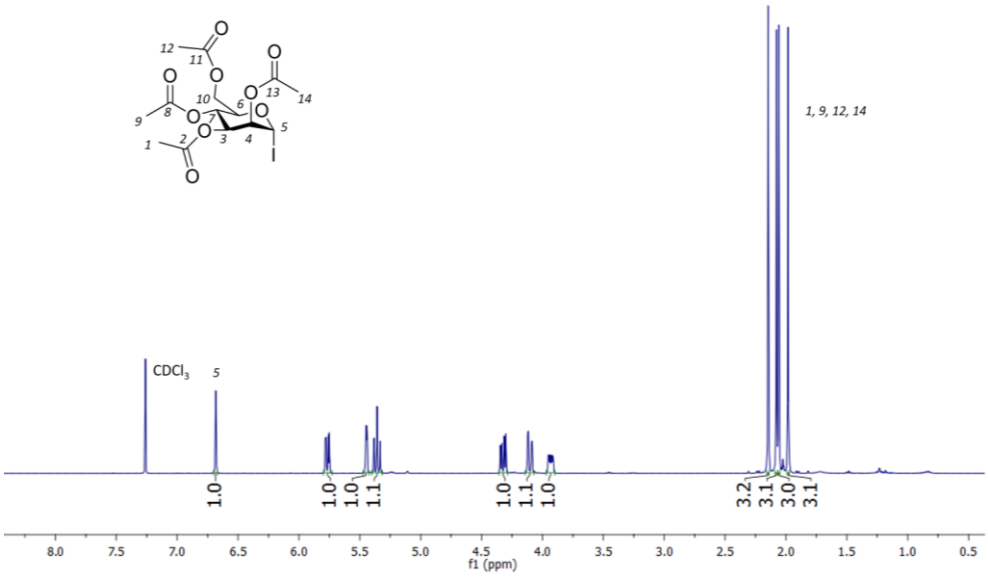

Figure S14 - ^{1}H NMR spectrum of 2,3,4,6 tetra-O-acetyl-α-D-mannose-I **(12)** in $CDCl_3$.

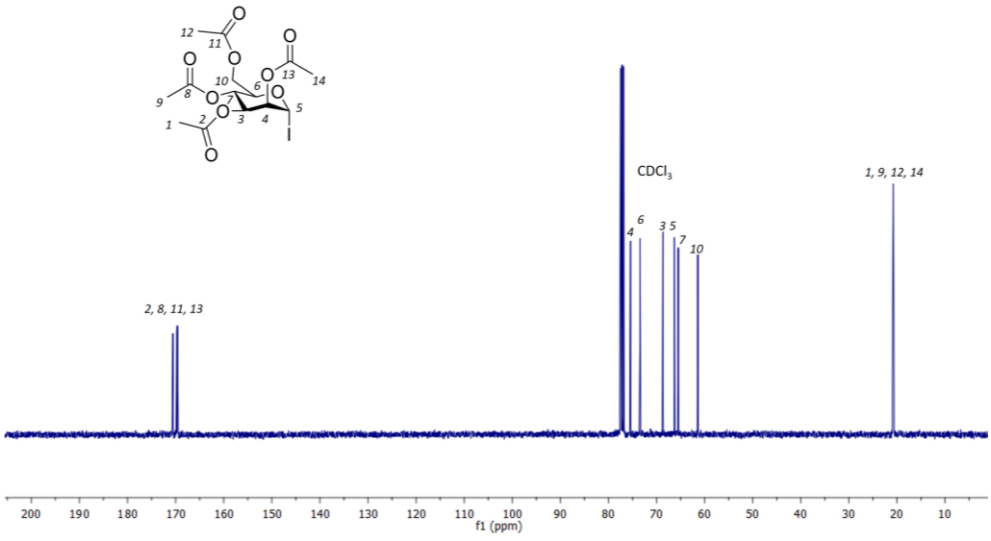

Figure S15 – ^{13}CNMR spectrum of 2,3,4,6 tetra-O-acetyl-α-D-mannose-I **(12)** in $CDCl_3$.

6.1.8 NMR spectrum of tetraacetate mannosylated-ethylethoxycarbamate cholesterol **(13)**

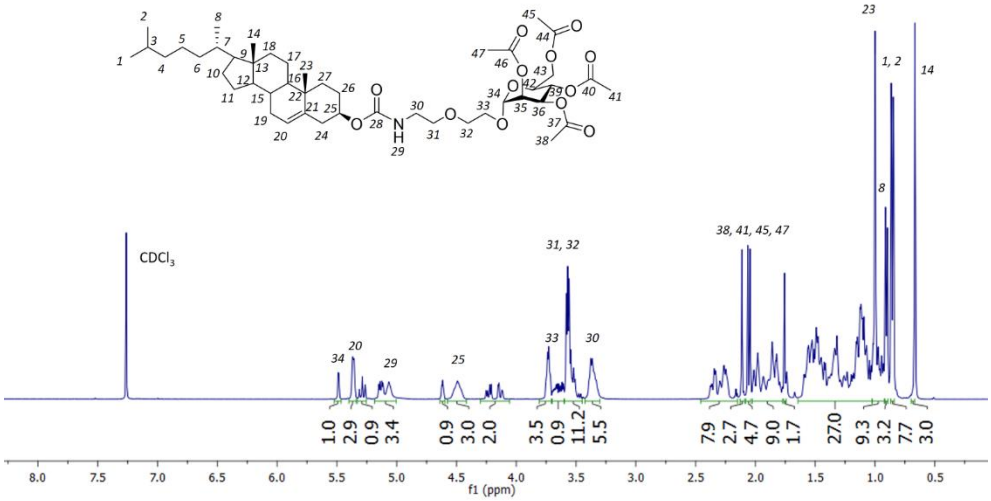

Figure S16 - ^{1}H NMR spectrum of tetraacetate mannosylated-ethylethoxycarbamate cholesterol **(13)** in $CDCl_3$.

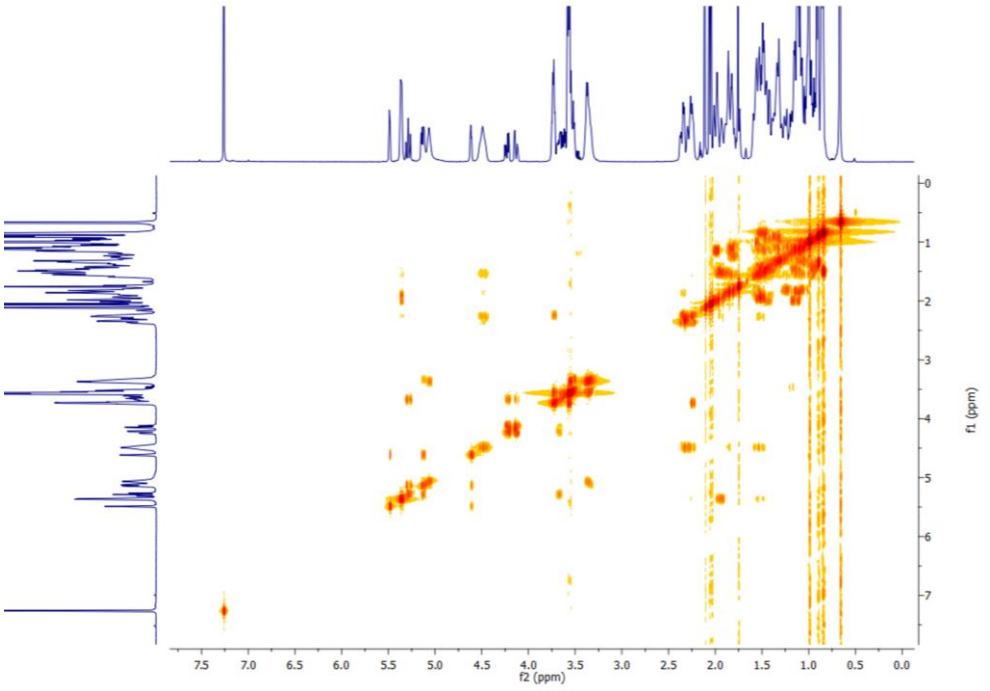

Figure S17 – COSY NMR spectrum of tetraacetate mannosylated-ethylethoxycarbamate cholesterol **(13)** in $CDCl_3$.

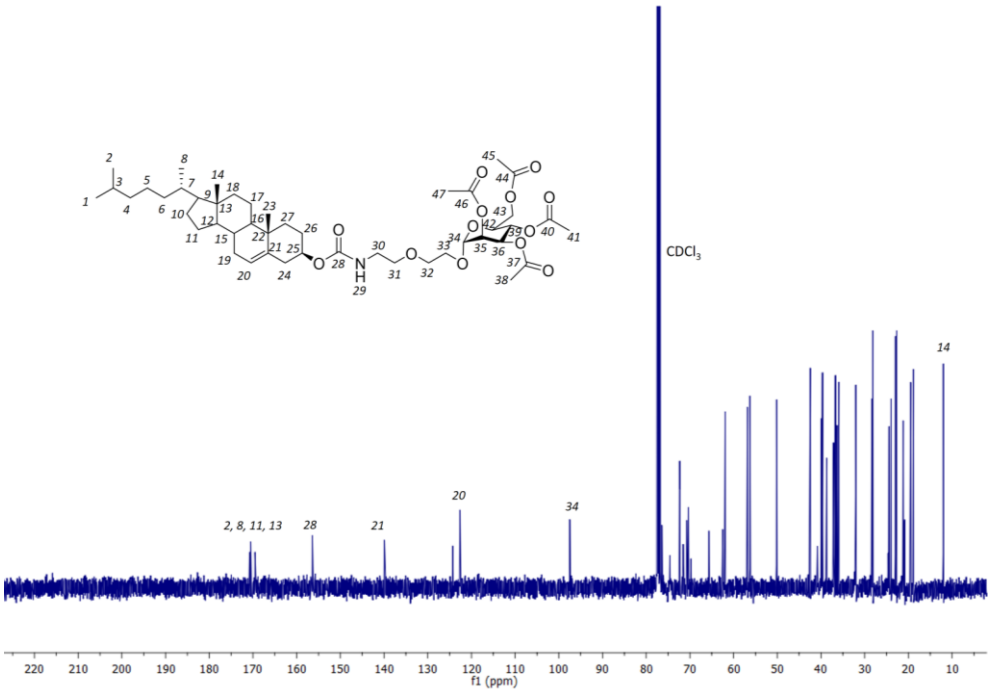

Figure S18 - ^{13}CNMR spectrum of tetraacetate mannosylated-ethylethoxycarbamate cholesterol **(13)** in $CDCl_3$.

6.1.9 NMR spectra of mannosylated-ethylethoxycarbamate cholesterol **(14)**

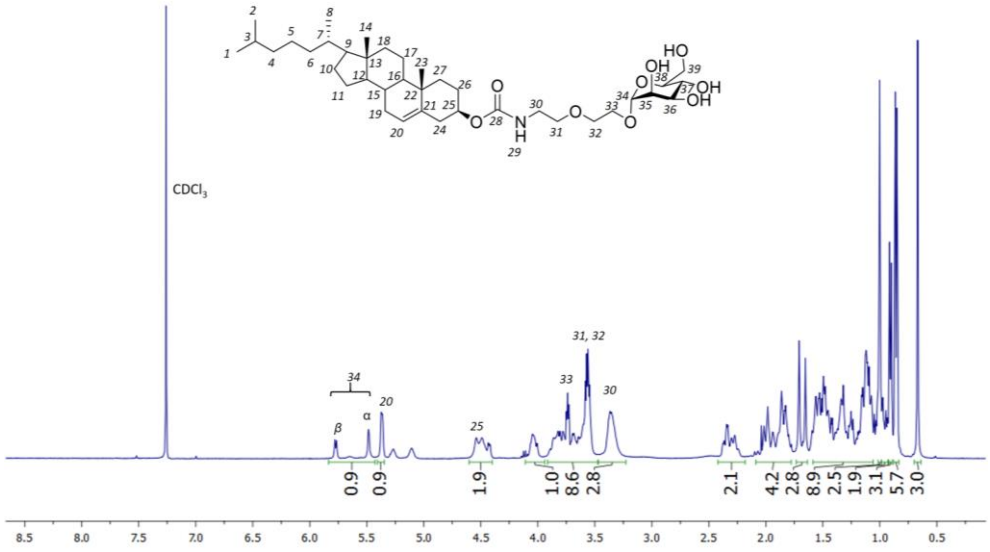

Figure S19 - ^{1}HNMR spectrum of mannosylated-ethylethoxycarbamate cholesterol **(14)** in $CDCl_3$.

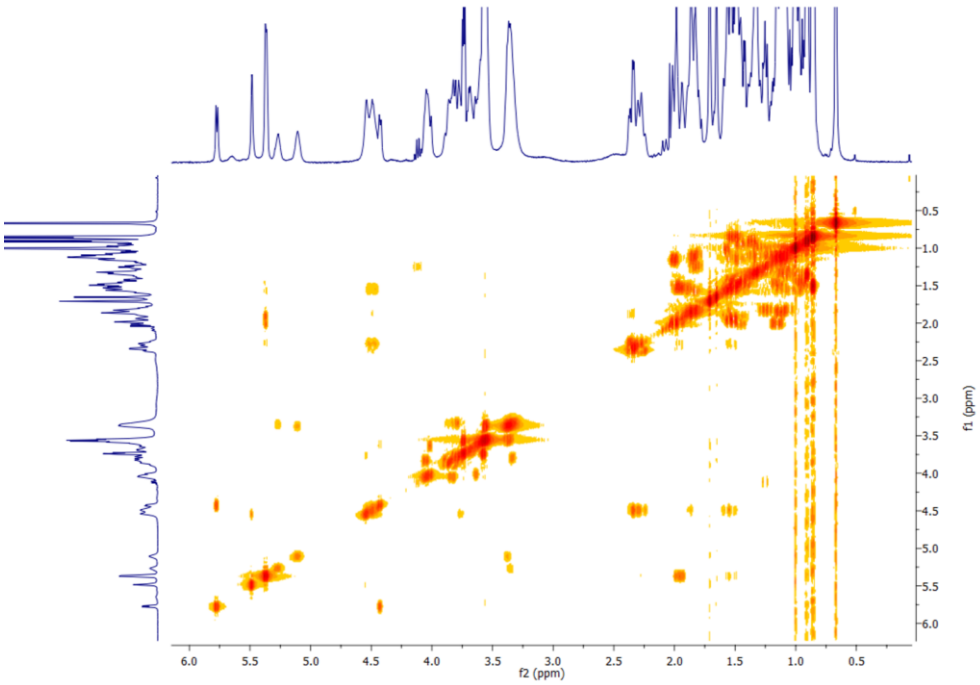

Figure S20 – COSY NMR spectrum of mannosylated-ethylethoxycarbamate cholesterol **(14)** in $CDCl_3$.

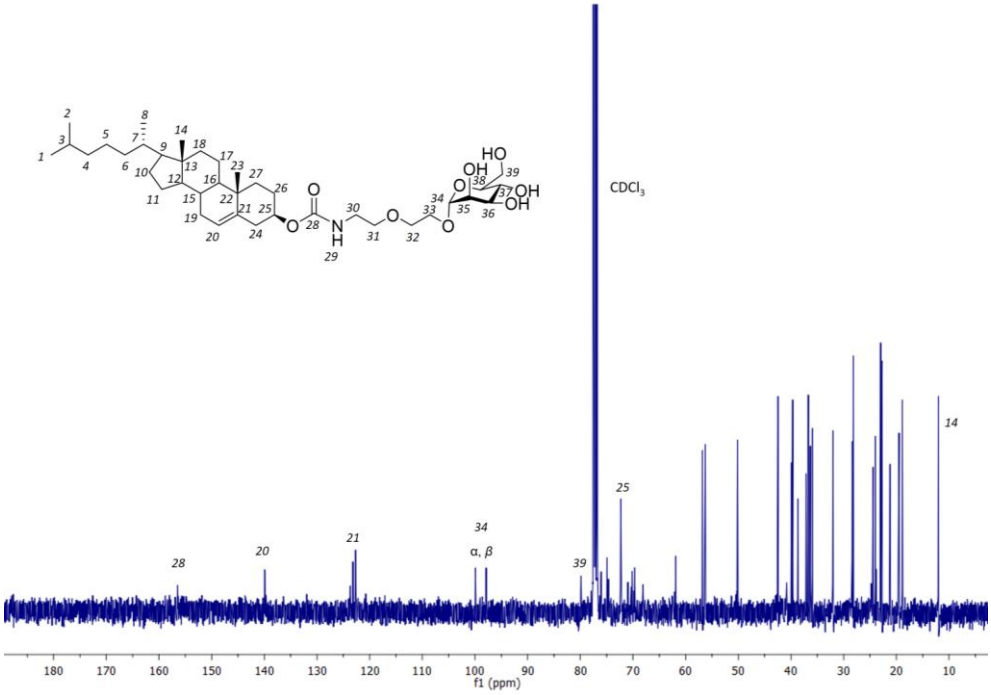

Figure S21 - ^{13}CNMR spectrum of mannosylated-ethylethoxycarbamate cholesterol **(14)** in $CDCl_3$.

6.1.10 NMR spectra of Cholesterol-(2-ethylethoxycarbamate) 2-bromopropionyl ester **(15)**

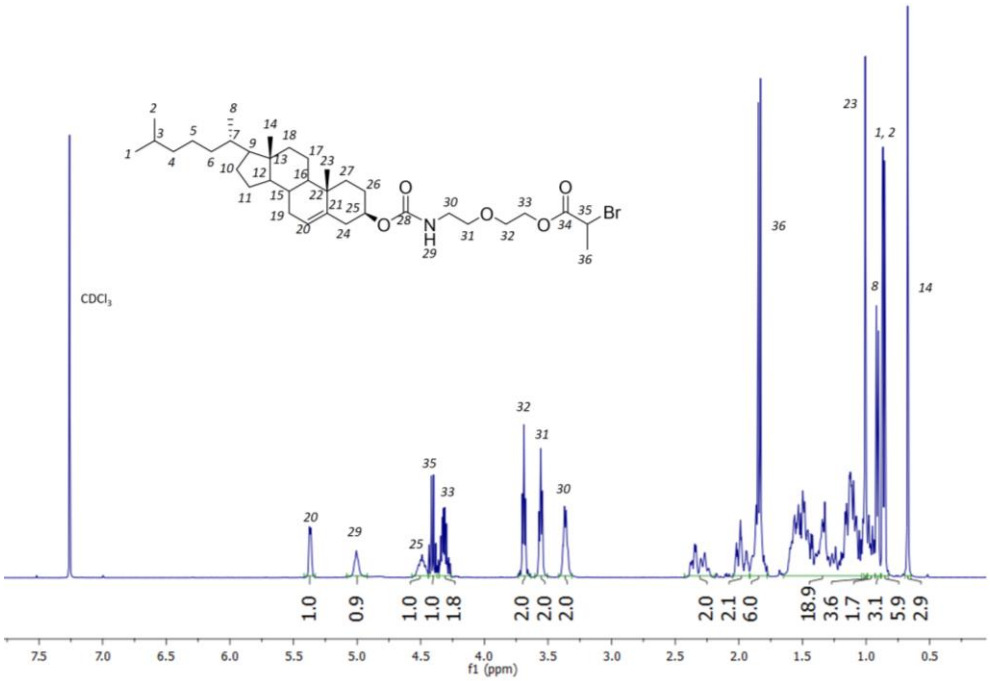

Figure S22 – ^{1}H NMR spectrum of Cholesterol-(2-ethylethoxycarbamate) 2-bromopropionyl ester **(15)** in $CDCl_3$.

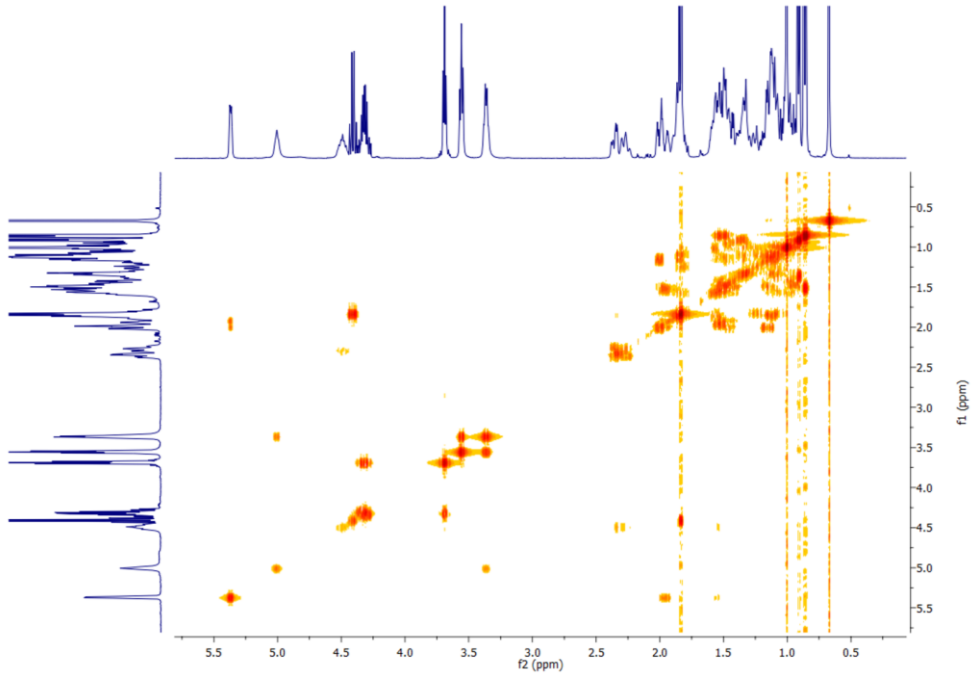

Figure S23 - COSY NMR spectrum of Cholesterol-(2-ethylethoxycarbamate) 2-bromopropionyl ester **(15)** in $CDCl_3$.

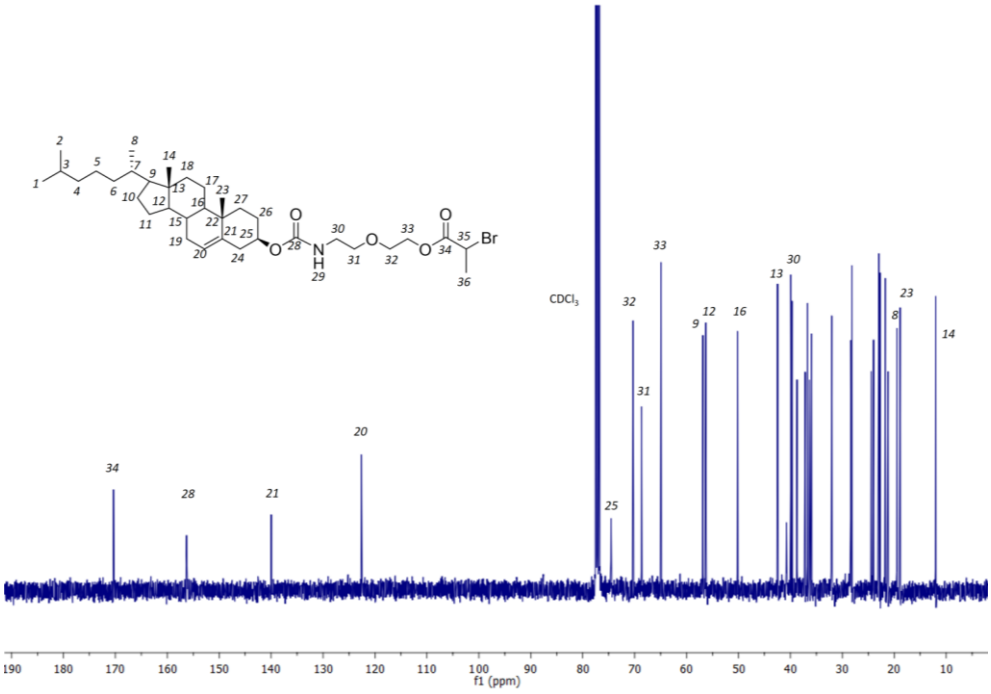

Figure S24 - ^{13}C NMR spectrum of Cholesterol-(2-ethylethoxycarbamate) 2-bromopropionyl ester **(15)** in $CDCl_3$.

6.1.11 NMR spectra of Cholesterol-10-methyl-1,9-dioxo-12-thioxo-5,8-dioxa-15,16-dihydroxy-11,13-dithia-2-azahexadecane **(16)**

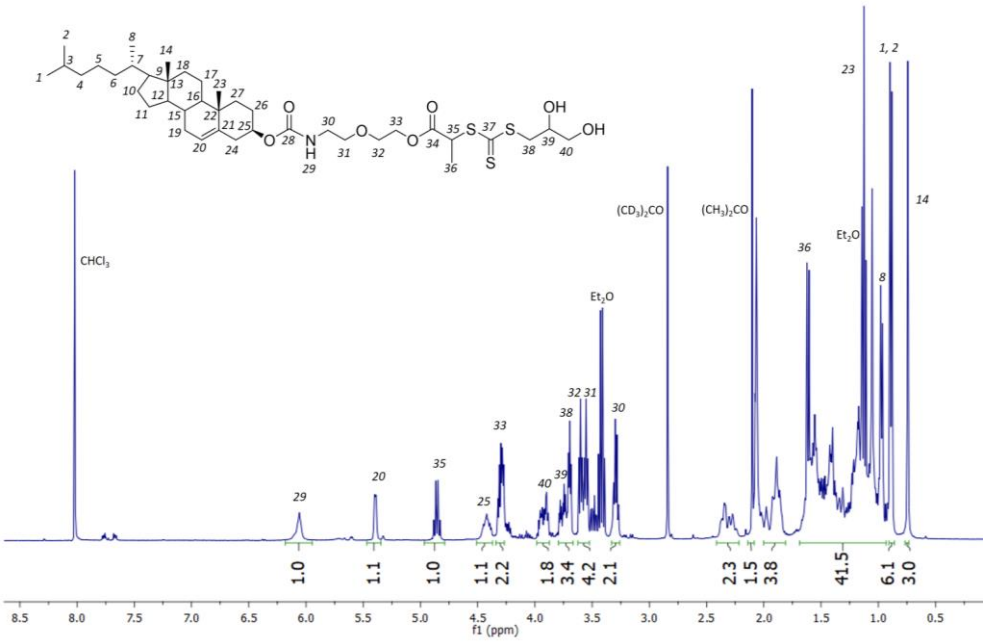

Figure S25 - ^{1}H NMR spectrum of Cholesterol-10-methyl-1,9-dioxo-12-thioxo-5,8-dioxa-15,16-dihydroxy-11,13-dithia-2-azahexadecane **(16)** in $(CD_3)_2CO$.

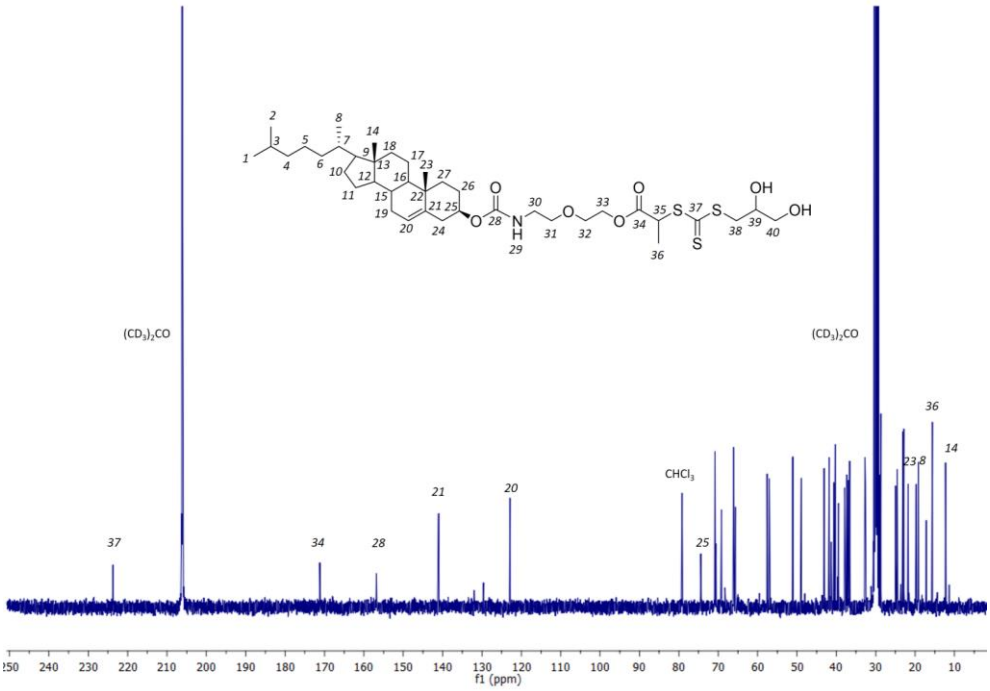

Figure S26 - ^{13}C NMR spectrum of Cholesterol-10-methyl-1,9-dioxo-12-thioxo-5,8-dioxa-15,16-dihydroxy-11,13-dithia-2-azahexadecane **(16)** in $(CD_3)_2CO$.

6.1.12 NMR spectra of sodium 3-(trithiocarboxyl)propane-1-sulfonate **(17)**

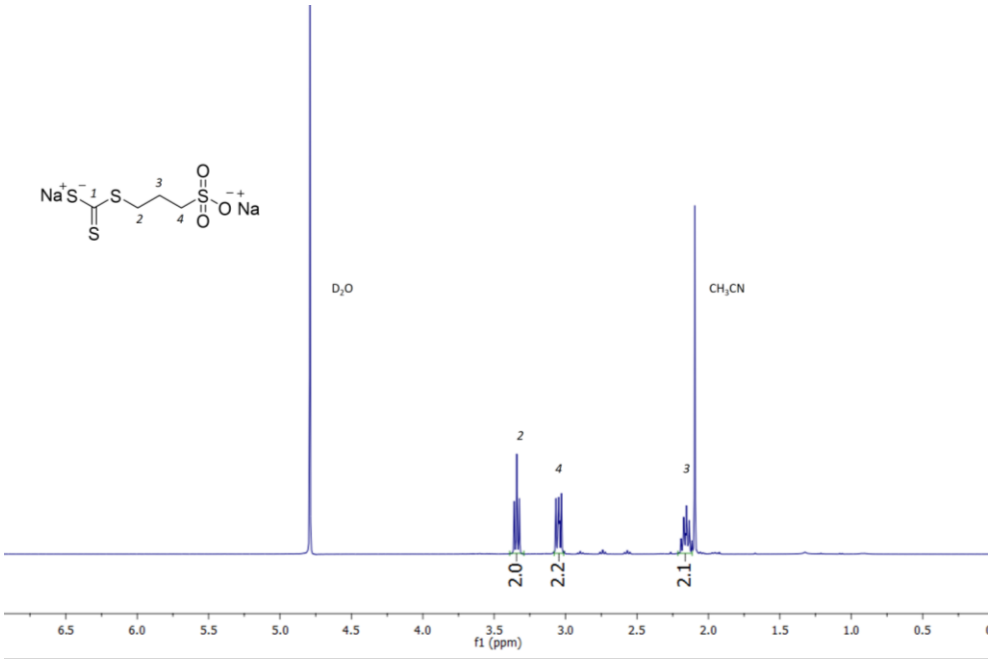

Figure S27 - ^{1}H NMR spectrum of sodium 3-(trithiocarboxyl)propane-1-sulfonate **(17)** in D_2O.

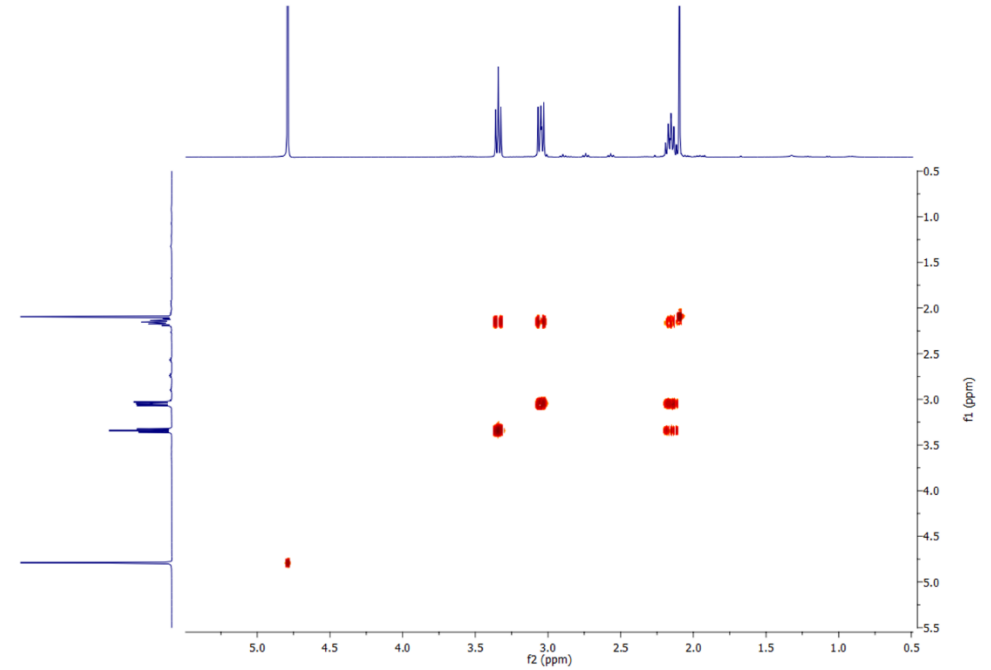

Figure S28 – COSY NMR spectrum of sodium 3-(trithiocarboxyl)propane-1-sulfonate **(17)** in D_2O.

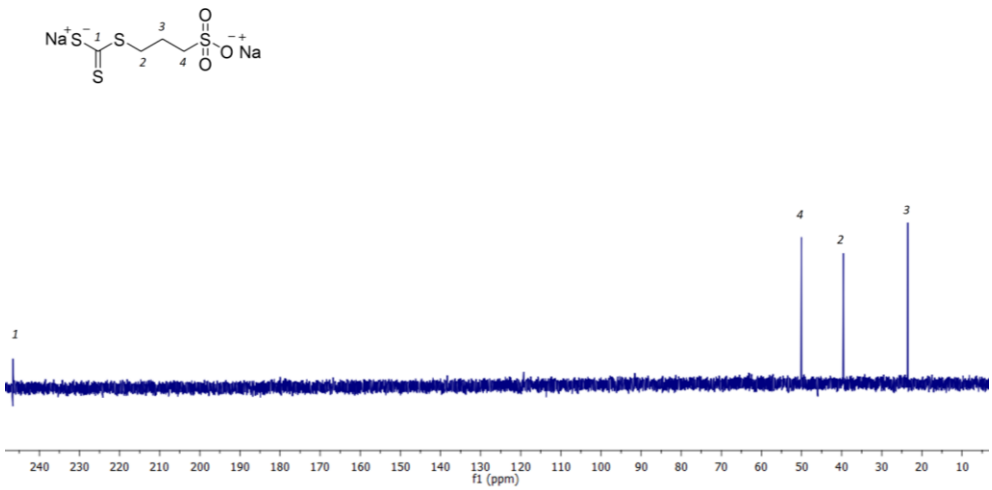

Figure S29 – ^{13}C NMR spectrum of sodium 3-(trithiocarboxyl)propane-1-sulfonate **(17)** in D_2O.

6.1.13 NMR spectra of Sodium 1-(cholesterol)-10-methyl-1,9-dioxo-12-thioxo-5,8-dioxa-11,13-dithia-2-azahexadecane-16-sulfonate **(18)**

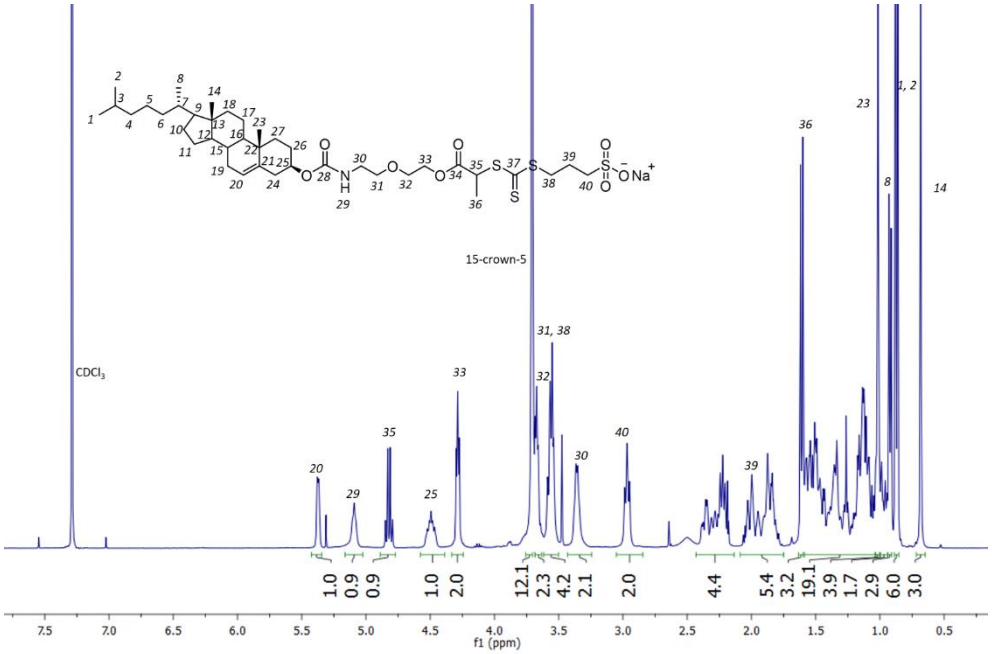

Figure S30 – ^{1}H NMR spectrum of Sodium 1-(cholesterol)-10-methyl-1,9-dioxo-12-thioxo-5,8-dioxa-11,13-dithia-2-azahexadecane-16-sulfonate **(18)** in $CDCl_3$.

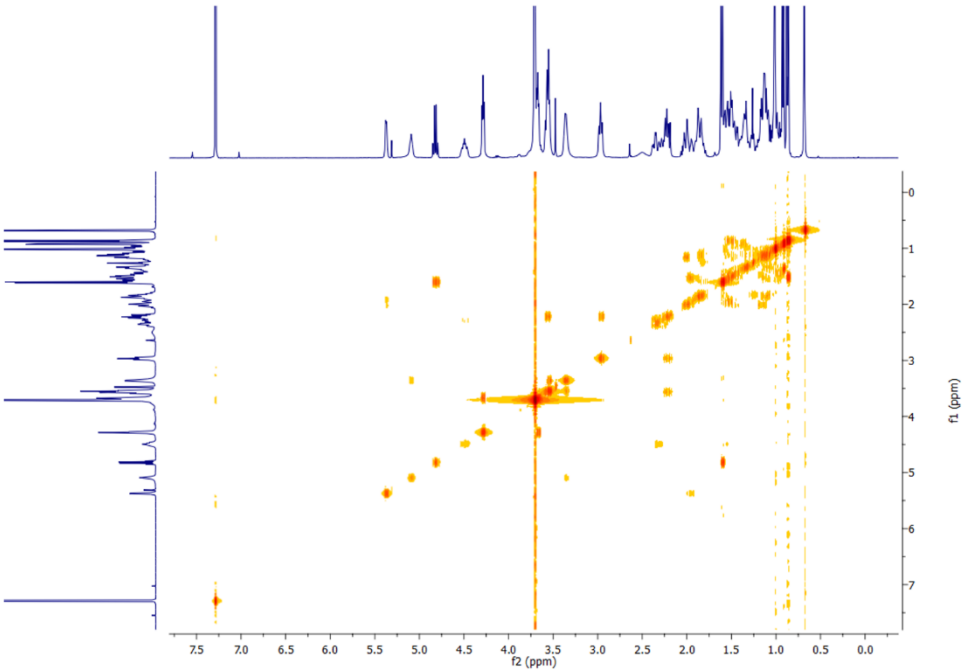

Figure S31 - COSY NMR spectrum of Sodium 1-(cholesterol)-10-methyl-1,9-dioxo-12-thioxo-5,8-dioxa-11,13-dithia-2-azahexadecane-16-sulfonate **(18)** in $CDCl_3$.

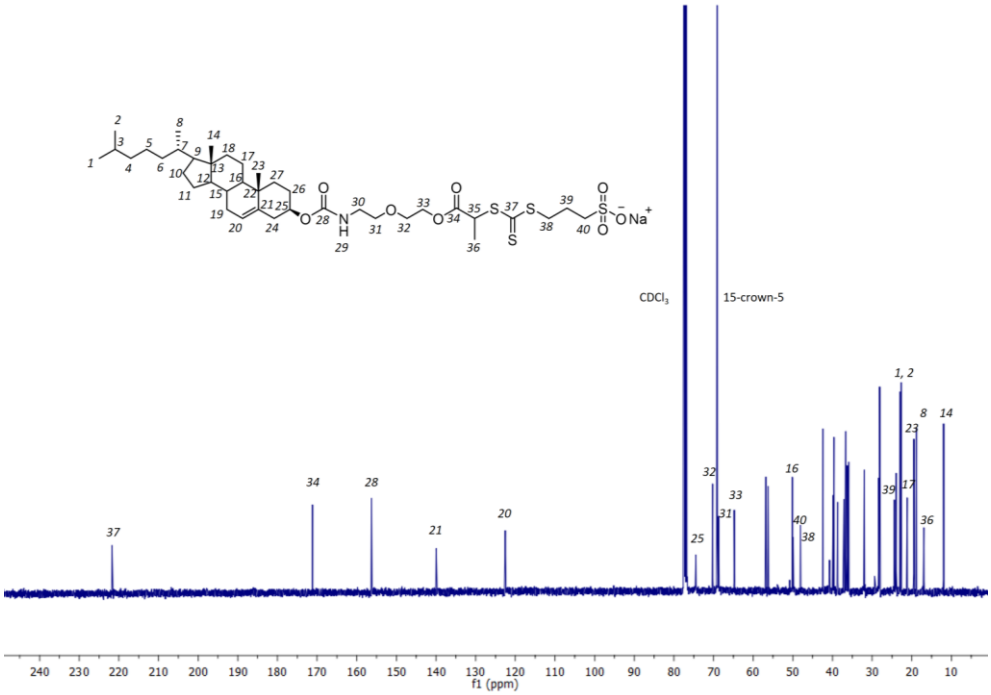

Figure S32 - ^{13}C NMR spectrum of Sodium 1-(cholesterol)-10-methyl-1,9-dioxo-12-thioxo-5,8-dioxa-11,13-dithia-2-azahexadecane-16-sulfonate **(18)** in $CDCl_3$.

6.1.14 NMR spectra of 2'-acrylamidoethyl-2,3,4,6-tetra-O-acetyl-β-D-galactopyranoside **(19)**

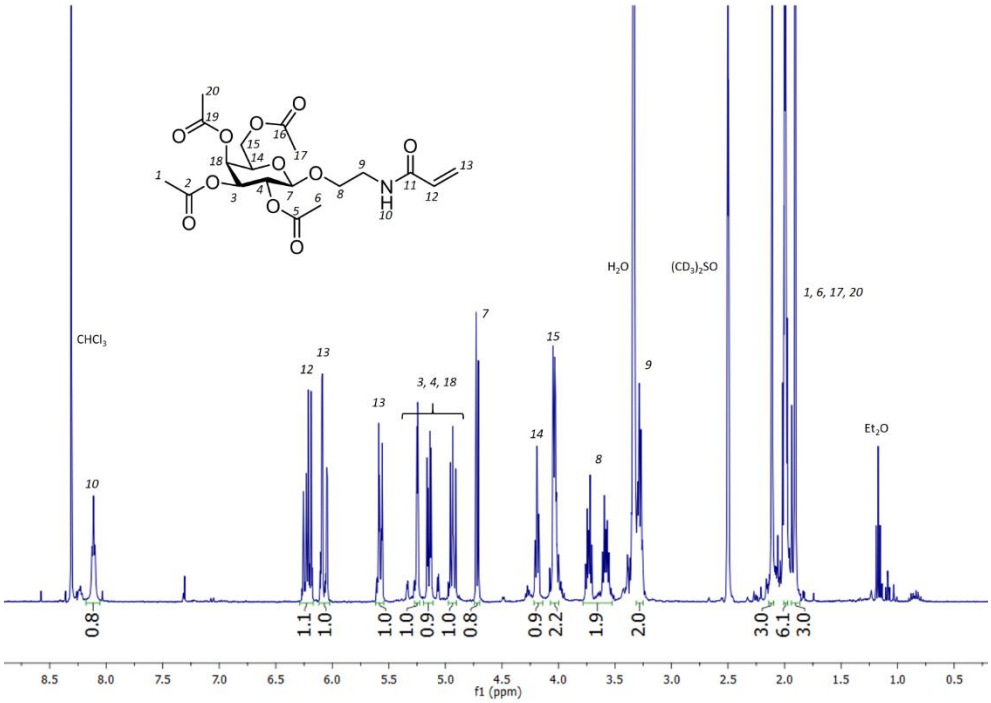

Figure S33 - ^{1}H NMR spectrum of 2'-acrylamidoethyl-2,3,4,6-tetra-O-acetyl-β-D-galactopyranoside **(19)** in $(CD_3)_2SO$.

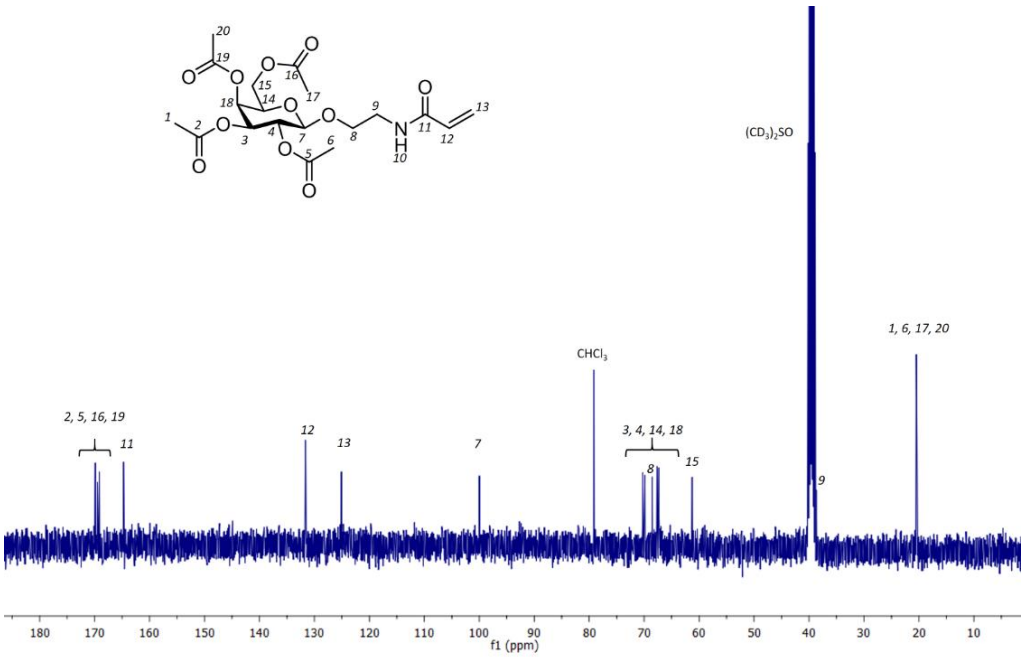

Figure S34 - ^{13}C NMR spectrum of 2'-acrylamidoethyl-2,3,4,6-tetra-O-acetyl-β-D-galactopyranoside **(19)** in $(CD_3)_2SO$.

6.1.15 NMR spectra of 2'-acrylamidoethyl -β-D-galactopyranoside **(20)**

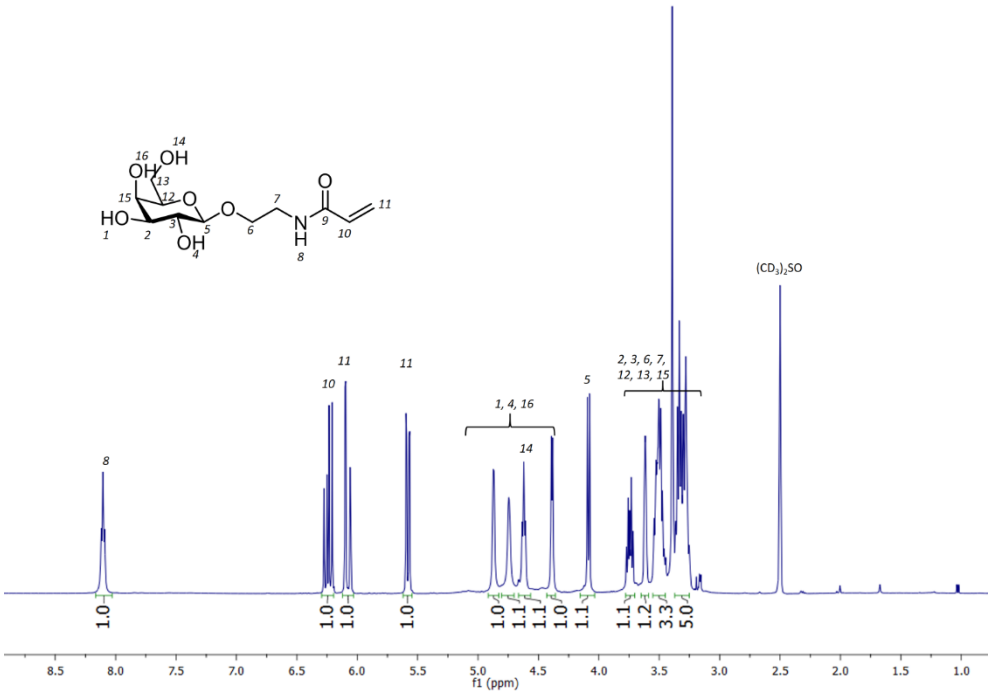

Figure S35 - ^{1}H NMR spectrum of 2'-acrylamidoethyl -β-D-galactopyranoside **(20)** in $(CD_3)_2SO$.

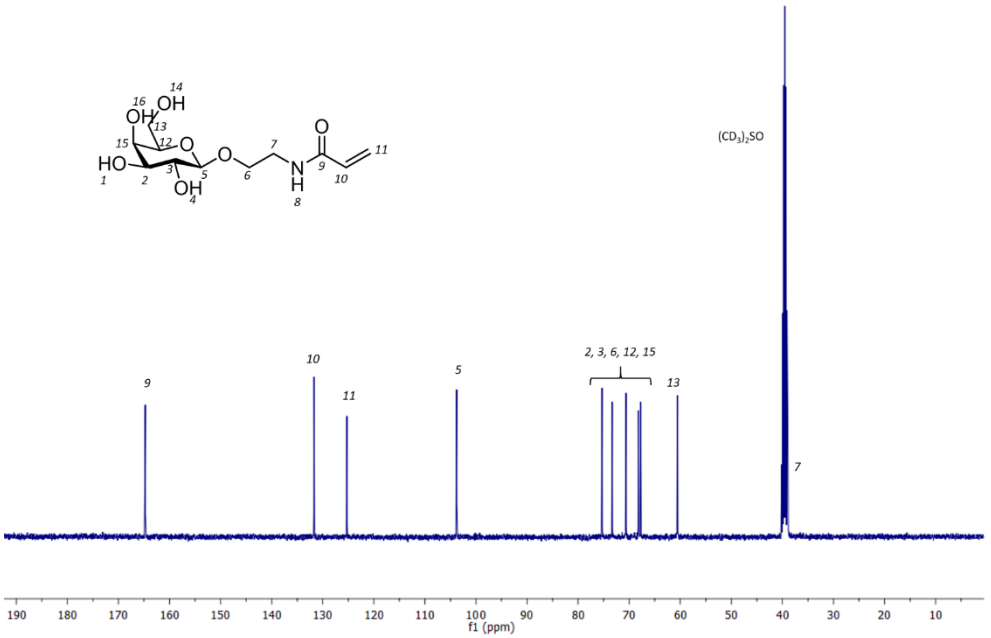

Figure S36 - ^{13}C NMR spectrum of 2'-acrylamidoethyl -β-D-galactopyranoside **(20)** in $(CD_3)_2SO$.

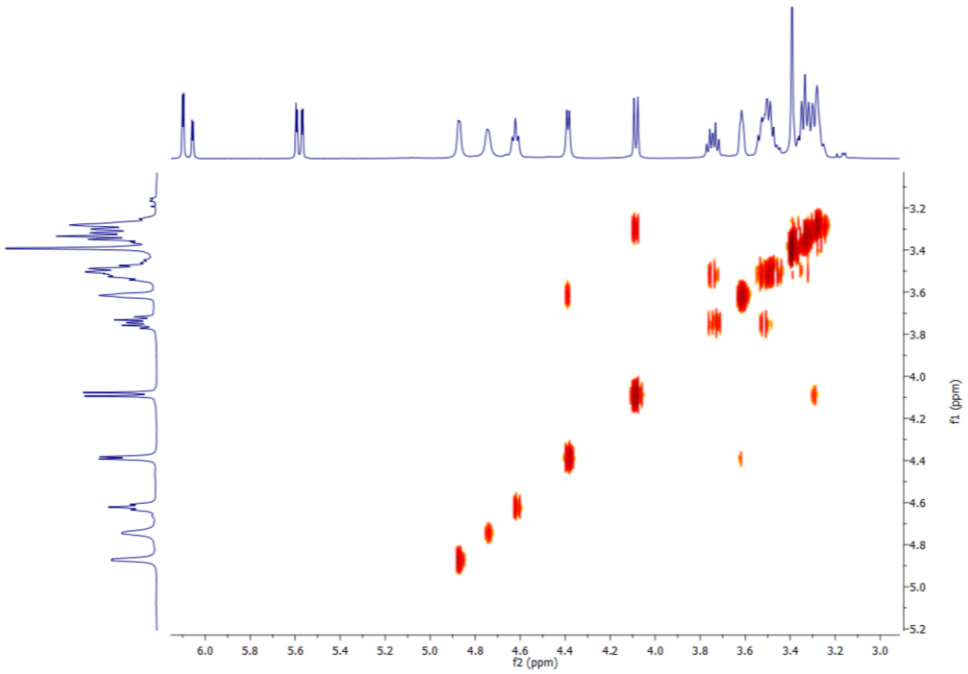

Figure S37 – COSY NMR spectrum of 2'-acrylamidoethyl -β-D-galactopyranoside **(20)** in $(CD_3)_2SO$.

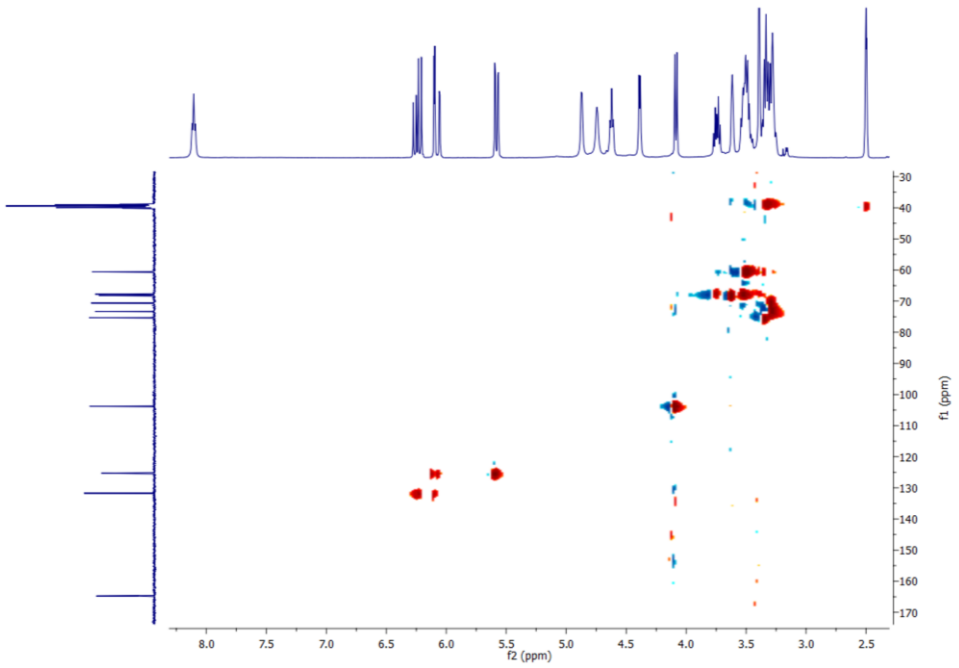

Figure S38 - HSQC NMR spectrum of 2'-acrylamidoethyl -β-D-galactopyranoside **(20)** in $(CD_3)_2SO$.

6.1.16 NMR spectra of 2'-acrylamidoethyl-2,3,4,6-tetra-O-acetyl-α-D-mannosepyranoside **(21)**

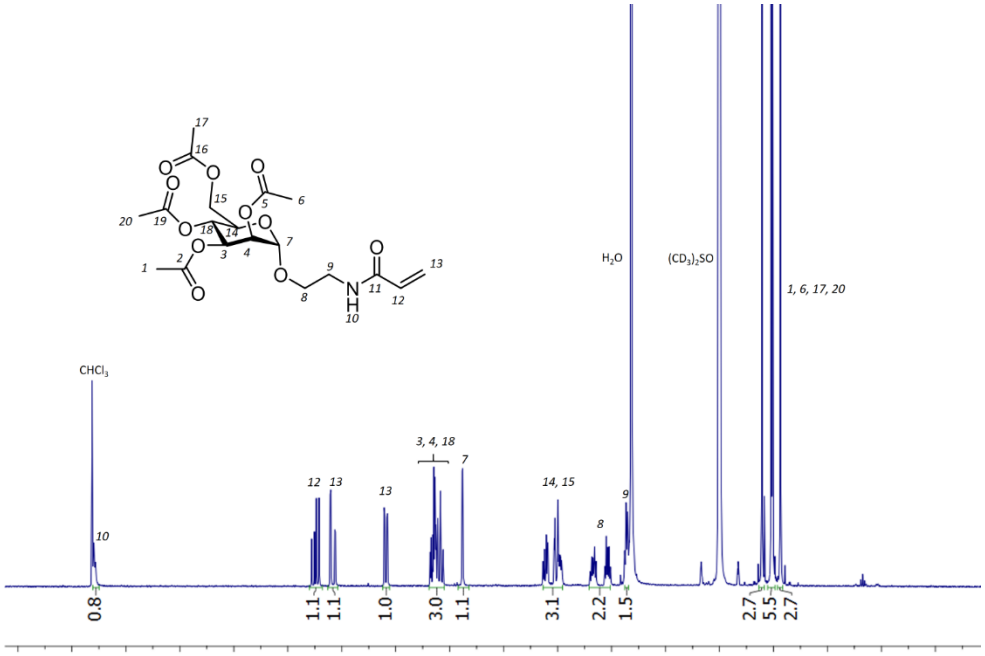

Figure S39 - ^{1}H NMR spectrum of 2'-acrylamidoethyl-2,3,4,6-tetra-O-acetyl-α-D-mannosepyranoside **(21)** in $(CD_3)_2SO$.

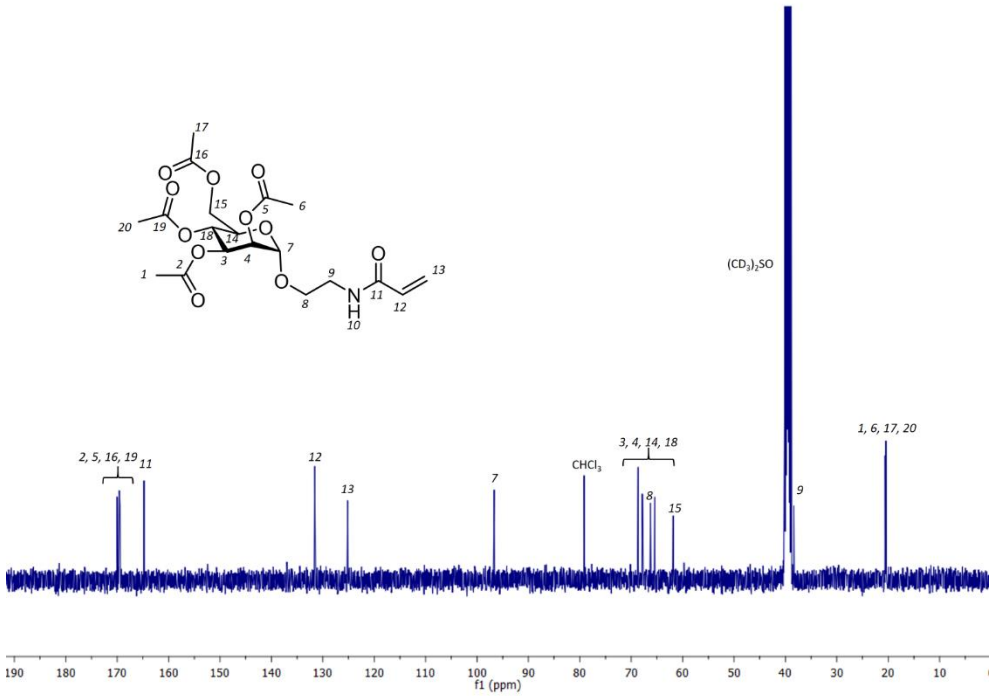

Figure S40 – ^{13}C NMR spectrum of 2'-acrylamidoethyl-2,3,4,6-tetra-O-acetyl-α-D-mannosepyranoside **(21)** in $(CD_3)_2SO$.

6.1.17 NMR spectra of 2'-acrylamidoethyl-α-D-mannosepyranoside **(22)**

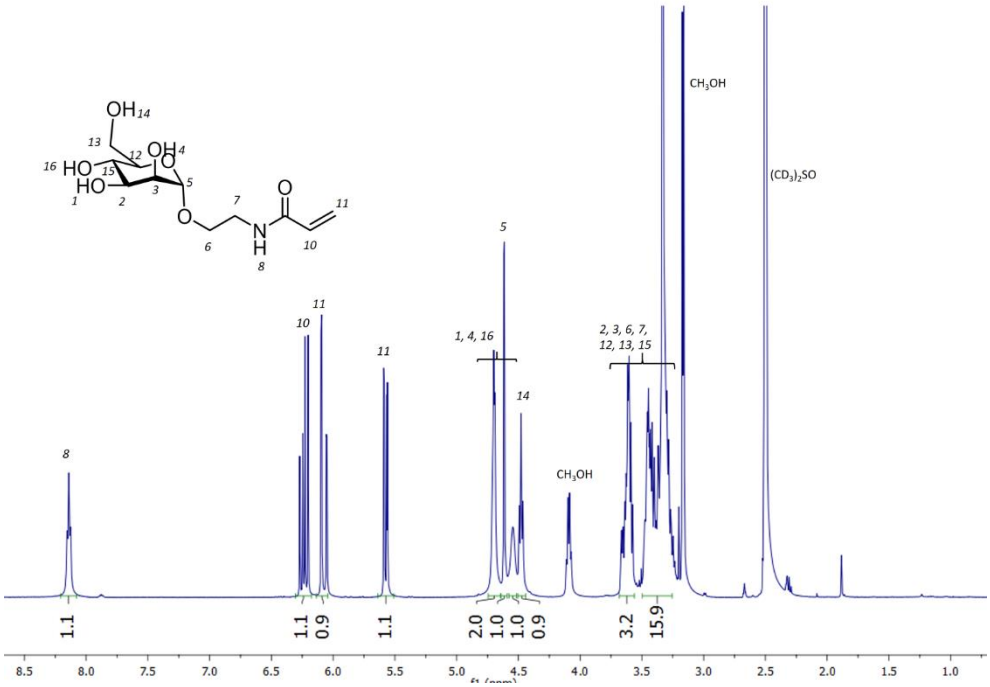

Figure S41 - ^{1}H NMR spectrum of 2'-acrylamidoethyl-α-D-mannosepyranoside **(22)** in $(CD_3)_2SO$.

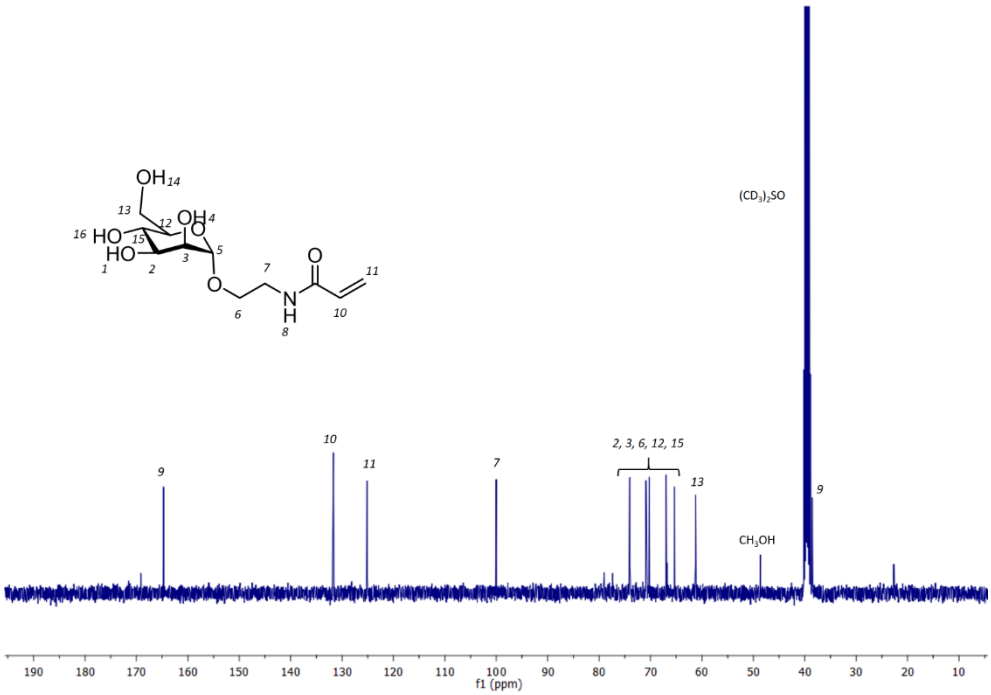

Figure S42 - ^{13}C NMR spectrum of 2'-acrylamidoethyl-α-D-mannosepyranoside **(22)** in $(CD_3)_2SO$.

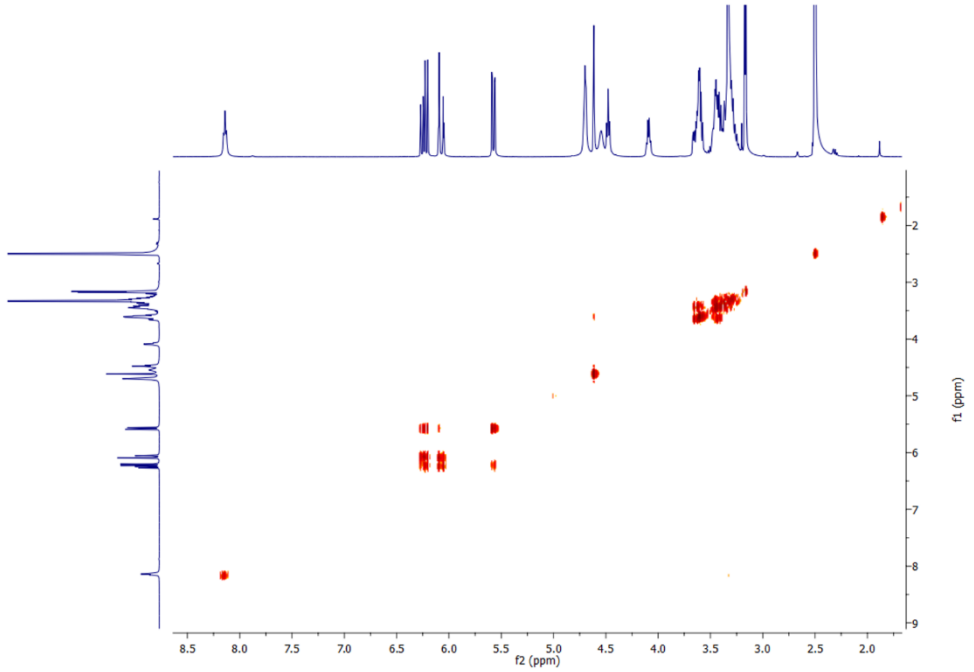

Figure S43 - COSY NMR spectrum of 2'-acrylamidoethyl-α-D-mannosepyranoside **(22)** in $(CD_3)_2SO$.

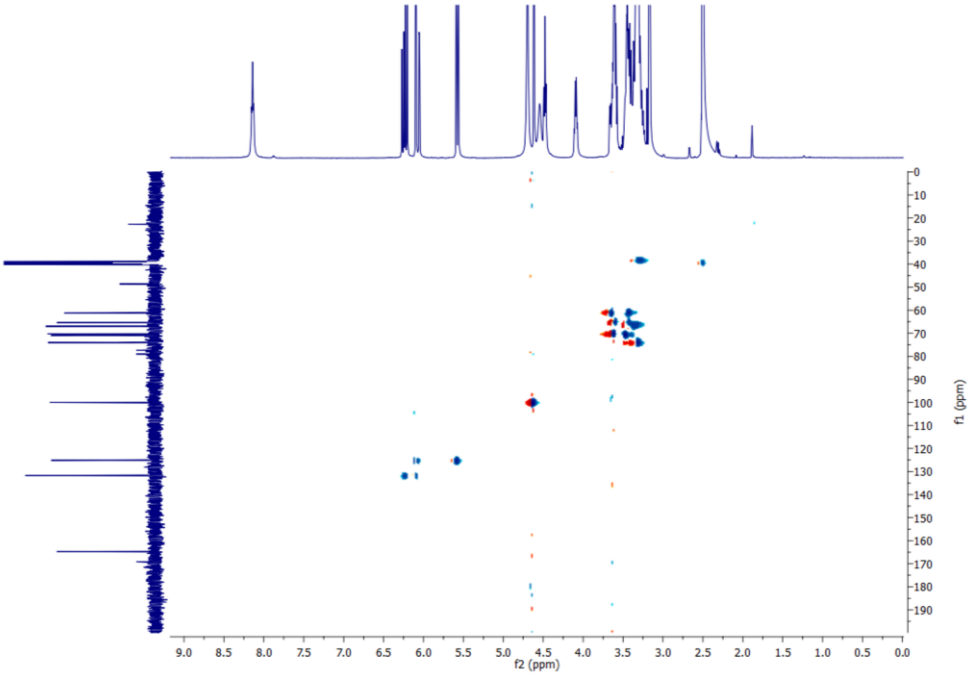

Figure S44 – HSQC NMR spectrum of 2'-acrylamidoethyl-α-D-mannosepyranoside **(22)** in $(CD_3)_2SO$.

6.1.18 NMR spectrum of cholesterol-terminated poly(N-hydroxyethyl acrylamide)$_{25}$ **(23)**

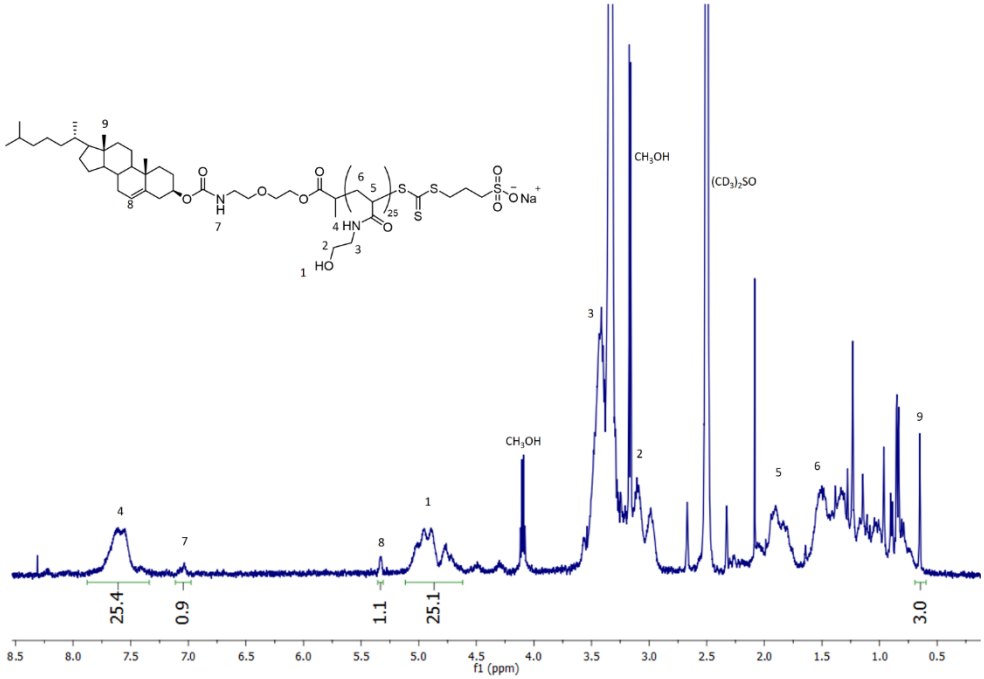

Figure S45 – ^{1}H NMR spectrum of cholesterol-terminated poly(N-hydroxyethyl acrylamide)$_{25}$ **(23)** in $(CD_3)_2SO$.

6.1.19 NMR spectra of cholesterol-terminated glycopolymers **(24, 25, 26, 27)**

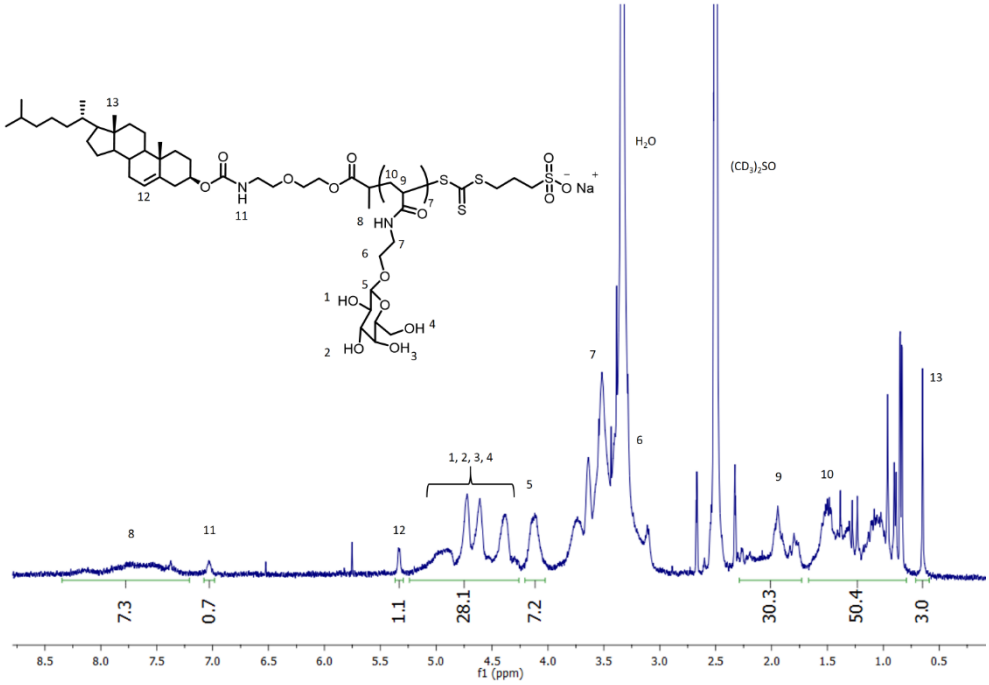

Figure S46 - ^{1}H NMR spectrum of Cholesterol-Gal_7 **(24)** in $(CD_3)_2SO$.

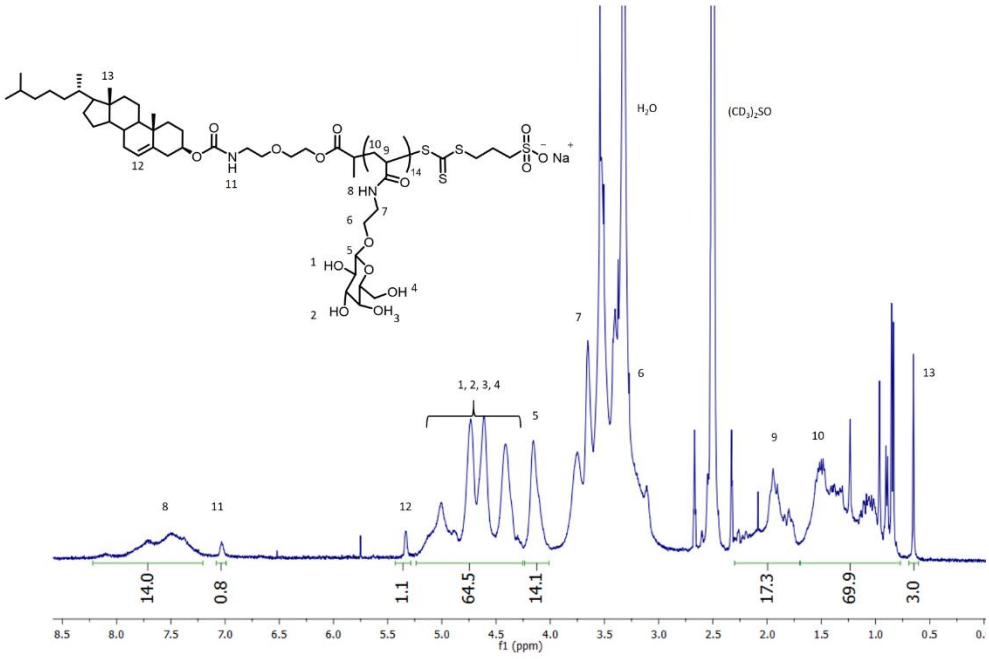

Figure S47 - ^{1}H NMR spectrum of Cholesterol-Gal_{14} **(25)** in $(CD_3)_2SO$.

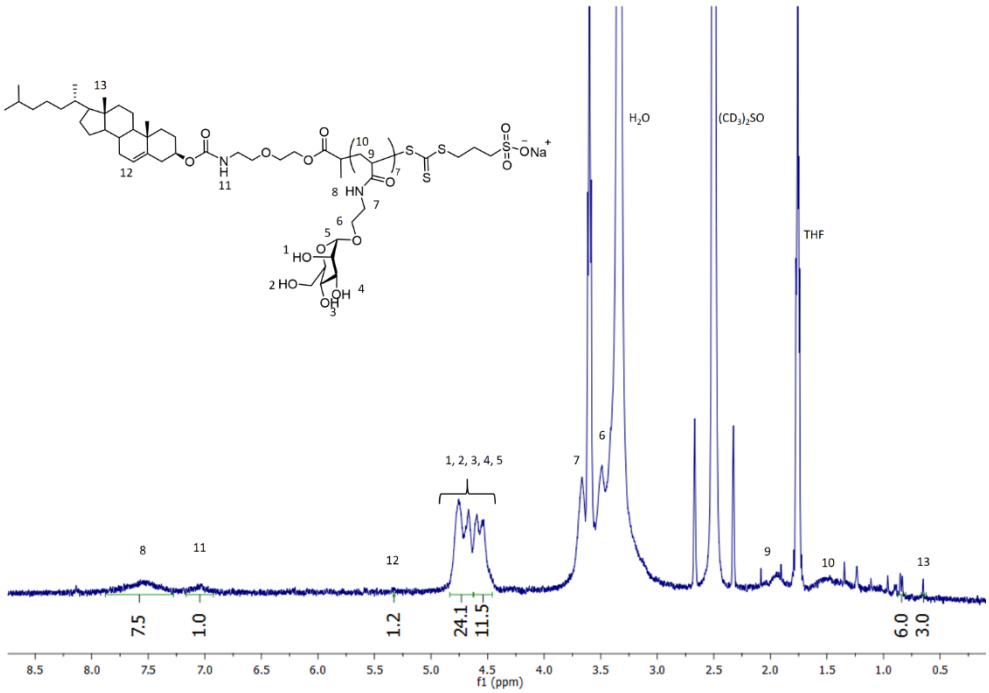

Figure S48 - ^{1}H NMR spectrum of Cholesterol-Man_7 **(26)** in $(CD_3)_2SO$.

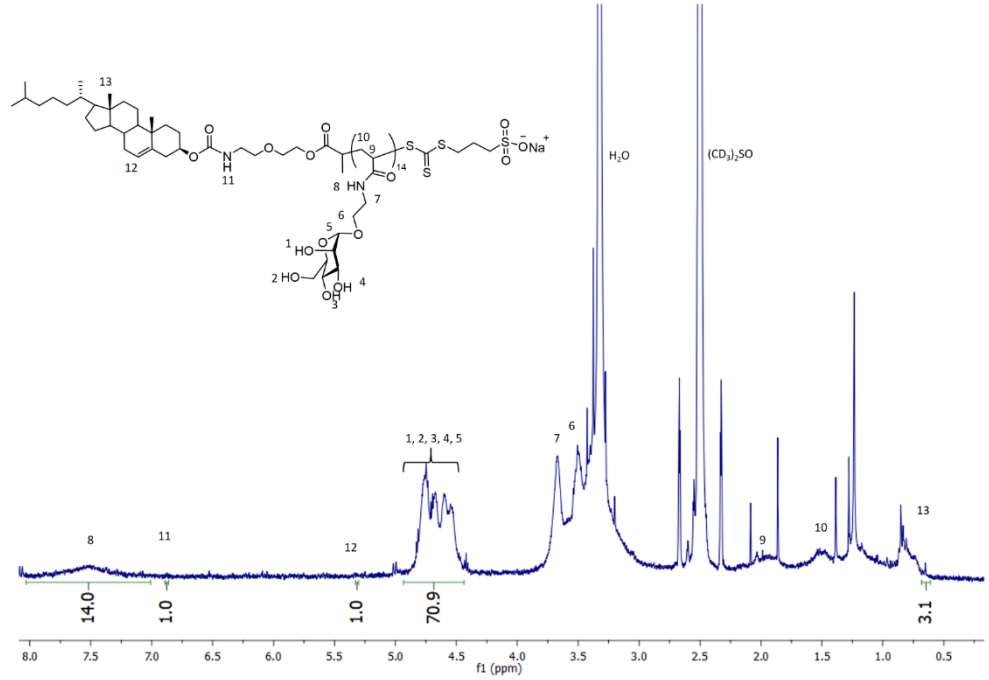

Figure S49 - ^{1}H NMR spectrum of Cholesterol-Man_7 **(27)** in $(CD_3)_2SO$.

6.1.20 Mass spectrum of cholesterol-terminated glycopolymer **(26)**

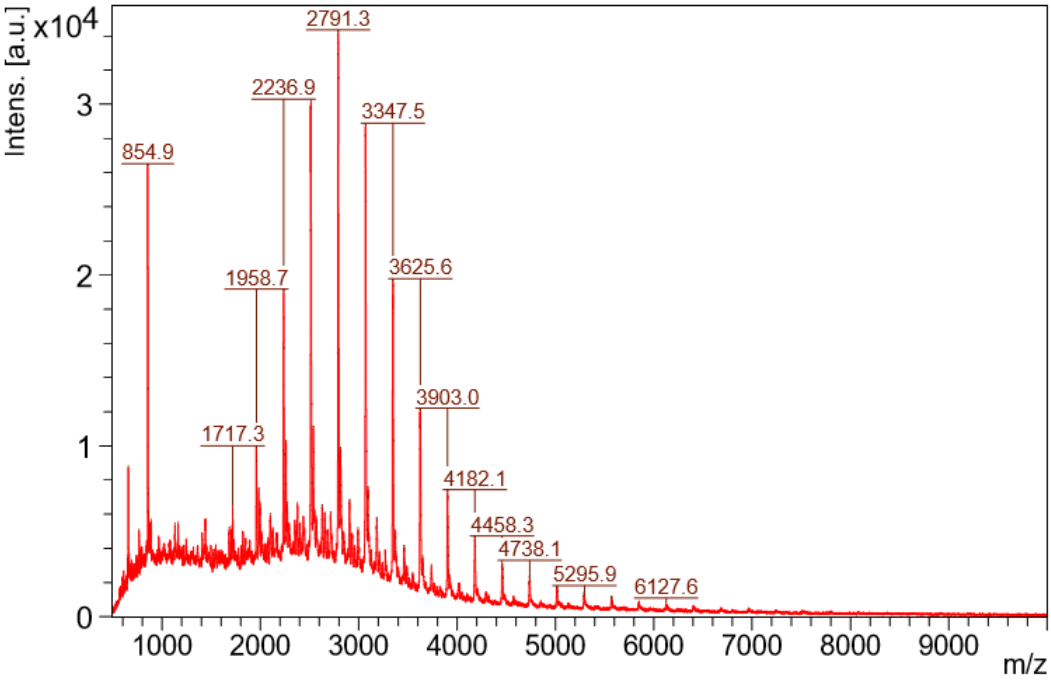

Figure S50 – MALDI-TOF mass spectrum of Chol-Man_7 **(26)**.

6.2 Supplementary Information Chapter 2 – SEC chromatograms

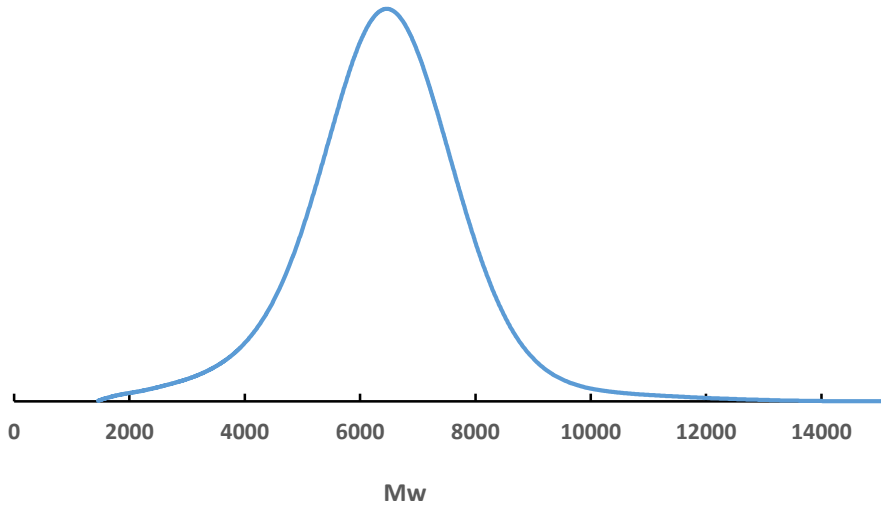

Figure S51 - SEC analysis of cholesterol-terminated poly(N-hydroxyethyl acrylamide)$_{25}$ **(23)** M_n (SEC): 5.85 kDa, Đ 1.05.

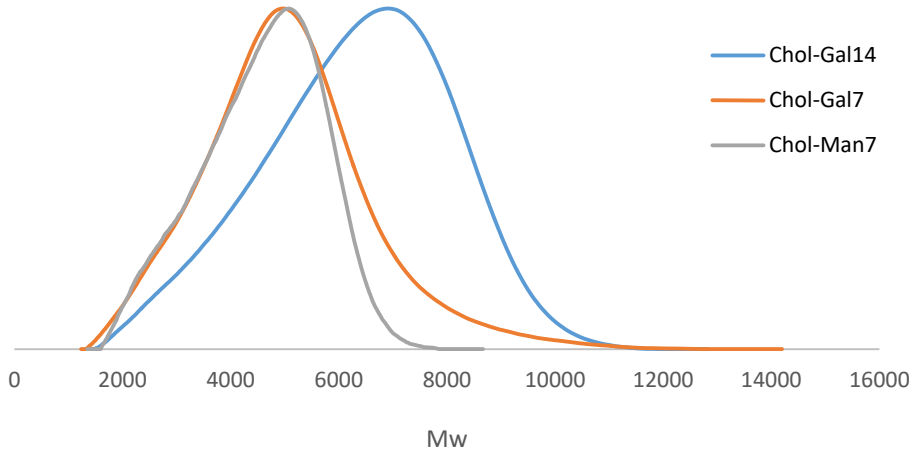

Figure S52 – SEC analysis of glycopolymer Chol-Gal$_7$ **(24)**, Chol-Gal$_{14}$ **(25)**, Chol-Man$_7$ **(26)**.

6.3 Supplementary Information Chapter 3

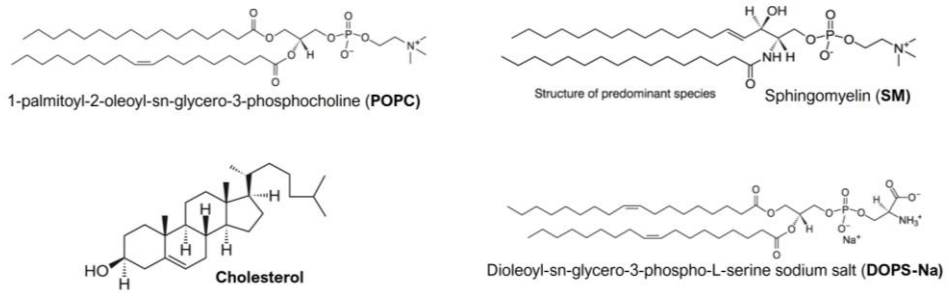

Figure S53 – Chemical structures of (phospho)lipids used for liposome formulations.

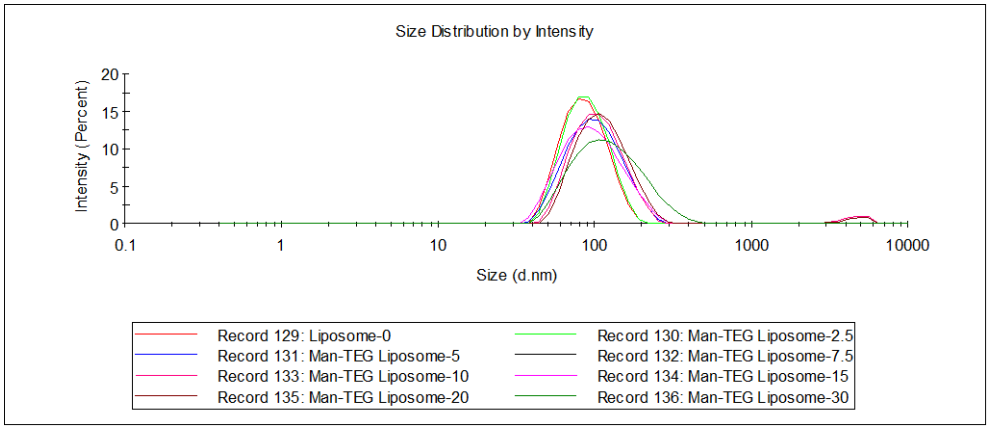

Figure S54 - Particle size distribution of Man-TEG liposome formulations.

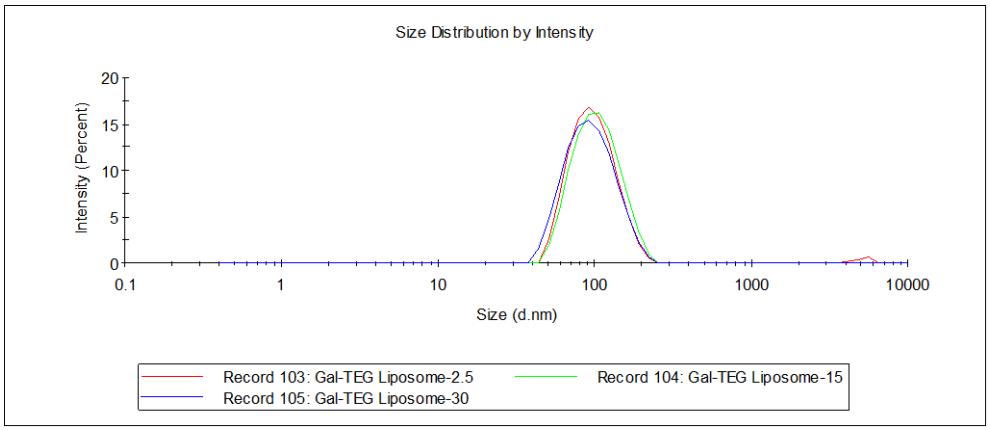

Figure S55 - Particle size distribution of Gal-TEG liposome formulations.

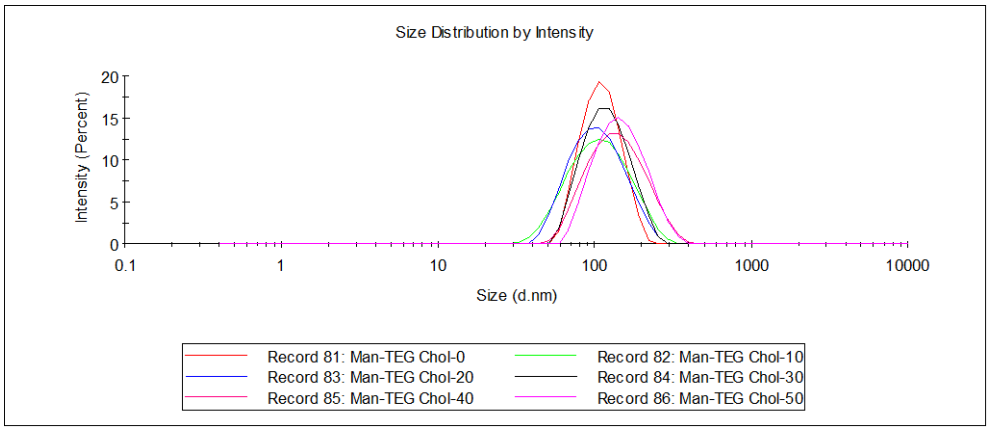

Figure S56 - Particle size distribution for Man-TEG liposome formulations with variable cholesterol content.

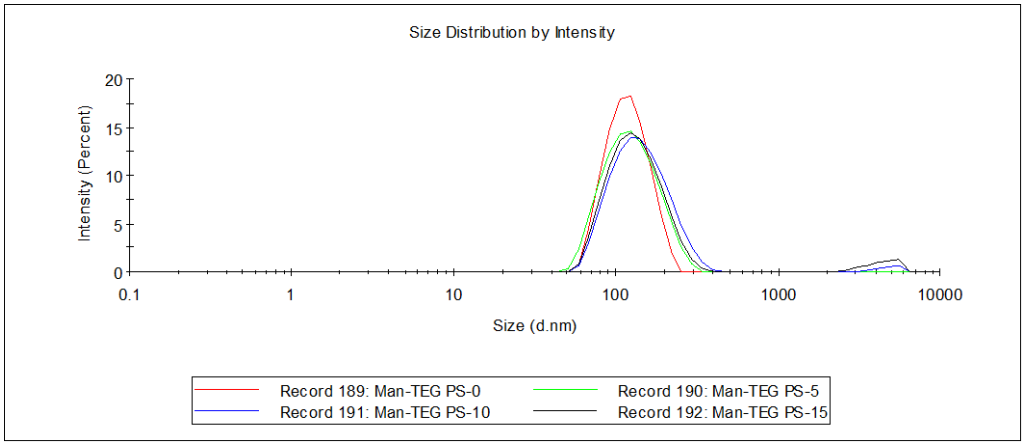

Figure S57 - Particle size distribution for Man-TEG liposome formulations with variable PS content.

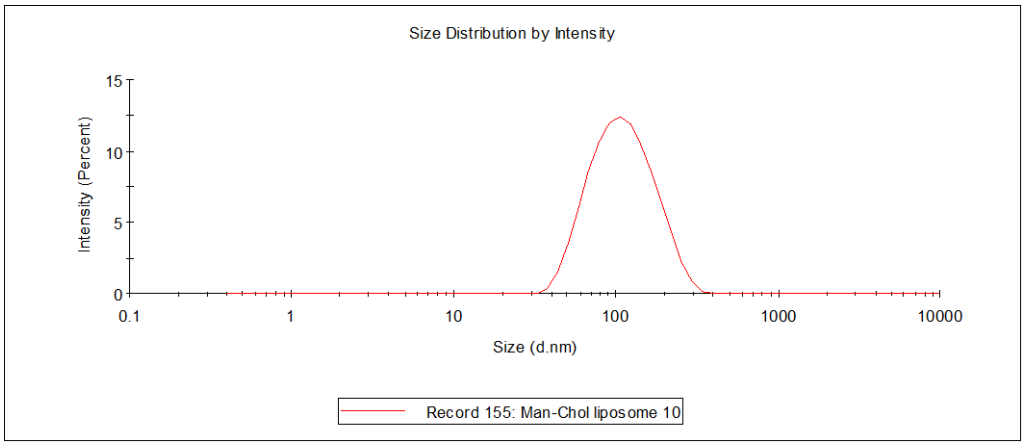

Figure S58 - Particle size distribution for Man-Chol liposome formulation.

Table S1 - Z-average and PdI values from DLS.

Formulation	Z-Average[1] d. nm	PdI[1]
Liposome-0	82.68 ± 0.22	0.154 ± 0.07
Man-TEG Liposome-2.5	102.2 ± 0.55	0.163 ± 0.02
Man-TEG Liposome-5	99.75 ± 0.63	0.101 ± 0.01
Man-TEG Liposome-7.5	112.2 ± 0.99	0.123 ± 0.64
Man-TEG Liposome -10	103.3 ± 0.68	0.234 ± 0.09
Man-TEG Liposome-15	105.8 ± 0.28	0.172 ± 0.02
Man-TEG Liposome-20	108.1 ± 0.64	0.180 ± 0.01
Man-TEG Liposome -30	117.7± 0.67	0.148± 0.09
Gal-TEG Liposome-2.5	87.06 ± 0.62	0.177 ± 0.01
Gal-TEG Liposome-15	96.21 ± 0.65	0.178 ± 0.08
Gal-TEG Liposome-30	94.22 ± 0.14	0.142 ± 0.03
Man-TEG Chol-0	105.2 ± 0.46	0.079 ± 0.02
Man-TEG Chol-10	93.23 ± 0.47	0.180 ± 0.01
Man-TEG Chol-20	95.37 ± 0.81	0.116 ± 0.01
Man-TEG Chol-30	111.4 ± 0.60	0.095 ± 0.01
Man-TEG Chol-40	120.7± 0.67	0.148 ± 0.10
Man-TEG Chol-50	136.4 ± 1.18	0.079 ± 0.01
Man-TEG PS 0	111.6*	0.075*
Man-TEG PS-5	114.2*	0.117*
Man-TEG PS-10	132.7*	0.163*
Man-TEG PS-15	131.1*	0.205*
Man-Chol Liposome 10	109.9 ± 0.10	0.088± 0.01

[1] Average values ± S.D. (n=3); * n=1 due to time constraint:

Table S2 – Concanavalin A aggregation assays Rate constant (K) ± Standard Error (S.E.) and goodness of fit determined by GraphPad Prism 7.03©, using nonlinear regression, one phase association analysis.

Formulation	Rate constant (K) ± S.E.	Goodness of Fit (R^2)
Liposome-0	1.345e-005 ± 3.149e-007	0.6034
Man-TEG Liposome-2.5	0.001249 ± 9.826e-006	0.9998
Man-TEG Liposome-5	0.01141 ± 1.989e-005	0.9996
Man-TEG Liposome-7.5	0.01745 ± 0.00008	0.9954
Man-TEG Liposome -10	0.02239 ± 0.00017	0.9854
Man-TEG Liposome-15	0.02035 ± 0.00015	0.987
Man-TEG Liposome-20	0.01896 ± 0.00014	0.988
Man-TEG Liposome -30	0.02019 ± 0.00016	0.9853
Gal-TEG Liposome-2.5	0.00035 ± 0.0002	0.9697
Gal-TEG Liposome-15	0.00045 ± 0.0002	0.9112
Gal-TEG Liposome-30	0.00135 ± 0.0006	0.9464
Liposome-0 without Con A	0.0004 ± 0.0000	0.7842
Man-TEG Liposome-2.5 without Con A	0.0008 ± 0.0002	0.9924
Man-TEG Liposome-30 without Con A	0.00065 ± 0.00007	0.8968
Man-TEG Chol-0	0.00033 ± 0.00003	0.9987
Man-TEG Chol-10	0.01278 ± 0.00004	0.9982
Man-TEG Chol-20	0.01214 ± 0.00002	0.9996
Man-TEG Chol-30	0.01378 ± 0.00006	0.9965
Man-TEG Chol-40	0.02159 ± 0.00014	0.9894
Man-TEG Chol-50	0.02198 ± 0.00017	0.9853
Man-TEG PS 0	0.01584 ± 0.00014	0.9844
Man-TEG PS-5	0.01266 ± 0.00002	0.9996
Man-TEG PS-10	0.01614 ± 0.00009	0.9933
Man-TEG PS-15	0.01261 ± 0.00002	0.9994

6.4 Supplementary Information Chapter 4

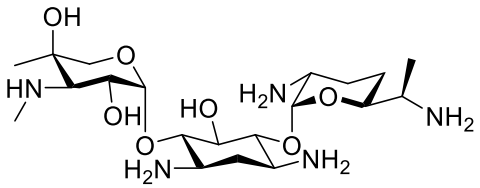

Figure S59 – Chemical structure of gentamicin.

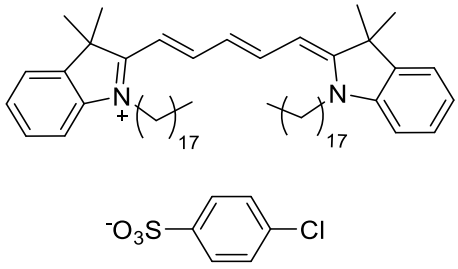

Figure S60 – Chemical structure of 1,1'-dioctadecyl-3,3,3',3'-tetramethylindodicarbocyanine 4-chlorobenzenesulfonate salt (DID).

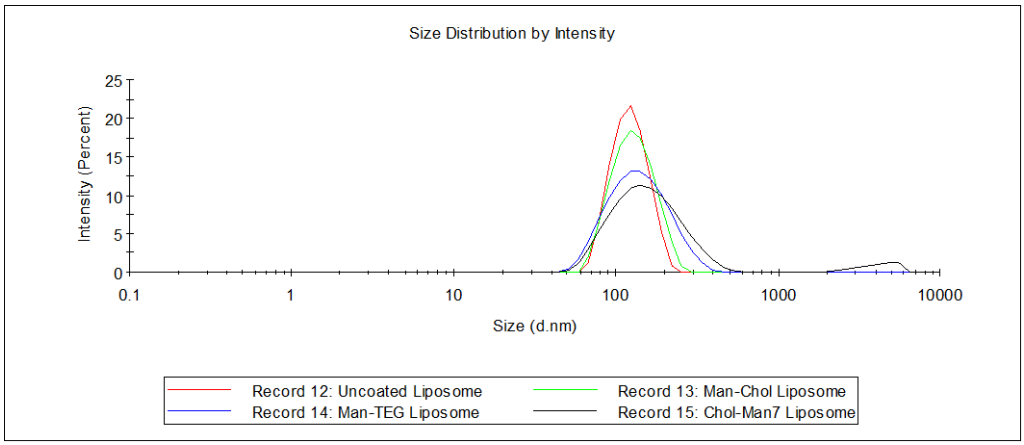

Figure S61 - Particle size distribution for liposome formulations used for uptake studies.

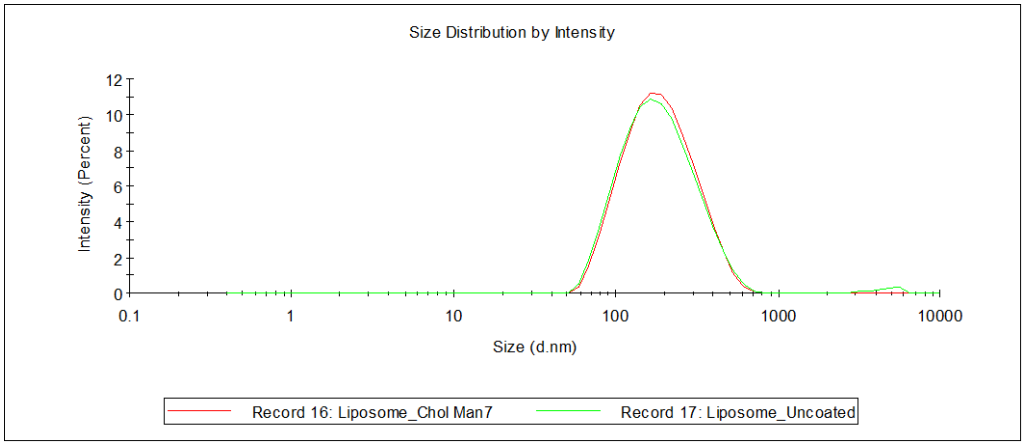

Figure S62 - Particle size distribution for liposome formulations used for gentamicin delivery study.

Table S3 – Lipid content, Z-average/PdI values from DLS and DID Encapsulation Efficiency of liposome formulations for *in vitro* studies.

	Molar Ratio %						
Formulation	Ligand	Chol	SM	POPC	Z-Average[2] d. (nm)	PdI[2]	EE%[3]
Untargeted Liposome[1]	0	40	10	49.5	116.5 ± 1.08	0.014 ± 0.01	93
Man-TEG Liposome[1]	10	40	10	39.5	123.5 ± 1.51	0.058 ± 0.01	86
Man-Chol Liposome[1]	10	30	10	49.5	128.6 ± 2.40	0.128 ± 0.02	71
Chol-Man_7 Liposome[1]	10	30	10	49.5	150.5 ± 1.22	0.266 ± 0.03	59
Gentamicin - untargeted Liposome	0	40	10	49.5	167.3 ± 1.20	0.281 ± 0.02	-
Gentamicin - Chol-Man_7 Liposome	10	30	10	49.5	161.7 ± 1.24	0.188 ± 0.01	-

[1] 0.5% molar ratio DID; [2] Average values ± S.D. (n=3); DID [3]Encapsulation Efficiency %

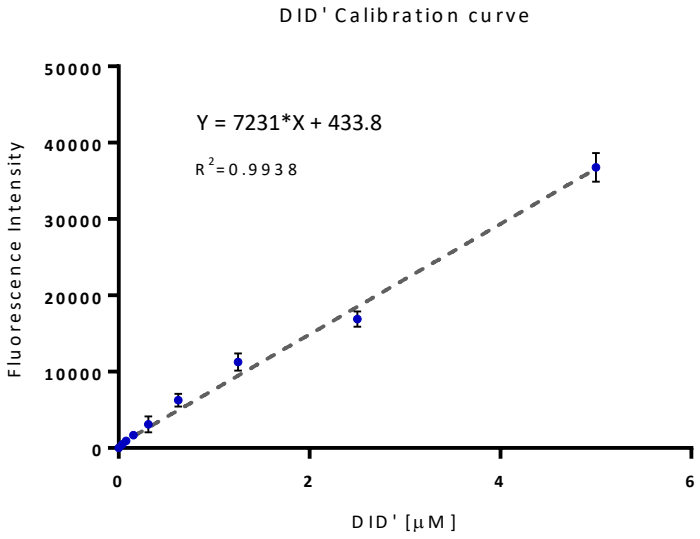

Figure S63 – Calibration curve of DID concentration, µM

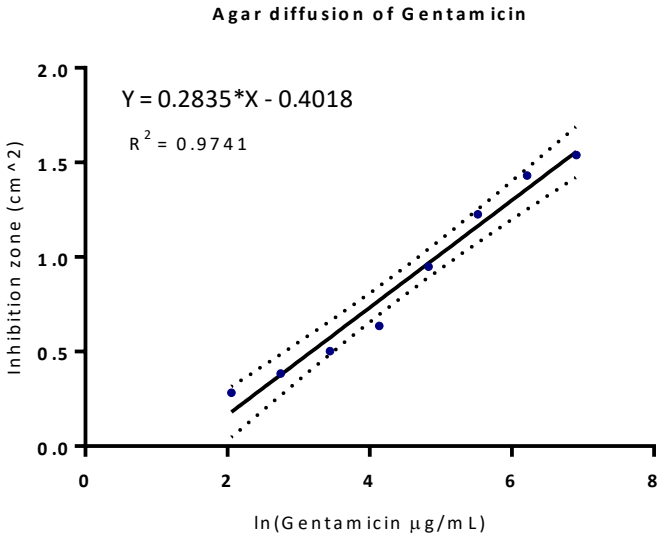

Figure S64 - Calibration curve of gentamicin in *S. aureus* inhibition assay.